

Overview of Airborne-Electromagnetic and -Magnetic Geophysical Data Collection Using the RESOLVE[®] and GEOTEM[®] Surveys Near Red Deer, Central Alberta

Overview of Airborne- Electromagnetic and -Magnetic Geophysical Data Collection Using the RESOLVE® and GEOTEM® Surveys near Red Deer, Central Alberta

S.R. Slattery¹ and L.D. Andriashek²

¹ Formerly of Alberta Geological Survey (see page ii for current address)

² Energy Resources Conservation Board
Alberta Geological Survey

©Her Majesty the Queen in Right of Alberta, 2012
ISBN 978-0-7785-8654-8

The Energy Resources Conservation Board/Alberta Geological Survey (ERCB/AGS), its employees and contractors make no warranty, guarantee or representation, express or implied, or assume any legal liability regarding the correctness, accuracy, completeness or reliability of this publication. Any reference to proprietary software and/or any use of proprietary data formats do not constitute endorsement by ERCB/AGS of any manufacturer's product.

If you use information from this publication in other publications or presentations, please acknowledge the ERCB/AGS. We recommend the following reference format:

Slattery, S.R. and Andriashek, L.D. (2012): Overview of airborne-electromagnetic and -magnetic geophysical survey data collection using the RESOLVE[®] and GEOTEM[®] surveys near Red Deer, central Alberta; Energy Resources Conservation Board, ERCB/AGS Open File Report 2012-07, 246 p.

Author address:

Shawn Slattery
Syncrude Canada Ltd.
P.O. Bag 4009, M.D. A 250
Fort McMurray, AB T9H 3L1
Canada
Tel: 780.715.9579
E-mail: slattery.shawn@syncrude.com

Published June 2012 by:

Energy Resources Conservation Board
Alberta Geological Survey
4th Floor, Twin Atria Building
4999 – 98th Avenue
Edmonton, AB T6B 2X3
Canada

Tel: 780.422.1927
Fax: 780.422.1918
E-mail: AGS-Info@ercb.ca
Website: www.ags.gov.ab.ca

Contents

Acknowledgements.....	v
Abstract.....	vi
1 Introduction.....	1
2 Purpose and Scope.....	1
3 Location of Study Area and Geophysical Study Blocks.....	4
4 Methodology.....	4
4.1 Data Acquisition, Processing and Interpretations.....	4
4.2 RESOLVE® Frequency-Domain Geophysical Survey.....	6
4.3 GEOTEM® Time-Domain Geophysical Survey.....	7
References.....	8
Appendix 1 – RESOLVE® Survey for Alberta Energy Resources Conservation Board, Red Deer Area, Alberta.....	10
Appendix 2 – Logistics and Processing Report Airborne Magnetic and GEOTEM® Survey, Edmonton–Red Deer Area, Alberta.....	78
Appendix 3 – Interpretation of the GEOTEM® Airborne EM Data from the Alberta Energy Resources Conservation Board Groundwater Mapping Project, Red Deer–Edmonton Corridor Survey.....	165

Table

Table 1. Data sources and types available to validate airborne-electromagnetic (AEM) and airborne-magnetic (AM) geophysical data in the Edmonton–Calgary Corridor, Alberta.....	4
---	---

Figures

Figure 1. Digital elevation model (DEM) accented by hillshaded relief of surface topography of the Edmonton–Calgary Corridor (ECC), Alberta.....	2
Figure 2. a) Location of the 11 geophysical study blocks in the Edmonton–Calgary Corridor (ECC).....	3
Figure 3. a) Simplified, regional-scale cross-section, oriented west to east, of sediments and bedrock surveyed using the low-frequency, GEOTEM® time-domain survey, central Alberta. b) Simplified, local-scale cross-section, oriented west to east, of sediments and bedrock surveyed with the RESOLVE® frequency-domain survey, central Alberta.....	5
Figure 4. a) RESOLVE® frequency-domain survey in operation. The main part of the geophysical system is contained within a cylindrical tube, commonly referred to as a receiver, which is towed beneath the helicopter. b) The RESOLVE® receiver is approximately 9 m in length.....	6
Figure 5. a) The GEOTEM® survey technique in flight.....	7

Acknowledgements

Comments from T.G. Lemay and N. Atkinson of the Alberta Geological Survey improved an earlier version of this report. We also thank J. Dawson for editing the report.

Abstract

This report is one in a series of eight Alberta Geological Survey (AGS) Open File reports that provide an overview of airborne-electromagnetic and -magnetic geophysical surveys completed over the Edmonton–Calgary Corridor (ECC) by Fugro Airborne Surveys. These surveys were completed between November 2007 and February 2010 as part of a joint AGS and Alberta Environment and Sustainable Resource Development (ESRD) study to determine the usefulness of the RESOLVE[®], GEOTEM[®] and TEMPEST[®] geophysical survey techniques in mapping the distribution and physical attributes of sediment- and bedrock-aquifer complexes over areas of formerly glaciated terrain.

The ECC was selected as the first test area to support the AGS-ESRD groundwater mapping program as it represents the region with the highest rates of industrial and urban growth in the province. Since this growth will exert increasing demands on water resources in the ECC, it is necessary to reassess the spatial distribution of previously mapped, as well as unmapped, aquifer complexes in the region. By doing so, Alberta may better predict and manage current and/or future stresses on existing aquifer systems caused by industrial, agricultural and urban development. Airborne geophysical survey methods were selected as one of the tools in completing this assessment.

The ECC is an ideal area to evaluate the usefulness of airborne-electromagnetic and -magnetic geophysical survey techniques due to the wealth of existing surficial and subsurface geological datasets (i.e., geological mapping, lithologs, petrophysical data, field observations, etc.). These datasets provide users with a means to calibrate and verify airborne geophysical data, analyses and interpretations within the ECC.

This report describes data collection methods using the Fugro Airborne Surveys' RESOLVE[®] and GEOTEM[®] survey techniques and data processing. Geophysical interpretations of these data, completed for the four study blocks near the city of Red Deer, Alberta, by Fugro Airborne Surveys and Larch Consulting Ltd., are included as appendices in this report.

1 Introduction

In recognition of increasing rates of urbanization and industrialization in Alberta, and the foreseeable pressures that this will have on existing water supplies, the Alberta Geological Survey (AGS) in partnership with Alberta Environment and Sustainable Resource Development (ESRD) has initiated a multiyear project to characterize nonsaline aquifer complexes within the province. The Edmonton–Calgary Corridor (ECC), the region with the most industrial and urban development in Alberta, was selected as the first study area by AGS and ESRD (Figure 1).

It is inevitable that future groundwater use in the ECC will place additional stress on existing aquifer systems. Therefore, reassessing previously mapped aquifers, potentially locating unmapped aquifers and implementing management strategies that ensure groundwater resources exist for future use are essential. As management strategies and decision-making tools will require more accurate geological and hydrogeological models, innovative approaches to data collection will be required. In complicated geological terrains, such as the ECC, where hydraulic pathways within glacial sediments and between glacial sediments and underlying bedrock formations are poorly understood, continuous high-resolution geological mapping of both glacial sediments and bedrock formations is necessary to better understand and illustrate the architecture of geological strata. A better understanding of the geological architecture within the ECC will allow for improved geological modelling, which in turn will allow for a better hydrogeological model of the ECC. It is anticipated that this model will form the cornerstone for numerous applications, such as groundwater exploration programs, aquifer protection studies and significant recharge area identification. More importantly, this model will form the framework for groundwater-flow modelling exercises and future water-budget calculations leading to improved water management decisions.

Recognizing the need for high-quality regional geological data, AGS and ESRD have collaborated to obtain airborne-geophysical survey data for near-continuous coverage of the ECC. A similar approach has been taken in other areas of formerly glaciated terrain by geological surveys in the United States, Europe and the United Kingdom (cf. Smith et al., 2003, 2006, 2007; Lahti et al., 2005; Wiederhold et al., 2009). Despite the success of these surveys in mapping the distribution of near-surface and subsurface aquifers, one of the main objectives of our investigation is to evaluate and compare the usefulness of these same types of airborne-geophysical survey techniques in mapping the distribution of aquifers in the ECC.

Between November 2007 and February 2010, airborne-electromagnetic (AEM) and airborne-magnetic (AM) surveys were completed by Fugro Airborne Surveys over 11 study blocks in the ECC on behalf of AGS and ESRD. The airborne-geophysical surveys were undertaken using one or a combination of the following survey techniques: fixed-wing, GEOTEM® or TEMPEST® time-domain or helicopter-borne, RESOLVE® frequency-domain (Figure 2a). This report provides an overview of data collection using the RESOLVE® frequency-domain and GEOTEM® time-domain survey techniques, data processing and the interpretation of data completed over four study blocks near the city of Red Deer, central Alberta (Figure 2b). Information on GEOTEM® and TEMPEST® time-domain airborne-geophysical survey techniques completed over the remaining study blocks in the ECC are presented in separate Open File reports ((Slattery and Andriashek, 2012a–g).

2 Purpose and Scope

The reasons for completing AEM and AM geophysical surveys in the ECC are multifaceted. First, it is to evaluate the effectiveness of frequency- and time-domain geophysical surveys to determine the spatial distribution of near-surface and subsurface electrical and magnetic properties of sediments and bedrock. It is anticipated that these properties will be related to geological and hydrogeological features in the ECC,

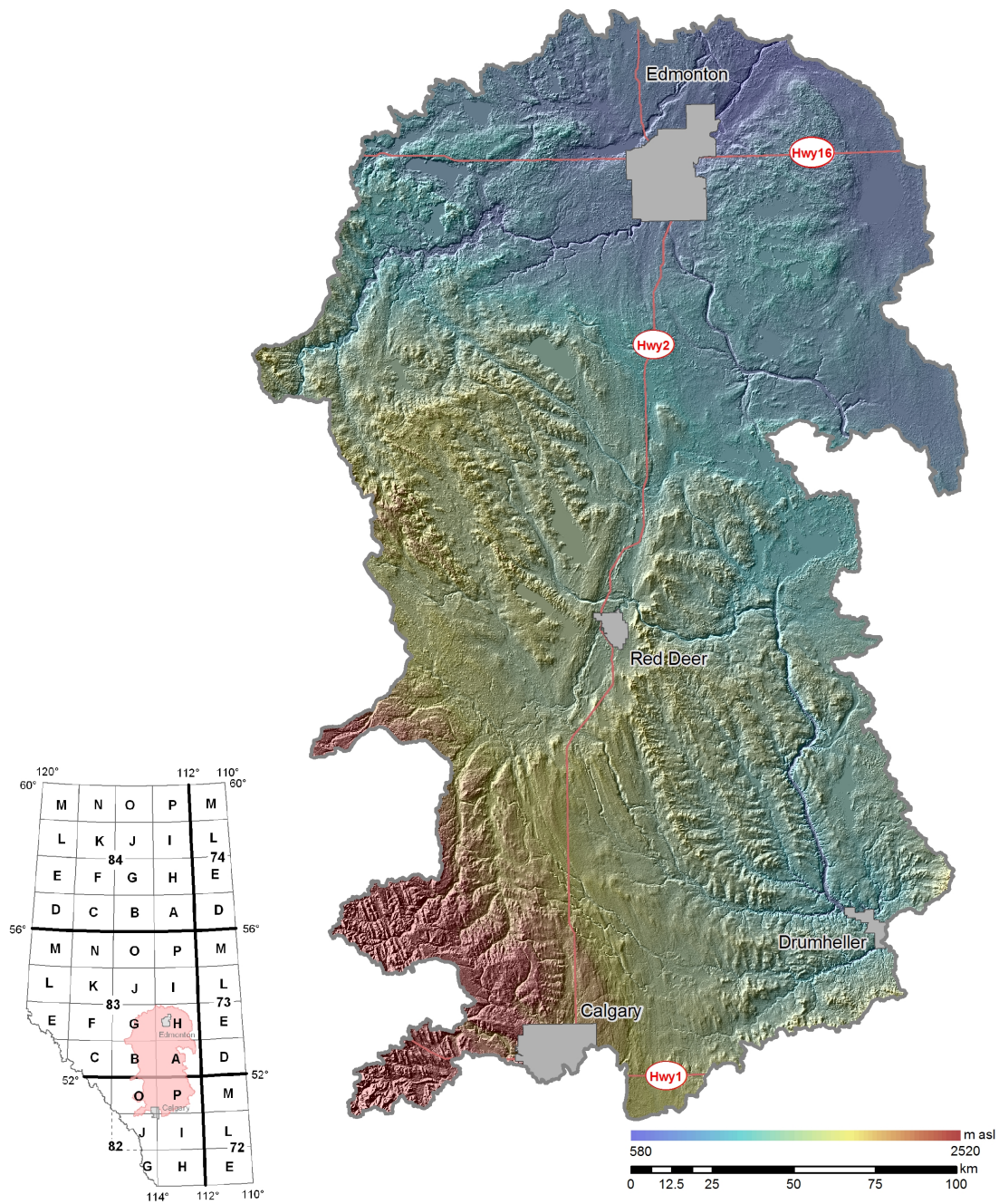


Figure 1. Digital elevation model (DEM) accented by hillshaded relief of surface topography of the Edmonton–Calgary Corridor (ECC), Alberta. Elevation of surface topography in metres above sea level is defined by colour ramp. Vertical exaggeration is 20x. Inset map depicts location of the ECC, Alberta.

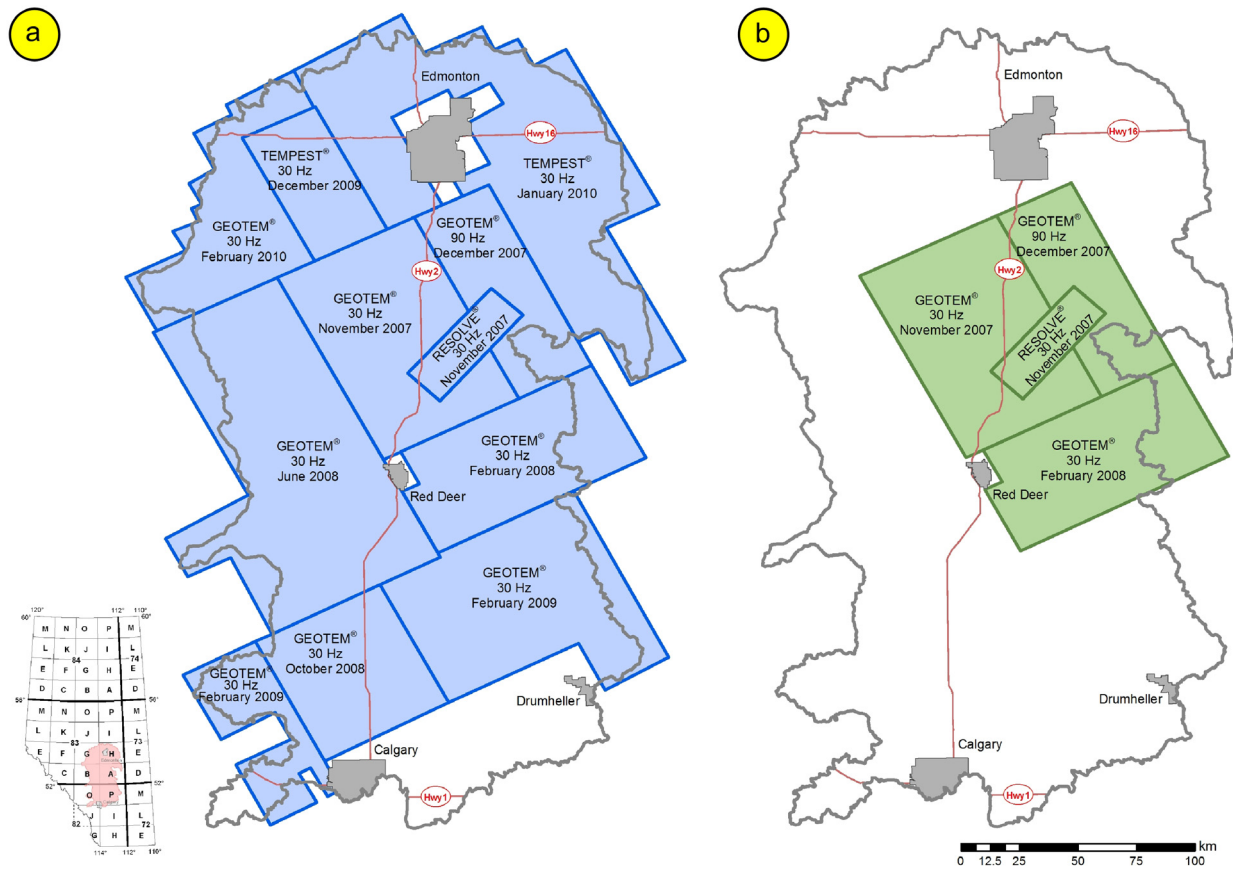


Figure 2. a) Location of the 11 geophysical study blocks in the Edmonton–Calgary Corridor (ECC). The type of geophysical survey and when it was completed are provided on each study block. b) Location of the four study blocks (the first survey area) near the city of Red Deer, Alberta. Inset map depicts location of the ECC, Alberta.

which will provide a better understanding of the geological architecture. This, in turn, will allow for more accurate geological and hydrogeological models to support improved water management decisions.

Second, the selection of the ECC for AEM and AM surveying was influenced by the widespread availability of existing surface and subsurface geological and geophysical data in the region (Table 1). These data are needed to validate the results and interpretations of the AEM and AM survey data. If the interpretation of AEM and AM survey data correlates with geological data and ground and downhole geophysical data, then AEM and AM surveying techniques could be used to interpret the geological framework in those areas that have limited subsurface geological and geophysical data. In such areas, AEM and AM surveys may provide a more time- and cost-effective means to acquire continuous, high-quality geological data than traditional drilling methods and geological mapping investigations.

Third, the geological setting of the ECC is such that aquifer complexes can occur at various depths and have a variety of sediment and rock properties. Low-frequency (30 and 90 hertz [Hz]), GEOTEM® time-domain surveys were completed to provide greater penetration depths and summary electromagnetic (EM) and magnetic data to improve the delineation of regional-scale geological strata in the ECC. The AGS and ESRD tested the RESOLVE® frequency-domain survey in areas where more detailed resolution of the near-surface geology was required. Simplified cross-sections of the geological settings are depicted in Figure 3.

Table 1. Data sources and types available to validate airborne-electromagnetic (AEM) and airborne-magnetic (AM) geophysical data in the Edmonton–Calgary Corridor, Alberta. Abbreviations: ESRD, Alberta Environment and Sustainable Resource Development; AGS, Alberta Geological Survey; ERCB, Energy Resources Conservation Board.

Data Source	Data Class	Number of Data Points
ESRD digital water-well database	Water-well records and litholog records	234 902
AGS geotechnical database	Geotechnical borehole records	1202
ERCB oil-and gas–well database	Oil-and-gas–well and petrophysical records	5161
AGS borehole database	Geological borehole and petrophysical records	363
AGS field observations	Field-based geological data	322

3 Location of Study Area and Geophysical Study Blocks

The ECC study area occupies approximately 49 500 km² and lies within portions of NTS 82I, J, O and P and 83A, B, G and H. Ten subwatershed boundaries define the irregularly shaped boundary of the ECC study area (Figure 1).

Between November 2007 and February 2010, AEM and AM surveys were completed over 11 study blocks in the ECC (Figure 2a). Data collection over the first survey area, located near the city of Red Deer, Alberta (Figure 2b), was completed in three stages. Data collection for the first stage of the survey was completed in November 2007 over the central study block of the survey area using a helicopter-borne, RESOLVE[®] frequency-domain survey method (Figure 2b). The survey was flown over 4279.4 line kilometres (line-km), including 394.0 line-km of tie lines, using frequencies of 400, 1800, 3300, 8200, 40 000 and 140 000 Hz. Flight lines were completed in a northwest-southeast direction with a line separation of 200 m. Tie lines were completed in a perpendicular (northeast-southwest) direction to the flight lines with a line separation of 2000 m.

During the second stage of the survey, completed between November and December 2007, data were acquired over the northern half of the first survey area using a fixed-wing, GEOTEM[®] time-domain survey. Data collection was completed using a base pulse repetition rate of 90 Hz over the northeastern study block of the survey area whereas a base pulse repetition rate of 30 Hz was used over the northwestern study block of the survey area (Figure 2b). Data were recorded along flight lines oriented northwest to southeast with a line separation of approximately 800 m. Tie lines were approximately 1500 m apart in a northeast-southwest direction.

The third and final stage of the survey was completed during February 2008 over the southern study block of the first survey area (Figure 2b). Data were acquired using a fixed wing, GEOTEM[®] time-domain survey with a base pulse repetition rate of 30 Hz. Data were recorded along flight lines oriented northeast to southwest, with tie lines oriented in a northwest-southeast direction at 8 m intervals along the flight lines. Additional information on these survey techniques is presented in the following section and in Appendices 1 and 2.

4 Methodology

4.1 Data Acquisition, Processing and Interpretations

Digital data from the AEM and AM surveys were acquired by the contractor, Fugro Airborne Surveys, using the RESOLVE[®] and GEOTEM[®] survey techniques. These techniques are briefly described below and presented in Appendices 1 and 2. For additional information, the reader is referred to Fraser (1978), Smith et al. (2003, 2006, 2007), Paine and Minty (2005) and Siemon (2006).

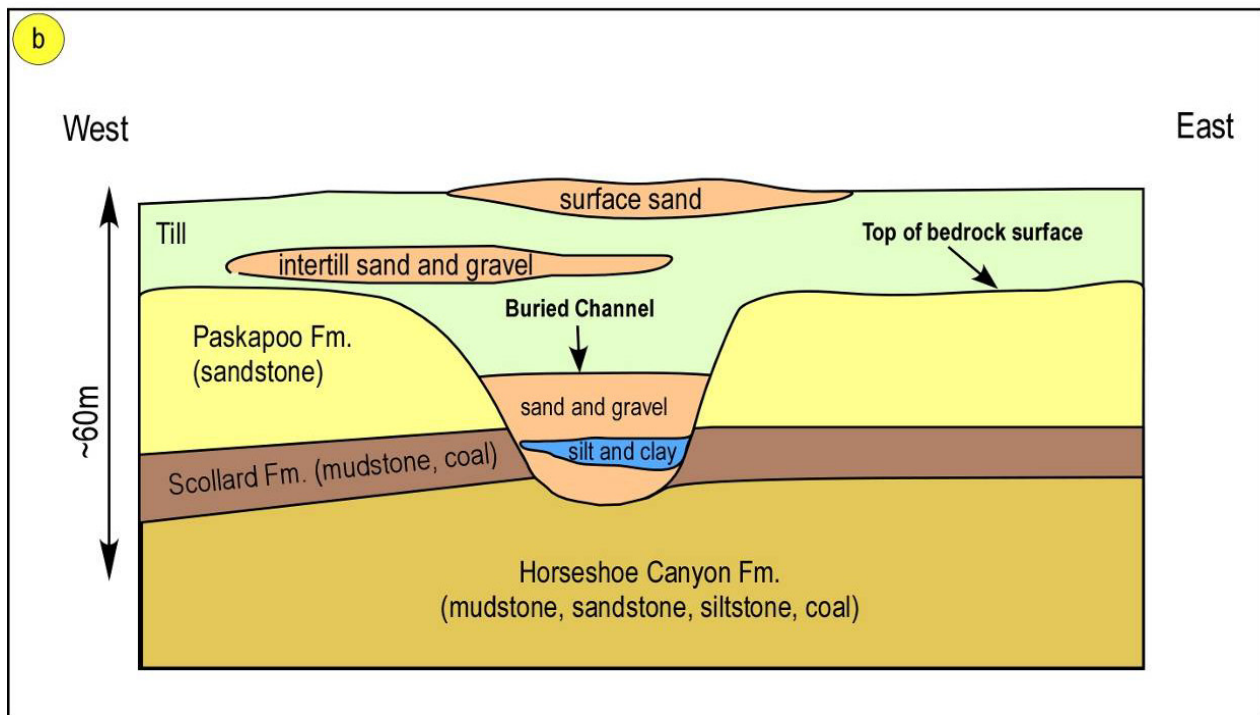
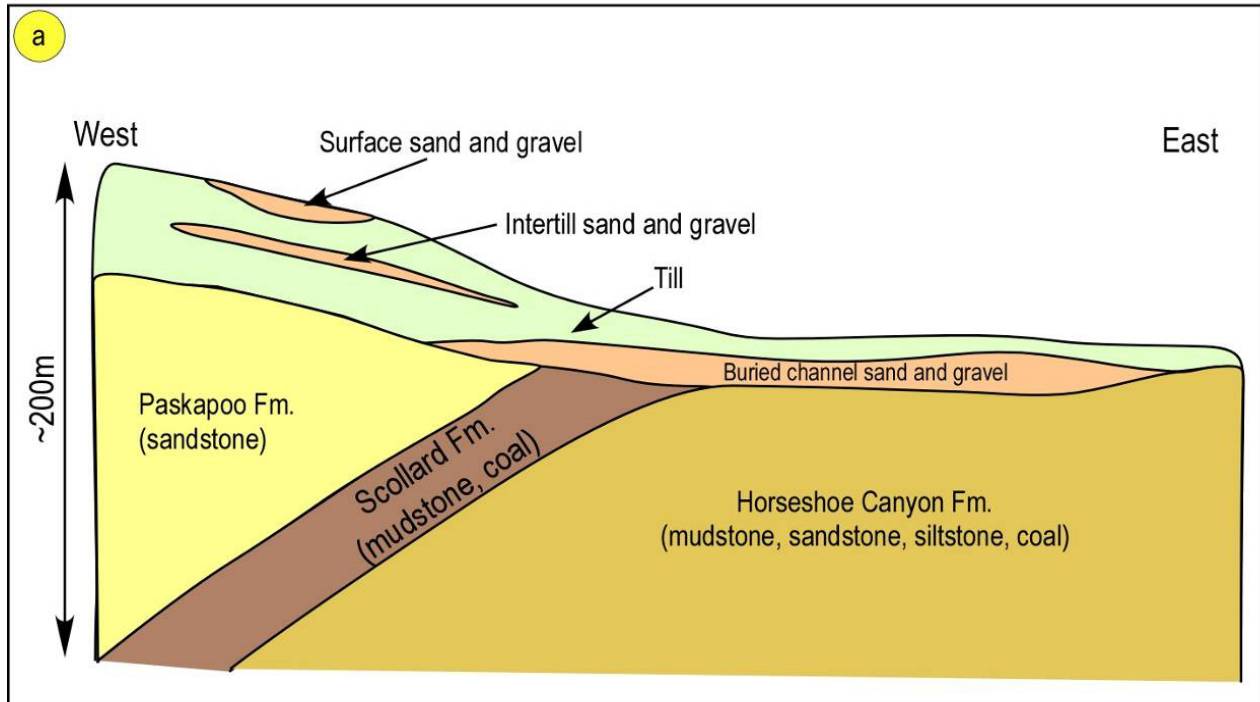


Figure 3. a) Simplified, regional-scale cross-section, oriented west to east, of sediments and bedrock surveyed using the low-frequency, GEOTEM® time-domain survey, central Alberta. b) Simplified, local-scale cross-section, oriented west to east, of sediments and bedrock surveyed with the RESOLVE® frequency-domain survey, central Alberta.

Additional data processing and interpretation were completed by a second contractor, Larch Consulting Ltd. The results by Larch are presented in Appendix 3. Datasets provided to AGS and ESRD from the contractors included both unprocessed and processed tabular datasets, as well as grid-based digital maps illustrating ground resistivity in relation to depth below ground surface. The AGS and ESRD did not process any of the geophysical data.

4.2 RESOLVE® Frequency-Domain Geophysical Survey

The RESOLVE® survey is a helicopter-borne, frequency-domain EM survey designed specifically for locating conductive anomalies and mapping earth resistivities. It is completed using a unique six-frequency system, with the EM response measured by horizontal coplanar coils at approximately 400, 1800, 8200, 40 000 and 140 000 Hz and one coaxial coil at approximately 3300 Hz. Appendix 1 details the specific frequencies, separation, and orientation of the coil pairs.

Ancillary equipment used in this survey consisted of a magnetometer, radar and laser altimeters, a video camera, a digital data recorder and an electronic navigation system. The instrumentation was installed in a modified AS350-B2 helicopter. The helicopter flew with an EM sensor height of approximately 30 m. The main part of the geophysical system is contained within a cylindrical tube, commonly referred to as a receiver, which is towed beneath the helicopter (Figure 4; Appendix 1). All data recorded by the

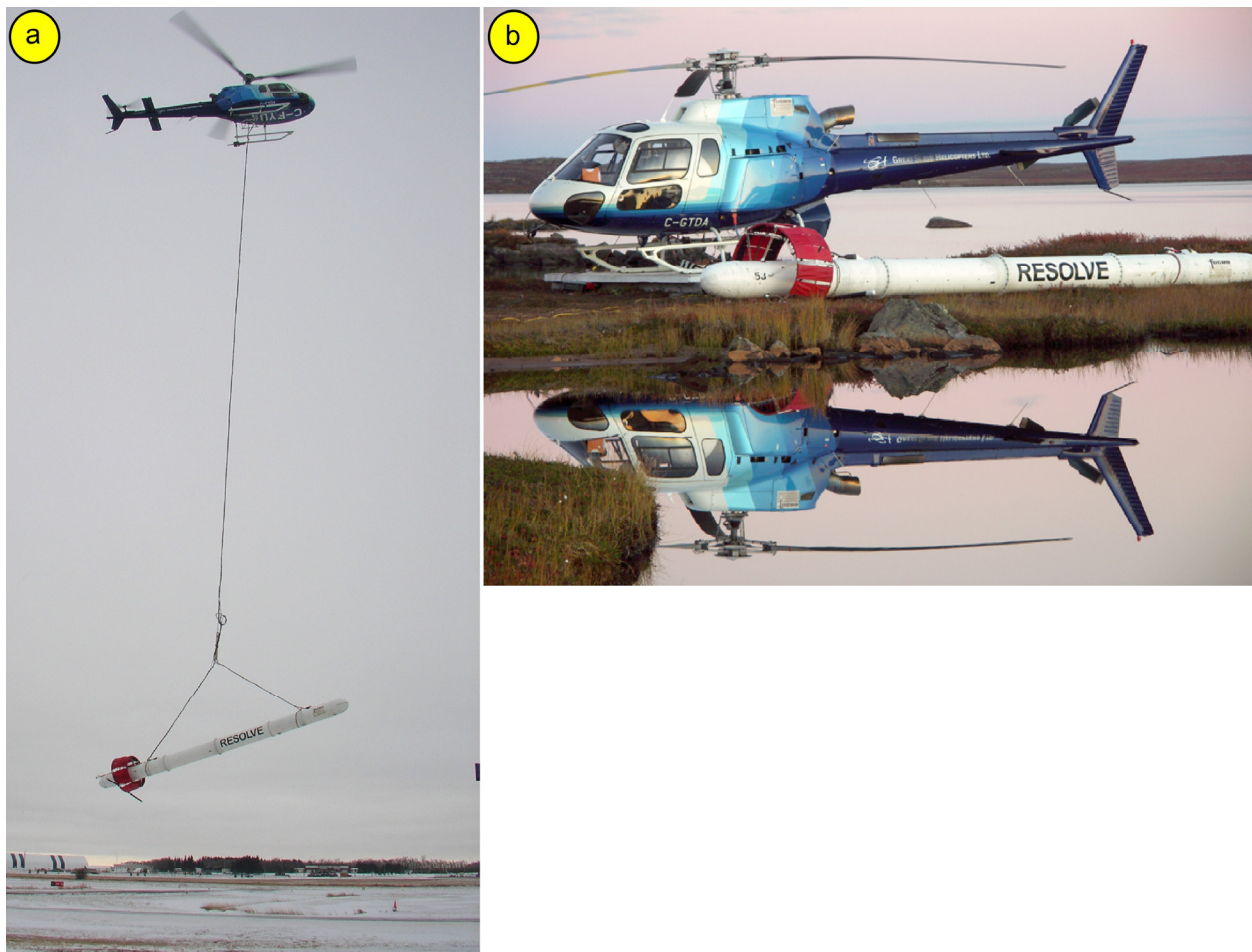


Figure 4. a) RESOLVE® frequency-domain survey in operation. The main part of the geophysical system is contained within a cylindrical tube, commonly referred to as a receiver, which is towed beneath the helicopter. b) The RESOLVE® receiver is approximately 9 m in length.

measurement systems in the receiver are transmitted through a cable to a processing and digital recording system located in the helicopter (Appendix 1). Measurements of the geophysical data (EM and total field magnetic) are made approximately every 3 m along the flight line. Additional information on the RESOLVE[®] survey technique is provided in Appendix 1.

4.3 GEOTEM[®] Time-Domain Geophysical Survey

The fixed-wing, GEOTEM[®] time-domain survey technique consists of a towed-bird EM system. The survey technique is based on the premise that fluctuations in the primary EM field produced in the transmitting loop will result in eddy currents being generated in any conductors in the ground. The eddy currents then decay to produce a secondary EM field that may be sensed in the receiver coil. Each primary pulse causes decaying eddy currents in the ground to produce a secondary magnetic field. This secondary magnetic field, in turn, induces a voltage in the receiver coils, which is the EM response. Good conductors decay slowly, whereas poor conductors decay more rapidly.

The primary EM pulses are created by a series of discontinuous sinusoidal current pulses fed into a three- or six-turn transmitting loop surrounding the aircraft and fixed to the nose, tail and wing tips. For this survey, instrumentation was installed on a modified Casa 212 aircraft (Figure 5). The base frequency rate is selectable: 25, 30, 75, 90, 125, 150, 225 and 270 Hz, and the length of the pulse can be adjusted to suit specific targets. Standard pulse widths available are 0.6, 1.0, 2.0 and 4.0 ms, and the receiver is a three-axis (x, y, z) induction coil that is towed by the aircraft on a 135 m long, nonmagnetic cable (refer to Appendix 2, Figure 3). The usual mean terrain clearance for the aircraft is 120 m with the EM receiver normally being situated 50 m below and 130 m behind the aircraft. Additional information on the GEOTEM[®] survey technique is provided in Appendix 2.



Figure 5. a) The GEOTEM[®] survey technique in flight. Note the transmitting loop fixed to the aircraft's nose, tail and wing tips. Primary electromagnetic pulses are created by a series of discontinuous, sinusoidal current pulses and transmitted into the transmitting loop. b) Modified Casa 212 aircraft used by Fugro Airborne Surveys in this study.

5 References

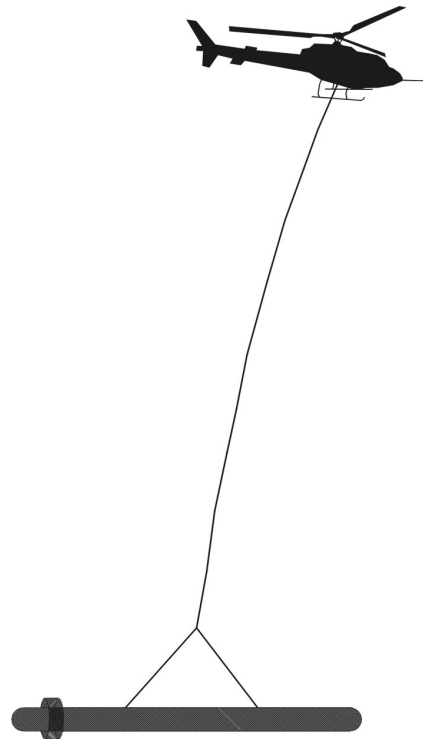
- Fraser, D.C. (1978): Resistivity mapping with an airborne multicoil electromagnetic system; *Geophysics*, v. 43, p. 144–172.
- Lahti, M., Vanhala, H., Mattsson, A., Beamish, D. and Lerssi, J. (2005): Environmental applications of airborne geophysics – groundwater and contaminated soil in Finland, Germany and United Kingdom; Geological Survey of Finland, Special Paper 39, p. 155–175.
- Paine, J.G. and Minty, B.R.S. (2005): Airborne hydrogeophysics; *in* *Hydrogeophysics*, Y. Rubin and S.S. Hubbard (ed.), Water Science and Technology Library, v. 50, p. 333–357.
- Simon, B. (2006): Electromagnetic methods – frequency domain – airborne techniques; *in* *Groundwater geophysics – a tool for hydrogeology*, R. Kirsch (ed.), Springer-Verlag, p. 155–170.
- Slattery, S.R. and Andriashek, L.D. (2012a): Overview of airborne-electromagnetic and -magnetic geophysical data collection using the GEOTEM[®] survey technique in the Sylvan Lake area, central Alberta; Energy Resources Conservation Board, ERCB/AGS Open File Report 2012-08, 175 p.
- Slattery, S.R. and Andriashek, L.D. (2012b): Overview of airborne-electromagnetic and -magnetic geophysical data collection using the GEOTEM[®] survey technique north of Calgary, Alberta; Energy Resources Conservation Board, ERCB/AGS Open File Report 2012-09, 169 p.
- Slattery, S.R. and Andriashek, L.D. (2012c): Overview of airborne-electromagnetic and -magnetic geophysical survey data collection using the GEOTEM[®] survey technique near Three Hills and Cochrane, Alberta; Energy Resources Conservation Board, ERCB/AGS Open File Report 2012-10, 92 p.
- Slattery, S.R. and Andriashek, L.D. (2012d): Overview of airborne-electromagnetic and -magnetic geophysical data collection using the TEMPEST[®] survey technique near Edmonton, Alberta; Energy Resources Conservation Board, ERCB/AGS Open File Report 2012-11, 38 p.
- Slattery, S.R. and Andriashek, L.D. (2012e): Overview of airborne-electromagnetic and -magnetic geophysical data collection using the GEOTEM[®] survey technique near Drayton Valley, central Alberta; Energy Resources Conservation Board, ERCB/AGS Open File Report 2012-12, 92 p.
- Slattery, S.R. and Andriashek, L.D. (2012f): Overview of airborne-electromagnetic and magnetic-geophysical data collection and interpretation in the Edmonton–Calgary Corridor, Alberta; Energy Resources Conservation Board, ERCB/AGS Open File Report 2012-13, 208 p.
- Slattery, S.R. and Andriashek, L.D. (2012g): Overview of airborne-electromagnetic and -magnetic geophysical data collection using the TEMPEST[®] survey technique near Wabamun, central Alberta; Energy Resources Conservation Board, ERCB/AGS Open File Report 2012-14, 38 p.
- Smith, B.D., Irvine, R., Blome, C.D., Clark, A.K. and Smith, D.V. (2003): Preliminary results, helicopter electromagnetic and magnetic survey of the Seco Creek area, Medina and Uvalde counties, Texas; Proceedings for the Symposium on the Application of Geophysics to Environmental and Engineering Problems, San Antonio, Texas, 15 p.
- Smith, B.D., Thamke, J.N., Cain, M.J., Tyrrell, C. and Hill, P.L. (2006): Helicopter electromagnetic and magnetic survey maps and data, East Poplar Oil Field area, Fort Peck Indian Reservation, northeastern Montana, August 2004; United States Geological Survey, Open File Report 2006-1216, 23 p., 1 plate.
- Smith, B.D., Grauch, V.J.S., McCafferty, A.E., Smith, D.V., Rodriguez, B.R., Pool, D.R., Deszcz-Pan, M. and Labson, V.F. (2007): Airborne electromagnetic and magnetic surveys for ground-water resources: a decade of study by the U.S. Geological Survey; *in* *Proceedings of Exploration 07: Fifth Decennial International Conference on Mineral Exploration*, B. Milkereit (ed.), p. 895–899.

Wiederhold, H., Schaumann, G. and Steuer, A. (2009): Airborne geophysical investigations for hydrogeological purposes in northern Germany; Near Surface 2009 – 15th European Meeting of Environmental and Engineering Geophysics, September 7–9, 2009, Dublin, Ireland, 5 p.

**Appendix 1 – RESOLVE® Survey for Alberta Energy Resources Conservation Board,
Red Deer Area, Alberta**

**RESOLVE SURVEY
FOR
ALBERTA ENERGY RESOURCES CONSERVATION BOARD
RED DEER AREA
ALBERTA**

NTS: 83A/11, 12, 13, 14



Fugro Airborne Surveys Corp.
Mississauga, Ontario

March 4, 2008

SUMMARY

This report describes the logistics, data acquisition, processing and presentation of results of a RESOLVE airborne geophysical survey carried out for Alberta Energy Resources Conservation Board, over a property located near Red Deer, Alberta. Total coverage of the survey block amounted to 4279.4 km. The survey was flown from November 22nd to December 6th, 2007.

The purpose of the survey was to detect conductivity contrasts within the survey area. This was accomplished by using a RESOLVE multi-coil, multi-frequency electromagnetic system, supplemented by a high sensitivity cesium magnetometer. The information from these sensors was processed to produce maps that display the magnetic and conductive properties of the survey area. A GPS electronic navigation system ensured accurate positioning of the geophysical data with respect to the base map.

The survey data were processed and compiled in the Fugro Airborne Surveys Toronto office. Map products and digital data were provided in accordance with the scales and formats specified in the Survey Agreement.

CONTENTS

1.INTRODUCTION.....	1.1
2.SURVEY OPERATIONS.....	2.1
3.SURVEY EQUIPMENT	3.1
Electromagnetic System.....	3.1
In-Flight EM System Calibration.....	3.2
Airborne Magnetometer.....	3.4
Magnetic Base Station	3.4
Navigation (Global Positioning System).....	3.6
Radar Altimeter	3.8
Barometric Pressure and Temperature Sensors.....	3.9
Laser Altimeter	3.9
Digital Data Acquisition System	3.10
Video Flight Path Recording System.....	3.10
4.QUALITY CONTROL AND IN-FIELD PROCESSING.....	4.1
5.DATA PROCESSING.....	5.1
Flight Path Recovery	5.1
Electromagnetic Data	5.1
Apparent Resistivity.....	5.2
Resistivity-depth Sections	5.3
Total Magnetic Field.....	5.5
Calculated Vertical Magnetic Gradient.....	5.6
Contour, Colour and Shadow Map Displays	5.6
6.PRODUCTS.....	6.1
Base Maps	6.1

APPENDICES

- A. List of Personnel
- B. Background Information
- C. Data Archive Description
- D. Data Processing Flowcharts
- E. Glossary

1. INTRODUCTION

A RESOLVE electromagnetic/resistivity/magnetic survey was flown for Alberta Energy Resources Conservation Board, from November 22nd to December 6th, 2007 over a survey block located near Red Deer, Alberta. The survey area can be located on NTS map sheets 83A/11, 12, 13, 14 (Figure 2).

Survey coverage consisted of approximately 4279.4 line-km, including 394.0 line-km of tie lines. Flight lines were flown in an azimuthal direction of 138°/318° with a line separation of 200 metres. Tie lines were flown orthogonal to the traverse lines (48°/228°) with a line separation of 2000 metres.

The survey employed the RESOLVE electromagnetic system. Ancillary equipment consisted of a magnetometer, radar and laser altimeters, video camera, a digital data recorder and an electronic navigation system. The instrumentation was installed in an AS350-B2 turbine helicopter (Registration C-FYDA) that was provided by Great Slave Helicopters Ltd. The helicopter flew with an EM sensor height of approximately 30 metres.



Figure 1: Fugro Airborne Surveys RESOLVE EM bird

2. SURVEY OPERATIONS

The base of operations for the survey was established at Wetaskiwin Airport, Wetaskiwin, Alberta. The survey area, coloured in magenta on the location map, is located on NTS map sheets 83A/11, 12, 13, 14 (Figure 2).

Table 2-1 lists the corner coordinates of the survey area in NAD83, Alberta 10TM (Forest), central meridian -115°.

Table 2-1

Block	Corners	X-UTM (E)	Y-UTM (N)
07116-1	1	588561	5837285
	2	619341	5867852
	3	632081	5855404
	4	602206	5823947

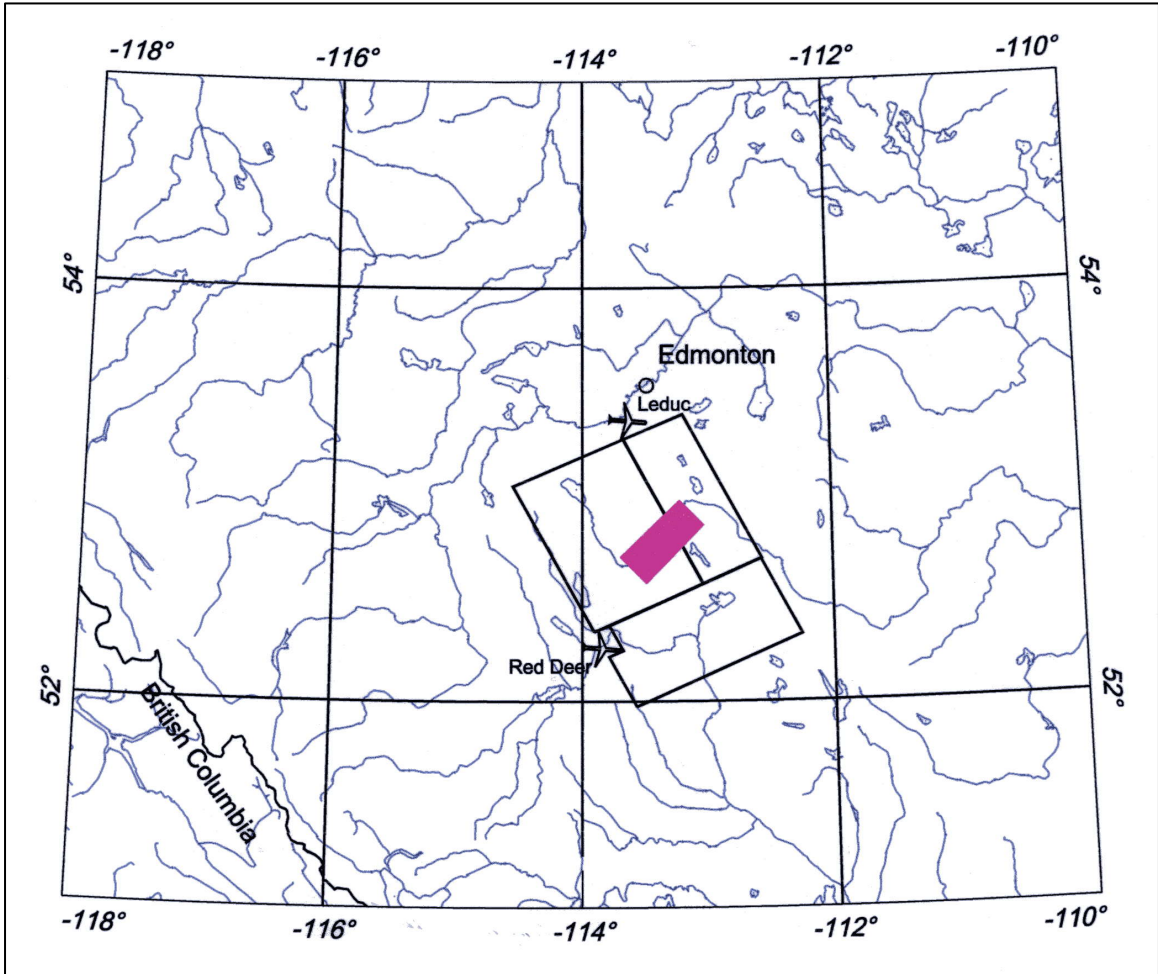


Figure 2
Red Deer Survey Area Location
Job # 07116

The survey specifications were as follows:

Parameter	Specifications
Traverse line direction	138°/318°
Traverse line spacing	200 m
Tie line direction	48°/228°
Tie line spacing	2000 m
Sample interval	10 Hz, 3.3 m @ 120 km/h
Aircraft mean terrain clearance	58 m
EM sensor mean terrain clearance	30 m
Mag sensor mean terrain clearance	30 m
Navigation (guidance)	±5 m, Real-time GPS
Post-survey flight path	±2 m, Differential GPS

3. SURVEY EQUIPMENT

This section provides a brief description of the geophysical instruments used to acquire the survey data and the calibration procedures employed. The geophysical equipment was installed in an AS350-B2 helicopter. This aircraft provides a safe and efficient platform for surveys of this type.

Electromagnetic System

Model: RESOLVE

Type: Towed bird, symmetric dipole configuration operated at a nominal survey altitude of 30 metres. Coil separation is 7.9 metres for 400 Hz, 1800 Hz, 8200 Hz, 40 000 Hz and 140 000 Hz, and 9.0 metres for the 3300 Hz coil-pair.

Coil orientations, frequencies and dipole moments	<u>Atm²</u>	<u>orientation</u>	<u>nominal</u>	<u>actual</u>
	310	coplanar /	400 Hz	396 Hz
	175	coplanar /	1800 Hz	1773 Hz
	211	coaxial /	3300 Hz	3247 Hz
	70	coplanar /	8200 Hz	8220 Hz
	35	coplanar /	40 000 Hz	39 880 Hz
	18	coplanar /	140 000 Hz	132 700 Hz

Channels recorded: 6 in-phase channels
6 quadrature channels
2 monitor channels

Sensitivity: 0.12 ppm at 400 Hz Cp
0.12 ppm at 1800 Hz Cp
0.12 ppm at 3300 Hz Cx
0.24 ppm at 8200 Hz Cp
0.60 ppm at 40 000 Hz Cp
0.60 ppm at 140 000 Hz Cp

Sample rate: 10 per second, equivalent to 1 sample every 3.3 m, at a survey speed of 120 km/h.

The electromagnetic system utilizes a multi-coil coaxial/coplanar technique to energize conductors in different directions. The coaxial coils are vertical with their axes in the flight direction. The coplanar coils are horizontal. The secondary fields are sensed simultaneously by means of receiver coils that are maximum coupled to their respective transmitter coils. The system yields an in-phase and a quadrature channel from each transmitter-receiver coil-pair.

In-Flight EM System Calibration

Calibration of the system during the survey uses the Fugro AutoCal automatic, internal calibration process. At the beginning and end of each flight, and at intervals during the flight, the system is flown up to high altitude to remove it from any “ground effect” (response from the earth). Any remaining signal from the receiver coils (base level) is measured as the zero level, and is removed from the data collected until the time of the next calibration. Following the zero level setting, internal calibration coils, for which the response phase and amplitude have been determined at the factory, are automatically triggered – one for each frequency. The on-time of the coils is sufficient to determine an accurate response through any ambient noise. The receiver response to each calibration coil “event” is compared to the expected response (from the factory calibration) for both phase angle and amplitude, and any phase and gain corrections are automatically applied to bring the data to the correct value.

In addition, the outputs of the transmitter coils are continuously monitored during the survey, and the gains are adjusted to correct for any change in transmitter output.

Because the internal calibration coils are calibrated at the factory (on a resistive halfspace) ground calibrations using external calibration coils on-site are not necessary for system calibration. A check calibration may be carried out on-site to ensure all systems are working correctly. All system calibrations will be carried out in the air, at sufficient altitude that there will be no measurable response from the ground.

The internal calibration coils are rigidly positioned and mounted in the system relative to the transmitter and receiver coils. In addition, when the internal calibration coils are calibrated at the factory, a rigid jig is employed to ensure accurate response from the external coils.

Using real time Fast Fourier Transforms and the calibration procedures outlined above, the data are processed in real time, from measured total field at a high sampling rate, to in-phase and quadrature values at 10 samples per second.

Airborne Magnetometer

Model: Fugro D1344 processor with Scintrex CS2 sensor

Type: Optically pumped cesium vapour

Sensitivity: 0.01 nT

Sample rate: 10 per second

The magnetometer sensor is housed in the EM bird, 28 m below the helicopter.

Magnetic Base Station

Primary

Model: GEM Systems GSM-19T

Type: Digital recording proton precession

Sensitivity: 0.10 nT

Sample rate: 3 second intervals

Backup

Model: Fugro CF1 base station with timing provided by integrated GPS

Sensor type: Geometrics G822 or Scintrex CS-2

Counter specifications: Accuracy: ± 0.1 nT
Resolution: 0.01 nT
Sample rate: 1 Hz

GPS specifications: Model: Marconi Allstar
Type: Code and carrier tracking of L1 band,
12-channel, C/A code at 1575.42 MHz
Sensitivity: -90 dBm, 1.0 second update

Accuracy: Manufacturer's stated accuracy for differential corrected GPS is 2 metres

Environmental

Monitor specifications:

Temperature:

- Accuracy: $\pm 1.5^{\circ}\text{C}$ max
- Resolution: 0.0305°C
- Sample rate: 1 Hz
- Range: -40°C to $+75^{\circ}\text{C}$

Barometric pressure:

- Model: Motorola MPXA4115A
- Accuracy: $\pm 3.0^{\circ}$ kPa max (-20°C to 105°C temp. ranges)
- Resolution: 0.013 kPa
- Sample rate: 1 Hz
- Range: 55 kPa to 108 kPa

A digital recorder is operated in conjunction with the base station magnetometer to record the diurnal variations of the earth's magnetic field. The clock of the base station is synchronized with that of the airborne system, using GPS time, to permit subsequent removal of diurnal drift. The locations of the magnetic base stations are given below in table 3-1.

Table 3-1 Magnetic Base Station Locations

Status	Make	Sensor Type	Location Name	WGS84 Latitude (deg-min-sec)	WGS84 Longitude (deg-min-sec)	WGS84 Elevation (m)
Primary	GEM (Proton)	GEM GSM-19T	Wetaskiwin Airport	52°58'3.67603"N	113°24'46.54418"W	748.32
Secondary	CF1 (Cesium)	Scintrex CS2	Wetaskiwin Airport	52°58'3.67603"N	113°24'46.54418"W	748.32

Navigation (Global Positioning System)

Airborne Receiver for Flight Path Recovery

Model:	Novatel OEM4
Type:	Code and carrier tracking of L1-C/A code at 1575.42 MHz and L2-P code at 1227.0 MHz. Dual frequency, 24-channel
Sample rate:	10 Hz update
Accuracy:	Better than 1 metre in differential mode
Antenna:	Mounted at centre of EM bird

Airborne Receiver for Guidance

Model:	Novatel OEM4
Type:	Code and carrier tracking of L1-C/A code at 1575.42 MHz and L2-P code at 1227.0 MHz. Dual frequency, 24-channel
Sample rate:	10 Hz update
Accuracy:	Better than 1 metre in differential mode
Antenna:	Mounted on the tail of the helicopter

Primary Base Station for Post-Survey Differential Correction

Model:	Novatel OEM4
Type:	Code and carrier tracking of L1-C/A code at 1575.42 MHz and L2-P code at 1227.0 MHz. Dual frequency, 24-channel
Sample rate:	10 Hz update
Accuracy:	Better than 1 metre in differential mode

Secondary GPS Base Station

Model:	Marconi Allstar OEM, CMT-1200
Type:	Code and carrier tracking of L1 band, 12-channel, C/A code at 1575.42 MHz
Sensitivity:	-90 dBm, 1.0 second update
Accuracy:	Manufacturer's stated accuracy for differential corrected GPS is 2 metres.

The Novatel OEM4 is a line of sight, satellite navigation system that utilizes time-coded signals from at least four of forty-eight available satellites. Both Russian GLONASS and American NAVSTAR satellite constellations are used to calculate the position and to provide real time guidance to the helicopter. For flight path processing a Novatel OEM4 was used as the mobile receiver. A similar system was used as the primary base station receiver. The mobile and base station raw XYZ data were recorded, thereby permitting post-survey differential corrections for theoretical accuracies of better than 2 metres. A Marconi Allstar GPS unit, part of the CF-1, was used as a secondary (back-up) base station.

Each base station receiver is able to calculate its own latitude and longitude. The GPS records data relative to the WGS84 ellipsoid, which is the basis of the revised North American Datum (NAD83). Conversion software is used to transform the WGS84 coordinates to the UTM system displayed on the maps. The locations of the base stations are given below in table 3-2.

Table 3-1 GPS Base Station Locations

Status	Make	Location Name	WGS84 Latitude	WGS84 Longitude	WGS84 Elevation (m)
Primary	Novatel OEM4	Wetaskiwin Airport	52°58'3.69254"N	113°24'45.84793"W	749.15
Secondary	CF1 Marconi	Wetaskiwin Airport	52°58'3.67603"N	113°24'46.54418"W	748.32

Radar Altimeter

Manufacturer: Honeywell/Sperry

Model: AT220 or RT300

Type: Short pulse modulation, 4.3 GHz

Sensitivity: 0.3 m

Sample rate: 2 per second

The radar altimeter measures the vertical distance between the helicopter and the ground.

This information is used in the processing algorithm that determines conductor depth.

Barometric Pressure and Temperature Sensors

Model: DIGHEM D 1300

Type: Motorola MPX4115AP analog pressure sensor
AD592AN high-impedance remote temperature sensors

Sensitivity: Pressure: 150 mV/kPa
Temperature: 100 mV/°C or 10 mV/°C (selectable)

Sample rate: 10 per second

The D1300 circuit is used in conjunction with one barometric sensor and up to three temperature sensors. Two sensors (baro and temp) are installed in the EM console in the aircraft, to monitor pressure (1KPA) and internal operating temperatures (2TDC).

Laser Altimeter

Manufacturer: Optech

Model ADMGPA100

Type: Fixed pulse repetition rate of 2 kHz

Sensitivity: ±5 cm from 10°C to 30°C
±10 cm from -20°C to +50°C

Sample rate: 2 per second

The laser altimeter is housed in the EM bird, and measures the distance from the EM bird to ground, except in areas of dense tree cover.

Digital Data Acquisition System

Manufacturer: Fugro
Model: HeliDAS
Recorder: Compact Flash Card

The stored data are downloaded to the field workstation PC at the survey base, for verification, backup and preparation of in-field products.

Video Flight Path Recording System

Type: Panasonic WVCD/32 Colour Video Camera
Recorder: Axis 241S video server and tablet computer

Fiducial numbers are recorded continuously and are displayed on the margin of each image. This procedure ensures accurate correlation of data with respect to visible features on the ground.

4. QUALITY CONTROL AND IN-FIELD PROCESSING

Digital data for each flight were transferred to the field workstation, in order to verify data quality and completeness. A database was created and updated using Geosoft Oasis Montaj and proprietary Fugro Atlas software. This allowed the field personnel to calculate, display and verify both the positional (flight path) and geophysical data on a screen or printer. Records were examined as a preliminary assessment of the data acquired for each flight.

In-field processing of Fugro survey data consists of differential corrections to the airborne GPS data, verification of EM calibrations, drift correction of the raw airborne EM data, spike rejection and filtering of all geophysical and ancillary data, verification of flight videos, calculation of preliminary resistivity data, diurnal correction, and preliminary levelling of magnetic data.

All data, including base station records, were checked on a daily basis, to ensure compliance with the survey contract specifications. Reflights were required if any of the following specifications were not met.

Navigation - Positional (x,y) accuracy of better than 10 m, with a CEP (circular error of probability) of 95%.

- Flight Path - No lines to exceed $\pm 25\%$ departure from nominal line spacing over a continuous distance of more than 1 km, except for reasons of safety.

- Clearance - Mean terrain sensor clearance of 30 m, ± 10 m, except where precluded by safety considerations, e.g., restricted or populated areas, severe topography, obstructions, tree canopy, aerodynamic limitations, etc.

- Airborne Mag - The non-normalized 4th difference will not exceed 1.6 nT over a continuous distance of 1 kilometre excluding areas where this specification is exceeded due to natural anomalies.

- Base Mag - Diurnal variations not to exceed 10 nT over a straight line time chord of 1 minute.

- EM - Spheric pulses may occur having strong peaks but narrow widths. The EM data area considered acceptable when their occurrence is less than 10 spheric events exceeding the stated noise specification for a given frequency per 100 samples continuously over a distance of 2,000 metres.

Frequency	Coil Orientation	Peak to Peak Noise Envelope (ppm)
400 Hz	horizontal coplanar	10.0
1800 Hz	horizontal coplanar	10.0
3300 Hz	vertical coaxial	10.0
8200 Hz	horizontal coplanar	20.0
40 000 Hz	horizontal coplanar	40.0
140 000 Hz	horizontal coplanar	50.0

5. DATA PROCESSING

Flight Path Recovery

The raw range data from at least four satellites are simultaneously recorded by both the base and mobile GPS units. The geographic positions of both units, relative to the model ellipsoid, are calculated from this information. Differential corrections, which are obtained from the base station, are applied to the mobile unit data to provide a post-flight track of the aircraft, accurate to within 2 m. Speed checks of the flight path are also carried out to determine if there are any spikes or gaps in the data.

The corrected WGS84 latitude/longitude coordinates are transformed to the coordinate system used on the final maps. Images or plots are then created to provide a visual check of the flight path.

Electromagnetic Data

EM data are processed at the recorded sample rate of 10 samples/second. Spheric rejection median and Hanning filters are then applied to reduce noise to acceptable levels.

Apparent Resistivity

The apparent resistivities in ohm-m are generated from the in-phase and quadrature EM components for all of the coplanar frequencies, using a pseudo-layer half-space model. The inputs to the resistivity algorithm are the in-phase and quadrature amplitudes of the secondary field. The algorithm calculates the apparent resistivity in ohm-m, and the apparent height of the bird above the conductive source. Any difference between the apparent height and the true height, as measured by the radar altimeter, is called the pseudo-layer and reflects the difference between the real geology and a homogeneous halfspace. This difference is often attributed to the presence of a highly resistive upper layer. Any errors in the altimeter reading, caused by heavy tree cover, are included in the pseudo-layer and do not affect the resistivity calculation. The apparent depth estimates, however, will reflect the altimeter errors. Apparent resistivities calculated in this manner may differ from those calculated using other models.

In areas where the effects of magnetic permeability or dielectric permittivity have suppressed the in-phase responses, the calculated resistivities will be erroneously high. Various algorithms and inversion techniques can be used to partially correct for the effects of permeability and permittivity.

Apparent resistivity maps portray all of the information for a given frequency over the entire survey area. This full coverage contrasts with the electromagnetic anomaly map, which provides information only over interpreted conductors. The large dynamic range afforded by

the multiple frequencies makes the apparent resistivity parameter an excellent mapping tool.

The preliminary apparent resistivity maps and images are carefully inspected to identify any lines or line segments that might require base level adjustments. Subtle changes between in-flight calibrations of the system can result in line-to-line differences that are more recognizable in resistive (low signal amplitude) areas. If required, manual level adjustments are carried out to eliminate or minimize resistivity differences that can be attributed, in part, to changes in operating temperatures. These levelling adjustments are usually very subtle, and do not result in the degradation of discrete anomalies.

After the manual levelling process is complete, revised resistivity grids are created. The resulting grids can be subjected to a microlevelling technique in order to smooth the data for contouring. The coplanar resistivity parameter has a broad 'footprint' that requires very little filtering.

Resistivity-depth Sections

The apparent resistivities for all frequencies can be displayed simultaneously as coloured resistivity-depth sections. Usually, only the coplanar data are displayed as the close frequency separation between the coplanar and adjacent coaxial data tends to distort the section. The sections can be plotted using the topographic elevation profile as the surface. The digital terrain values, in metres a.m.s.l., can be calculated from the GPS Z-value or barometric altimeter, minus the aircraft radar altimeter.

Resistivity-depth sections can be generated in three formats:

- (1) Sengpiel resistivity sections, where the apparent resistivity for each frequency is plotted at the depth of the centroid of the in-phase current flow¹; and,
- (2) Differential resistivity sections, where the differential resistivity is plotted at the differential depth².
- (3) Occam³ or Multi-layer⁴ inversion.

Both the Sengpiel and differential methods are derived from the pseudo-layer half-space model. Both yield a coloured resistivity-depth section that attempts to portray a smoothed approximation of the true resistivity distribution with depth. Resistivity-depth sections are most useful in conductive layered situations, but may be unreliable in areas of moderate to high resistivity where signal amplitudes are weak. In areas where in-phase responses have been suppressed by the effects of magnetite, or adversely affected by cultural features, the computed resistivities shown on the sections may be unreliable.

¹ Sengpiel, K.P., 1988, Approximate Inversion of Airborne EM Data from Multilayered Ground: Geophysical Prospecting 36, 446-459.

² Huang, H. and Fraser, D.C., 1993, Differential Resistivity Method for Multi-frequency Airborne EM Sounding: presented at Intern. Airb. EM Workshop, Tucson, Ariz.

³ Constable et al, 1987, Occam's inversion: a practical algorithm for generating smooth models from electromagnetic sounding data: Geophysics, 52, 289-300.

⁴ Huang H., and Palacky, G.J., 1991, Damped least-squares inversion of time domain airborne EM data based on singular value decomposition: Geophysical Prospecting, 39, 827-844.

Both the Occam and multi-layer inversions compute the layered earth resistivity model that would best match the measured EM data. The Occam inversion uses a series of thin, fixed layers (usually 20 x 5m and 10 x 10m layers) and computes resistivities to fit the EM data. The multi-layer inversion computes the resistivity and thickness for each of a defined number of layers (typically 3-5 layers) to best fit the data.

Total Magnetic Field

A fourth difference editing routine was applied to the magnetic data to remove any spikes.

The aeromagnetic data were corrected for diurnal variation using the magnetic base station data. The results were then levelled using tie and traverse line intercepts. Manual adjustments were applied to any lines that required levelling, as indicated by shadowed images of the gridded magnetic data. The manually levelled data were then subjected to a microlevelling filter.

Calculated Vertical Magnetic Gradient

The diurnally-corrected total magnetic field data were subjected to a processing algorithm that enhances the response of magnetic bodies in the upper 500 m and attenuates the response of deeper bodies. The resulting vertical gradient map provides better definition and resolution of near-surface magnetic units. It also identifies weak magnetic features that may not be evident on the total field map. However, regional magnetic variations and changes in lithology may be better defined on the total magnetic field map.

Contour, Colour and Shadow Map Displays

The geophysical data are interpolated onto a regular grid using a modified Akima spline technique. The resulting grid is suitable for image processing and generation of contour maps. The grid cell size is 20% of the line interval.

Colour maps are produced by interpolating the grid down to the pixel size. The parameter is then incremented with respect to specific amplitude ranges to provide colour "contour" maps.

Monochromatic shadow maps or images are generated by employing an artificial sun to cast shadows on a surface defined by the geophysical grid. There are many variations in the shadowing technique. These techniques can be applied to total field or enhanced magnetic data, magnetic derivatives, resistivity, etc. The shadowing technique is also used as a quality control method to detect subtle changes between lines.

6. PRODUCTS

This section lists the final maps and products that have been provided under the terms of the survey agreement. Other products can be prepared from the existing dataset, if requested. These include magnetic enhancements or derivatives, percent magnetite, resistivities corrected for magnetic permeability and/or dielectric permittivity, digital terrain, resistivity-depth sections, inversions, and overburden thickness. Most parameters can be displayed as contours, profiles, or in colour.

Base Maps

Base maps of the survey area were produced by scanning published topographic maps to a bitmap (.bmp) format. This process provides a relatively accurate, distortion-free base that facilitates correlation of the navigation data to the map coordinate system. The topographic files were combined with geophysical data for plotting the final maps. All maps were created using the following parameters:

Projection Description:

Datum:	NAD83
Ellipsoid:	GRS80
Projection:	Alberta 10 TM (Forest)
Central Meridian:	-115°
False Northing:	0
False Easting:	500000
Scale Factor:	0.9992

The following parameters are presented on two map sheets, at a scale of 1:50 000. All maps include flight lines and topography.

Table 6-1 Final Products

Final Product	Number of sets of colour maps
Total Magnetic Field	1
Calculated Vertical Magnetic Gradient	1
Resistivity (5 metre depth)	1
Resistivity (10 metre depth)	1
Resistivity (20 metre depth)	1
Resistivity (30 metre depth)	1
Resistivity (50 metre depth)	1

Additional Products

Digital Archive (see Archive Description)	1 DVD
Survey Report	2 copies
Digital Flight Path Video	2 DVDs
Resistivity Depth Sections	all lines

APPENDIX A

LIST OF PERSONNEL

The following personnel were involved in the acquisition, processing, and presentation of data, relating to a RESOLVE airborne geophysical survey carried out for Alberta Energy Resources Conservation Board, Red Deer, Alberta.

David Miles	Manager, Helicopter Operations
Emily Farquhar	Manager, Data Processing and Interpretation
Nicholas Gavican	Geophysical Operator
Tai-chyi Shei	Field Geophysicist
Tianyou Chen	Field Geophysicist
Glenn Charbonneau	Pilot (Great Slave Helicopters Ltd.)
Russell Imrie	Geophysical Data Processor
Ruth Pritchard	Geophysicist
Lyn Vanderstarren	Drafting Supervisor
Susan Pothiah	Word Processing Operator
Albina Tonello	Secretary/Expeditor

The survey consisted of 4279.4 km of coverage, flown from November 22nd to December 6th, 2007.

All personnel are employees of Fugro Airborne Surveys, except where indicated.

APPENDIX B

BACKGROUND INFORMATION

BACKGROUND INFORMATION

Electromagnetics

Fugro electromagnetic responses fall into two general classes, discrete and broad. The discrete class consists of sharp, well-defined anomalies from discrete conductors such as sulphide lenses and steeply dipping sheets of graphite and sulphides. The broad class consists of wide anomalies from conductors having a large horizontal surface such as flatly dipping graphite or sulphide sheets, saline water-saturated sedimentary formations, conductive overburden and rock, kimberlite pipes and geothermal zones. A vertical conductive slab with a width of 200 m would straddle these two classes.

The vertical sheet (half plane) is the most common model used for the analysis of discrete conductors. All anomalies plotted on the geophysical maps are analyzed according to this model. The following section entitled **Discrete Conductor Analysis** describes this model in detail, including the effect of using it on anomalies caused by broad conductors such as conductive overburden.

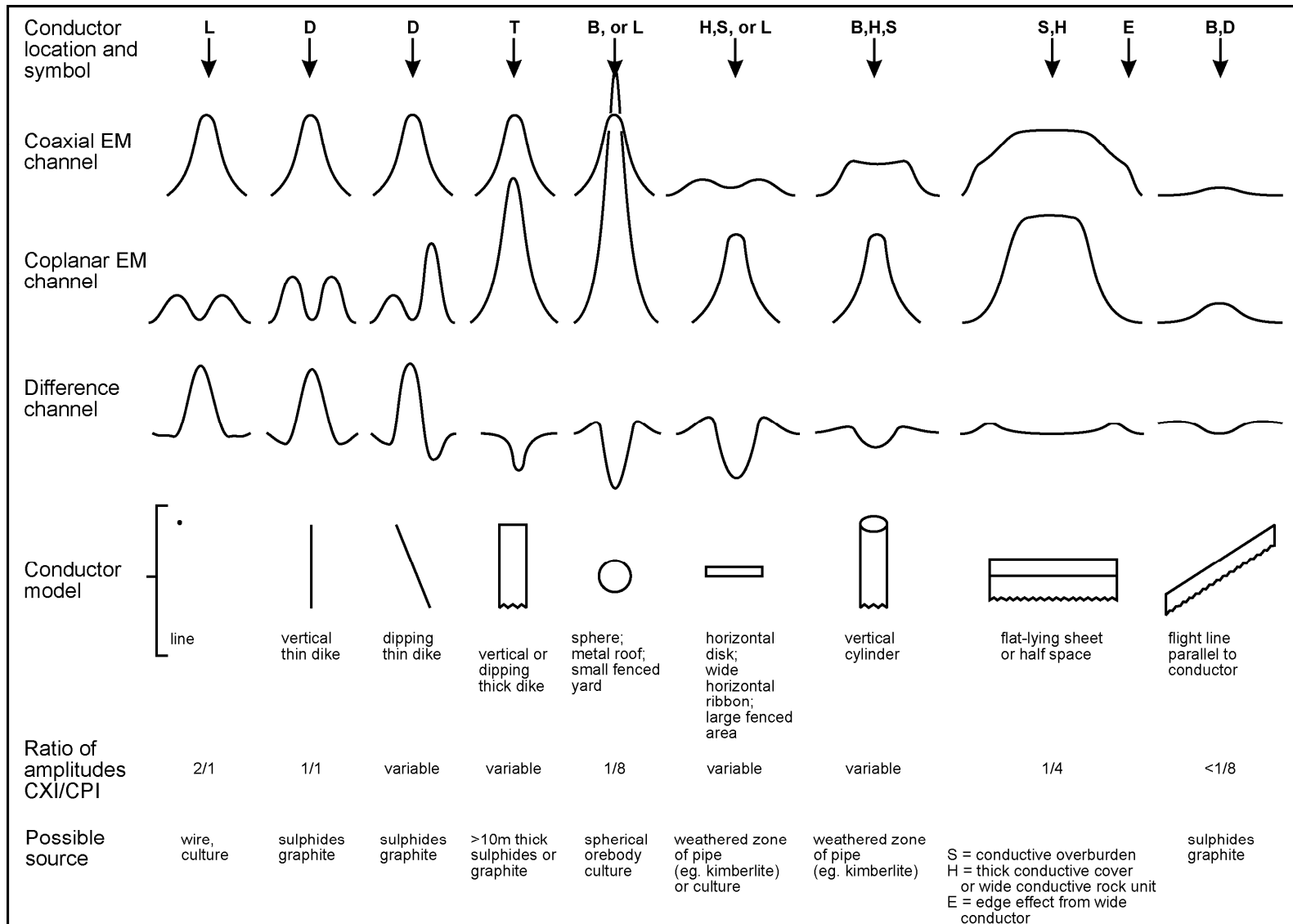
The conductive earth (half-space) model is suitable for broad conductors. Resistivity contour maps result from the use of this model. A later section entitled **Resistivity Mapping** describes the method further, including the effect of using it on anomalies caused by discrete conductors such as sulphide bodies.

Geometric Interpretation

The geophysical interpreter attempts to determine the geometric shape and dip of the conductor. Figure B-1 shows typical HEM anomaly shapes which are used to guide the geometric interpretation.

Discrete Conductor Analysis

The EM anomalies appearing on the electromagnetic map are analyzed by computer to give the conductance (i.e., conductivity-thickness product) in siemens (mhos) of a vertical sheet model. This is done regardless of the interpreted geometric shape of the conductor. This is not an unreasonable procedure, because the computed conductance increases as the electrical quality of the conductor increases, regardless of its true shape. DIGHEM anomalies are divided into seven grades of conductance, as shown in Table B-1. The conductance in siemens (mhos) is the reciprocal of resistance in ohms.



Typical HEM anomaly shapes
Figure B-1

- Appendix B.3 -

The conductance value is a geological parameter because it is a characteristic of the conductor alone. It generally is independent of frequency, flying height or depth of burial, apart from the averaging over a greater portion of the conductor as height increases. Small anomalies from deeply buried strong conductors are not confused with small anomalies from shallow weak conductors because the former will have larger conductance values.

Table B-1. EM Anomaly Grades

Anomaly Grade	Siemens
7	> 100
6	50 - 100
5	20 - 50
4	10 - 20
3	5 - 10
2	1 - 5
1	< 1

Conductive overburden generally produces broad EM responses which may not be shown as anomalies on the geophysical maps. However, patchy conductive overburden in otherwise resistive areas can yield discrete anomalies with a conductance grade (cf. Table B-1) of 1, 2 or even 3 for conducting clays which have resistivities as low as 50 ohm-m. In areas where ground resistivities are below 10 ohm-m, anomalies caused by weathering variations and similar causes can have any conductance grade. The anomaly shapes from the multiple coils often allow such conductors to be recognized, and these are indicated by the letters S, H, and sometimes E on the geophysical maps (see EM legend on maps).

For bedrock conductors, the higher anomaly grades indicate increasingly higher conductances. Examples: the New Inco copper discovery (Noranda, Canada) yielded a grade 5 anomaly, as did the neighbouring copper-zinc Magusi River ore body; Matabi (copper-zinc, Sturgeon Lake, Canada) and Whistle (nickel, Sudbury, Canada) gave grade 6; and the Montcalm nickel-copper discovery (Timmins, Canada) yielded a grade 7 anomaly. Graphite and sulphides can span all grades but, in any particular survey area, field work may show that the different grades indicate different types of conductors.

Strong conductors (i.e., grades 6 and 7) are characteristic of massive sulphides or graphite. Moderate conductors (grades 4 and 5) typically reflect graphite or sulphides of a less massive character, while weak bedrock conductors (grades 1 to 3) can signify poorly connected graphite or heavily disseminated sulphides. Grades 1 and 2 conductors may not respond to ground EM equipment using frequencies less than 2000 Hz.

The presence of sphalerite or gangue can result in ore deposits having weak to moderate conductances. As an example, the three million ton lead-zinc deposit of Restigouche Mining Corporation near Bathurst, Canada, yielded a well-defined grade 2 conductor. The 10 percent by volume of sphalerite occurs as a coating around the fine grained massive pyrite, thereby inhibiting electrical conduction. Faults, fractures and shear zones may produce anomalies that typically have low conductances (e.g., grades 1 to 3). Conductive rock formations can yield anomalies of any conductance grade. The conductive materials in

- Appendix B.4 -

such rock formations can be salt water, weathered products such as clays, original depositional clays, and carbonaceous material.

For each interpreted electromagnetic anomaly on the geophysical maps, a letter identifier and an interpretive symbol are plotted beside the EM grade symbol. The horizontal rows of dots, under the interpretive symbol, indicate the anomaly amplitude on the flight record. The vertical column of dots, under the anomaly letter, gives the estimated depth. In areas where anomalies are crowded, the letter identifiers, interpretive symbols and dots may be obliterated. The EM grade symbols, however, will always be discernible, and the obliterated information can be obtained from the anomaly listing appended to this report.

The purpose of indicating the anomaly amplitude by dots is to provide an estimate of the reliability of the conductance calculation. Thus, a conductance value obtained from a large ppm anomaly (3 or 4 dots) will tend to be accurate whereas one obtained from a small ppm anomaly (no dots) could be quite inaccurate. The absence of amplitude dots indicates that the anomaly from the coaxial coil-pair is 5 ppm or less on both the in-phase and quadrature channels. Such small anomalies could reflect a weak conductor at the surface or a stronger conductor at depth. The conductance grade and depth estimate illustrates which of these possibilities fits the recorded data best.

The conductance measurement is considered more reliable than the depth estimate. There are a number of factors that can produce an error in the depth estimate, including the averaging of topographic variations by the altimeter, overlying conductive overburden, and the location and attitude of the conductor relative to the flight line. Conductor location and attitude can provide an erroneous depth estimate because the stronger part of the conductor may be deeper or to one side of the flight line, or because it has a shallow dip. A heavy tree cover can also produce errors in depth estimates. This is because the depth estimate is computed as the distance of bird from conductor, minus the altimeter reading. The altimeter can lock onto the top of a dense forest canopy. This situation yields an erroneously large depth estimate but does not affect the conductance estimate.

Dip symbols are used to indicate the direction of dip of conductors. These symbols are used only when the anomaly shapes are unambiguous, which usually requires a fairly resistive environment.

A further interpretation is presented on the EM map by means of the line-to-line correlation of bedrock anomalies, which is based on a comparison of anomaly shapes on adjacent lines. This provides conductor axes that may define the geological structure over portions of the survey area. The absence of conductor axes in an area implies that anomalies could not be correlated from line to line with reasonable confidence.

The electromagnetic anomalies are designed to provide a correct impression of conductor quality by means of the conductance grade symbols. The symbols can stand alone with geology when planning a follow-up program. The actual conductance values are printed in the attached anomaly list for those who wish quantitative data. The anomaly ppm and depth are indicated by inconspicuous dots which should not distract from the conductor patterns, while being helpful to those who wish this information. The map provides an

- Appendix B.5 -

interpretation of conductors in terms of length, strike and dip, geometric shape, conductance, depth, and thickness. The accuracy is comparable to an interpretation from a high quality ground EM survey having the same line spacing.

The appended EM anomaly list provides a tabulation of anomalies in ppm, conductance, and depth for the vertical sheet model. No conductance or depth estimates are shown for weak anomalous responses that are not of sufficient amplitude to yield reliable calculations.

Since discrete bodies normally are the targets of EM surveys, local base (or zero) levels are used to compute local anomaly amplitudes. This contrasts with the use of true zero levels which are used to compute true EM amplitudes. Local anomaly amplitudes are shown in the EM anomaly list and these are used to compute the vertical sheet parameters of conductance and depth.

Questionable Anomalies

The EM maps may contain anomalous responses that are displayed as asterisks (*). These responses denote weak anomalies of indeterminate conductance, which may reflect one of the following: a weak conductor near the surface, a strong conductor at depth (e.g., 100 to 120 m below surface) or to one side of the flight line, or aerodynamic noise. Those responses that have the appearance of valid bedrock anomalies on the flight profiles are indicated by appropriate interpretive symbols (see EM legend on maps). The others probably do not warrant further investigation unless their locations are of considerable geological interest.

The Thickness Parameter

A comparison of coaxial and coplanar shapes can provide an indication of the thickness of a steeply dipping conductor. The amplitude of the coplanar anomaly (e.g., CPI channel) increases relative to the coaxial anomaly (e.g., CXI) as the apparent thickness increases, i.e., the thickness in the horizontal plane. (The thickness is equal to the conductor width if the conductor dips at 90 degrees and strikes at right angles to the flight line.) This report refers to a conductor as thin when the thickness is likely to be less than 3 m, and thick when in excess of 10 m. Thick conductors are indicated on the EM map by parentheses "()". For base metal exploration in steeply dipping geology, thick conductors can be high priority targets because many massive sulphide ore bodies are thick. The system cannot sense the thickness when the strike of the conductor is subparallel to the flight line, when the conductor has a shallow dip, when the anomaly amplitudes are small, or when the resistivity of the environment is below 100 ohm-m.

Resistivity Mapping

Resistivity mapping is useful in areas where broad or flat lying conductive units are of interest. One example of this is the clay alteration which is associated with Carlin-type

- Appendix B.6 -

deposits in the south west United States. The resistivity parameter was able to identify the clay alteration zone over the Cove deposit. The alteration zone appeared as a strong resistivity low on the 900 Hz resistivity parameter. The 7,200 Hz and 56,000 Hz resistivities showed more detail in the covering sediments, and delineated a range front fault. This is typical in many areas of the south west United States, where conductive near surface sediments, which may sometimes be alkalic, attenuate the higher frequencies.

Resistivity mapping has proven successful for locating diatremes in diamond exploration. Weathering products from relatively soft kimberlite pipes produce a resistivity contrast with the unaltered host rock. In many cases weathered kimberlite pipes were associated with thick conductive layers that contrasted with overlying or adjacent relatively thin layers of lake bottom sediments or overburden.

Areas of widespread conductivity are commonly encountered during surveys. These conductive zones may reflect alteration zones, shallow-dipping sulphide or graphite-rich units, saline ground water, or conductive overburden. In such areas, EM amplitude changes can be generated by decreases of only 5 m in survey altitude, as well as by increases in conductivity. The typical flight record in conductive areas is characterized by in-phase and quadrature channels that are continuously active. Local EM peaks reflect either increases in conductivity of the earth or decreases in survey altitude. For such conductive areas, apparent resistivity profiles and contour maps are necessary for the correct interpretation of the airborne data. The advantage of the resistivity parameter is that anomalies caused by altitude changes are virtually eliminated, so the resistivity data reflect only those anomalies caused by conductivity changes. The resistivity analysis also helps the interpreter to differentiate between conductive bedrock and conductive overburden. For example, discrete conductors will generally appear as narrow lows on the contour map and broad conductors (e.g., overburden) will appear as wide lows.

The apparent resistivity is calculated using the pseudo-layer (or buried) half-space model defined by Fraser (1978)⁵. This model consists of a resistive layer overlying a conductive half-space. The depth channels give the apparent depth below surface of the conductive material. The apparent depth is simply the apparent thickness of the overlying resistive layer. The apparent depth (or thickness) parameter will be positive when the upper layer is more resistive than the underlying material, in which case the apparent depth may be quite close to the true depth.

The apparent depth will be negative when the upper layer is more conductive than the underlying material, and will be zero when a homogeneous half-space exists. The apparent depth parameter must be interpreted cautiously because it will contain any errors that might exist in the measured altitude of the EM bird (e.g., as caused by a dense tree cover). The inputs to the resistivity algorithm are the in-phase and quadrature components of the coplanar coil-pair. The outputs are the apparent resistivity of the conductive half-space (the source) and the sensor-source distance. The flying height is not an input variable, and the output resistivity and sensor-source distance are independent of the flying height when the

⁵ Resistivity mapping with an airborne multicoil electromagnetic system: Geophysics, v. 43, p.144-172

- Appendix B.7 -

conductivity of the measured material is sufficient to yield significant in-phase as well as quadrature responses. The apparent depth, discussed above, is simply the sensor-source distance minus the measured altitude or flying height. Consequently, errors in the measured altitude will affect the apparent depth parameter but not the apparent resistivity parameter.

The apparent depth parameter is a useful indicator of simple layering in areas lacking a heavy tree cover. Depth information has been used for permafrost mapping, where positive apparent depths were used as a measure of permafrost thickness. However, little quantitative use has been made of negative apparent depths because the absolute value of the negative depth is not a measure of the thickness of the conductive upper layer and, therefore, is not meaningful physically. Qualitatively, a negative apparent depth estimate usually shows that the EM anomaly is caused by conductive overburden. Consequently, the apparent depth channel can be of significant help in distinguishing between overburden and bedrock conductors.

Interpretation in Conductive Environments

Environments having low background resistivities (e.g., below 30 ohm-m for a 900 Hz system) yield very large responses from the conductive ground. This usually prohibits the recognition of discrete bedrock conductors. However, Fugro data processing techniques produce three parameters that contribute significantly to the recognition of bedrock conductors in conductive environments. These are the in-phase and quadrature difference channels (DIFI and DIFQ, which are available only on systems with “common” frequencies on orthogonal coil pairs), and the resistivity and depth channels (RES and DEP) for each coplanar frequency.

The EM difference channels (DIFI and DIFQ) eliminate most of the responses from conductive ground, leaving responses from bedrock conductors, cultural features (e.g., telephone lines, fences, etc.) and edge effects. Edge effects often occur near the perimeter of broad conductive zones. This can be a source of geologic noise. While edge effects yield anomalies on the EM difference channels, they do not produce resistivity anomalies. Consequently, the resistivity channel aids in eliminating anomalies due to edge effects. On the other hand, resistivity anomalies will coincide with the most highly conductive sections of conductive ground, and this is another source of geologic noise. The recognition of a bedrock conductor in a conductive environment therefore is based on the anomalous responses of the two difference channels (DIFI and DIFQ) and the resistivity channels (RES). The most favourable situation is where anomalies coincide on all channels.

The DEP channels, which give the apparent depth to the conductive material, also help to determine whether a conductive response arises from surficial material or from a conductive zone in the bedrock. When these channels ride above the zero level on the depth profiles (i.e., depth is negative), it implies that the EM and resistivity profiles are responding primarily to a conductive upper layer, i.e., conductive overburden. If the DEP channels are below the zero level, it indicates that a resistive upper layer exists, and this usually implies the existence of a bedrock conductor. If the low frequency DEP channel is below the zero level

and the high frequency DEP is above, this suggests that a bedrock conductor occurs beneath conductive cover.

Reduction of Geologic Noise

Geologic noise refers to unwanted geophysical responses. For purposes of airborne EM surveying, geologic noise refers to EM responses caused by conductive overburden and magnetic permeability. It was mentioned previously that the EM difference channels (i.e., channel DIFI for in-phase and DIFQ for quadrature) tend to eliminate the response of conductive overburden.

Magnetite produces a form of geological noise on the in-phase channels. Rocks containing less than 1% magnetite can yield negative in-phase anomalies caused by magnetic permeability. When magnetite is widely distributed throughout a survey area, the in-phase EM channels may continuously rise and fall, reflecting variations in the magnetite percentage, flying height, and overburden thickness. This can lead to difficulties in recognizing deeply buried bedrock conductors, particularly if conductive overburden also exists. However, the response of broadly distributed magnetite generally vanishes on the in-phase difference channel DIFI. This feature can be a significant aid in the recognition of conductors that occur in rocks containing accessory magnetite.

EM Magnetite Mapping

The information content of HEM data consists of a combination of conductive eddy current responses and magnetic permeability responses. The secondary field resulting from conductive eddy current flow is frequency-dependent and consists of both in-phase and quadrature components, which are positive in sign. On the other hand, the secondary field resulting from magnetic permeability is independent of frequency and consists of only an in-phase component which is negative in sign. When magnetic permeability manifests itself by decreasing the measured amount of positive in-phase, its presence may be difficult to recognize. However, when it manifests itself by yielding a negative in-phase anomaly (e.g., in the absence of eddy current flow), its presence is assured. In this latter case, the negative component can be used to estimate the percent magnetite content.

A magnetite mapping technique, based on the low frequency coplanar data, can be complementary to magnetometer mapping in certain cases. Compared to magnetometry, it is far less sensitive but is more able to resolve closely spaced magnetite zones, as well as providing an estimate of the amount of magnetite in the rock. The method is sensitive to 1/4% magnetite by weight when the EM sensor is at a height of 30 m above a magnetitic half-space. It can individually resolve steep dipping narrow magnetite-rich bands which are separated by 60 m. Unlike magnetometry, the EM magnetite method is unaffected by remanent magnetism or magnetic latitude.

The EM magnetite mapping technique provides estimates of magnetite content which are usually correct within a factor of 2 when the magnetite is fairly uniformly distributed. EM

magnetite maps can be generated when magnetic permeability is evident as negative in-phase responses on the data profiles.

Like magnetometry, the EM magnetite method maps only bedrock features, provided that the overburden is characterized by a general lack of magnetite. This contrasts with resistivity mapping which portrays the combined effect of bedrock and overburden.

The Susceptibility Effect

When the host rock is conductive, the positive conductivity response will usually dominate the secondary field, and the susceptibility effect⁶ will appear as a reduction in the in-phase, rather than as a negative value. The in-phase response will be lower than would be predicted by a model using zero susceptibility. At higher frequencies the in-phase conductivity response also gets larger, so a negative magnetite effect observed on the low frequency might not be observable on the higher frequencies, over the same body. The susceptibility effect is most obvious over discrete magnetite-rich zones, but also occurs over uniform geology such as a homogeneous half-space.

High magnetic susceptibility will affect the calculated apparent resistivity, if only conductivity is considered. Standard apparent resistivity algorithms use a homogeneous half-space model, with zero susceptibility. For these algorithms, the reduced in-phase response will, in most cases, make the apparent resistivity higher than it should be. It is important to note that there is nothing wrong with the data, nor is there anything wrong with the processing algorithms. The apparent difference results from the fact that the simple geological model used in processing does not match the complex geology.

Measuring and Correcting the Magnetite Effect

Theoretically, it is possible to calculate (forward model) the combined effect of electrical conductivity and magnetic susceptibility on an EM response in all environments. The difficulty lies, however, in separating out the susceptibility effect from other geological effects when deriving resistivity and susceptibility from EM data.

Over a homogeneous half-space, there is a precise relationship between in-phase, quadrature, and altitude. These are often resolved as phase angle, amplitude, and altitude. Within a reasonable range, any two of these three parameters can be used to calculate the half space resistivity. If the rock has a positive magnetic susceptibility, the in-phase component will be reduced and this departure can be recognized by comparison to the other parameters.

⁶ Magnetic susceptibility and permeability are two measures of the same physical property. Permeability is generally given as relative permeability, μ_r , which is the permeability of the substance divided by the permeability of free space ($4 \pi \times 10^{-7}$). Magnetic susceptibility k is related to permeability by $k = \mu_r - 1$. Susceptibility is a unitless measurement, and is usually reported in units of 10^{-6} . The typical range of susceptibilities is -1 for quartz, 130 for pyrite, and up to 5×10^5 for magnetite, in 10^{-6} units (Telford et al, 1986).

The algorithm used to calculate apparent susceptibility and apparent resistivity from HEM data, uses a homogeneous half-space geological model. Non half-space geology, such as horizontal layers or dipping sources, can also distort the perfect half-space relationship of the three data parameters. While it may be possible to use more complex models to calculate both rock parameters, this procedure becomes very complex and time-consuming. For basic HEM data processing, it is most practical to stick to the simplest geological model.

Magnetite reversals (reversed in-phase anomalies) have been used for many years to calculate an “FeO” or magnetite response from HEM data (Fraser, 1981). However, this technique could only be applied to data where the in-phase was observed to be negative, which happens when susceptibility is high and conductivity is low.

Applying Susceptibility Corrections

Resistivity calculations done with susceptibility correction may change the apparent resistivity. High-susceptibility conductors, that were previously masked by the susceptibility effect in standard resistivity algorithms, may become evident. In this case the susceptibility corrected apparent resistivity is a better measure of the actual resistivity of the earth. However, other geological variations, such as a deep resistive layer, can also reduce the in-phase by the same amount. In this case, susceptibility correction would not be the best method. Different geological models can apply in different areas of the same data set. The effects of susceptibility, and other effects that can create a similar response, must be considered when selecting the resistivity algorithm.

Susceptibility from EM vs Magnetic Field Data

The response of the EM system to magnetite may not match that from a magnetometer survey. First, HEM-derived susceptibility is a rock property measurement, like resistivity. Magnetic data show the total magnetic field, a measure of the potential field, not the rock property. Secondly, the shape of an anomaly depends on the shape and direction of the source magnetic field. The electromagnetic field of HEM is much different in shape from the earth's magnetic field. Total field magnetic anomalies are different at different magnetic latitudes; HEM susceptibility anomalies have the same shape regardless of their location on the earth.

In far northern latitudes, where the magnetic field is nearly vertical, the total magnetic field measurement over a thin vertical dike is very similar in shape to the anomaly from the HEM-derived susceptibility (a sharp peak over the body). The same vertical dike at the magnetic equator would yield a negative magnetic anomaly, but the HEM susceptibility anomaly would show a positive susceptibility peak.

Effects of Permeability and Dielectric Permittivity

Resistivity algorithms that assume free-space magnetic permeability and dielectric permittivity, do not yield reliable values in highly magnetic or highly resistive areas. Both magnetic polarization and displacement currents cause a decrease in the in-phase component, often resulting in negative values that yield erroneously high apparent resistivities. The effects of magnetite occur at all frequencies, but are most evident at the lowest frequency. Conversely, the negative effects of dielectric permittivity are most evident at the higher frequencies, in resistive areas.

The table below shows the effects of varying permittivity over a resistive (10,000 ohm-m) half space, at frequencies of 56,000 Hz (DIGHEM^V) and 102,000 Hz (RESOLVE).

Apparent Resistivity Calculations Effects of Permittivity on In-phase/Quadrature/Resistivity

Freq (Hz)	Coil	Sep (m)	Thres (ppm)	Alt (m)	In Phase	Quad Phase	App Res	App Depth (m)	Permittivity
56,000	CP	6.3	0.1	30	7.3	35.3	10118	-1.0	1 Air
56,000	CP	6.3	0.1	30	3.6	36.6	19838	-13.2	5 Quartz
56,000	CP	6.3	0.1	30	-1.1	38.3	81832	-25.7	10 Epidote
56,000	CP	6.3	0.1	30	-10.4	42.3	76620	-25.8	20 Granite
56,000	CP	6.3	0.1	30	-19.7	46.9	71550	-26.0	30 Diabase
56,000	CP	6.3	0.1	30	-28.7	52.0	66787	-26.1	40 Gabbro
102,000	CP	7.86	0.1	30	32.5	117.2	9409	-0.3	1 Air
102,000	CP	7.86	0.1	30	11.7	127.2	25956	-16.8	5 Quartz
102,000	CP	7.86	0.1	30	-14.0	141.6	97064	-26.5	10 Epidote
102,000	CP	7.86	0.1	30	-62.9	176.0	83995	-26.8	20 Granite
102,000	CP	7.86	0.1	30	-107.5	215.8	73320	-27.0	30 Diabase
102,000	CP	7.86	0.1	30	-147.1	259.2	64875	-27.2	40 Gabbro

Methods have been developed (Huang and Fraser, 2000, 2001) to correct apparent resistivities for the effects of permittivity and permeability. The corrected resistivities yield more credible values than if the effects of permittivity and permeability are disregarded.

Recognition of Culture

Cultural responses include all EM anomalies caused by man-made metallic objects. Such anomalies may be caused by inductive coupling or current gathering. The concern of the interpreter is to recognize when an EM response is due to culture. Points of consideration used by the interpreter, when coaxial and coplanar coil-pairs are operated at a common frequency, are as follows:

1. Channels CXPL and CPPL monitor 60 Hz radiation. An anomaly on these channels shows that the conductor is radiating power. Such an indication is normally a guarantee that the conductor is cultural. However, care must be taken to ensure that the conductor is not a geologic body that strikes across a power line, carrying leakage currents.
2. A flight that crosses a "line" (e.g., fence, telephone line, etc.) yields a centre-peaked coaxial anomaly and an m-shaped coplanar anomaly.⁷ When the flight crosses the cultural line at a high angle of intersection, the amplitude ratio of coaxial/coplanar response is 2. Such an EM anomaly can only be caused by a line. The geologic body that yields anomalies most closely resembling a line is the vertically dipping

⁷ See Figure B-1 presented earlier.

- Appendix B.13 -

thin dike. Such a body, however, yields an amplitude ratio of 1 rather than 2. Consequently, an m-shaped coplanar anomaly with a CXI/CPI amplitude ratio of 2 is virtually a guarantee that the source is a cultural line.

3. A flight that crosses a sphere or horizontal disk yields centre-peaked coaxial and coplanar anomalies with a CXI/CPI amplitude ratio (i.e., coaxial/coplanar) of 1/8. In the absence of geologic bodies of this geometry, the most likely conductor is a metal roof or small fenced yard.⁸ Anomalies of this type are virtually certain to be cultural if they occur in an area of culture.
4. A flight that crosses a horizontal rectangular body or wide ribbon yields an m-shaped coaxial anomaly and a centre-peaked coplanar anomaly. In the absence of geologic bodies of this geometry, the most likely conductor is a large fenced area.⁵ Anomalies of this type are virtually certain to be cultural if they occur in an area of culture.
5. EM anomalies that coincide with culture, as seen on the camera film or video display, are usually caused by culture. However, care is taken with such coincidences because a geologic conductor could occur beneath a fence, for example. In this example, the fence would be expected to yield an m-shaped coplanar anomaly as in case #2 above. If, instead, a centre-peaked coplanar anomaly occurred, there would be concern that a thick geologic conductor coincided with the cultural line.
6. The above description of anomaly shapes is valid when the culture is not conductively coupled to the environment. In this case, the anomalies arise from inductive coupling to the EM transmitter. However, when the environment is quite conductive (e.g., less than 100 ohm-m at 900 Hz), the cultural conductor may be conductively coupled to the environment. In this latter case, the anomaly shapes tend to be governed by current gathering. Current gathering can completely distort the anomaly shapes, thereby complicating the identification of cultural anomalies. In such circumstances, the interpreter can only rely on the radiation channels and on the camera film or video records.

Magnetic Responses

The measured total magnetic field provides information on the magnetic properties of the earth materials in the survey area. The information can be used to locate magnetic bodies of direct interest for exploration, and for structural and lithological mapping.

⁸ It is a characteristic of EM that geometrically similar anomalies are obtained from: (1) a planar conductor, and (2) a wire which forms a loop having dimensions identical to the perimeter of the equivalent planar conductor.

- Appendix B.14 -

The total magnetic field response reflects the abundance of magnetic material in the source. Magnetite is the most common magnetic mineral. Other minerals such as ilmenite, pyrrhotite, franklinite, chromite, hematite, arsenopyrite, limonite and pyrite are also magnetic, but to a lesser extent than magnetite on average.

In some geological environments, an EM anomaly with magnetic correlation has a greater likelihood of being produced by sulphides than one which is non-magnetic. However, sulphide ore bodies may be non-magnetic (e.g., the Kidd Creek deposit near Timmins, Canada) as well as magnetic (e.g., the Mattabi deposit near Sturgeon Lake, Canada).

Iron ore deposits will be anomalously magnetic in comparison to surrounding rock due to the concentration of iron minerals such as magnetite, ilmenite and hematite.

Changes in magnetic susceptibility often allow rock units to be differentiated based on the total field magnetic response. Geophysical classifications may differ from geological classifications if various magnetite levels exist within one general geological classification. Geometric considerations of the source such as shape, dip and depth, inclination of the earth's field and remanent magnetization will complicate such an analysis.

In general, mafic lithologies contain more magnetite and are therefore more magnetic than many sediments which tend to be weakly magnetic. Metamorphism and alteration can also increase or decrease the magnetization of a rock unit.

Textural differences on a total field magnetic contour, colour or shadow map due to the frequency of activity of the magnetic parameter resulting from inhomogeneities in the distribution of magnetite within the rock, may define certain lithologies. For example, near surface volcanics may display highly complex contour patterns with little line-to-line correlation.

Rock units may be differentiated based on the plan shapes of their total field magnetic responses. Mafic intrusive plugs can appear as isolated "bulls-eye" anomalies. Granitic intrusives appear as sub-circular zones, and may have contrasting rings due to contact metamorphism. Generally, granitic terrain will lack a pronounced strike direction, although granite gneiss may display strike.

Linear north-south units are theoretically not well-defined on total field magnetic maps in equatorial regions due to the low inclination of the earth's magnetic field. However, most stratigraphic units will have variations in composition along strike that will cause the units to appear as a series of alternating magnetic highs and lows.

Faults and shear zones may be characterized by alteration that causes destruction of magnetite (e.g., weathering) that produces a contrast with surrounding rock. Structural breaks may be filled by magnetite-rich, fracture filling material as is the case with diabase dikes, or by non-magnetic felsic material.

Faulting can also be identified by patterns in the magnetic total field contours or colours. Faults and dikes tend to appear as lineaments and often have strike lengths of several

- Appendix B.15 -

kilometres. Offsets in narrow, magnetic, stratigraphic trends also delineate structure. Sharp contrasts in magnetic lithologies may arise due to large displacements along strike-slip or dip-slip faults.

APPENDIX C

DATA ARCHIVE DESCRIPTION

APPENDIX C

ARCHIVE DESCRIPTION

CDVD00287

This final data archive contains XYZ files database and grids of an airborne geophysical survey conducted by FUGRO AIRBORNE SURVEYS CORP. on behalf of the Alberta Energy Resources Conservation Board in Alberta over the Edmonton-Red Deer Area flown from November 23 to December 6, 2007

Job # 07116

ReadMe.TXT - This file

Grids in Geosoft format with corresponding .GI files

\Grids\

MAG.GRD	- Residual Magnetic Field nT
CVG.GRD	- Calculated Vertical Gradient from Residual
Magnetic Field nT/m	
RES5M.GRD	- Resistivity Depth Slice 5m
RES10M.GRD	- Resistivity Depth Slice 10m
RES20M.GRD	- Resistivity Depth Slice 20m
RES30M.GRD	- Resistivity Depth Slice 30m
RES50M.GRD	- Resistivity Depth Slice 50m
R_1.GRD	- Inversion Resistivity layer 1
R_2.GRD	- Inversion Resistivity layer 2
R_3.GRD	- Inversion Resistivity layer 3
R_4.GRD	- Inversion Resistivity layer 4
T_1.GRD	- Apparent thickness layer 1
T_2.GRD	- Apparent thickness layer 2
T_3.GRD	- Apparent thickness layer 3

\Linedata\

ARC.GDB	- Final data archive in Geosoft database format
ARC.XYZ	- Final data archive in Geosoft XYZ format

\Plots\
Final colour maps in PDF format

MAG.GRD	- Residual Magnetic Field nT
CVG.GRD	- Calculated Vertical Gradient from Residual
Magnetic Field nT/m	
RES5M.PDF	- Resistivity Depth Slice 5m
RES10M.PDF	- Resistivity Depth Slice 10m
RES20M.PDF	- Resistivity Depth Slice 20m
RES30M.PDF	- Resistivity Depth Slice 30m
RES50M.PDF	- Resistivity Depth Slice 50m

\Profiles Profiles in SEGY format 3 lines per plot

\Report\

07116rep.pdf

- Logistics report

Geosoft GDB ARCHIVE SUMMARY

#	CHANNAME	UNITS	DESCRIPTION
1	X_10TM	m	UTME-Alberta 10 TM
2	Y_10TM	m	UTMN-Alberta 10 TM
3	FID	n/a	Synchronization Counter
4	X_NAD83	m	UTME-NAD83 Z12N
5	Y_NAD83	m	UTMN-NAD83 Z12N
6	Z	m	GPS antenna height above WGS 84 ellipsoid
7	LAT_WGS84	deg	Latitude (WGS84)
8	LON_WGS84	deg	Longitude (WGS84)
9	ALTRAD_HELI	m	Helicopter to Earth-Surface, Radar Altimeter
10	ALTRAD_BIRD	m	Em Bird to Earth-Surface, Radar Altimeter
11	ALTLAS_BIRD	m	Em Bird to Earth-Surface, Laser Altimeter
12	DEM	m	Digital Elevation Model
13	MAGSP	nT	Despiked Uncorrected Total Magnetic Field
14	DIURNAL	nT	Recorded Daily Variations of Magnetic Field
15	DIURNAL_COR	nT	Base removed, interpolated and filtered diurnal
16	MAGLD	nT	Lagged diurnally corrected Total Magnetic Field
17	IGRF	nT	International Geomagnetic Reference Field (2005 model)
18	MAG	nT	Igrf corrected, Leveled Total Magnetic Field
19	CPI400	ppm	Leveled Inphase-Coplanar 396 Hz
20	CPQ400	ppm	Leveled Quadrature-Coplanar 396 Hz
21	CPI1800	ppm	Leveled Inphase-Coplanar 1773 Hz
22	CPQ1800	ppm	Leveled Quadrature-Coplanar 1773 Hz
23	CXI3300	ppm	Leveled Inphase-Coaxial 3247 Hz
24	CXQ3300	ppm	Leveled Quadrature-Coaxial 3247 Hz
25	CPI8200	ppm	Leveled Inphase-Coplanar 8220 Hz
26	CPQ8200	ppm	Leveled Quadrature-Coplanar 8220 Hz
27	CPI40K	ppm	Leveled Inphase-Coplanar 39880 Hz
28	CPQ40K	ppm	Leveled Quadrature-Coplanar 39880 Hz
29	CPI140K	ppm	Leveled Inphase-Coplanar 132700 Hz
30	CPQ140K	ppm	Leveled Quadrature-Coplanar 132700 Hz
31	RES400	ohm.m	Apparent Resistivity 396 Hz
32	RES1800	ohm.m	Apparent Resistivity 1773 Hz
33	RES8200	ohm.m	Apparent Resistivity 8220 Hz
34	RES40K	ohm.m	Apparent Resistivity 39880 Hz
35	RES140K	ohm.m	Apparent Resistivity 132700 Hz
36	DEP400	m	Apparent Depth 396 Hz
37	DEP1800	m	Apparent Depth 1773 Hz
38	DEP8200	m	Apparent Depth 8220 Hz
39	DEP40k	m	Apparent Depth 39880 Hz
40	DEP140k	m	Apparent Depth 132700 Hz
41	CPPL	n/a	Coplanar Powerline Monitor
42	CXSP	n/a	Coaxial Spherics Monitor
43	DRES400	ohm.m	Differential Resistivity 396 Hz
44	DRES1800	ohm.m	Differential Resistivity 1773 Hz
45	DRES8200	ohm.m	Differential Resistivity 8220 Hz
46	DRES40K	ohm.m	Differential Resistivity 39880 Hz

47	DRES140K	ohm.m	Differential Resistivity	132700 Hz
48	DDEP400	m	Differential Depth	396 Hz
49	DDEP1800	m	Differential Depth	1773 Hz
50	DDEP8200	m	Differential Depth	8220 Hz
51	DDEP40k	m	Differential Depth	39880 Hz
52	DDEP140k	m	Differential Depth	132700 Hz
53	RES5M	ohm.m	Resistivity Depth Slice	5m
54	RES10M	ohm.m	Resistivity Depth Slice	10m
55	RES20M	ohm.m	Resistivity Depth Slice	20m
56	RES30M	ohm.m	Resistivity Depth Slice	30m
57	RES50M	ohm.m	Resistivity Depth Slice	50m
58	R_1	ohm.m	Inversion Resistivity layer	1
59	R_2	ohm.m	Inversion Resistivity layer	2
60	R_3	ohm.m	Inversion Resistivity layer	3
61	R_4	ohm.m	Inversion Resistivity layer	4
62	T_1	m	Apparent thickness layer	1
63	T_2	m	Apparent thickness layer	2
64	T_3	m	Apparent thickness layer	3

The coordinate system for all grids and the data archive is projected as follows

Channel names	X_10TM,Y_10TM
Length Units	metres
Projection	Alberta 10TM
Type	Transverse Mercator
Latitude Origin	0
Longitude Origin	115 West
Scale factor	0.9992
False easting	500000
False northing	0
Datum	NAD83
Ellipsoid	GRS 1980
Major Axis	6378137
Eccentricity	0.08181919104
Prime Mer	0
Local Datum Transform	NAD83 Canada

If you have any problems with this archive please contact

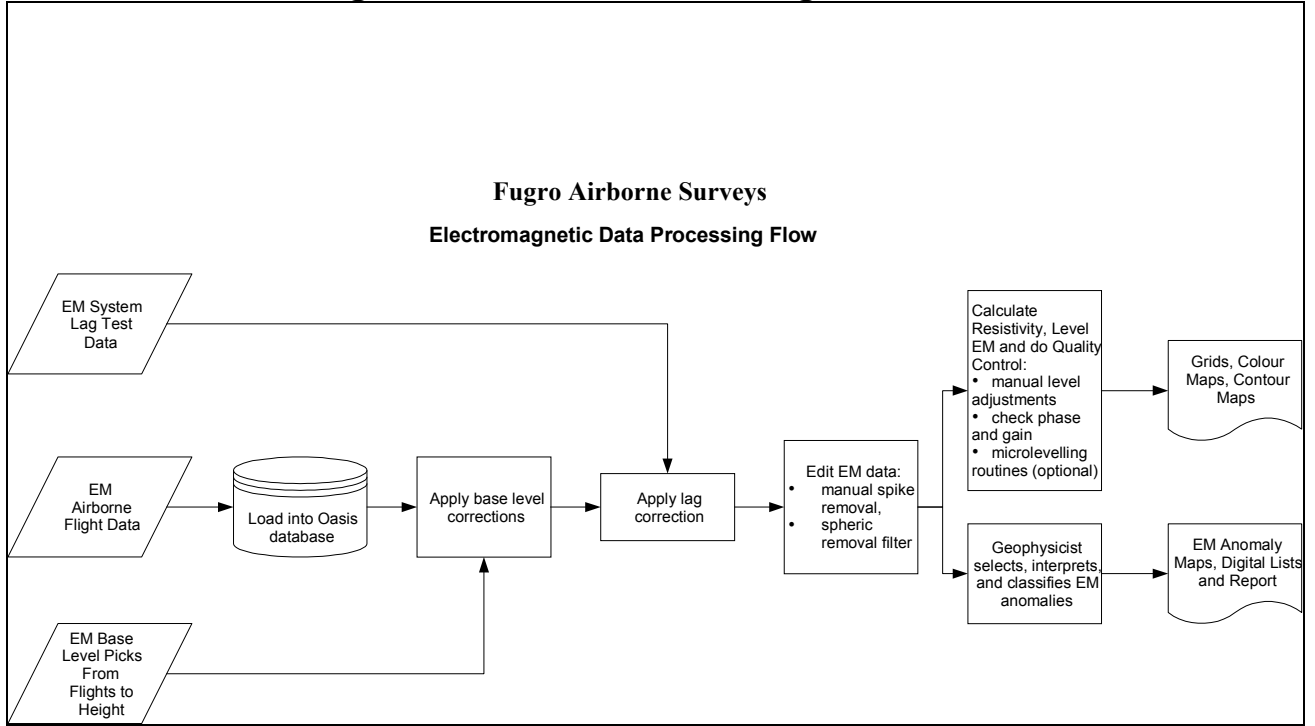
Processing Manager
FUGRO AIRBORNE SURVEYS CORP.
2270 Argentia Road, Unit 2
Mississauga, Ontario
Canada L5N 6A6
Tel (905) 812-0212
Fax (905) 812-1504
E-mail toronto@fugroairborne.com

APPENDIX D

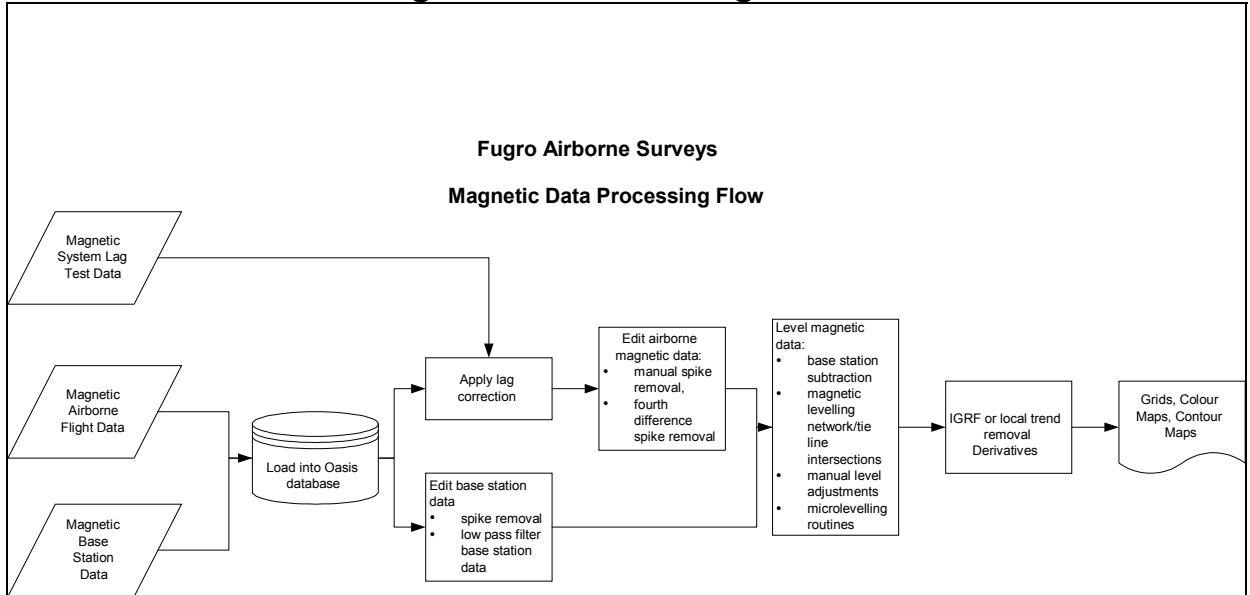
**DATA PROCESSING
FLOWCHARTS**

APPENDIX D

Processing Flow Chart - Electromagnetic Data



Processing Flow Chart - Magnetic Data



APPENDIX E

GLOSSARY

APPENDIX E

GLOSSARY OF AIRBORNE GEOPHYSICAL TERMS

Note: The definitions given in this glossary refer to the common terminology as used in airborne geophysics.

altitude attenuation: the absorption of gamma rays by the atmosphere between the earth and the detector. The number of gamma rays detected by a system decreases as the altitude increases.

apparent- : the *physical parameters* of the earth measured by a geophysical system are normally expressed as apparent, as in “apparent *resistivity*”. This means that the measurement is limited by assumptions made about the geology in calculating the response measured by the geophysical system. Apparent resistivity calculated with *HEM*, for example, generally assumes that the earth is a *homogeneous half-space* – not layered.

amplitude: The strength of the total electromagnetic field. In *frequency domain* it is most often the sum of the squares of *in-phase* and *quadrature* components. In multi-component electromagnetic surveys it is generally the sum of the squares of all three directional components.

analytic signal: The total amplitude of all the directions of magnetic *gradient*. Calculated as the sum of the squares.

anisotropy: Having different *physical parameters* in different directions. This can be caused by layering or fabric in the geology. Note that a unit can be anisotropic, but still *homogeneous*.

anomaly: A localized change in the geophysical data characteristic of a discrete source, such as a conductive or magnetic body: something locally different from the *background*.

B-field: In time-domain *electromagnetic* surveys, the magnetic field component of the (electromagnetic) *field*. This can be measured directly, although more commonly it is calculated by integrating the time rate of change of the magnetic field dB/dt , as measured with a receiver coil.

background: The “normal” response in the geophysical data – that response observed over most of the survey area. *Anomalies* are usually measured relative to the background. In airborne gamma-ray spectrometric surveys the term defines the *cosmic*, radon, and aircraft responses in the absence of a signal from the ground.

base-level: The measured values in a geophysical system in the absence of any outside signal. All geophysical data are measured relative to the system base level.

base frequency: The frequency of the pulse repetition for a *time-domain electromagnetic* system. Measured between subsequent positive pulses.

- Appendix E.2 -

bird: A common name for the pod towed beneath or behind an aircraft, carrying the geophysical sensor array.

bucking: The process of removing the strong **signal** from the **primary field** at the **receiver** from the data, to measure the **secondary field**. It can be done electronically or mathematically. This is done in **frequency-domain EM**, and to measure **on-time** in **time-domain EM**.

calibration coil: A wire coil of known size and dipole moment, which is used to generate a field of known **amplitude** and **phase** in the receiver, for system calibration. Calibration coils can be external, or internal to the system. Internal coils may be called Q-coils.

coaxial coils: [CX] Coaxial coils in an HEM system are in the vertical plane, with their axes horizontal and collinear in the flight direction. These are most sensitive to vertical conductive objects in the ground, such as thin, steeply dipping conductors perpendicular to the flight direction. Coaxial coils generally give the sharpest anomalies over localized conductors. (See also **coplanar coils**)

coil: A multi-turn wire loop used to transmit or detect electromagnetic fields. Time varying **electromagnetic** fields through a coil induce a voltage proportional to the strength of the field and the rate of change over time.

compensation: Correction of airborne geophysical data for the changing effect of the aircraft. This process is generally used to correct data in **fixed-wing time-domain electromagnetic** surveys (where the transmitter is on the aircraft and the receiver is moving), and magnetic surveys (where the sensor is on the aircraft, turning in the earth's magnetic field).

component: In **frequency domain electromagnetic** surveys this is one of the two **phase** measurements – **in-phase or quadrature**. In “multi-component” electromagnetic surveys it is also used to define the measurement in one geometric direction (vertical, horizontal in-line and horizontal transverse – the Z, X and Y components).

Compton scattering: gamma ray photons will bounce off electrons as they pass through the earth and atmosphere, reducing their energy and then being detected by **radiometric** sensors at lower energy levels. See also **stripping**.

conductance: See **conductivity thickness**

conductivity: [σ] The facility with which the earth or a geological formation conducts electricity. Conductivity is usually measured in milli-Siemens per metre (mS/m). It is the reciprocal of **resistivity**.

conductivity-depth imaging: see **conductivity-depth transform**.

- Appendix E.3 -

conductivity-depth transform: A process for converting electromagnetic measurements to an approximation of the conductivity distribution vertically in the earth, assuming a *layered earth*. (Macnae and Lamontagne, 1987; Wolfgram and Karlik, 1995)

conductivity thickness: [σt] The product of the *conductivity*, and thickness of a large, tabular body. (It is also called the “conductivity-thickness product”) In electromagnetic geophysics, the response of a thin plate-like conductor is proportional to the conductivity multiplied by thickness. For example a 10 metre thickness of 20 Siemens/m mineralization will be equivalent to 5 metres of 40 S/m; both have 200 S conductivity thickness. Sometimes referred to as conductance.

conductor: Used to describe anything in the ground more conductive than the surrounding geology. Conductors are most often clays or graphite, or hopefully some type of mineralization, but may also be man-made objects, such as fences or pipelines.

coplanar coils: [CP] In HEM, the coplanar coils lie in the horizontal plane with their axes vertical, and parallel. These coils are most sensitive to massive conductive bodies, horizontal layers, and the *halfspace*.

cosmic ray: High energy sub-atomic particles from outer space that collide with the earth’s atmosphere to produce a shower of gamma rays (and other particles) at high energies.

counts (per second): The number of *gamma-rays* detected by a gamma-ray *spectrometer*. The rate depends on the geology, but also on the size and sensitivity of the detector.

culture: A term commonly used to denote any man-made object that creates a geophysical anomaly. Includes, but not limited to, power lines, pipelines, fences, and buildings.

current channelling: See current gathering.

current gathering: The tendency of electrical currents in the ground to channel into a conductive formation. This is particularly noticeable at higher frequencies or early time channels when the formation is long and parallel to the direction of current flow. This tends to enhance anomalies relative to inductive currents (see also *induction*). Also known as current channelling.

daughter products: The radioactive natural sources of gamma-rays decay from the original “parent” element (commonly potassium, uranium, and thorium) to one or more lower-energy “daughter” elements. Some of these lower energy elements are also radioactive and decay further. *Gamma-ray spectrometry* surveys may measure the gamma rays given off by the original element or by the decay of the daughter products.

- Appendix E.4 -

dB/dt : As the **secondary electromagnetic field** changes with time, the magnetic field [**B**] component induces a voltage in the receiving **coil**, which is proportional to the rate of change of the magnetic field over time.

decay: In **time-domain electromagnetic** theory, the weakening over time of the **eddy currents** in the ground, and hence the **secondary field** after the **primary field** electromagnetic pulse is turned off. In **gamma-ray spectrometry**, the radioactive breakdown of an element, generally potassium, uranium, thorium, or one of their **daughter** products.

decay constant: see time constant.

decay series: In **gamma-ray spectrometry**, a series of progressively lower energy **daughter products** produced by the radioactive breakdown of uranium or thorium.

depth of exploration: The maximum depth at which the geophysical system can detect the target. The depth of exploration depends very strongly on the type and size of the target, the contrast of the target with the surrounding geology, the homogeneity of the surrounding geology, and the type of geophysical system. One measure of the maximum depth of exploration for an electromagnetic system is the depth at which it can detect the strongest conductive target – generally a highly conductive horizontal layer.

differential resistivity: A process of transforming **apparent resistivity** to an approximation of layer resistivity at each depth. The method uses multi-frequency HEM data and approximates the effect of shallow layer **conductance** determined from higher frequencies to estimate the deeper conductivities (Huang and Fraser, 1996)

dipole moment: [NIA] For a transmitter, the product of the area of a **coil**, the number of turns of wire, and the current flowing in the coil. At a distance significantly larger than the size of the coil, the magnetic field from a coil will be the same if the dipole moment product is the same. For a receiver coil, this is the product of the area and the number of turns. The sensitivity to a magnetic field (assuming the source is far away) will be the same if the dipole moment is the same.

diurnal: The daily variation in a natural field, normally used to describe the natural fluctuations (over hours and days) of the earth's magnetic field.

dielectric permittivity: [ϵ] The capacity of a material to store electrical charge, this is most often measured as the relative permittivity [ϵ_r], or ratio of the material dielectric to that of free space. The effect of high permittivity may be seen in HEM data at high frequencies over highly resistive geology as a reduced or negative **in-phase**, and higher **quadrature** data.

drape: To fly a survey following the terrain contours, maintaining a constant altitude above the local ground surface. Also applied to re-processing data collected at varying altitudes above ground to simulate a survey flown at constant altitude.

- Appendix E.5 -

drift: Long-time variations in the base-level or calibration of an instrument.

eddy currents: The electrical currents induced in the ground, or other conductors, by a time-varying *electromagnetic field* (usually the *primary field*). Eddy currents are also induced in the aircraft's metal frame and skin; a source of *noise* in EM surveys.

electromagnetic: [EM] Comprised of a time-varying electrical and magnetic field. Radio waves are common electromagnetic fields. In geophysics, an electromagnetic system is one which transmits a time-varying *primary field* to induce *eddy currents* in the ground, and then measures the *secondary field* emitted by those eddy currents.

energy window: A broad spectrum of *gamma-ray* energies measured by a spectrometric survey. The energy of each gamma-ray is measured and divided up into numerous discrete energy levels, called windows.

equivalent (thorium or uranium): The amount of radioelement calculated to be present, based on the gamma-rays measured from a *daughter* element. This assumes that the *decay series* is in equilibrium – progressing normally.

exposure rate: in radiometric surveys, a calculation of the total exposure rate due to gamma rays at the ground surface. It is used as a measurement of the concentration of all the *radioelements* at the surface. See also: **natural exposure rate**.

fiducial, or fid: Timing mark on a survey record. Originally these were timing marks on a profile or film; now the term is generally used to describe 1-second interval timing records in digital data, and on maps or profiles.

Figure of Merit: (FOM) A sum of the 12 distinct magnetic noise variations measured by each of four flight directions, and executing three aircraft attitude variations (yaw, pitch, and roll) for each direction. The flight directions are generally parallel and perpendicular to planned survey flight directions. The FOM is used as a measure of the *manoeuvre noise* before and after **compensation**.

fixed-wing: Aircraft with wings, as opposed to “rotary wing” helicopters.

footprint: This is a measure of the area of sensitivity under the aircraft of an airborne geophysical system. The footprint of an *electromagnetic* system is dependent on the altitude of the system, the orientation of the transmitter and receiver and the separation between the receiver and transmitter, and the conductivity of the ground. The footprint of a *gamma-ray spectrometer* depends mostly on the altitude. For all geophysical systems, the footprint also depends on the strength of the contrasting *anomaly*.

frequency domain: An *electromagnetic* system which transmits a *primary field* that oscillates smoothly over time (sinusoidal), inducing a similarly varying electrical current in the ground. These systems generally measure the changes in the *amplitude* and *phase* of

- Appendix E.6 -

the **secondary field** from the ground at different frequencies by measuring the **in-phase** and **quadrature** phase components. See also **time-domain**.

full-stream data: Data collected and recorded continuously at the highest possible sampling rate. Normal data are stacked (see **stacking**) over some time interval before recording.

gamma-ray: A very high-energy photon, emitted from the nucleus of an atom as it undergoes a change in energy levels.

gamma-ray spectrometry: Measurement of the number and energy of natural (and sometimes man-made) gamma-rays across a range of photon energies.

gradient: In magnetic surveys, the gradient is the change of the magnetic field over a distance, either vertically or horizontally in either of two directions. Gradient data is often measured, or calculated from the total magnetic field data because it changes more quickly over distance than the **total magnetic field**, and so may provide a more precise measure of the location of a source. See also **analytic signal**.

ground effect: The response from the earth. A common calibration procedure in many geophysical surveys is to fly to altitude high enough to be beyond any measurable response from the ground, and there establish **base levels** or **backgrounds**.

half-space: A mathematical model used to describe the earth – as infinite in width, length, and depth below the surface. The most common halfspace models are **homogeneous** and **layered earth**.

heading error: A slight change in the magnetic field measured when flying in opposite directions.

HEM: Helicopter ElectroMagnetic, This designation is most commonly used for helicopter-borne, **frequency-domain** electromagnetic systems. At present, the transmitter and receivers are normally mounted in a **bird** carried on a sling line beneath the helicopter.

herringbone pattern: A pattern created in geophysical data by an asymmetric system, where the **anomaly** may be extended to either side of the source, in the direction of flight. Appears like fish bones, or like the teeth of a comb, extending either side of centre, each tooth an alternate flight line.

homogeneous: This is a geological unit that has the same **physical parameters** throughout its volume. This unit will create the same response to an HEM system anywhere, and the HEM system will measure the same apparent **resistivity** anywhere. The response may change with system direction (see **anisotropy**).

- Appendix E.7 -

HTEM: Helicopter Time-domain ElectroMagnetic, This designation is used for the new generation of helicopter-borne, **time-domain** electromagnetic systems.

in-phase: the component of the measured **secondary field** that has the same phase as the transmitter and the **primary field**. The in-phase component is stronger than the **quadrature** phase over relatively higher **conductivity**.

induction: Any time-varying electromagnetic field will induce (cause) electrical currents to flow in any object with non-zero **conductivity**. (see **eddy currents**)

induction number: also called the “response parameter”, this number combines many of the most significant parameters affecting the **EM** response into one parameter against which to compare responses. For a **layered earth** the response parameter is $\mu\omega\sigma h^2$ and for a large, flat, **conductor** it is $\mu\omega\sigma h$, where μ is the **magnetic permeability**, ω is the angular **frequency**, σ is the **conductivity**, t is the thickness (for the flat conductor) and h is the height of the system above the conductor.

inductive limit: When the frequency of an EM system is very high, or the **conductivity** of the target is very high, the response measured will be entirely **in-phase** with no **quadrature** (phase angle =0). The in-phase response will remain constant with further increase in conductivity or frequency. The system can no longer detect changes in conductivity of the target.

infinite: In geophysical terms, an “infinite” dimension is one much greater than the **footprint** of the system, so that the system does not detect changes at the edges of the object.

International Geomagnetic Reference Field: [IGRF] An approximation of the smooth magnetic field of the earth, in the absence of variations due to local geology. Once the IGRF is subtracted from the measured magnetic total field data, any remaining variations are assumed to be due to local geology. The IGRF also predicts the slow changes of the field up to five years in the future.

inversion, or inverse modeling: A process of converting geophysical data to an earth model, which compares theoretical models of the response of the earth to the data measured, and refines the model until the response closely fits the measured data (Huang and Palacky, 1991)

layered earth: A common geophysical model which assumes that the earth is horizontally layered – the **physical parameters** are constant to **infinite** distance horizontally, but change vertically.

magnetic permeability: [μ] This is defined as the ratio of magnetic induction to the inducing magnetic field. The relative magnetic permeability [μ_r] is often quoted, which is the ratio of the rock permeability to the permeability of free space. In geology and geophysics, the **magnetic susceptibility** is more commonly used to describe rocks.

- Appendix E.8 -

magnetic susceptibility: [**k**] A measure of the degree to which a body is magnetized. In SI units this is related to relative **magnetic permeability** by $k = \mu_r - 1$, and is a dimensionless unit. For most geological material, susceptibility is influenced primarily by the percentage of magnetite. It is most often quoted in units of 10^{-6} . In HEM data this is most often apparent as a negative ***in-phase*** component over high susceptibility, high **resistivity** geology such as diabase dikes.

manoeuvre noise: variations in the magnetic field measured caused by changes in the relative positions of the magnetic sensor and magnetic objects or electrical currents in the aircraft. This type of noise is generally corrected by magnetic **compensation**.

model: Geophysical theory and applications generally have to assume that the geology of the earth has a form that can be easily defined mathematically, called the model. For example steeply dipping **conductors** are generally modeled as being **infinite** in horizontal and depth extent, and very thin. The earth is generally modeled as horizontally layered, each layer infinite in extent and uniform in characteristic. These models make the mathematics to describe the response of the (normally very complex) earth practical. As theory advances, and computers become more powerful, the useful models can become more complex.

natural exposure rate: in radiometric surveys, a calculation of the total exposure rate due to natural-source gamma rays at the ground surface. It is used as a measurement of the concentration of all the natural **radioelements** at the surface. See also: **exposure rate**.

noise: That part of a geophysical measurement that the user does not want. Typically this includes electronic interference from the system, the atmosphere (***sferics***), and man-made sources. This can be a subjective judgment, as it may include the response from geology other than the target of interest. Commonly the term is used to refer to high frequency (short period) interference. See also ***drift***.

Occam's inversion: an ***inversion*** process that matches the measured **electromagnetic** data to a theoretical model of many, thin layers with constant thickness and varying resistivity (Constable et al, 1987).

off-time: In a ***time-domain electromagnetic*** survey, the time after the end of the ***primary field pulse***, and before the start of the next pulse.

on-time: In a ***time-domain electromagnetic*** survey, the time during the ***primary field pulse***.

overburden: In engineering and mineral exploration terms, this most often means the soil on top of the unweathered bedrock. It may be sand, glacial till, or weathered rock.

- Appendix E.9 -

Phase, phase angle: The angular difference in time between a measured sinusoidal electromagnetic field and a reference – normally the primary field. The phase is calculated from $\tan^{-1}(\textit{in-phase} / \textit{quadrature})$.

physical parameters: These are the characteristics of a geological unit. For electromagnetic surveys, the important parameters are **conductivity**, **magnetic permeability** (or **susceptibility**) and **dielectric permittivity**; for magnetic surveys the parameter is magnetic susceptibility, and for gamma ray spectrometric surveys it is the concentration of the major radioactive elements: potassium, uranium, and thorium.

permittivity: see **dielectric permittivity**.

permeability: see **magnetic permeability**.

primary field: the EM field emitted by a transmitter. This field induces **eddy currents** in (energizes) the conductors in the ground, which then create their own **secondary fields**.

pulse: In time-domain EM surveys, the short period of intense **primary** field transmission. Most measurements (the **off-time**) are measured after the pulse. **On-time** measurements may be made during the pulse.

quadrature: that component of the measured **secondary field** that is phase-shifted 90° from the **primary field**. The quadrature component tends to be stronger than the **in-phase** over relatively weaker **conductivity**.

Q-coils: see **calibration coil**.

radioelements: This normally refers to the common, naturally-occurring radioactive elements: potassium (K), uranium (U), and thorium (Th). It can also refer to man-made radioelements, most often cobalt (Co) and cesium (Cs)

radiometric: Commonly used to refer to **gamma ray** spectrometry.

radon: A radioactive daughter product of uranium and thorium, radon is a gas which can leak into the atmosphere, adding to the non-geological background of a gamma-ray spectrometric survey.

receiver: the **signal** detector of a geophysical system. This term is most often used in active geophysical systems – systems that transmit some kind of signal. In airborne **electromagnetic** surveys it is most often a **coil**. (see also, **transmitter**)

resistivity: [ρ] The strength with which the earth or a geological formation resists the flow of electricity, typically the flow induced by the **primary field** of the electromagnetic transmitter. Normally expressed in ohm-metres, it is the reciprocal of **conductivity**.

resistivity-depth transforms: similar to **conductivity depth transforms**, but the calculated **conductivity** has been converted to **resistivity**.

resistivity section: an approximate vertical section of the resistivity of the layers in the earth. The resistivities can be derived from the **apparent resistivity**, the **differential resistivities**, **resistivity-depth transforms**, or **inversions**.

Response parameter: another name for the **induction number**.

secondary field: The field created by conductors in the ground, as a result of electrical currents induced by the **primary field** from the **electromagnetic** transmitter. Airborne **electromagnetic** systems are designed to create and measure a secondary field.

Sengpiel section: a **resistivity section** derived using the **apparent resistivity** and an approximation of the depth of maximum sensitivity for each frequency.

sferic: Lightning, or the **electromagnetic** signal from lightning, it is an abbreviation of "atmospheric discharge". These appear to magnetic and electromagnetic sensors as sharp "spikes" in the data. Under some conditions lightning storms can be detected from hundreds of kilometres away. (see **noise**)

signal: That component of a measurement that the user wants to see – the response from the targets, from the earth, etc. (See also **noise**)

skin depth: A measure of the depth of penetration of an electromagnetic field into a material. It is defined as the depth at which the primary field decreases to 1/e of the field at the surface. It is calculated by approximately $503 \times \sqrt{(\text{resistivity}/\text{frequency})}$. Note that depth of penetration is greater at higher **resistivity** and/or lower **frequency**.

spectrometry: Measurement across a range of energies, where **amplitude** and energy are defined for each measurement. In gamma-ray spectrometry, the number of gamma rays are measured for each energy **window**, to define the **spectrum**.

spectrum: In **gamma ray spectrometry**, the continuous range of energy over which gamma rays are measured. In **time-domain electromagnetic** surveys, the spectrum is the energy of the **pulse** distributed across an equivalent, continuous range of frequencies.

spheric: see **sferic**.

stacking: Summing repeat measurements over time to enhance the repeating **signal**, and minimize the random **noise**.

stripping: Estimation and correction for the gamma ray photons of higher and lower energy that are observed in a particular **energy window**. See also **Compton scattering**.

susceptibility: See *magnetic susceptibility*.

tau: [τ] Often used as a name for the *time constant*.

TDEM: *time domain electromagnetic*.

thin sheet: A standard model for electromagnetic geophysical theory. It is usually defined as a thin, flat-lying conductive sheet, *infinite* in both horizontal directions. (see also *vertical plate*)

tie-line: A survey line flown across most of the *traverse lines*, generally perpendicular to them, to assist in measuring *drift* and *diurnal* variation. In the short time required to fly a tie-line it is assumed that the drift and/or diurnal will be minimal, or at least changing at a constant rate.

time constant: The time required for an *electromagnetic* field to decay to a value of 1/e of the original value. In *time-domain* electromagnetic data, the time constant is proportional to the size and *conductance* of a tabular conductive body. Also called the decay constant.

Time channel: In *time-domain electromagnetic* surveys the decaying *secondary field* is measured over a period of time, and the divided up into a series of consecutive discrete measurements over that time.

time-domain: *Electromagnetic* system which transmits a pulsed, or stepped *electromagnetic* field. These systems induce an electrical current (*eddy current*) in the ground that persists after the *primary field* is turned off, and measure the change over time of the *secondary field* created as the currents *decay*. See also *frequency-domain*.

total energy envelope: The sum of the squares of the three *components* of the *time-domain electromagnetic secondary field*. Equivalent to the *amplitude* of the secondary field.

transient: Time-varying. Usually used to describe a very short period pulse of *electromagnetic* field.

transmitter: The source of the *signal* to be measured in a geophysical survey. In airborne *EM* it is most often a *coil* carrying a time-varying electrical current, transmitting the *primary field*. (see also *receiver*)

traverse line: A normal geophysical survey line. Normally parallel traverse lines are flown across the property in spacing of 50 m to 500 m, and generally perpendicular to the target geology.

- Appendix E.12 -

vertical plate: A standard model for electromagnetic geophysical theory. It is usually defined as thin conductive sheet, *infinite* in horizontal dimension and depth extent. (see also *thin sheet*)

waveform: The shape of the *electromagnetic pulse* from a *time-domain* electromagnetic transmitter.

window: A discrete portion of a *gamma-ray spectrum* or *time-domain electromagnetic decay*. The continuous energy spectrum or *full-stream* data are grouped into windows to reduce the number of samples, and reduce *noise*.

Version 1.5, November 29, 2005
Greg Hodges,
Chief Geophysicist
Fugro Airborne Surveys, Toronto

Common Symbols and Acronyms

k	Magnetic susceptibility
ϵ	Dielectric permittivity
μ, μ_r	Magnetic permeability, relative permeability
ρ, ρ_a	Resistivity, apparent resistivity
σ, σ_a	Conductivity, apparent conductivity
σt	Conductivity thickness
τ	Tau, or time constant
Ωm	ohm-metres, units of resistivity
AGS	Airborne gamma ray spectrometry.
CDT	Conductivity-depth transform, conductivity-depth imaging (Macnae and Lamontagne, 1987; Wolfgram and Karlik, 1995)
CPI, CPQ	Coplanar in-phase, quadrature
CPS	Counts per second
CTP	Conductivity thickness product
CXI, CXQ	Coaxial, in-phase, quadrature
FOM	Figure of Merit
fT	femtoteslas, normal unit for measurement of B-Field
EM	Electromagnetic
keV	kilo electron volts – a measure of gamma-ray energy
MeV	mega electron volts – a measure of gamma-ray energy 1MeV = 1000keV
NIA	dipole moment: turns x current x Area
nT	nanotesla, a measure of the strength of a magnetic field
nG/h	nanoGreys/hour – gamma ray dose rate at ground level
ppm	parts per million – a measure of secondary field or noise relative to the primary or radioelement concentration.
pT/s	picoteslas per second: Units of decay of secondary field, dB/dt
S	siemens – a unit of conductance
x:	the horizontal component of an EM field parallel to the direction of flight.
y:	the horizontal component of an EM field perpendicular to the direction of flight.
z:	the vertical component of an EM field.

References:

Constable, S.C., Parker, R.L., And Constable, C.G., 1987, Occam's inversion: a practical algorithm for generating smooth models from electromagnetic sounding data: *Geophysics*, 52, 289-300

Huang, H. and Fraser, D.C, 1996. The differential parameter method for multifrequency airborne resistivity mapping. *Geophysics*, 55, 1327-1337

Huang, H. and Palacky, G.J., 1991, Damped least-squares inversion of time-domain airborne EM data based on singular value decomposition: *Geophysical Prospecting*, v.39, 827-844

Macnae, J. and Lamontagne, Y., 1987, Imaging quasi-layered conductive structures by simple processing of transient electromagnetic data: *Geophysics*, v52, 4, 545-554.

Sengpiel, K-P. 1988, Approximate inversion of airborne EM data from a multi-layered ground. *Geophysical Prospecting*, 36, 446-459

Wolfgram, P. and Karlik, G., 1995, Conductivity-depth transform of GEOTEM data: *Exploration Geophysics*, 26, 179-185.

Yin, C. and Fraser, D.C. (2002), The effect of the electrical anisotropy on the responses of helicopter-borne frequency domain electromagnetic systems, Submitted to *Geophysical Prospecting*

**Appendix 2 – Logistics and Processing Report Airborne Magnetic and GEOTEM®
Survey, Edmonton–Red Deer Area, Alberta**

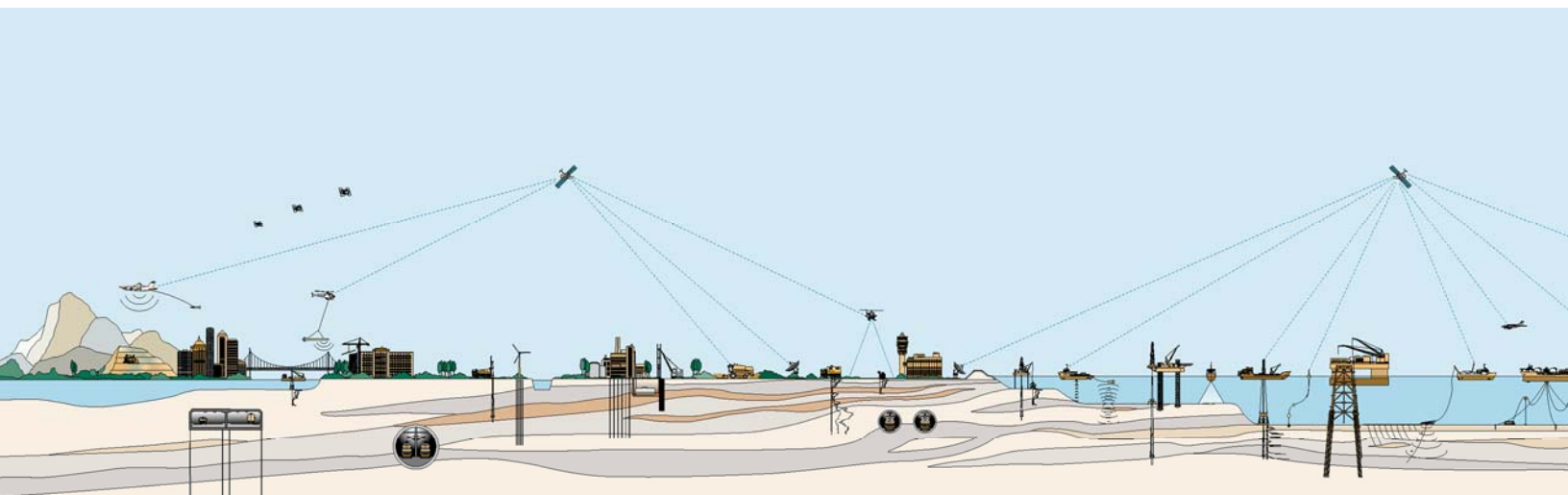


**LOGISTICS AND PROCESSING REPORT
Airborne Magnetic and GEOTEM[®] Survey**

EDMONTON – RED DEER AREA
ALBERTA

Job No. 07427 & 08401

Alberta Energy Resources Conservation Board





**LOGISTICS AND PROCESSING REPORT
AIRBORNE MAGNETIC AND GEOTEM[®] SURVEY
EDMONTON - RED DEER AREA
ALBERTA**

JOB NO. 07427

Client: Alberta Energy Resources Conservation Board
402, 4999-98 Avenue.
Edmonton, Alberta
T6B 2X3

Date of Report: March, 2008

TABLE OF CONTENTS

INTRODUCTION	5
SURVEY OPERATIONS	6
Location of the Survey Area	6
Aircraft and Geophysical On-Board Equipment	7
Base Station Equipment	11
Field Office Equipment	11
Survey Specifications	11
Field Crew	12
Production Statistics	12
QUALITY CONTROL AND COMPILATION PROCEDURES	13
DATA PROCESSING	14
Flight Path Recovery	14
Altitude Data	14
Base Station Diurnal Magnetics	14
Airborne Magnetics	14
<i>Residual Magnetic Intensity</i>	15
<i>Magnetic First Vertical Derivative</i>	15
Electromagnetics	15
<i>dB/dt data</i>	15
<i>B-field data</i>	16
<i>Coil Oscillation Correction</i>	17
<i>Apparent Resistivity</i>	18
<i>Resistivity-Depth-Images (RDI)</i>	18
FINAL PRODUCTS	19
Digital Archives	19
Maps	19
Profile Plots	19
Report	19

APPENDICES

- A FIXED-WING AIRBORNE ELECTROMAGNETIC SYSTEMS**
- B AIRBORNE TRANSIENT EM INTERPRETATION**
- C MULTICOMPONENT MODELING**
- D THE USEFULNESS OF MULTICOMPONENT, TIME-DOMAIN
AIRBORNE ELECTROMAGNETIC MEASUREMENT**
- E DATA ARCHIVE DESCRIPTION**
- F MAP PRODUCT GRIDS**
- G REFERENCE WAVEFORM**

I

Introduction

Between November 21st and December 18th, 2007 and between February 6th and February 18th, 2008, Fugro Airborne Surveys conducted a GEOTEM[®] electromagnetic and magnetic survey of the Edmonton – Red Deer Area on behalf of the Alberta Energy Resources Conservation Board. Using Leduc and Red Deer, Alberta as the bases of operations, a total of 17,497 line kilometres of data was collected using a Casa 212 modified aircraft (Figure 1).

The survey data were processed and compiled in the Fugro Airborne Surveys Ottawa office. The collected and processed data are presented on colour maps, and multi-parameter profiles. The following maps were produced: Residual Magnetic Intensity (RMI), First Vertical Derivative of RMI, Resistivity Depth Slice at 10m, Resistivity Depth Slice at 30m, Resistivity Depth Slice at 60m, Resistivity Depth Slice at 120m, Apparent Resistivity, and Flight Path. In addition, digital archives of the raw and processed survey data in line format, and gridded EM data were delivered.



Figure 1: Specially modified Casa 212 aircraft used by Fugro Airborne Surveys.

II

Survey Operations

Location of the Survey Area

The Edmonton – Red Deer Area (Figure 2) was flown with Leduc and Red Deer, Alberta as bases of operations. A total of 181 traverse lines were flown ranging in length from 87 km to 98 km, with a spacing of 800 m between lines and 15 tie lines were flown with a spacing of 15000 m between tie-lines, totalling 17,497 km for the complete survey.

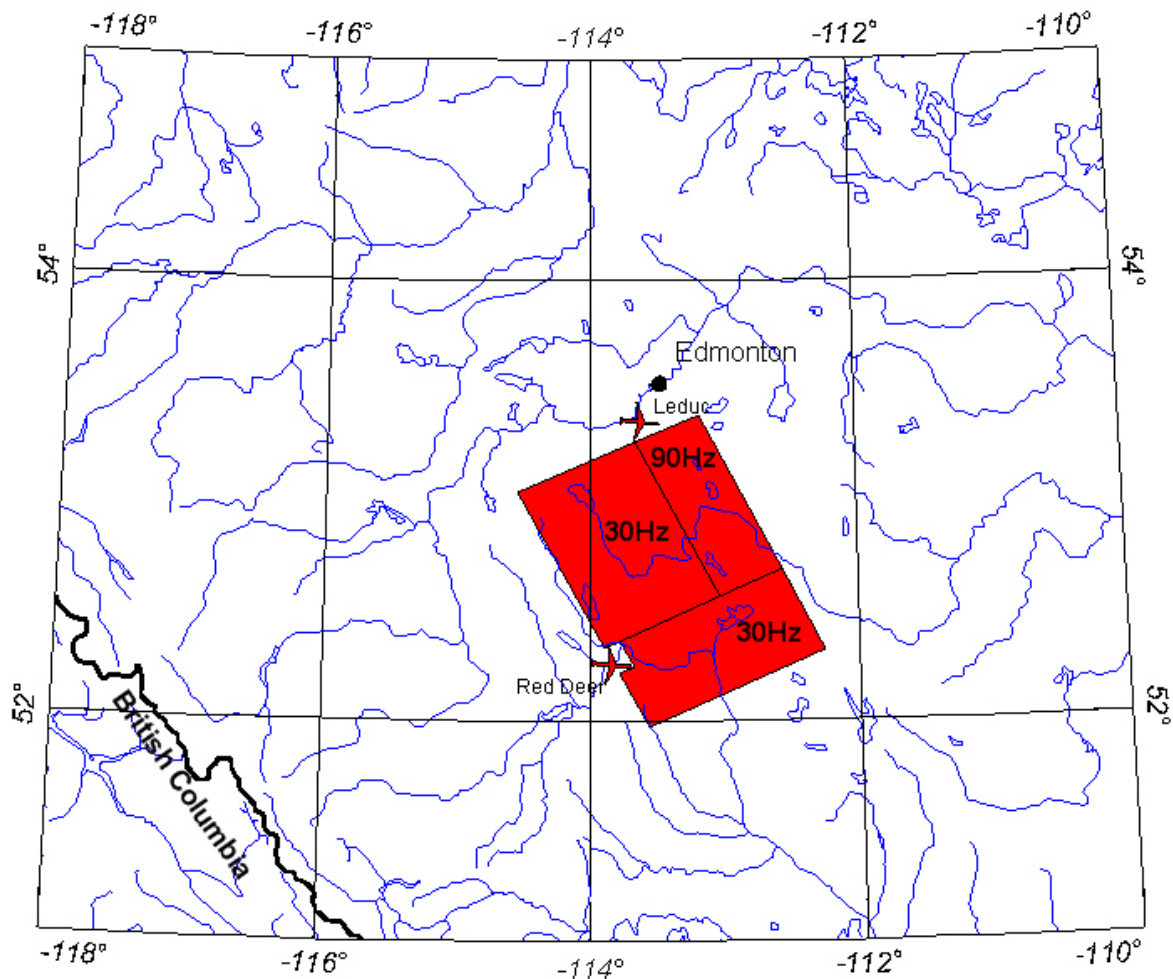


Figure 2: Survey location.

Aircraft and Geophysical On-Board Equipment

Aircraft:	Casa 212 (Twin Turbo Propeller)	
Operator:	FUGRO AIRBORNE SURVEYS	
Registration:	C-FDKM	
Survey Speed:	125 knots / 145 mph / 65 m/s	
Magnetometer:	Scintrex Cs-2 single cell cesium vapour, towed-bird installation, sensitivity = 0.01 nT ¹ , sampling rate = 0.1 s, ambient range 20,000 to 100,000 nT. The general noise envelope was kept below 0.5 nT. The nominal sensor height was ~73 m above ground.	
Electromagnetic system:	GEOTEM 20 channel Multicoil System	
Transmitter:	Vertical axis loop mounted on aircraft of 231 m ² Number of turns 6 Nominal height above ground of 120 m	
Receiver:	Multicoil system (x, y and z) with a final recording rate of 4 samples/second, for the recording of 20 channels of x, y and z-coil data. The nominal height above ground is ~75 m, placed ~130 m behind the centre of the transmitter loop.	
Base frequency:	30 Hz and 90 Hz	
Pulse width:	4045 μs (30Hz) 2110 μs (90Hz)	
Pulse delay:	33μs (30Hz) 27μs (90Hz)	
Off-time:	12589 μs (30Hz) 3346 μs (90Hz)	
Point value:	8.1μs (30Hz) 5.4 μs (90 Hz)	
Transmitter Current:	~670 A (30Hz) ~510 A (90Hz)	
Dipole moment:	~9.3x10 ⁵ Am ² (30Hz) ~7.1x10 ⁵ Am ² (90Hz)	

Figure 3: Mag and GEOTEM® Receivers



Figure 4: Modified Casa 212 in flight.

1 One nanotesla (nT) is the S.I. equivalent of one gamma.

Table 1: Electromagnetic Data Windows 30Hz.

Channel	Start (p)	End (p)	Width (p)	Start (ms)	End (ms)	Width (ms)	Mid (ms)
1	6	21	16	0.041	0.171	0.130	0.106
2	22	179	158	0.171	1.457	1.286	0.814
3	180	337	158	1.457	2.743	1.286	2.100
4	338	495	158	2.743	4.028	1.286	3.385
5	496	510	15	4.028	4.150	0.122	4.089
6	511	522	12	4.150	4.248	0.098	4.199
7	523	537	15	4.248	4.370	0.122	4.309
8	538	557	20	4.370	4.533	0.163	4.451
9	558	582	25	4.533	4.736	0.203	4.635
10	583	617	35	4.736	5.021	0.285	4.879
11	618	662	45	5.021	5.387	0.366	5.204
12	663	717	55	5.387	5.835	0.448	5.611
13	718	787	70	5.835	6.405	0.570	6.120
14	788	872	85	6.405	7.096	0.692	6.750
15	873	972	100	7.096	7.910	0.814	7.503
16	973	1097	125	7.910	8.927	1.017	8.419
17	1098	1247	150	8.927	10.148	1.221	9.538
18	1248	1447	200	10.148	11.776	1.628	10.962
19	1448	1697	250	11.776	13.810	2.035	12.793
20	1698	2048	351	13.810	16.667	2.856	15.238

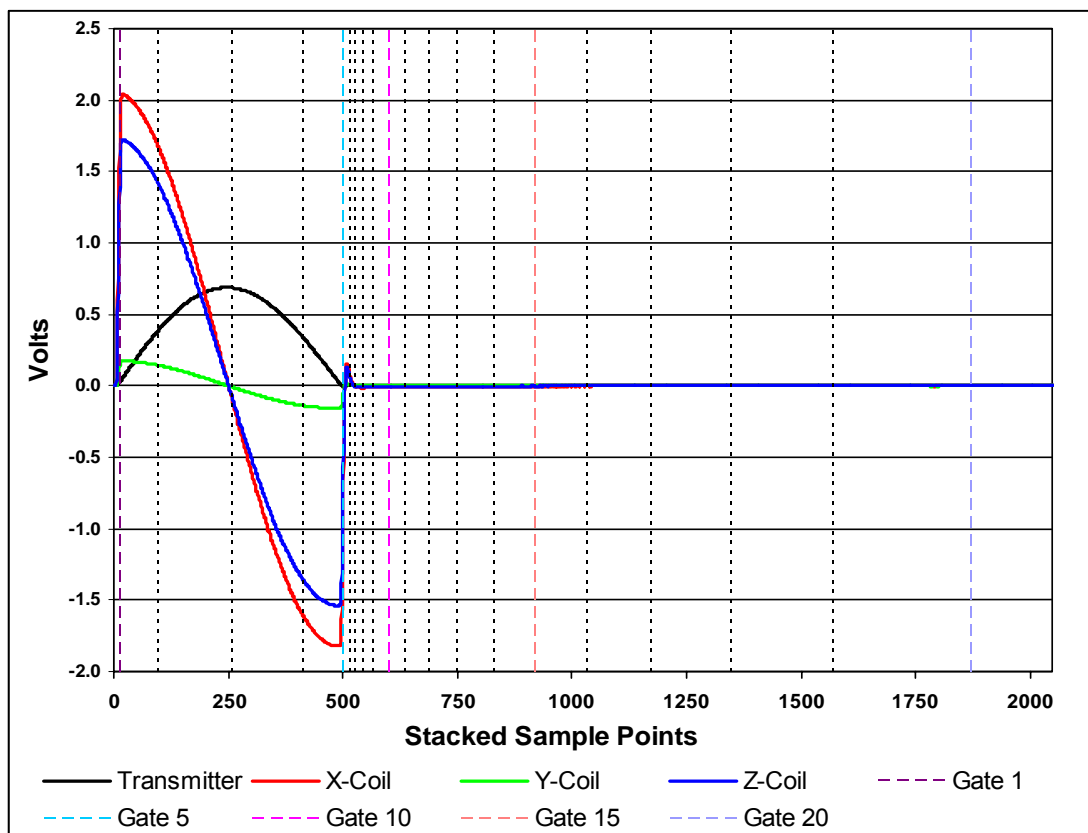


Figure 5: 30Hz GEOTEM Waveform and response with gate centres showing positions in sample points.

Table 2: Electromagnetic Data Windows 90Hz.

Channel	Start (p)	End (p)	Width (p)	Start (ms)	End (ms)	Width (ms)	Mid (ms)
1	6	26	21	0.027	0.141	0.114	0.084
2	27	146	120	0.141	0.792	0.651	0.467
3	147	264	118	0.792	1.432	0.640	1.112
4	265	384	120	1.432	2.083	0.651	1.758
5	385	406	22	2.083	2.203	0.119	2.143
6	407	426	20	2.203	2.311	0.109	2.257
7	427	446	20	2.311	2.420	0.109	2.365
8	447	466	20	2.420	2.528	0.109	2.474
9	467	486	20	2.528	2.637	0.109	2.582
10	487	511	25	2.637	2.772	0.136	2.705
11	512	536	25	2.772	2.908	0.136	2.840
12	537	566	30	2.908	3.071	0.163	2.989
13	567	596	30	3.071	3.234	0.163	3.152
14	597	636	40	3.234	3.451	0.217	3.342
15	637	676	40	3.451	3.668	0.217	3.559
16	677	721	45	3.668	3.912	0.244	3.790
17	722	771	50	3.912	4.183	0.271	4.047
18	772	831	60	4.183	4.508	0.326	4.346
19	832	906	75	4.508	4.915	0.407	4.712
20	907	1024	118	4.915	5.556	0.640	5.235

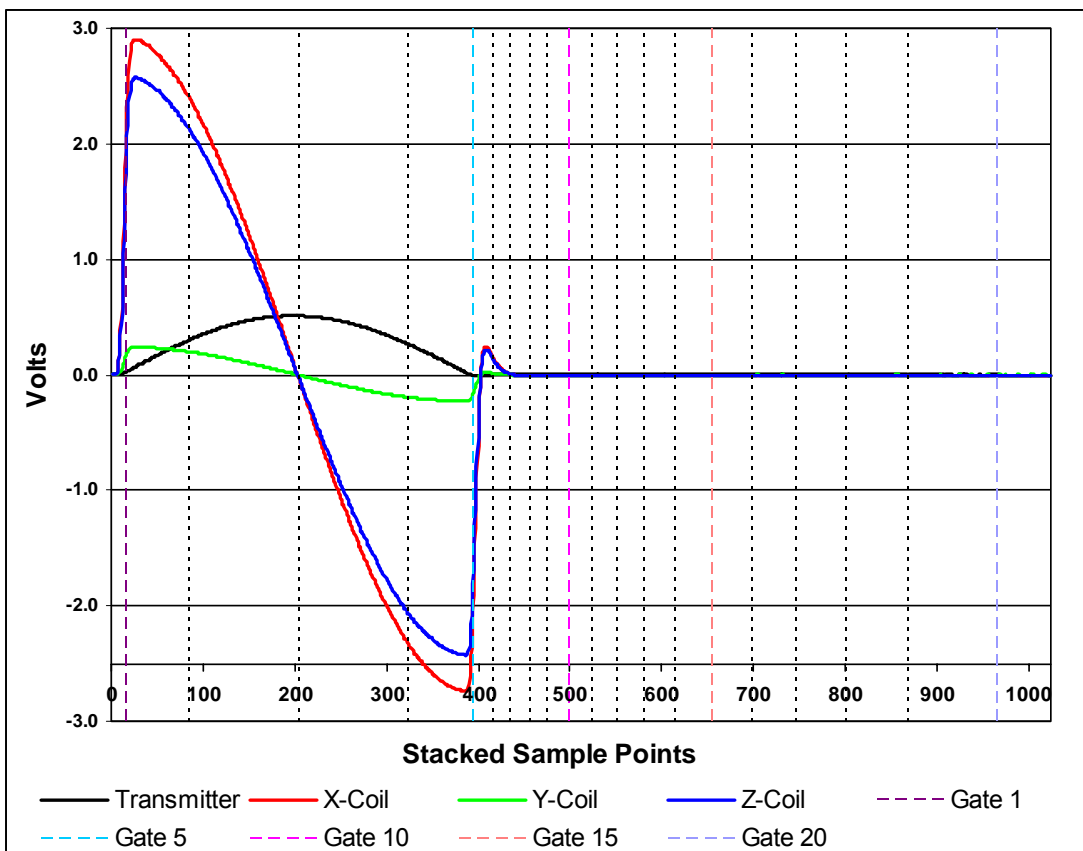


Figure 6: 90 Hz GEOTEM Waveform and response with gate centres showing positions in sample points.

Digital Acquisition: FUGRO AIRBORNE SURVEYS GEODAS SYSTEM.

Analogue Recorder: RMS GR-33, see below for analogue display and setup.

Barometric Altimeter: Rosemount 1241M, sensitivity 1 ft, 0.5 sec recording interval.

Radar Altimeter: King, accuracy 2%, sensitivity 1 ft, range 0 to 2500 ft, 0.5 sec recording interval.

Camera: Panasonic colour video, super VHS, model WV-CL302.

Electronic Navigation: NovAtel OEM4, 1 sec recording interval, with a resolution of 0.00001 degree and an accuracy of $\pm 5m$.

Analogue Recorder Display Setup:

Name	Description	Scale	Unit
ZF04	dB/dt Z coil Time Filtered Channel 04	20000	pV/cm
ZF12	dB/dt Z coil Time Filtered Channel 12	20000	pV/cm
ZF18	dB/dt Z coil Time Filtered Channel 18	20000	pV/cm
BZ4	B Field Z coil Time Filtered Channel 4	20000	fT/cm
BZ12	B Field Z coil Time Filtered Channel 12	20000	fT/cm
BZ18	B Field Z coil Time Filtered Channel 18	20000	fT/cm
XF4	dB/dt X coil Time Filtered Channel 4	20000	pV/cm
XF12	dB/dt X coil Time Filtered Channel 12	20000	pV/cm
XF18	dB/dt X coil Time Filtered Channel 18	20000	pV/cm
BX4	B Field X coil Time Filtered Channel 4	20000	fT/cm
BX12	B Field X coil Time Filtered Channel 12	20000	fT/cm
BX18	B Field X coil Time Filtered Channel 18	20000	fT/cm
BZ20	B-Field Z coil Raw channel 20	40000	fT/cm
BX20	B-Field X coil Raw channel 20	40000	fT/cm
X20	dB/dt X coil Raw channel 20	20000	pV/cm
Y20	dB/dt Y coil Raw channel 20	100000	pV/cm
Z20	dB/dt Z coil Raw channel 20	20000	pV/cm
X01	dB/dt X coil Raw channel 01	40000	pV/cm
XPL	Powerline Monitor	0.2	V/cm
XEFM	Earth Field Monitor	1	V/cm
XPRM	X Primary Field	0.4	V/cm
YPRM	Y Primary Field	133.3	V/cm
TPRM	Transmitter Primary Field	0.02	V/cm
CMAG	Coarse Total Field Magnetic Intensity	1000	nT/cm
FMAG	Fine Total Field Magnetic Intensity	50	nT/cm
4DIF	Magnetic 4th Difference Filtered	1	nT/cm
RADR	Radar Altimeter	50	ft/cm
BARO	Barometric Altimeter	200	ft/cm

Base Station Equipment

Magnetometer:	Scintrex CS-2 single cell cesium vapour, mounted in a magnetically quiet area, measuring the total intensity of the earth's magnetic field in units of 0.01 nT at intervals of 1 s, within a noise envelope of 0.20 nT.
GPS Receiver:	NovAtel OEM4, measuring all GPS channels, for up to 12 satellites.
Computer:	Laptop, Pentium model.
Data Logger:	CF1, SBBS (single board base station).

Field Office Equipment

Computer:	Dell Inspiron 9000 Series laptop.
Printer:	HP DeskJet 460 Mobile Printer.
DVD writer Drive:	Internal DVD+RW format.
Hard Drive:	500 GB Removable hard drive.

Survey Specifications

Northern 30Hz & 90Hz Blocks

Traverse Line Direction:	150° - 330°
Traverse Line Spacing:	800 m
Tie Line direction:	65° - 245°
Tie Line spacing:	15000 m

Southern 30Hz Extension Block

Traverse Line Direction:	65° - 245°
Traverse Line Spacing:	800 m
Tie Line direction:	150° - 330°
Tie Line spacing:	15000 m

Navigation:	Differential GPS. Traverse and tie line spacing was not to exceed the nominal by $> \pm 50$ m for ≥ 3 km.
Altitude:	The survey was flown at a mean terrain clearance of 120 m. Altitude was not to exceed 140 m over 3 km.
Magnetic Noise Levels:	The noise envelope on the magnetic data was not to exceed ± 0.25 nT over 3 km.
EM Noise Levels:	The noise envelope on the raw electromagnetic dB/dt X- and Z-coil channel 20 was not to exceed ± 3500 pT/s over a distance greater than 3 km as displayed on the raw analogue traces.

Field Crew

Data Processor:	S. Quinlan, J. Wollam, C. Swinwood, M. Noteboom
Pilots:	B. Gorell, T. Gaillot, D Wiens, P. MacNiel, K. Duncan, M. Melett
Electronics Operator:	M. Maierhofer, K. Lamirande, A. Aziz, A. Proulx
Engineer:	J. Robb, R. Constapel, R. Cameron

Production Statistics

Flying dates:	November 21 st - December 18 th 2007 and February 6 th - February 18 th 2008
Total production:	17,497 line kilometres
Number of production flights:	38
Days lost weather:	6

III

Quality Control and Compilation Procedures

In the field after each flight, all analogue records were examined as a preliminary assessment of the noise level of the recorded data. Altimeter deviations from the prescribed flying altitudes were also closely examined as well as the diurnal activity, as recorded on the base station.

All digital data were verified for validity and continuity. The data from the aircraft and base station were transferred to the PC's hard disk. Basic statistics were generated for each parameter recorded, these included: the minimum, maximum, and mean values; the standard deviation; and any null values located. All recorded parameters were edited for spikes or datum shifts, followed by final data verification via an interactive graphics screen with on-screen editing and interpolation routines.

The quality of the GPS navigation was controlled on a daily basis by recovering the flight path of the aircraft. The correction procedure employs the raw ranges from the base station to create improved models of clock error, atmospheric error, satellite orbit, and selective availability. These models are used to improve the conversion of aircraft raw ranges to aircraft position.

Checking all data for adherence to specifications was carried out in the field by the FUGRO AIRBORNE SURVEYS field geophysicist.

IV

Data Processing

Flight Path Recovery

GPS Recovery:	GPS positions recalculated from the recorded raw range data, and differentially corrected.
Projection:	Alberta 10 TM Projection
Datum:	NAD83
Central meridian:	115° West
False Easting:	500000 metres
False Northing:	0 metres
Scale factor:	0.9992

Altitude Data

Noise editing:	Alfatrim median filter used to eliminate the highest and lowest values from the statistical distribution of a 5 point sample window for the GPS elevation, and the two highest and lowest values from a 9 point sample window for the radar and barometric altimeters.
----------------	--

Base Station Diurnal Magnetics

Noise editing:	Alfatrim median filter used to eliminate the two highest and two lowest values from the statistical distribution of a 9 point sample window.
Culture editing:	Polynomial interpolation via a graphic screen editor.
Noise filtering:	Running average filter set to remove wavelengths less than 7 seconds.
Extraction of long wavelength component:	Running average filter to retain only wavelengths greater than 93 seconds (Northern 30Hz and 90Hz Blocks) and 463 seconds (Southern 30Hz Extension).

Airborne Magnetics

Lag correction:	3.2 s (Northern 30Hz & 90Hz Blocks), 3.6 s (Southern 30Hz Extension)
Noise editing:	4th difference editing routine set to remove spikes greater than 0.5 nT.
Noise filtering:	Triangular filter set to remove noise events having a wavelength less than 0.9 seconds.
Diurnal subtraction:	The long wavelength component of the diurnal was removed from the data with a base value of 58148 nT for the Northern 30Hz & 90Hz Blocks and

57590 nT for the Southern 30Hz Extension added back.

IGRF removal date: 2007.9 (Northern 30Hz & 90Hz Blocks), 2008.1 (Southern 30Hz Extension)

Gridding: The data was gridded using an akima routine with a grid cell size of 200 m.

Residual Magnetic Intensity

The residual magnetic intensity (RMI) is calculated from the total magnetic intensity (TMI), the diurnal, and the regional magnetic field. The TMI is measured in the aircraft, the diurnal is measured from the ground station and the regional magnetic field is calculated from the International Geomagnetic Reference Field (IGRF). The low frequency component of the diurnal is extracted from the filtered ground station data and removed from the TMI. The average of the diurnal is then added back in to obtain the resultant TMI. The regional magnetic field, calculated for the specific survey location and the time of the survey, is removed from the resultant TMI to obtain the RMI. The final step is to Tie line level and microlevel the RMI data.

Magnetic First Vertical Derivative

The first vertical derivative was calculated in the frequency domain from the final grid values to enhance subtleties related to geological structures.

A first vertical derivative has also been displayed in profile form. This was calculated from the line data by combining the transfer functions of the 1st vertical derivative and a low-pass filter (cut-off value = 0.045, roll-off value = 0.030). The low-pass filter was designed to attenuate the high frequencies representing non-geological signal, which are normally enhanced by the derivative operator. This parameter is also stored in the final digital archive.

Electromagnetics

dB/dt data

Lag correction: 3.0s

Data correction: The x, y and z-coil data were processed from the 20 raw channels recorded at 4 samples per second.

The following processing steps were applied to the dB/dt data from all coil sets:

- a) The data from channels 1 to 5 (on-time) and 6 to 20 (off-time) were corrected for drift in flight form (prior to cutting the recorded data back to the correct line limits) by passing a low order polynomial function through the baseline minima along each channel, via a graphic screen display;
- b) The data were edited for residual spheric spikes by examining the decay pattern of each individual EM transient. Bad decays (i.e. not fitting a normal exponential function) were deleted and replaced by interpolation;
- c) Noise filtering was done using an adaptive filter technique based on time domain triangular operators. Using a 2nd difference value to identify changes in gradient along each channel, minimal filtering (3 point convolution) is applied over the peaks of the anomalies, ranging in set increments up to a maximum amount of filtering in the resistive background areas (31 points for both the x-coil and the z-coil data);

- d) The filtered data from the x, y and z-coils were then re-sampled to a rate of 5 samples/s and combined into a common file for archiving.

B-field data

Processing steps: The processing of the B-Field data stream is very similar to the processing for the regular dB/dt data. The lag adjustment used was the same, followed by:

- 1) Drift adjustments;
- 2) Spike editing for spheric events;
- 3) Final noise filtering with an adaptive filter.

Note: The introduction of the B-Field data stream, as part of the GEOTEM[®] system, provides the explorationist with a more effective tool for exploration in a broader range of geological environments and for a larger class of target priorities.

The advantage of the B-Field data compared with the normal voltage data (dB/dt) are as follows:

1. A broader range of target conductance that the system is sensitive to. (The B-Field is sensitive to bodies with conductance as great as 100,000 Siemens);
2. Enhancement of the slowly decaying response of good conductors;
3. Suppression of rapidly decaying response of less conductive overburden;
4. Reduction in the effect of spherics on the data;
5. An enhanced ability to interpret anomalies due to conductors below thick conductive overburden;
6. Reduced dynamic range of the measured response (easier data processing and display).

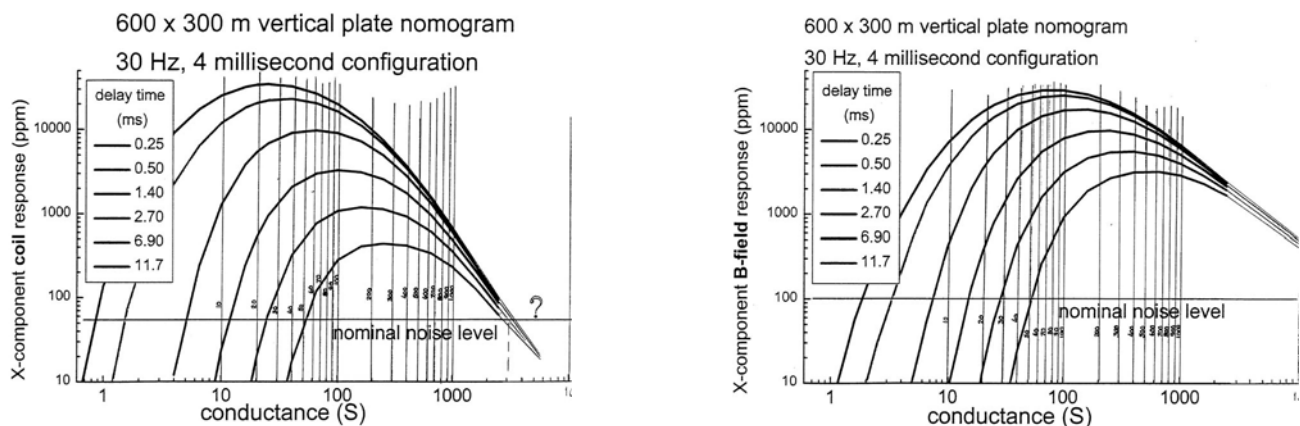


Figure 7: dB-dt vertical plate nomogram (left), B-field vertical plate nomogram (right).

Figure 7 displays the calculated vertical plate response for the GEOTEM[®] signal for the dB/dt and B-Field. For the dB/dt response, you will note that the amplitude of the early channel peaks at about 25 Siemens, and the late channels at about 250 Siemens. As the conductance exceeds 1000 Siemens the response curves quickly roll back into the noise level. For the B-Field response, the early channel amplitude peaks at about 80 Siemens and the late channel at about 550 Siemens. The projected extension of the graph in the direction of increasing conductance, where the response would roll back into the noise level, would be close to 100,000 Siemens. Thus, a strong conductor, having a conductance of several thousand Siemens, would be difficult to interpret on the dB/dt data, since the response would be mixed in with the background noise. However, this strong conductor would stand out clearly on the B-Field data, although it would have an unusual character, being a moderate to high amplitude response, exhibiting almost no decay.

In theory, the response from a super conductor (50,000 to 100,000 Siemens) would be seen on the B-Field data as a low amplitude, non-decaying anomaly, not visible in the off-time channels of the dB/dt stream. Caution must be exercised here, as this signature can also reflect a residual noise event in the B-Field data. In this situation, careful examination of the dB/dt on-time (in-pulse) data is required to resolve the ambiguity. If the feature were strictly a noise event, it would not be present in the dB/dt off-time data stream. This would locate the response at the resistive limit, and the mid in-pulse channel (normally identified as channel 3) would reflect little but background noise, or at best a weak negative peak. If, on the other hand, the feature does indeed reflect a superconductor, then this would locate the response at the inductive limit. In this situation, channel 3 of the dB/dt stream will be a mirror image of the transmitted pulse, i.e. a large negative.

Coil Oscillation Correction

The electromagnetic receiver sensor is housed in a bird which is towed behind the aircraft using a cable. Any changes in airspeed of the aircraft, variable crosswinds, or other turbulence will result in the bird swinging from side to side. This can result in the induction sensors inside the bird rotating about their mean orientation. The rotation is most marked when the air is particularly turbulent. The changes in orientation result in variable coupling of the induction coils to the primary and secondary fields. For example, if the sensor that is normally aligned to measure the x-axis response pitches upward, it will be measuring a response that will include a mixture of the X and Z component responses. The effect of coil oscillation on the data increases as the signal from the ground (conductivity) increases and may not be noticeable when flying over areas which are generally resistive. This becomes more of a concern when flying over highly conductive ground.

Using the changes in the coupling of the primary field, it is possible to estimate the pitch, roll and yaw of the receiver sensors. In the estimation process, it is assumed that a smoothed version of the primary field represents the primary field that would be measured when the sensors are in the mean orientation. The orientations are estimated using a non-linear inversion procedure, so erroneous orientations are sometimes obtained. These are reviewed and edited to insure smoothly varying values of orientations. These orientations can then be used to unmix the measured data to generate a response that would be measured if the sensors were in the correct orientation. For more information on this procedure, see:

http://www.fugroairborne.com/resources/technical_papers/airborne_em/atem.html

For the present dataset, the data from all 20 channels of dB/dt and B-Field parameters have been corrected for coil oscillation.

Apparent Resistivity

Fugro has developed an algorithm that converts the response in any measurement window (on- or off-time) into an apparent resistivity. This is performed using a look-up table that contains the response at a range of half-space resistivities and altimeter heights.

The apparent resistivity for the present dataset was calculated using dB/dt Z Coil channel 1 to provide the maximum information on the near-surface conductivity of the ground which, when combined with the magnetic signature, provides good geological mapping.

Resistivity-Depth-Images (RDI)

The Resistivity-Depth-Images (RDI) sections were calculated from the B Field Z-coil response, using an algorithm that converts the response in any measurement window (on- or off-time) into resistivity. For on-time data, it is not straightforward to identify which depth the apparent resistivity is associated, or identify any variation in resistivity with depth. Hence, the earth is assigned a constant value from surface to depth.

However, for the off-time data, the apparent resistivity can be associated with a depth. This depth, δ , depends on the magnetic permeability μ , the delay time t of the measurement window and the estimated apparent conductivity σ_{app} , i.e.

$$\delta = 0.55 \sqrt{\frac{t}{\mu \sigma_{app}}}$$

The electromagnetic method is most sensitive to conductive features so resistive features will be poorly resolved. The process of converting voltage data to resistivity as a function of depth tends to create smoother depth variations than can occur in reality.

The RDI sections, derived from each survey line, are created as individual grids. An additional set of RDI grids have been corrected for altitude variations such that the top of each section reflects the true terrain topography and it is these grids that are displayed on the multiplot profiles.

The RDI derived information is also provided as SEGY files and in a geosoft database as an array. The array consists of 151 levels of resistivity, from 0 to 300 metres depth. The resistivity values can be gridded to provide resistivity depth slices for desired depths. On this project, resistivity-depth slices were created for 10m, 30m, 60m, and 120m depth below the surface.

V

Final Products

Digital Archives

Line and grid data in the form of ASCII text files (*.xyz), Geosoft databases (*.gdb), SEG-Y Archives (*.sgy), Geosoft grids (*.grd), and ArcInfo grids (*.asc) have been written to DVD. The formats and layouts of these archives are further described in Appendix E (Data Archive Description). Hardcopies of all maps have been created as outlined below.

Maps

Colour

Scale: 1:250,000
Parameters: Residual Magnetic Intensity
First Vertical Derivative of the Residual Magnetic Intensity
Apparent Resistivity
Resistivity Depth Slice at 10m Depth
Resistivity Depth Slice at 30m Depth
Resistivity Depth Slice at 60m Depth
Resistivity Depth Slice at 120m Depth
Media/Copies: 1 Paper & 1 Digital (Geosoft .map format)

Profile Plots

Scale: 1:100,000
Parameters: Multi-channel presentation with 13 channels of both dB/dt and B-field X and Z-coil, Residual Magnetic Intensity, Calculated Magnetic Vertical Gradient, Radar Altimeter, EM Primary Field, Hz Monitor, Terrain, and Terrain adjusted Resistivity Depth Section.
Media/Copies: 1 Paper & 1 Digital (.emf format) of Each Line

Report

Media/Copies: 2 Paper & 1 digital (PDF format)

Appendix A

Fixed-Wing Airborne Electromagnetic Systems

FIXED-WING AIRBORNE ELECTROMAGNETIC SYSTEMS

General

The operation of a towed-bird time-domain electromagnetic system (EM) involves the measurement of decaying secondary electromagnetic fields induced in the ground by a series of short current pulses generated from an aircraft-mounted transmitter. Variations in the decay characteristics of the secondary field (sampled and displayed as windows) are analyzed and interpreted to provide information about the subsurface geology. The response of such a system utilizing a vertical-axis transmitter dipole and a multicomponent receiver coil has been documented by various authors including Smith and Keating (1991, *Geophysics* v.61, p. 74-81). To download this paper, see the website

http://www.fugroairborne.com/resources/technical_papers/airborne_em/multicomponent_EM.html

A number of factors combine to give the fixed-wing platforms excellent signal-to-noise ratio and depth of penetration: 1) the principle of sampling the induced secondary field in the absence of the primary field (during the “off-time”), 2) the large separation of the receiver coils from the transmitter, 3) the large dipole moment and 4) the power available from the fixed wing platform. Such a system is also relatively free of noise due to air turbulence. However, also sampling in the “on-time” can result in excellent sensitivity for mapping very resistive features and very conductive features, and thus mapping the geology (Annan et al., 1991, *Geophysics* v.61, p. 93-99) (for download see http://www.fugroairborne.com/resources/technical_papers/airborne_em/resistive_limit.html). The on-time and off-time parts of the half-cycle waveform are shown in Figure 1.

Through free-air model studies using the University of Toronto's Plate and Layered Earth programs it may be shown that the “depth of investigation” depends upon the geometry of the target. Typical depth limits would be 400 m below surface for a homogeneous half-space, 550 m for a flat-lying inductively thin sheet or 300 m for a large vertical plate conductor. These depth estimates are based on the assumptions that the overlying or surrounding material is resistive.

The method also offers very good discrimination of conductor geometry. This ability to distinguish between flat-lying and vertical conductors combined with excellent depth penetration results in good differentiation of bedrock conductors from surficial conductors (Appendix C).

Methodology

The Fugro time-domain fixed-wing electromagnetic systems (GEOTEM[®] and MEGATEM[®]) incorporate a high-speed digital EM receiver. The primary electromagnetic pulses are created by a series of discontinuous sinusoidal current pulses fed into a three- or six-turn transmitting loop surrounding the aircraft and fixed to the nose, tail and wing tips. The base frequency rate is selectable: 25, 30, 75, 90, 125, 150, 225 and 270 Hz. The length of the pulse can be tailored to suit the targets. Standard pulse widths available are 0.6, 1.0, 2.0 and 4.0 ms. The available off-time can be selected to be as great as 16 ms. The dipole moment depends on the pulse width, base frequency and aircraft used on the survey. Example pulse widths and off-time windows at different base frequencies are shown on Figure 2. The specific dipole moment, waveform and gate settings for this survey are given in the main body of the report.

The receiver is a three-axis (x,y,z) induction coil. In the fixed-wing systems, this is towed by the aircraft on a 135-metre cable. The tow cable is non-magnetic, to reduce noise levels. The usual mean terrain clearance for the aircraft is 120 m with the EM bird being situated nominally 50 m

below and 130 m behind the aircraft (see Figure 3).

Each primary pulse causes decaying eddy currents in the ground to produce a secondary magnetic field. This secondary magnetic field, in turn, induces a voltage in the receiver coils, which is the electromagnetic response. Good conductors decay slowly, while poor conductors more rapidly (see Figure 1).

The measured signals pass through anti-aliasing filters and are then digitized with an A/D converter at sampling rates of up to 80 kHz. The digital data flows from the A/D converter into an industrial-grade computer where the data are processed to reduce the noise.

Operations, which are carried out in the receiver, are:

1. *Primary-field removal:* In addition to measuring the secondary response from the ground, the receiver sensor coils also measure the primary response from the transmitter. During flight, the bird position and orientation changes slightly, and this has a very strong effect on the magnitude of the total response (primary plus secondary) measured at the receiver coils. The variable primary field response is distracting because it is unrelated to the ground response. The primary field can be measured by flying at an altitude such that no ground response is measurable. These calibration signals are used to define the shape of the primary waveform. By definition this primary field includes the response of the current in the transmitter loop plus the response of any slowly decaying eddy currents induced in the aircraft. We assume that the shape of the primary will be unchanged as the bird position changes, but that the amplitude will vary. The primary-field-removal procedure involves solving for the amplitude of the primary field in the measured response and removing this from the total response to leave a secondary response. Note that this procedure removes any (“in-phase”) response from the ground that has the same shape as the primary field. For more details on the primary-field removal procedure, see the paper on the web-site http://www.fugroairborne.com/resources/technical_papers/airborne_em/inphase.html
2. *Digital Stacking:* Stacking is carried out to reduce the effect of broadband noise on the data.
3. *Windowing of data:* The digital receiver samples the secondary and primary electromagnetic field at 64, 128 or 384 points per EM pulse and windows the signal in up to 20 time gates whose centres and widths are software selectable and which may be placed anywhere within or outside the transmitter pulse. This flexibility offers the advantage of arranging the gates to suit the goals of a particular survey, ensuring that the signal is appropriately sampled through its entire dynamic range. Example off-time windows are shown on Figure 1.
4. *Power Line Filtering:* Digital comb filters are applied to the data during real-time processing to remove power line interference while leaving the EM signal undisturbed. The RMS power line voltage (at all harmonics in the receiver passband) are computed, displayed and recorded for each data stack.
5. *Primary Field:* The primary field at the towed sensor is measured for each stack and recorded as a separate data channel to assess the variation in coupling between the transmitter and the towed sensor induced by changes in system geometry.
6. *Earth Field Monitor:* A monitor of sensor coil motion noise induced by coil motion in the Earth's magnetic field is also extracted in the course of the real-time digital processing. This information is also displayed on the real-time chart as well as being recorded for post-survey

diagnostic processes.

7. *Noise/Performance:* A monitor computes the RMS signal level on an early off-time window over a running 10-second window. This monitor provides a measure of noise levels in areas of low ground response. This information is printed at regular intervals on the side of the flight record and is recorded for every data stack.

One of the major roles of the digital receiver is to provide diagnostic information on system functions and to allow for identification of noise events, such as sferics, which may be selectively removed from the EM signal. The high digital sampling rate yields maximum resolution of the secondary field.

System Hardware

The airborne EM system consists of the aircraft, the on-board hardware, and the software packages controlling the hardware. The software packages in the data acquisition system and in the EM receiver were developed in-house, as were, certain elements of the hardware (transmitter, system timing clock, towed-bird sensor system).

Transmitter System

The transmitter system drives high-current pulses of an appropriate shape and duration through the coils mounted on the aircraft.

System Timing Clock

This subsystem provides appropriate timing signals to the transmitter, and also to the analog-to-digital converter, in order to produce output pulses and capture the ground response. All systems are synchronized to GPS time.

Towed-Bird Systems

A three-axis induction coil sensor is mounted inside a towed bird, which is typically 50 metres below and 130 metres behind the aircraft. (A second bird, housing the magnetometer sensor, is typically 50 metres below and 80 metres behind the aircraft.)

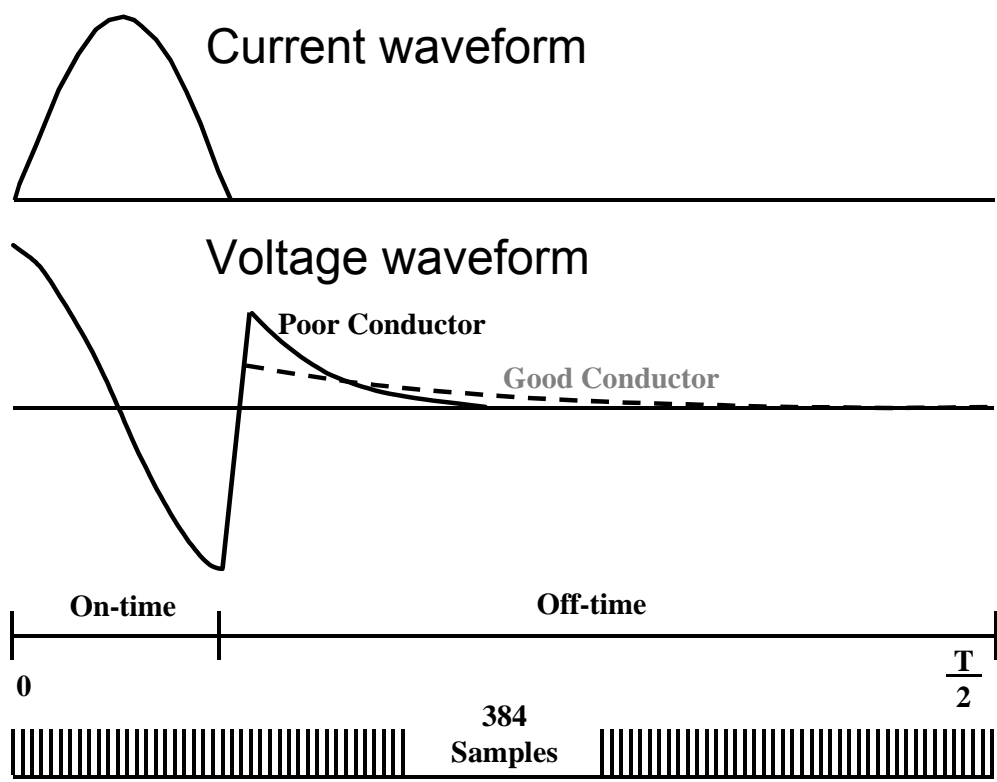


Figure 1. The waveforms and data sampling throughout the transmitter on- and off-time.

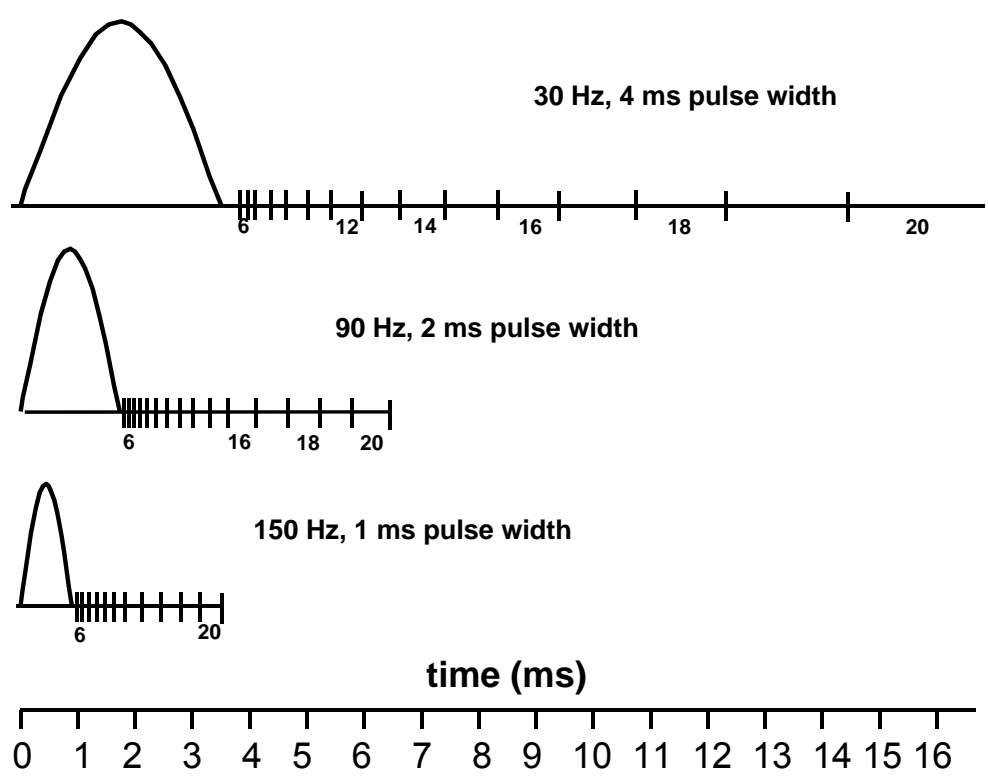


Figure 2. Pulse width and measurement windows for 150, 90 and 30 Hz base frequencies.

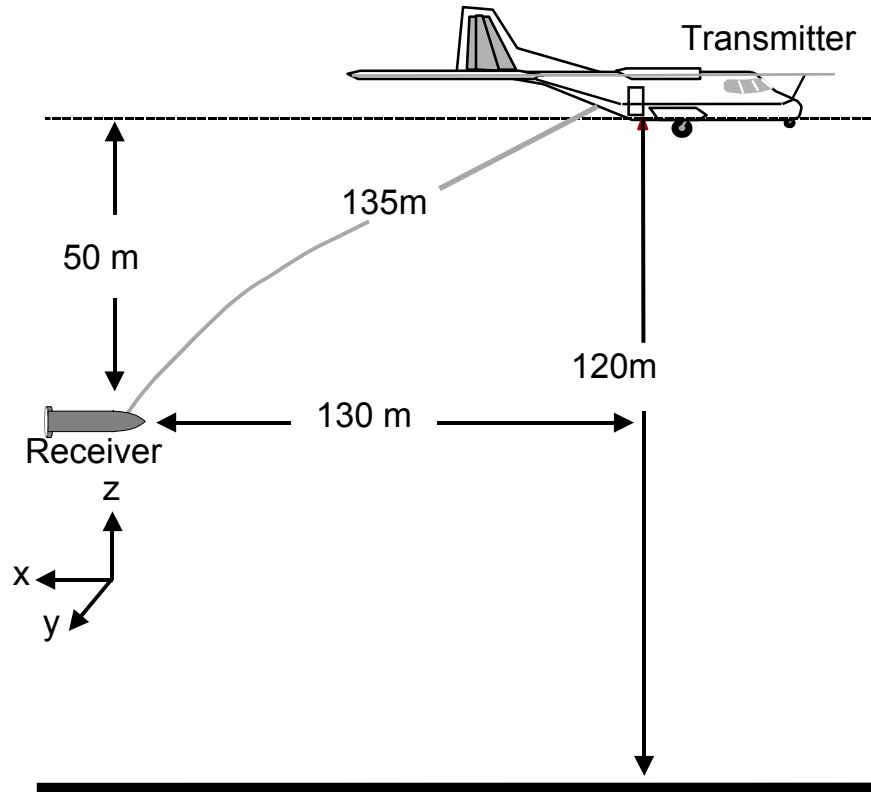


Figure 3. Nominal geometry of the fixed-wing electromagnetic system.

Appendix B

Airborne Transient EM Interpretation

Interpretation of transient electromagnetic data

Introduction

The basis of the transient electromagnetic (EM) geophysical surveying technique relies on the premise that changes in the primary EM field produced in the transmitting loop will result in eddy currents being generated in any conductors in the ground. The eddy currents then decay to produce a secondary EM field that may be sensed in the receiver coil.

MEGATEM[®] and GEOTEM[®] are airborne transient (or time-domain) towed-bird EM systems incorporating a high-speed digital receiver which records the secondary field response with a high degree of accuracy. Most often the earth's total magnetic field is recorded concurrently.

Although the approach to interpretation varies from one survey to another depending on the type of data presentation, objectives and local conditions, the following generalizations may provide the reader with some helpful background information.

The main purpose of the interpretation is to determine the probable origin of the responses detected during the survey and to suggest recommendations for further exploration. This is possible through an objective analysis of all characteristics of the different types of responses and associated magnetic anomalies, if any. If possible the airborne results are compared to other available data. Certitude is seldom reached, but a high probability is achieved in identifying the causes in most cases. One of the most difficult problems is usually the differentiation between surface conductor responses and bedrock conductor responses.

Types Of Conductors

Bedrock Conductors

The different types of bedrock conductors normally encountered are the following:

1. Graphites. Graphitic horizons (including a large variety of carbonaceous rocks) occur in sedimentary formations of the Precambrian as well as in volcanic tuffs, often concentrated in shear zones. They correspond generally to long, multiple conductors lying in parallel bands. They have no magnetic expression unless associated with pyrrhotite or magnetite. Their conductivity is variable but generally high.
2. Massive sulphides. Massive sulphide deposits usually manifest themselves as short conductors of high conductivity, often with a coincident magnetic anomaly. Some massive sulphides, however, are not magnetic, others are not very conductive (discontinuous mineralization or sphalerite), and some may be located among formational conductors so that one must not be too rigid in applying the selection criteria.

In addition, there are syngenetic sulphides whose conductive pattern may be similar to that of graphitic horizons but these are generally not as prevalent as graphites.

3. Magnetite and some serpentized ultrabasics. These rocks are conductive and very magnetic.
4. Manganese oxides. This mineralization may give rise to a weak EM response.

Surficial Conductors

1. Beds of clay and alluvium, some swamps, and brackish ground water are usually poorly conductive to moderately conductive.
2. Lateritic formations, residual soils and the weathered layer of the bedrock may cause surface anomalous zones, the conductivity of which is generally low to medium but can occasionally be high. Their presence is often related to the underlying bedrock.

Cultural Conductors (Man-Made)

3. Power lines. These frequently, but not always, produce a conductive type of response. In the case when the power line comb filter does not remove the radiated field, the anomalous response can exhibit phase changes between different windows. In the case of current induced by the EM system in a grounded wire, or steel pylon, the anomaly may look very much like a bedrock conductor.
4. Grounded fences or pipelines. These will invariably produce responses much like a bedrock conductor. Whenever they cannot be identified positively, a ground check is recommended.
5. General culture. Other localized sources such as certain buildings, bridges, irrigation systems, tailings ponds etc., may produce EM anomalies. Their instances, however, are rare and often they can be identified on the visual path recovery system.

Analysis Of The Conductors

The conductance of a plate is generally estimated assuming the plate is vertical and 600m by 300m. Hence the conductance alone is not generally a decisive criterion in the analysis of a conductor. In particular, one should note:

- Its shape and size,
- All local variations of characteristics within a conductive zone,
- Any associated geophysical parameter (e.g. magnetics),
- The geological environment,
- The structural context, and
- The pattern of surrounding conductors.

The first objective of the interpretation is to classify each conductive zone according to one of the three categories which best defines its probable origin. The categories are cultural, surficial and bedrock. A second objective is to assign to each zone a priority rating as to its potential as an economic prospect.

Bedrock Conductors

This category comprises those anomalies that cannot be classified according to the criteria established for cultural and surficial responses. It is difficult to assign a universal set of values that typify bedrock conductivity because any individual zone or anomaly might exhibit some, but not all, of these values and still be a bedrock conductor. The following criteria are considered indicative of a bedrock conductor:

1. An intermediate to high conductivity identified by a response with slow decay, with an anomalous response present in the later windows.
2. For vertical conductors, the anomaly should be narrow, relatively symmetrical, with a well-defined x-component peak.
3. If the conductor is thin, the response should show the characteristics evident in Figures 2 to 4. These figures illustrate how the response varies as a function of the flight direction for three bodies with different dips. The alternating character of the response as a result of line direction can be diagnostic of conductor geometry.
4. A small to intermediate amplitude. Large amplitudes are normally associated with surficial conductors. The amplitude varies according to the depth of the source.
5. A degree of continuity of the EM characteristics across several lines.
6. An associated magnetic response of similar dimensions. One should note, however, that those magnetic rocks that weather to produce a conductive upper layer would possess this magnetic association. In the absence of one or more of the characteristics defined in 1, 2, 3, 4 and 5, the related magnetic response cannot be considered significant.

Most obvious bedrock conductors occur in long, relatively monotonous, sometimes multiple zones following formational strike. Graphitic material is usually the most probable source. Massive syngenetic sulphides extending for many kilometres are known in nature but, in general, they are not common. Long formational structures associated with a strong magnetic expression may be indicative of banded iron formations.

In summary, a bedrock conductor reflecting the presence of a massive sulphide would normally exhibit the following characteristics:

- A high conductivity,
- A good anomaly shape (narrow and well-defined peak),
- A small to intermediate amplitude,
- An isolated setting,
- A short strike length (in general, not exceeding one kilometre), and
- Preferably, with a localized magnetic anomaly of matching dimensions.

Surficial Conductors

This term is used for geological conductors in the overburden, either glacial or residual in origin, and in the weathered layer of the bedrock. Most surficial conductors are probably caused by clay minerals. In some environments the presence of salts will contribute to the conductivity. Other possible electrolytic conductors are residual soils, swamps, brackish ground water and alluvium such as lake or river-bottom deposits, flood plains and estuaries.

Normally, most surficial materials have low to intermediate conductivity so they are not easily mistaken for highly conductive bedrock features. Also, many of them are wide and their anomaly shapes are typical of broad horizontal sheets.

When surficial conductivity is high it is usually still possible to distinguish between a horizontal plate

(more likely to be surficial material) and a vertical body (more likely to be a bedrock source) thanks to the asymmetry of the fixed-wing system responses observed at the edges of a broad conductor when flying adjacent lines in opposite directions. The configuration of the system is such that the response recorded at the leading edge is more pronounced than that registered at the trailing edge. Figure 1 illustrates the "edge effect". In practice there are many variations on this very diagnostic phenomenon.

One of the more ambiguous situations as to the true source of the response is when surface conductivity is related to bedrock lithology as for example, surface alteration of an underlying bedrock unit. At times, it is also difficult to distinguish between a weak conductor within the bedrock (e.g. near-massive sulphides) and a surficial source.

In the search for massive sulphides or other bedrock targets, surficial conductivity is generally considered as interference but there are situations where the interpretation of surficial-type conductors is the primary goal. When soils, weathered or altered products are conductive, and in-situ, the responses are a very useful aid to geologic mapping. Shears and faults are often identified by weak, usually narrow, anomalies.

Analysis of surficial conductivity can be used in the exploration for such features as lignite deposits, kimberlites, paleochannels and ground water. In coastal or arid areas, surficial responses may serve to define the limits of fresh, brackish and salty water.

Cultural Conductors

The majority of cultural anomalies occurs along roads and is accompanied by a response on the power line monitor. (This monitor is set to 50 or 60 Hz, depending on the local power grid.) In some cases, the current induced in the power line results in anomalies that could be mistaken for bedrock responses. There are also some power lines that have no response whatsoever.

The power line monitor, of course, is of great assistance in identifying cultural anomalies of this type. It is important to note, however, that geological conductors in the vicinity of power lines may exhibit a weak response on the monitor because of current induction via the earth.

Fences, pipelines, communication lines, railways and other man-made conductors can give rise to responses, the strength of which will depend on the grounding of these objects.

Another facet of this analysis is the line-to-line comparison of anomaly character along suspected man-made conductors. In general, the amplitude, the rate of decay, and the anomaly width should not vary a great deal along any one conductor, except for the change in amplitude related to terrain clearance variation. A marked departure from the average response character along any given feature gives rise to the possibility of a second conductor.

In most cases a visual examination of the site will suffice to verify the presence of a man-made conductor. If a second conductor is suspected the ground check is more difficult to accomplish. The object would be to determine if there is (i) a change in the man-made construction, (ii) a difference in the grounding conditions, (iii) a second cultural source, or (iv) if there is, indeed, a geological conductor in addition to the known man-made source.

The selection of targets from within extensive (formational) belts is much more difficult than in the case of isolated conductors. Local variations in the EM characteristics, such as in the amplitude,

decay, shape etc., can be used as evidence for a relatively localized occurrence. Changes in the character of the EM responses, however, may be simply reflecting differences in the conductive formations themselves rather than indicating the presence of massive sulphides and, for this reason, the degree of confidence is reduced.

Another useful guide for identifying localized variations within formational conductors is to examine the magnetic data in map or image form. Further study of the magnetic data can reveal the presence of faults, contacts, and other features, which, in turn, help define areas of potential economic interest.

Finally, once ground investigations begin, it must be remembered that the continual comparison of ground knowledge to the airborne information is an essential step in maximizing the usefulness of the airborne EM data.

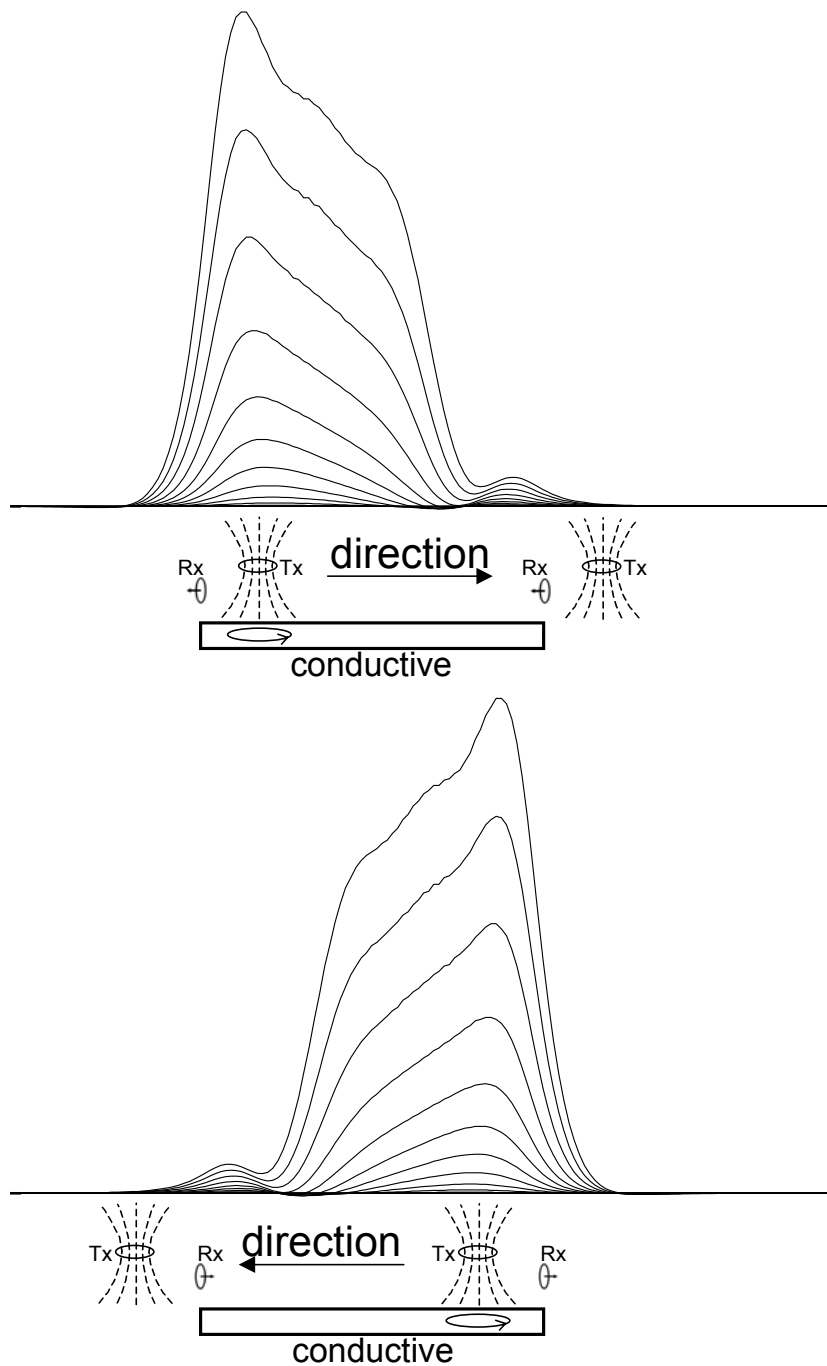


Figure 1. Illustration of how the x-component response varies depending on the flight direction. When the receiver flies onto the conductor, the transmitter is over the conductor and current is induced in the conductive material, resulting in a large response. When the receiver flies off the conductor, the transmitter is not over conductive material, so the response is small.

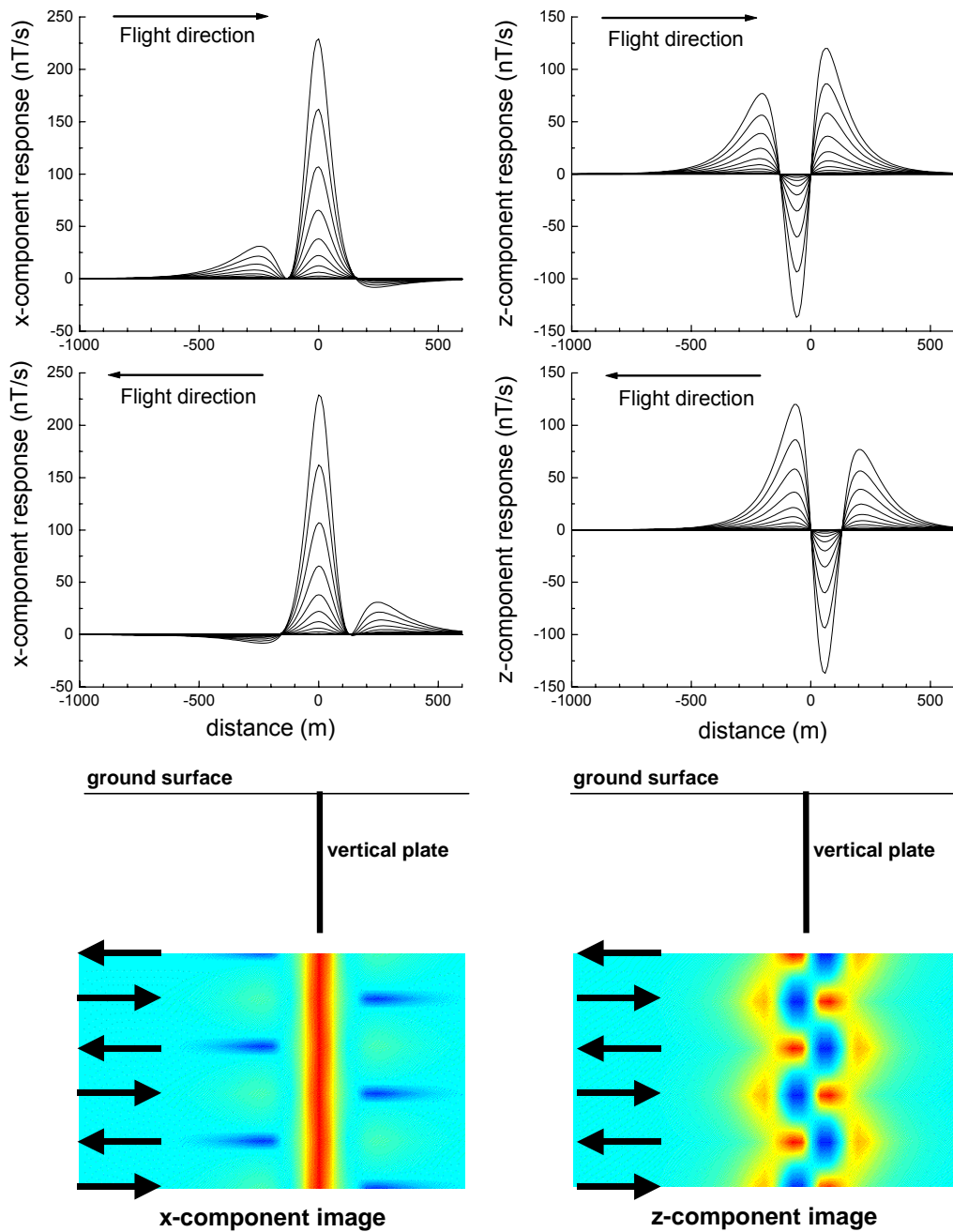


Figure 2. The response over a vertical plate. The left panels show the x-component, the right panels the z component. The top is flying left to right, the middle is right to left, the bottom is a plan image with the alternating flight directions shown with arrows.

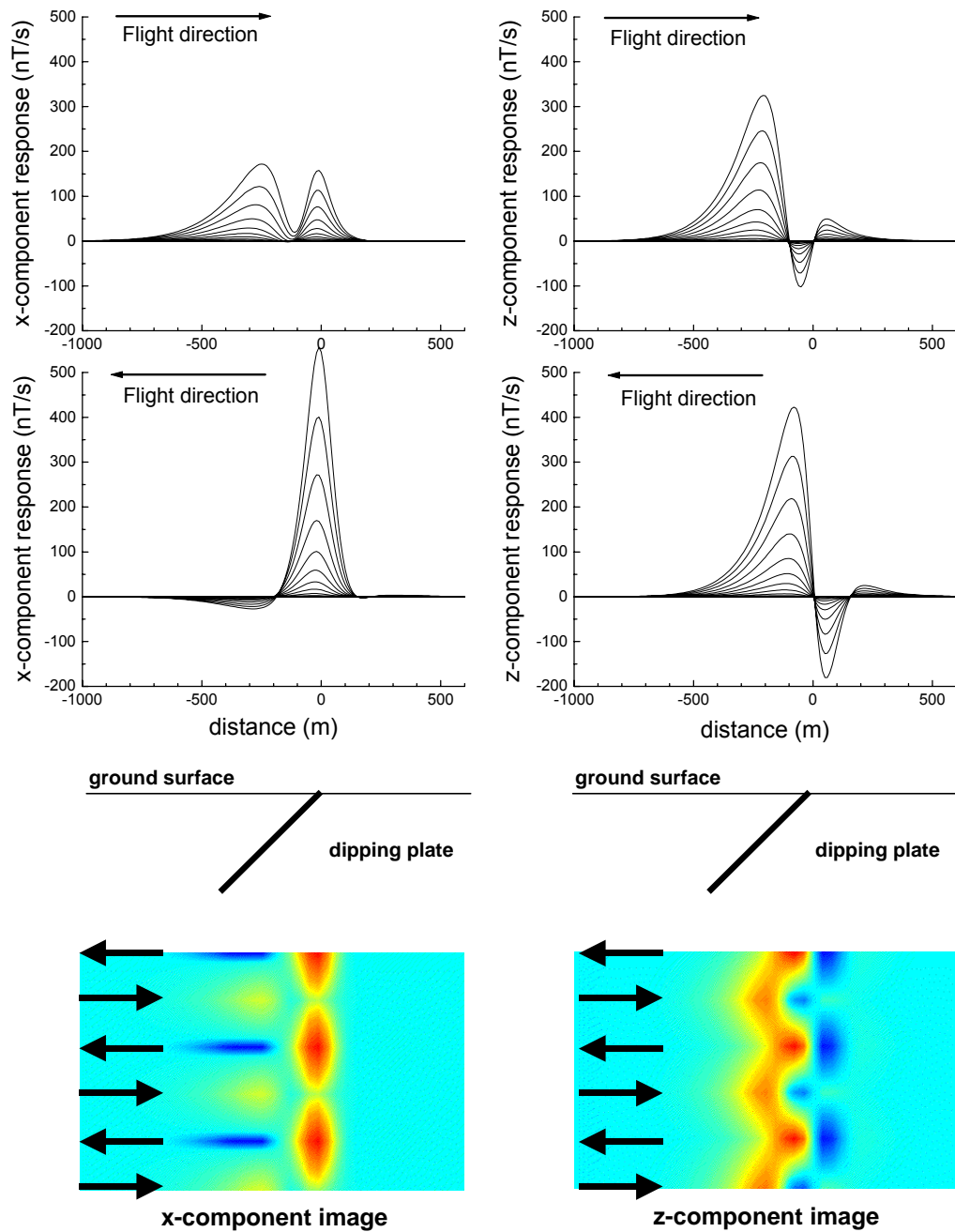


Figure 3. The response over a 45 degree dipping plate. The left panels show the x-component, the right panels the z component. The top is flying left to right, the middle is right to left, the bottom is a plan image with the alternating flight directions shown with arrows.

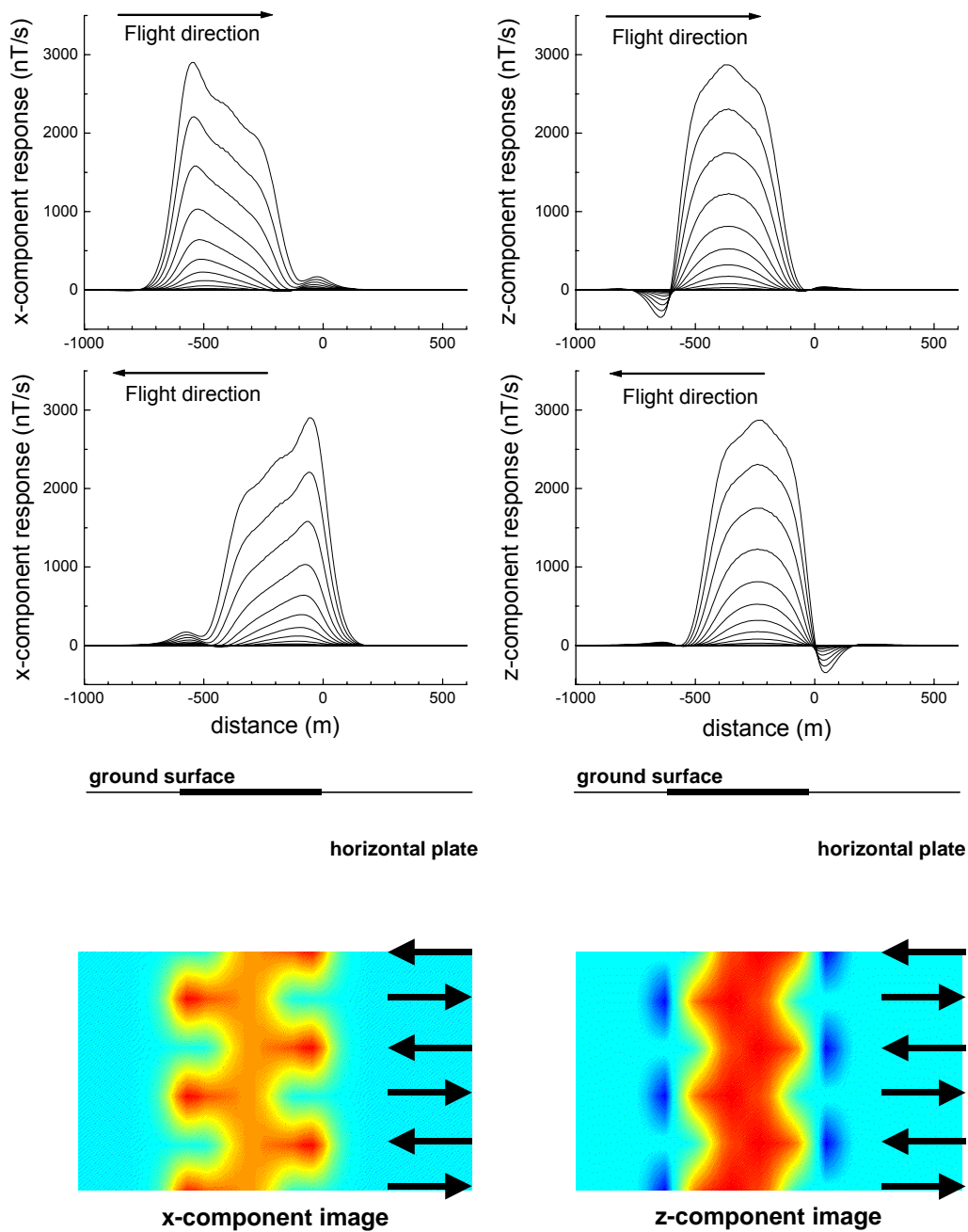


Figure 4. The response over a horizontal plate. The left panels show the x-component, the right panels the z component. The top is flying left to right, the middle is right to left, the bottom is a plan image with the alternating flight directions shown with arrows.

Appendix C

Multicomponent Modeling

Multicomponent fixed-wing airborne EM modeling

PLATE MODELING

The PLATE program has been used to generate synthetic responses over a number of plate models with varying depth of burial (0, 150 and 300 m) and dips (0, 45, 90 and 135 degrees). The geometry assumed for the fixed-wing airborne EM system is shown on the following page (Figure 1), and the transmitter waveform on the subsequent page (Figure 2). In these models, the receiver is 130 m behind and 50 m below the transmitter center.

In all cases the plate has a strike length of 600m, with a strike direction into the page. The width of the plate is 300m. As the flight path traverses the center of the plate, the y component is zero and has not been plotted.

The conductance of the plate is 20 S. In cases when the conductance is different, an indication of how the amplitudes may vary can be obtained from the nomogram included (Figure 3).

In the following profile plots (Figure 4 to 15) the plotting point is the receiver location and all of the component values are in nT/s, assuming a transmitter dipole moment of 900 000 Am². If the dipole moment is larger or smaller than 900 000 Am², then the response would be scaled up or down appropriately.

In the following profile plots (Figure 4 to 15) all components are in nT/s, for a transmitter dipole moment of 900 000 Am². If the dipole moment is larger or smaller, then the response should be scaled up or down appropriately.

The plotting point is the receiver location.

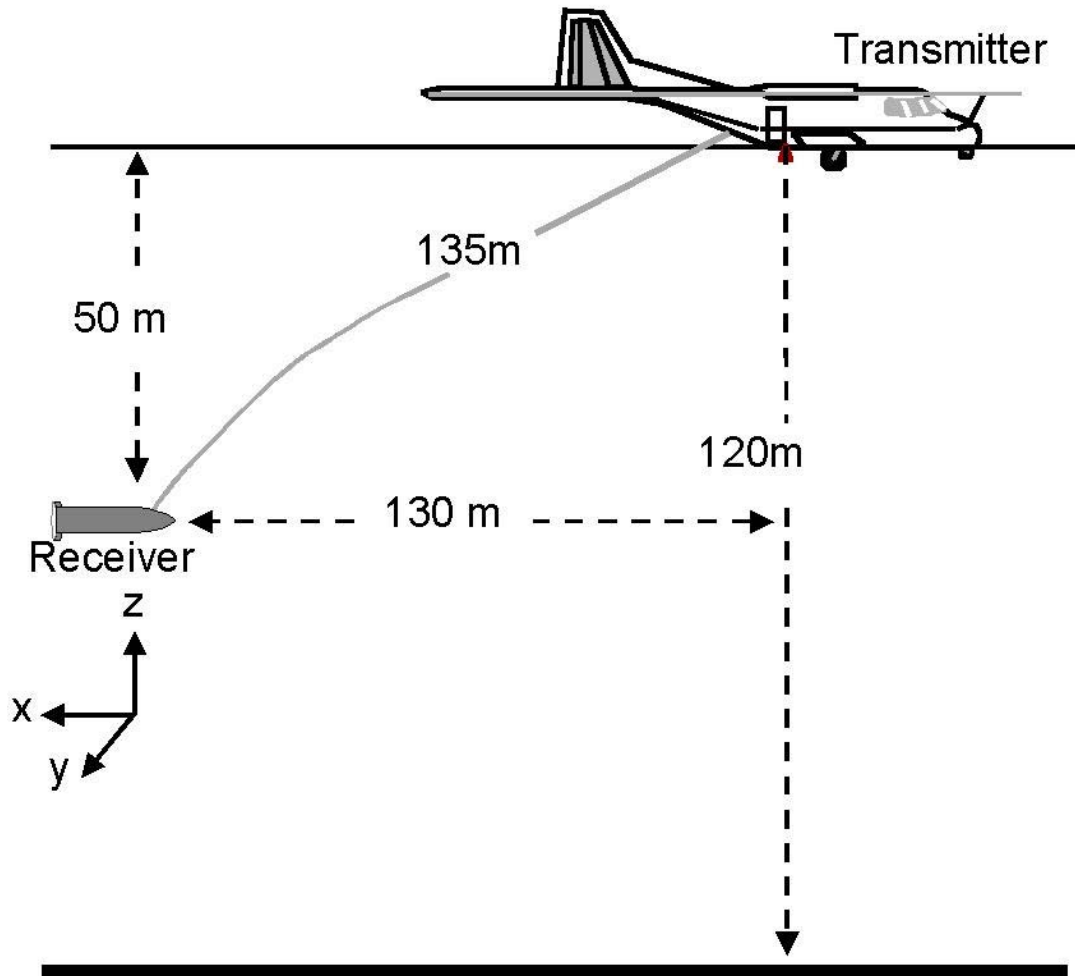


Figure 1. Nominal geometry of the MEGATEM/GEOTEM system.

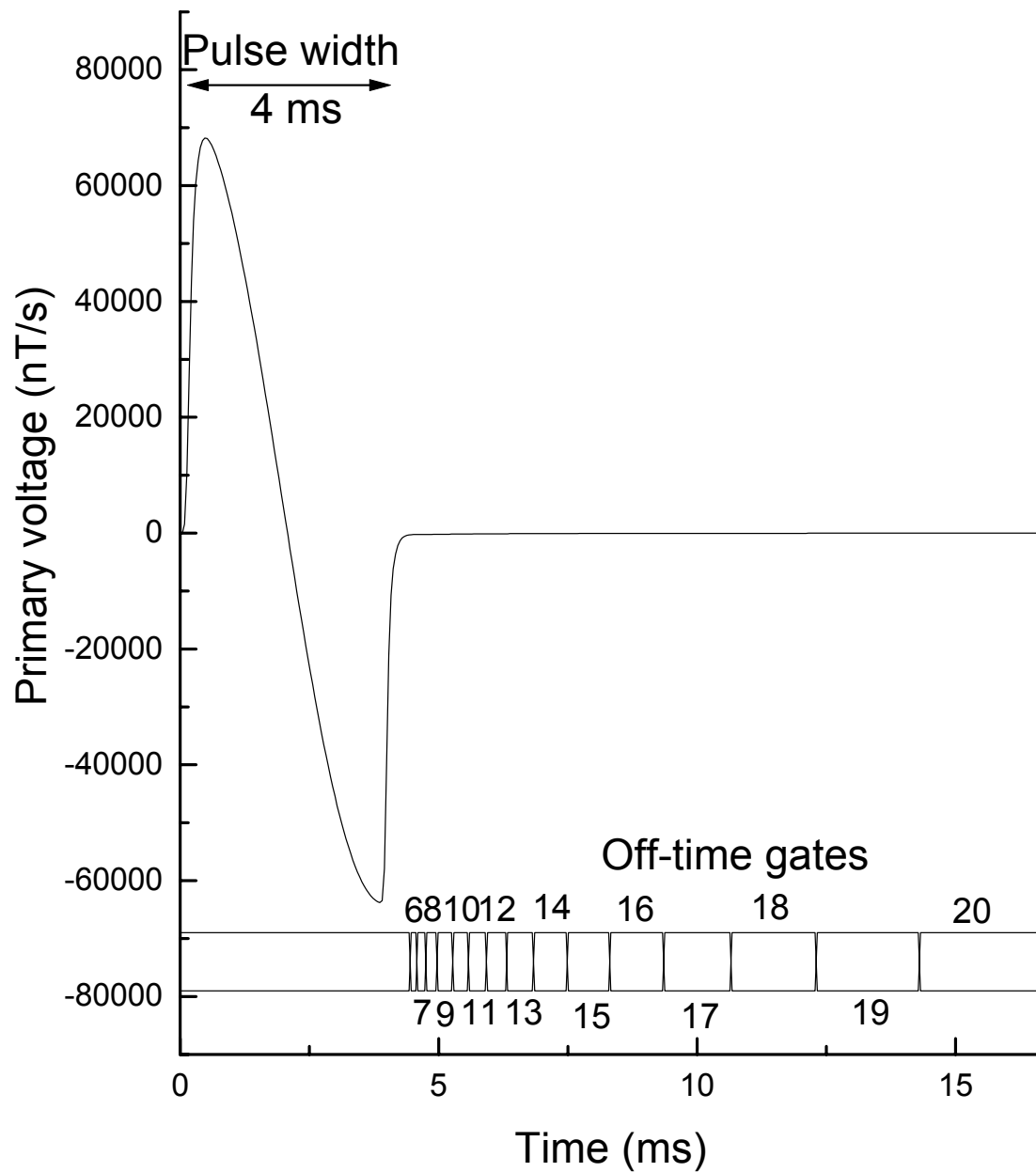


Figure 2. Theoretical transmitter waveform response in the receiver.

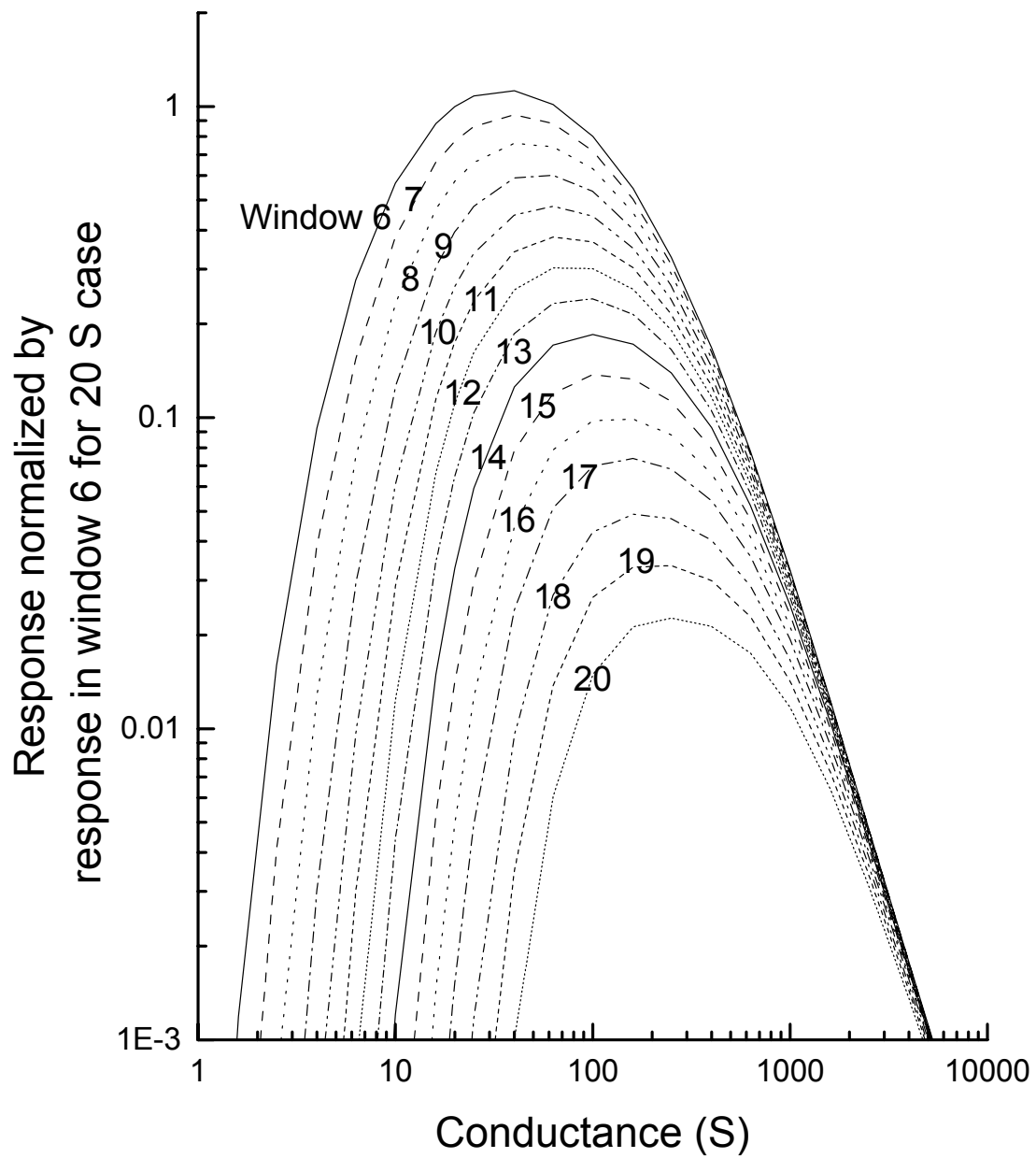


Figure 3. Nomogram for windows 6-20 normalized to a response from a 20 Siemen conductor in window 6.

Plate: dip=0; depth=0

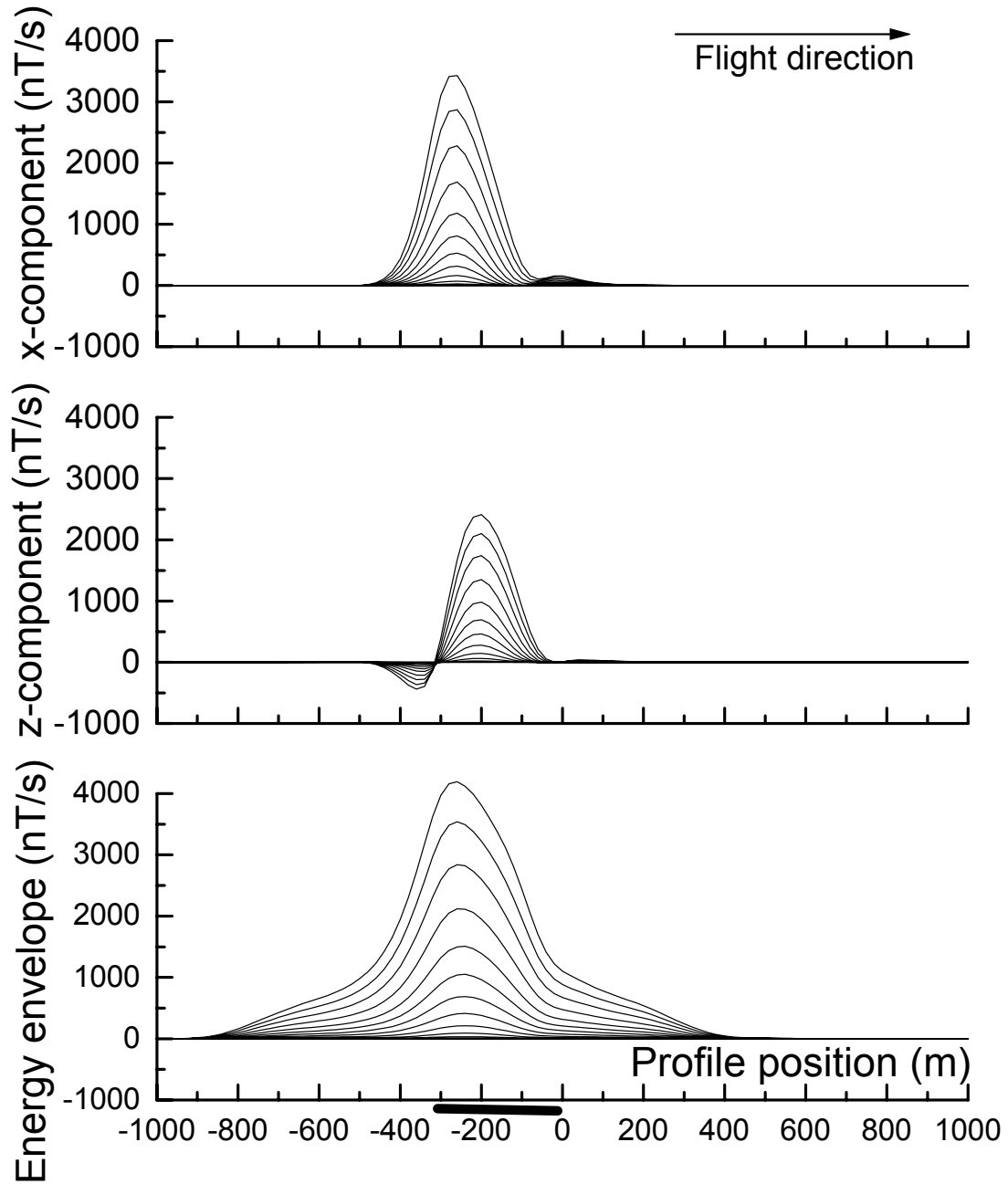


Figure 4.

Plate: dip=0; depth=150

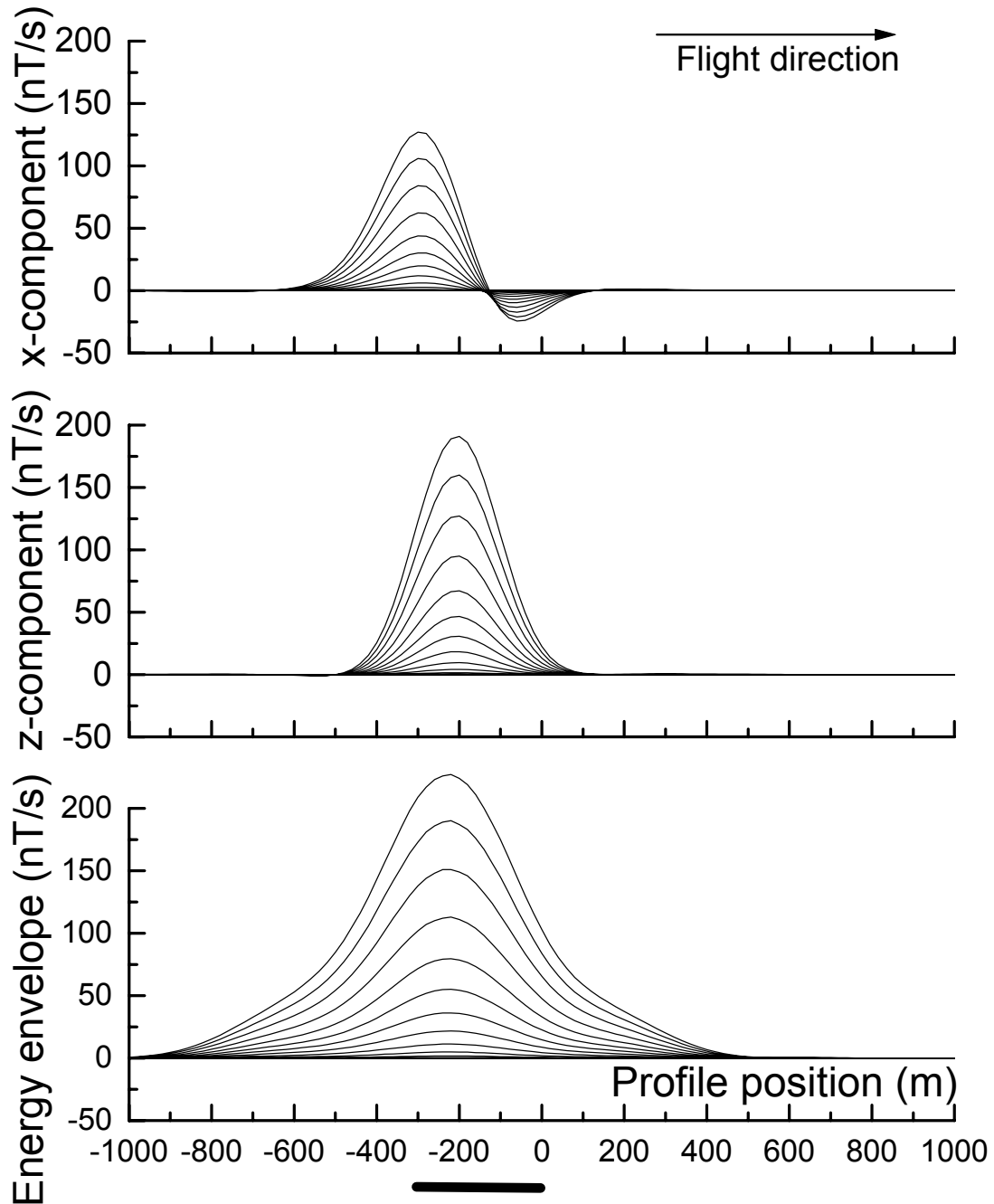


Figure 5.

Plate: dip=0; depth=300

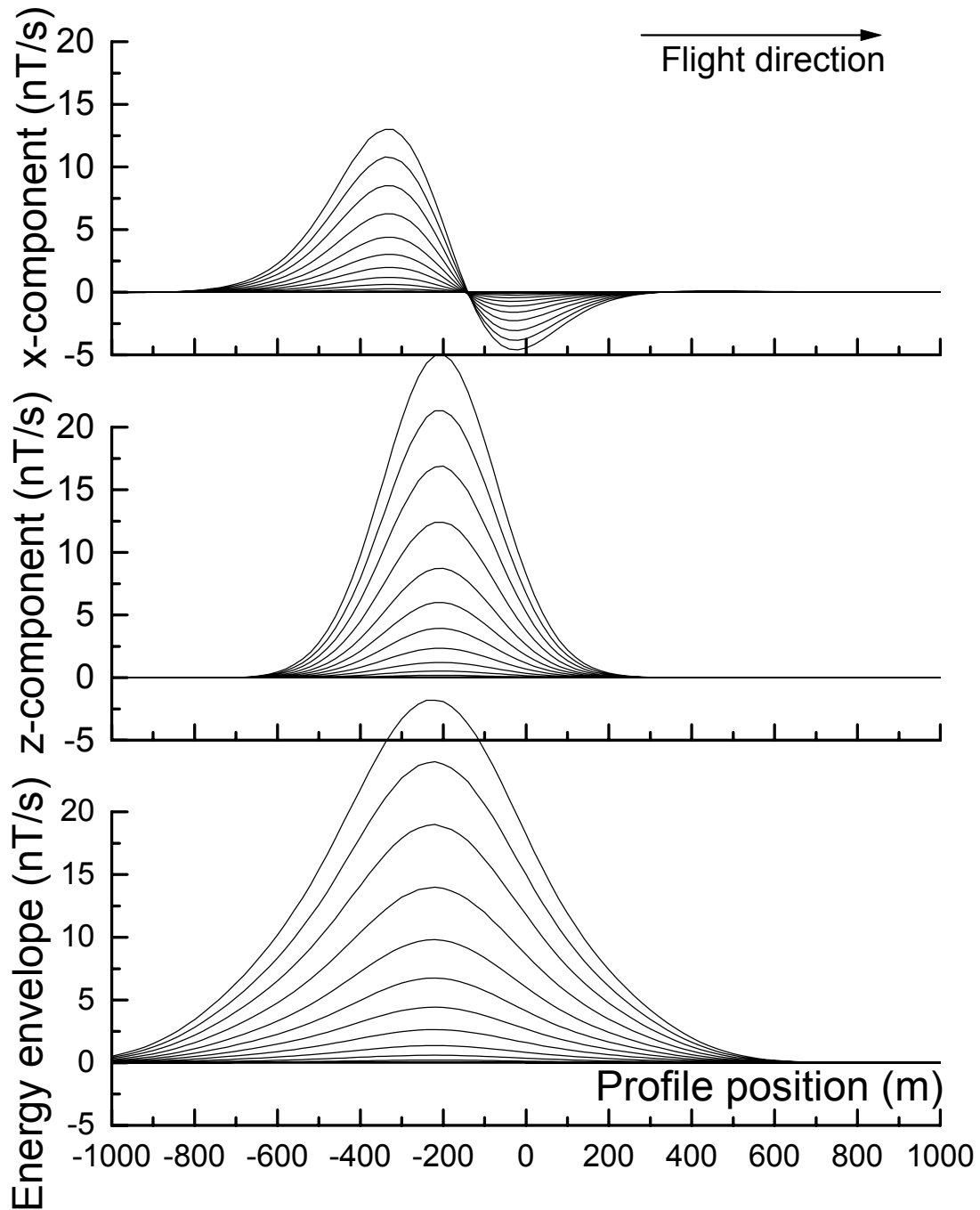


Figure 6.

Plate: dip=45; depth=0

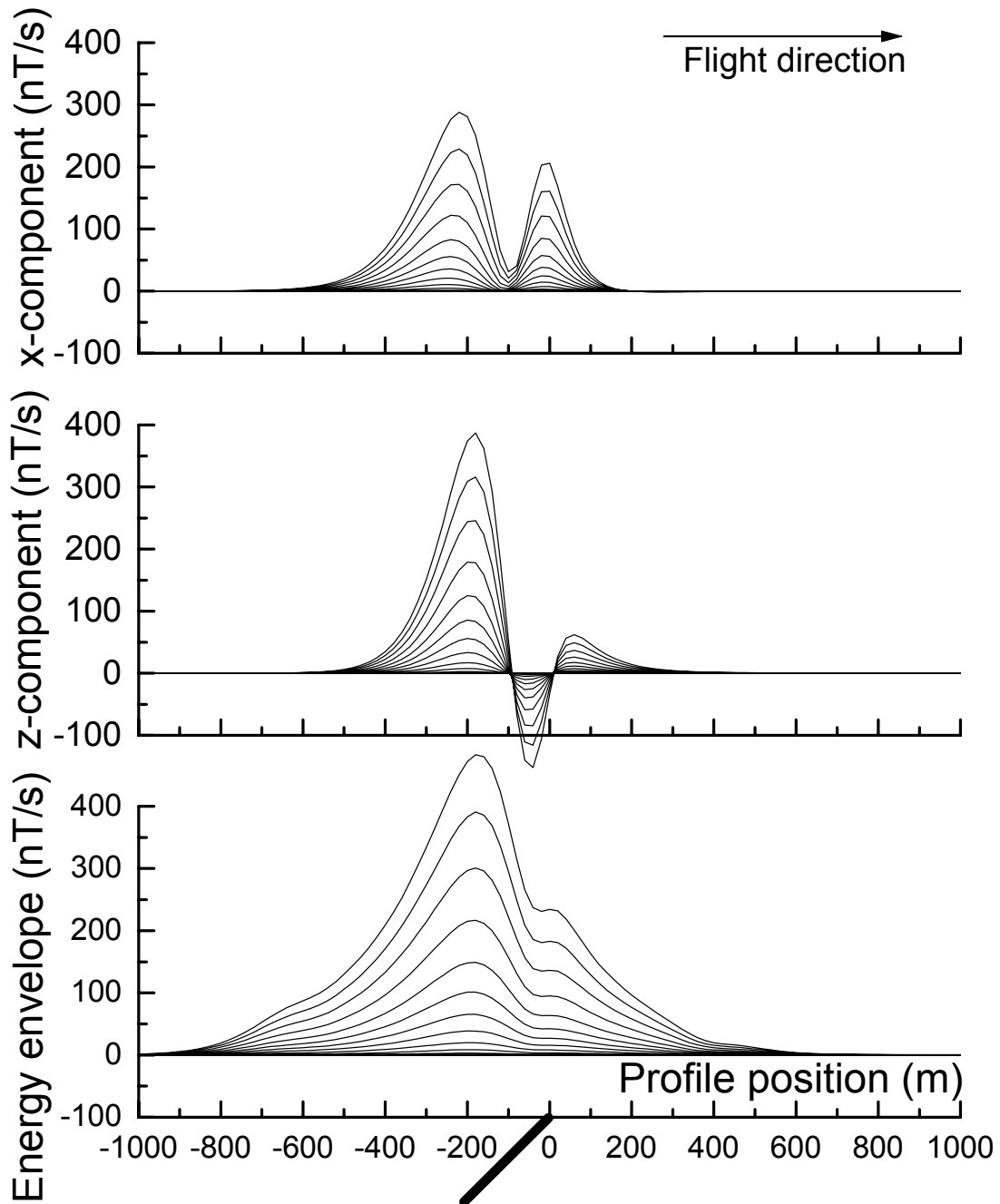


Figure 7.

Plate: dip=45; depth=150

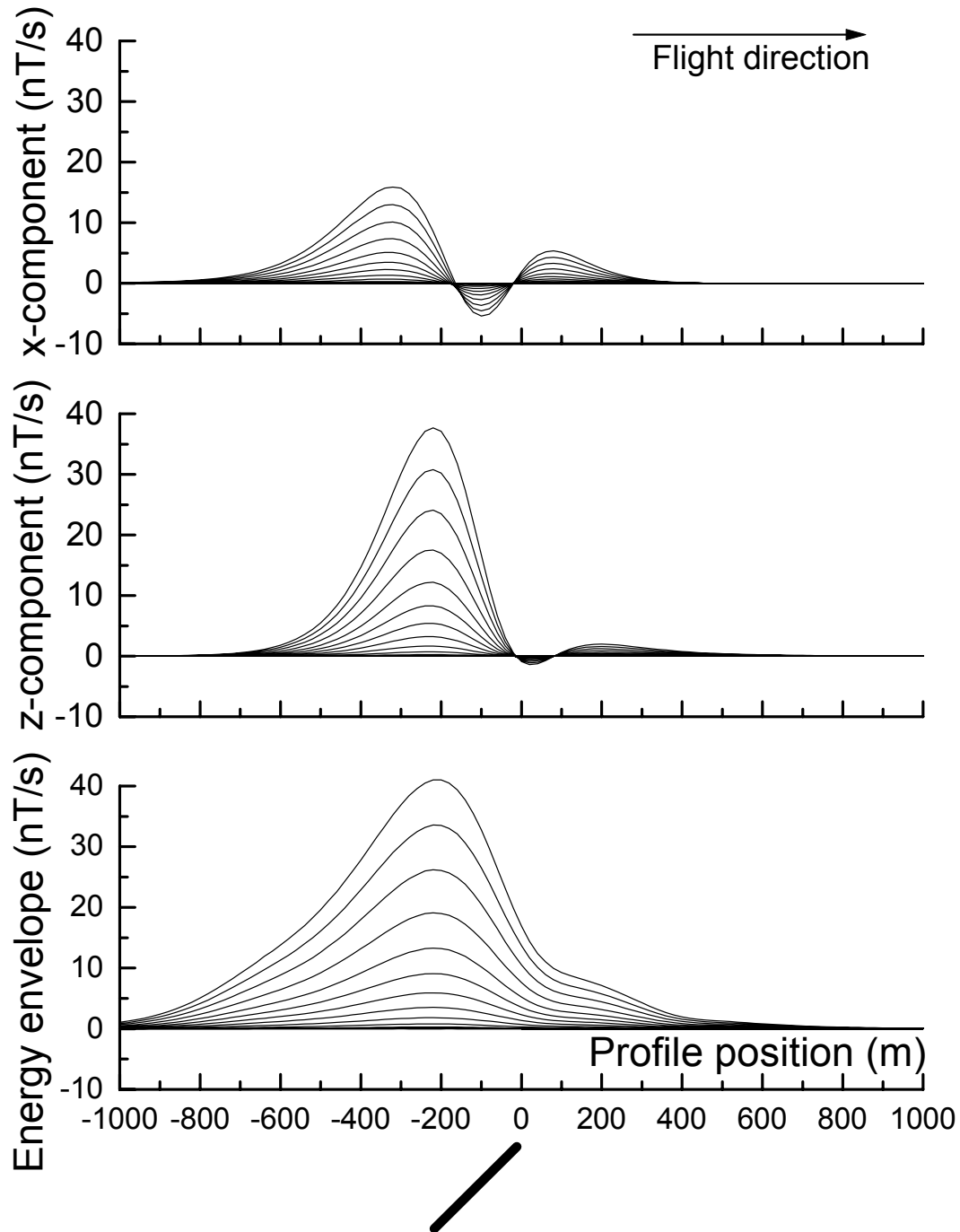


Figure 8.

Plate: dip=45; depth=300

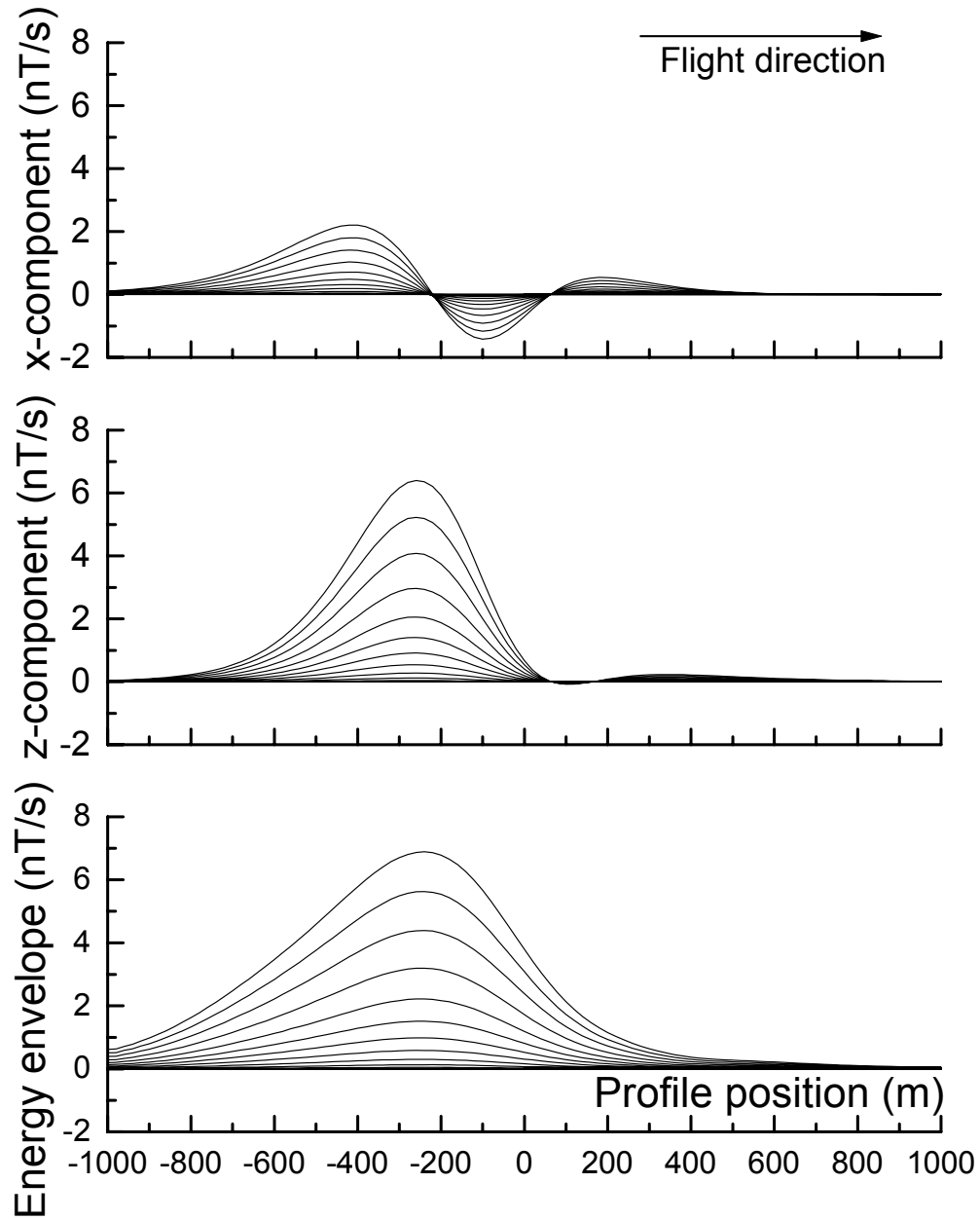


Figure 9.

Plate: dip=90; depth=0

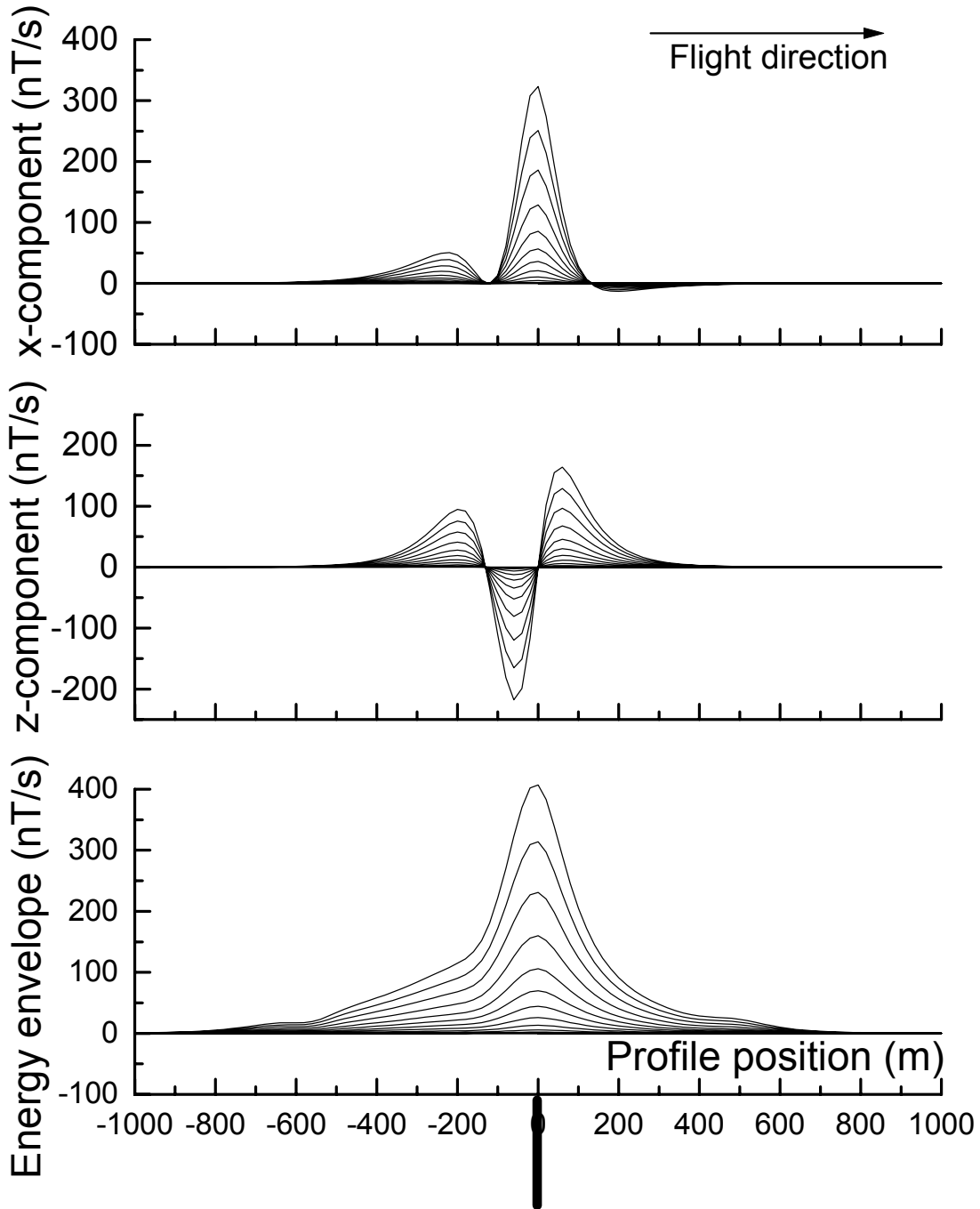


Figure 10.

Plate: dip=90; depth=150

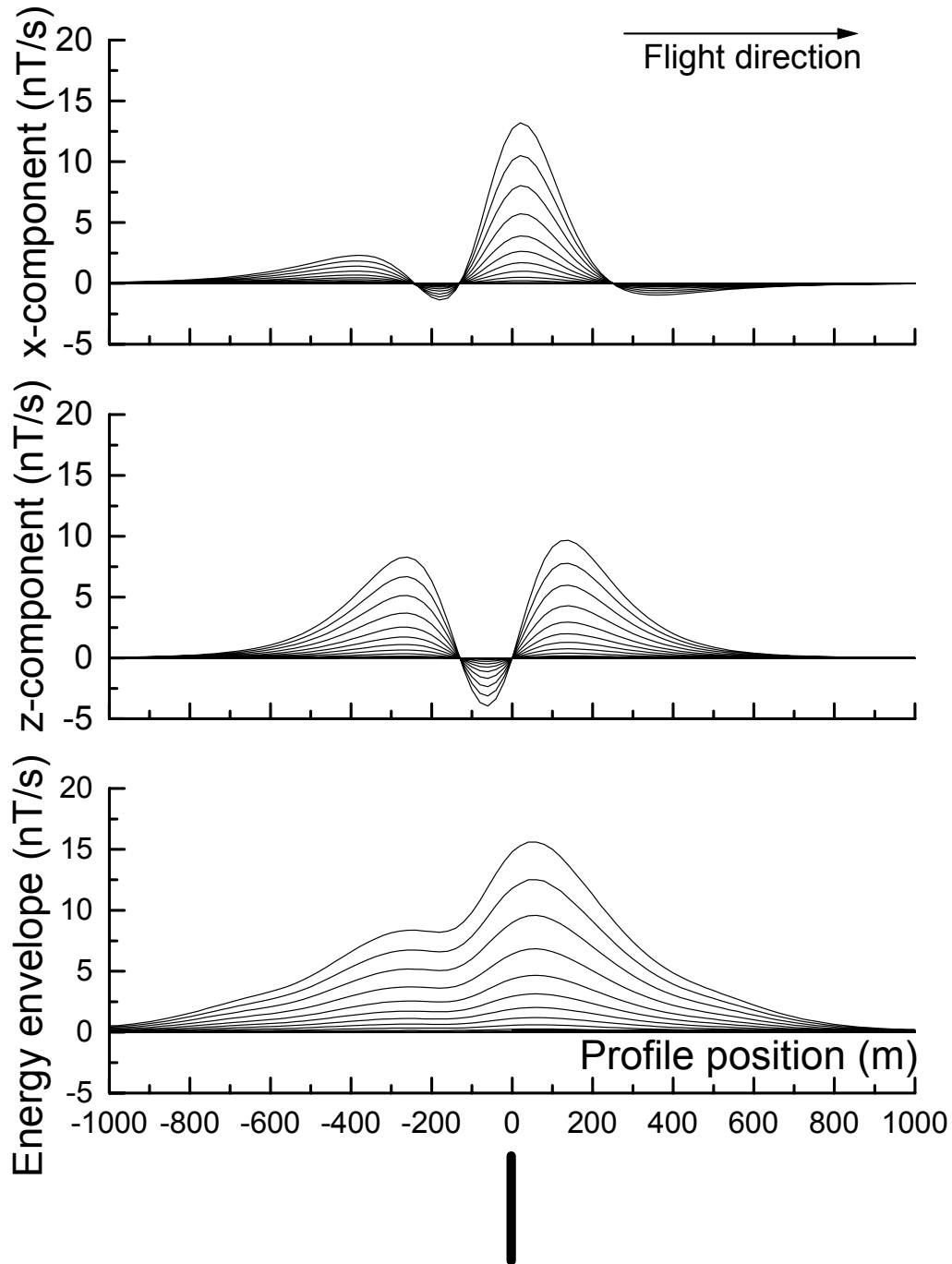


Figure 11.

Plate: dip=90; depth=300

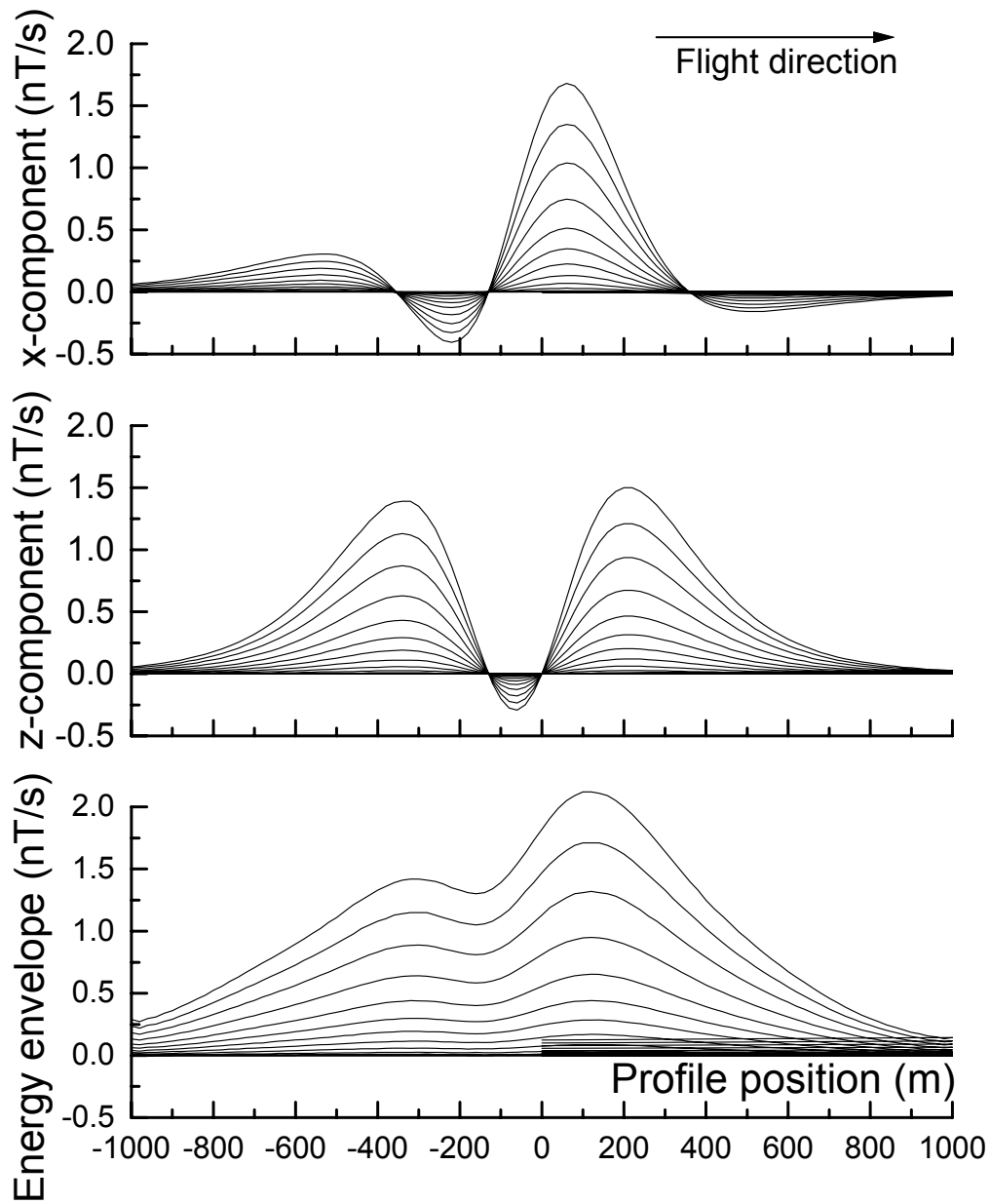


Figure 12.

Plate: dip=135; depth=0

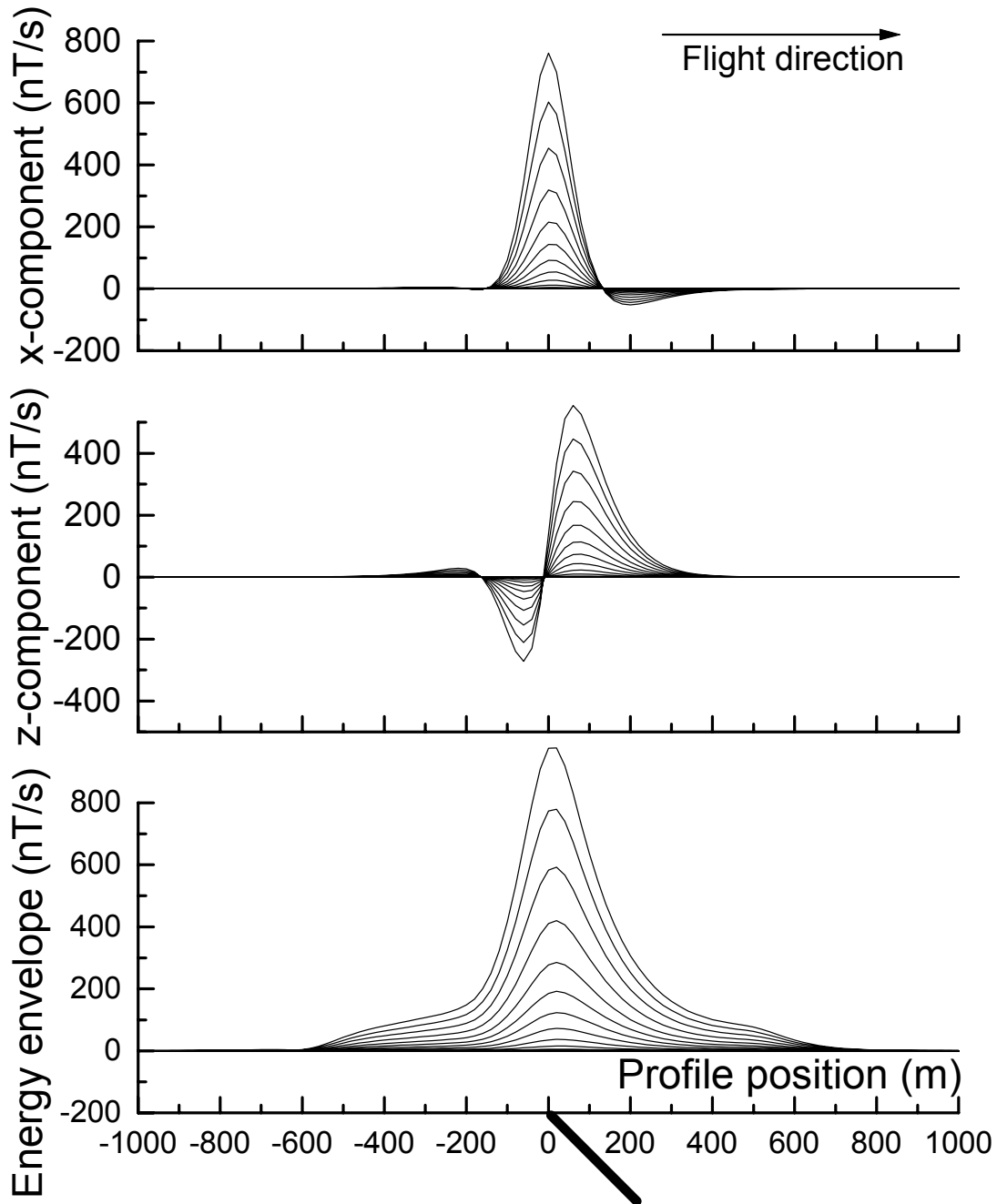


Figure 13.

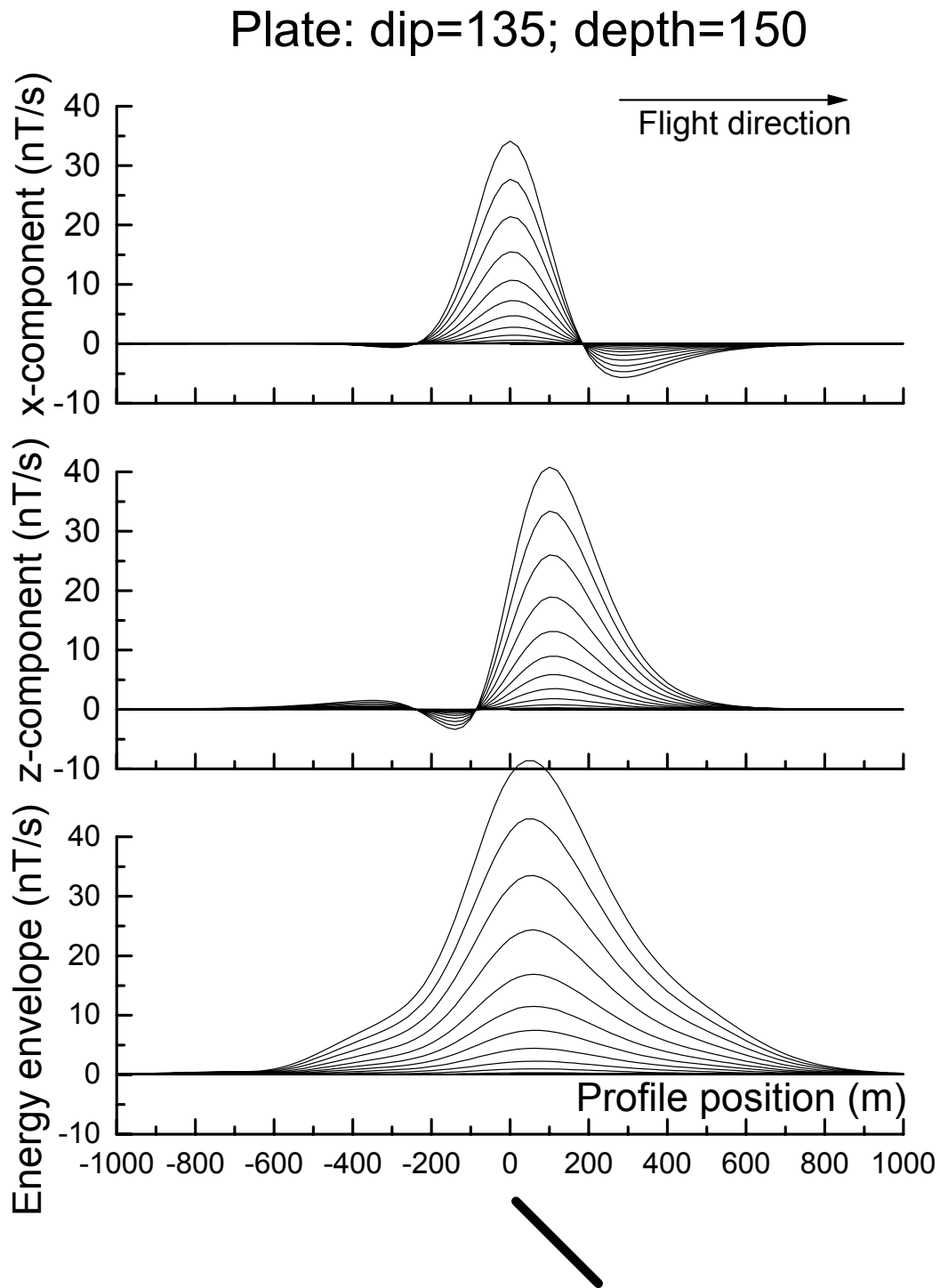


Figure 14.

Plate: dip=135; depth=300

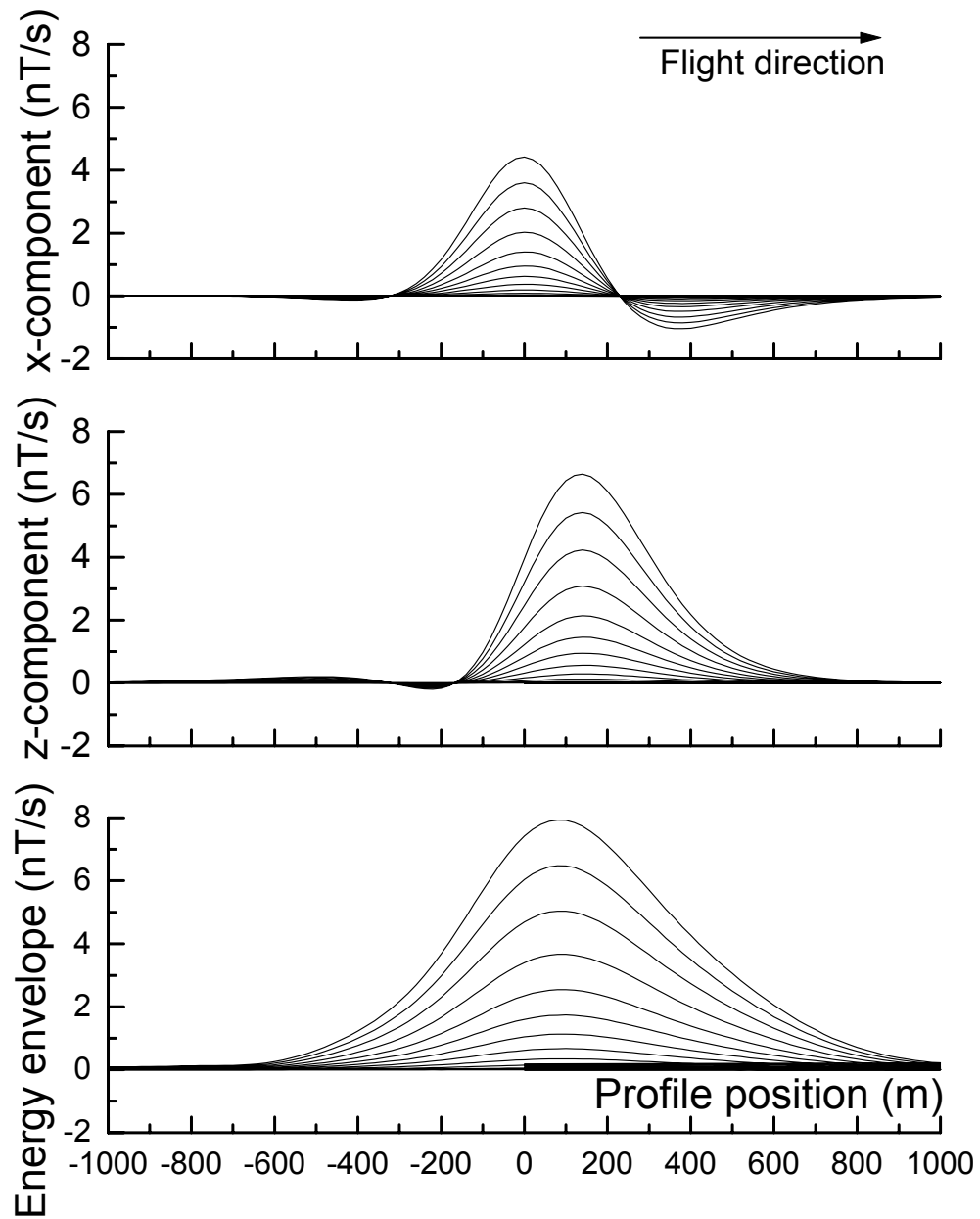


Figure 15.

SPHERE MODELING

The sphere in a uniform field program (Smith and Lee, Exploration Geophysics, 2001, pp 113-118) has been used to generate synthetic responses over a number of sphere models with varying depth of burial (0, 150 and 300 m). The geometry assumed for the fixed-wing airborne EM system and the waveform are as shown in Figures 1 and 2 above.

In all cases the sphere has a radius of 112 m. As the flight path traverses the center of the sphere, the y component is zero and has not been plotted.

The conductivity of the sphere is 1 S/m. In cases when the conductivity is different, an indication of how the amplitudes may vary can be obtained from the nomogram that follows (Figure 16).

In the following profile plots (Figure 17 to 19) all components are in nT/s, for a transmitter dipole moment of 900 000 Am². If the dipole moment is larger or smaller, then the response should be scaled up or down appropriately.

The plotting point is the receiver location.

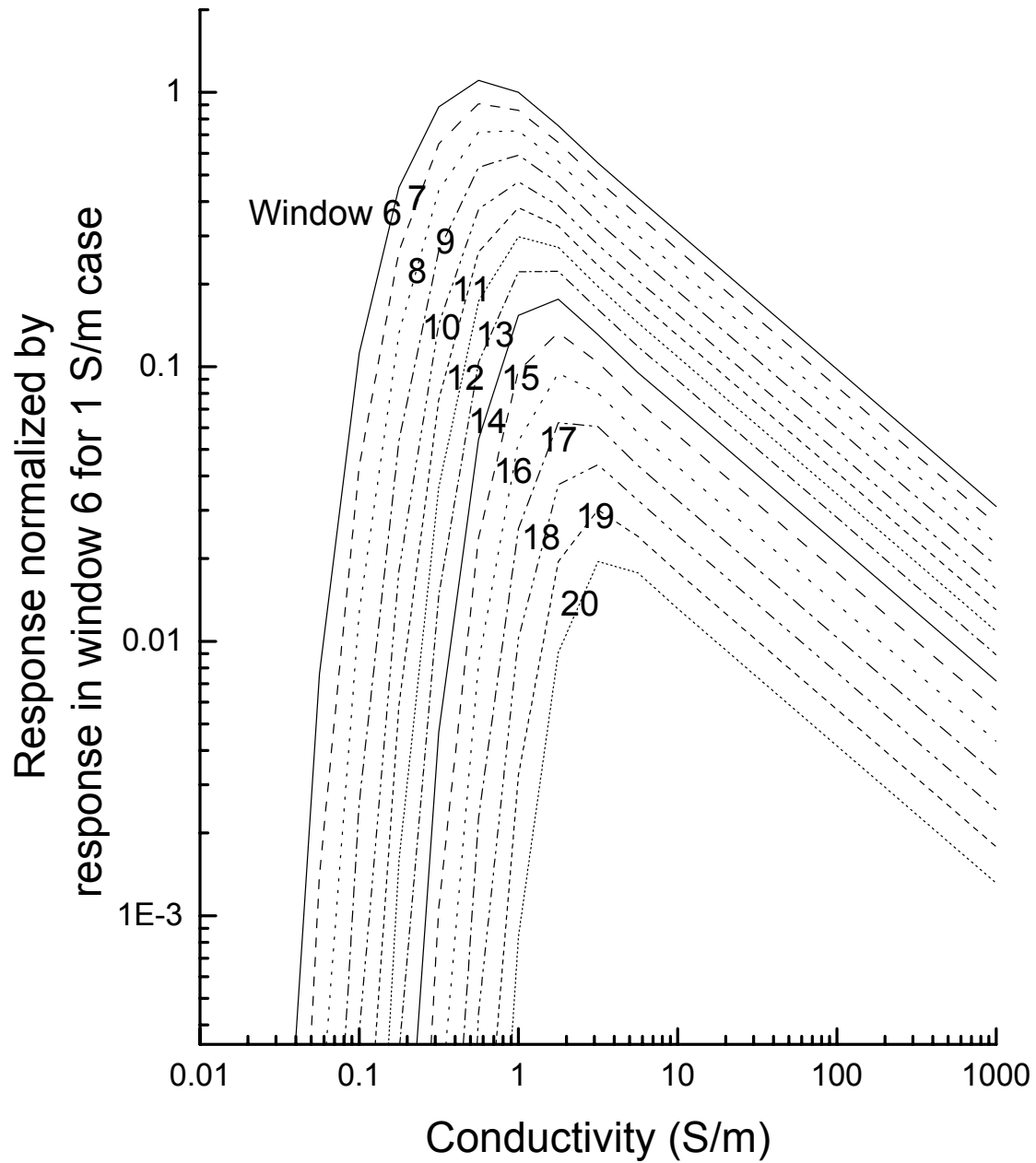


Figure 16. Nomogram for windows 6-20 normalized to a response from a 1 Siemen conductor in window 6.

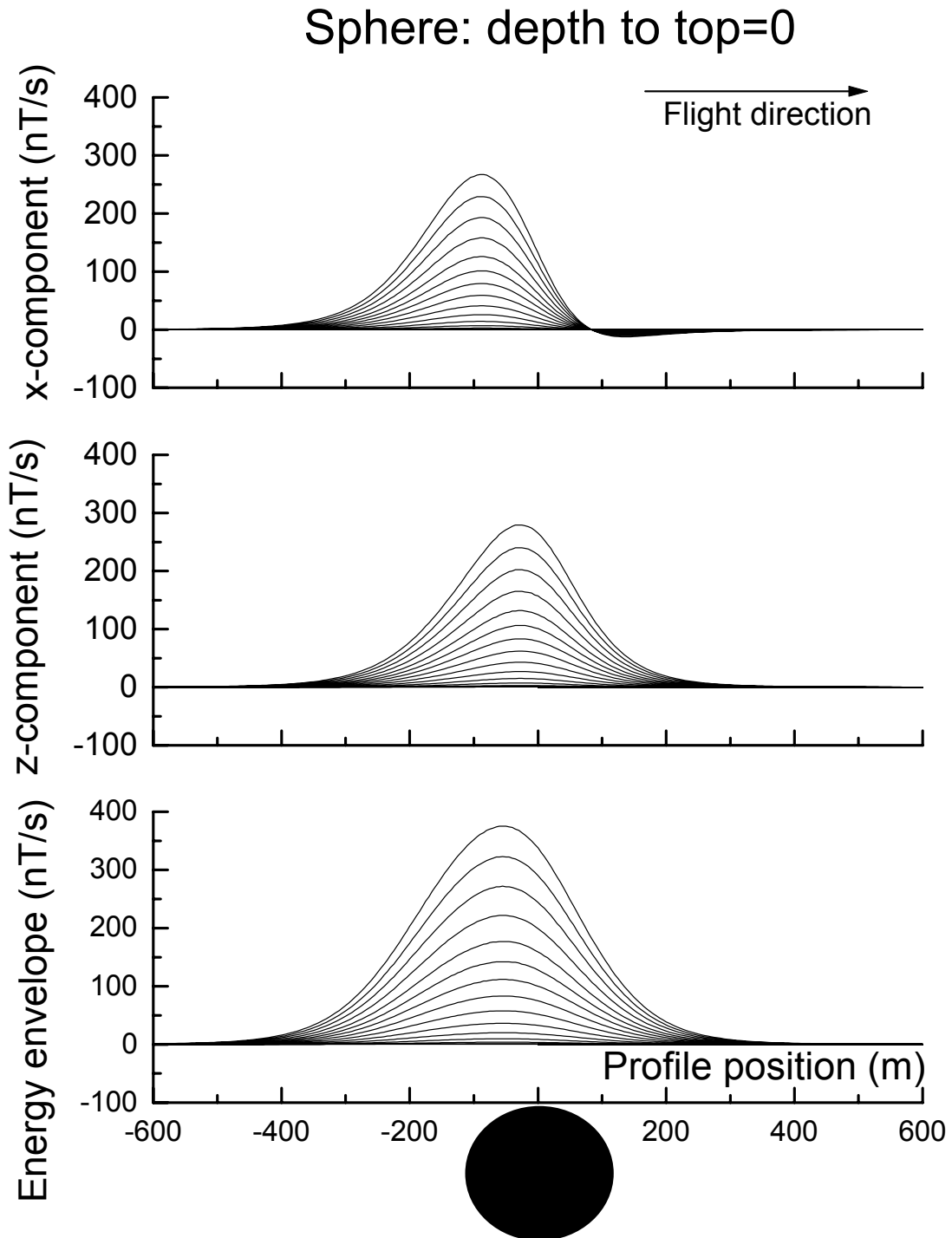


Figure 17.

Sphere: depth to top=150

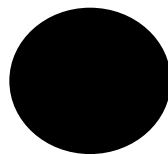
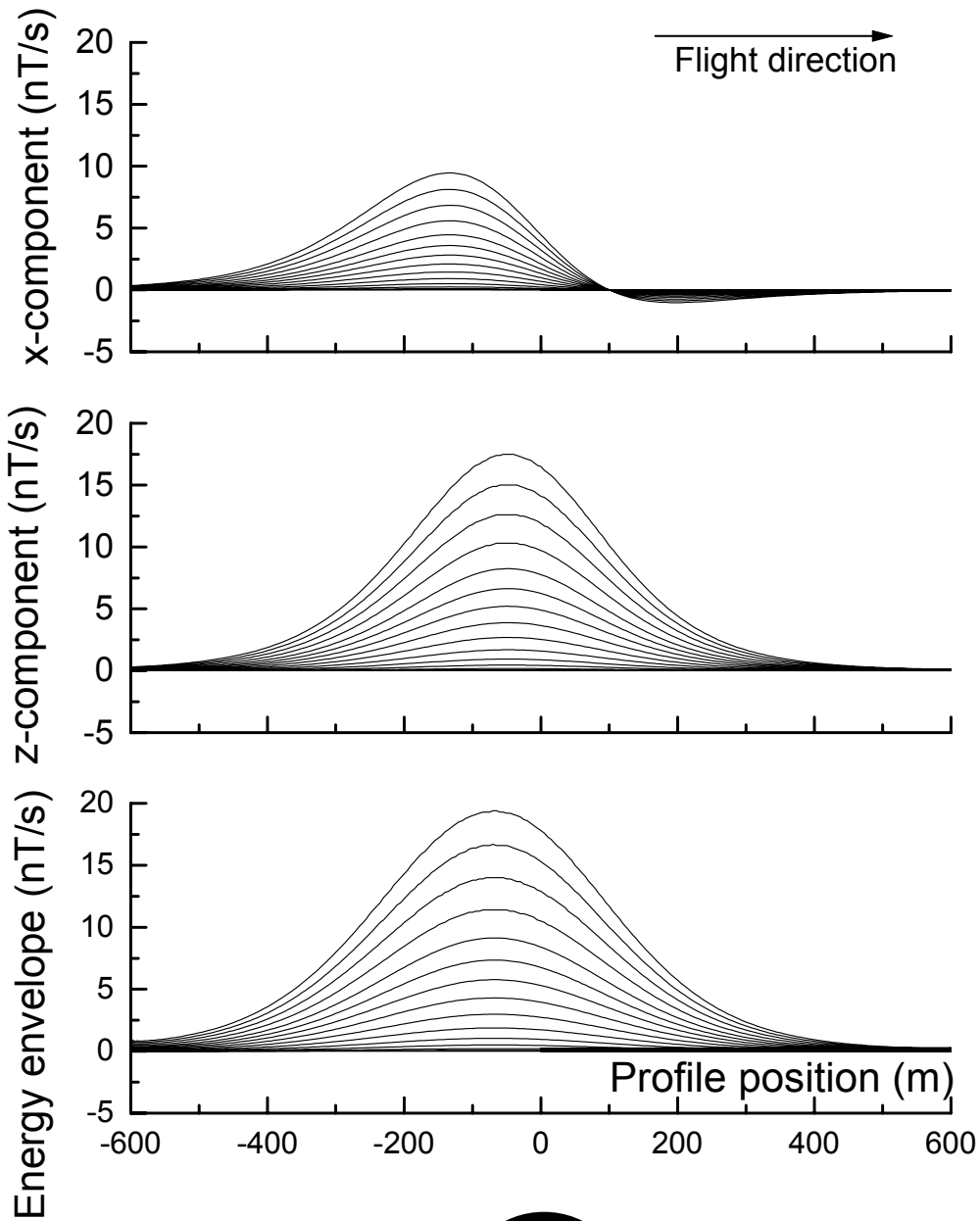


Figure 18.

Sphere: depth to top=300

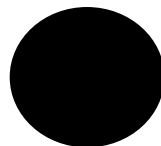
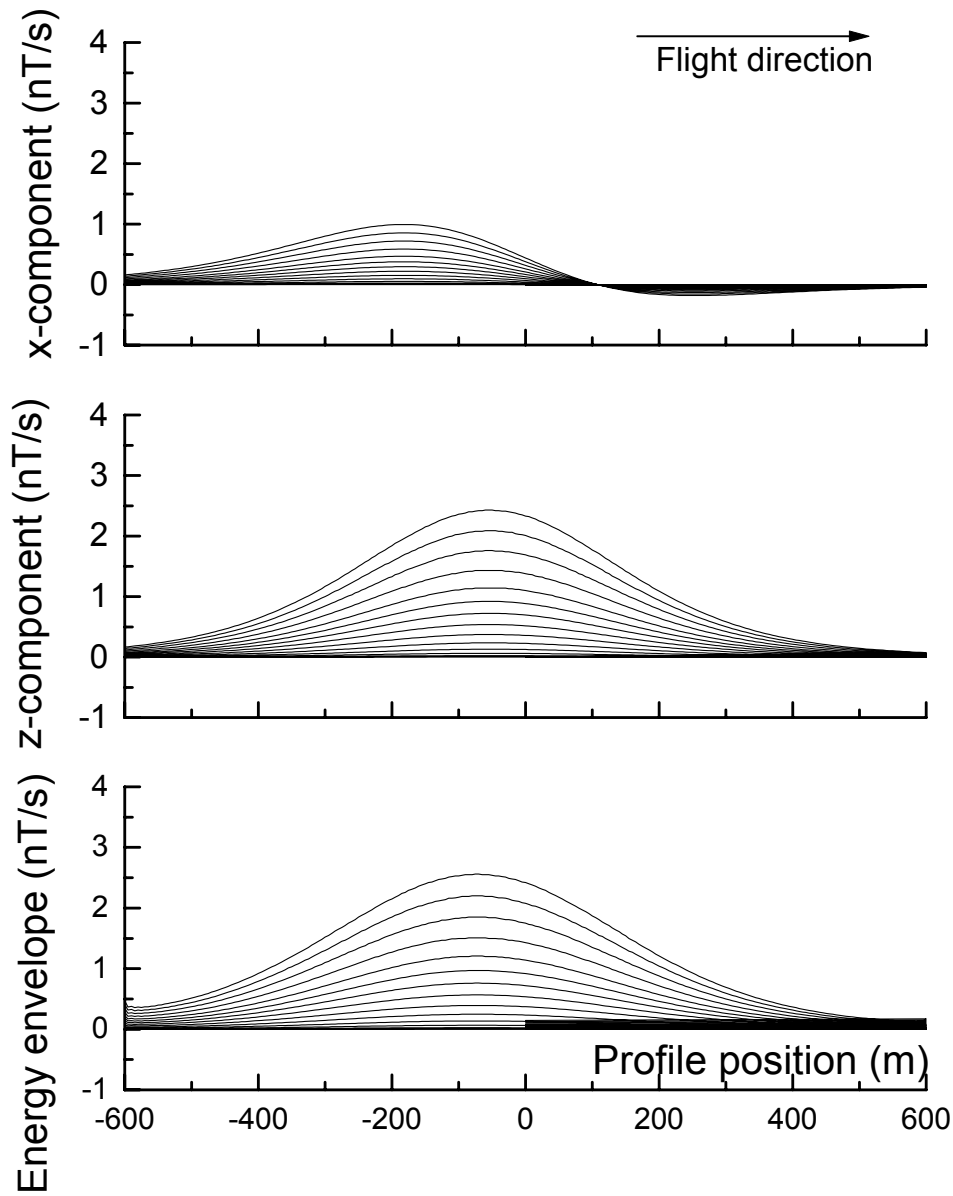


Figure 19.

Appendix D

The Usefulness of Multicomponent, Time-Domain Airborne Electromagnetic Measurement

GEOPHYSICS, VOL 61, NO. 1 (JANUARY-FEBRUARY 1996); P. 74-81, 17 FIGS.

The usefulness of multicomponent, time-domain airborne electromagnetic measurements

Richard S. Smith* and Pierre B. Keating ‡

ABSTRACT

Time-domain airborne electromagnetic (AEM) systems historically measure the inline horizontal (x) component. New versions of the electromagnetic systems are designed to collect two additional components [the vertical (z) and the lateral horizontal (y) component] to provide greater diagnostic information.

In areas where the geology is near horizontal, the z-component response provides greater signal to noise, particularly at late delay times. This allows the conductivity to be determined to greater depth. In a layered environment, the symmetry implies that the y component will be zero; hence a non-zero y component will indicate a lateral inhomogeneity.

The three components can be combined to give the “energy envelope” of the response. Over a vertical plate, the response profile of this envelope has a single positive peak and no side lobes. The shape of the energy envelope is dependent on the flight direction, but less so than the shape of the x component response profile.

In the interpretation of discrete conductors, the z component data can be used to ascertain the dip and depth to the conductor using simple rules of thumb. When the profile line is perpendicular to the strike direction and over the center of the conductor, the y component will be zero; otherwise it appears to be a combination of the x and z components. The extent of the contamination of the y component by the x and z components can be used to ascertain the strike direction and the lateral offset of the target, respectively.

Having the z and y component data increases the total response when the profile line has not traversed the target. This increases the possibility of detecting a target located between adjacent flight lines or beyond a survey boundary.

Presented at the Airborne Electromagnetics Workshop, Tucson, AZ, September 13-16, 1993. Manuscript received by the Editor February 28, 1994; revised manuscript received September 16, 1994.

*Geotrex, 2060 Walkley Rd., Ottawa, Ontario, K1G 3P5, Canada.

‡Geological Survey of Canada, 1 Observatory Crescent, Ottawa, Ontario K1A 0Y3, Canada.

© 1996 Society of Exploration Geophysicists. All rights reserved.

INTRODUCTION

The acquisition of multiple-component electromagnetic (EM) data is becoming more commonplace. In some techniques, such as those which use the plane-wave assumption (MT, CSAMT and VLF) more than one component has been acquired as a matter of routine for some time (see reviews by Vozoff, 1990, 1991; Zonge and Hughes, 1991; McNeill and Labson, 1991). Historically, commercially available controlled-waveform finite-source systems generally measure only one component. The only systems designed to acquire multiple component data are generally experimental [e.g., those described in the appendixes of Spies and Frischknecht (1991) or proprietary (the EMP system of Newmont Exploration).

Slingram EM systems, comprising a moving dipolar transmitter and a moving receiver, generally only measure one component of the response. Although the MaxMin system was designed with a capability to measure a second (minimum coupled) component, this capability is not used extensively in practice. The only systems that use two receiver coils in practice are those that measure the wavetilt or polarization ellipse (Frischknecht et al., 1991).

Historically, time-domain EM systems have been capable of collecting multicomponent data in a sequential manner by reorienting the sensor for each component direction. The usefulness of additional components is discussed by Macnae (1984) for the case of the UTEM system. Macnae concluded that, as extra time was required to acquire the additional components, this time was better spent collecting more densely spaced vertical-component data. The vertical-component, which is less subject to spheric noise, could subsequently be converted to the horizontal components using the Hilbert transform operators.

Recent instrument developments have been towards multicomponent systems. For example, commercially available ground-EM systems such as the Geonics PROTEM, the Zonge GDP-32 and the SIROTEM have been expanded to include multiple input channels that allow three (or more) components to be acquired simultaneously. There is also a version of the UTEM system currently being developed at Lamontagne Geophysics Ltd. These multichannel receivers require complimentary multicomponent sensors -- for ground-based systems these have been developed by Geonics Ltd and Zonge Engineering and Research Organization. The interpretation of fixed-source, multi-component ground-EM data is described in Barnett (1984) and Macnae (1984).

In the past, multi-component borehole measurements have been hindered by the lack of availability of multi-component sensor probes. Following the development of two prototype probes (Lee, 1986; Hodges et al., 1991), multi-component sensors are now available from Crone Geophysics and Exploration Ltd and Geonics. Three component UTEM and SIROTEM borehole sensors are also in development at Lamontagne and Monash University (Cull, 1993), respectively. Hodges et al. (1991) present an excellent discussion of techniques that can be used to interpret three-component borehole data.

Airborne systems such as frequency-domain helicopter electromagnetic methods acquire data using multiple sensors. However, each receiver has a corresponding transmitter that either operates at a different frequency or has a different coil orientation (Palacky and West, 1991). Hence, these systems are essentially multiple single-component systems. The exception to this rule is the now superseded Dighem III system (Fraser, 1972) which used one transmitter and three receivers.

The only multicomponent airborne EM (AEM) system currently in operation is the SPECTREM system (Macnae, et al., 1991). This is a proprietary system (owned and operated by

Anglo-American Corporation of South Africa Ltd.), based on the PROSPECT system (Annan, 1986). The Prospect system was originally designed to acquire the x , y and z components, but SPECTREM is apparently only collecting two components (x and z) at the time of writing. Other multi-component systems currently in development are:

- 1) the SALTMAP system,
- 2) a helicopter time-domain system (Hogg, 1986), and
- 3) a new version of the GEOTEM[®] system (GEOTEM is a registered trademark of Geotrex).

Apart from a few type curves in Hogg (1986), there is little literature available which describes how to interpret data from these systems.

This paper is intended to give an insight into the types of responses expected with the new multi-component AEM systems, and the information that can be extracted from the data. The insight could be of some assistance in interpreting data from multicomponent moving-source ground EM systems (should this type of data be acquired).

The use of multi-component data will be discussed for a number of different applications. For illustration purposes, this paper will use the transmitter-receiver geometry of the GEOTEM system (Figure 1), which is comparable to the other fixed-wing geometries (SPECTREM and SALTMAP). The GEOTEM system is a digital transient EM system utilizing a bipolar half-sinusoidal current waveform [for more details refer to Annan and Lockwood (1991)]. The sign convention used in this paper is shown in Figure 1, with the y component being into the page. In a practical EM system, the receiver coils will rotate in flight. We will assume that the three components of the measured primary field and an assumed bird position have been used to correct for any rotation of the coil.

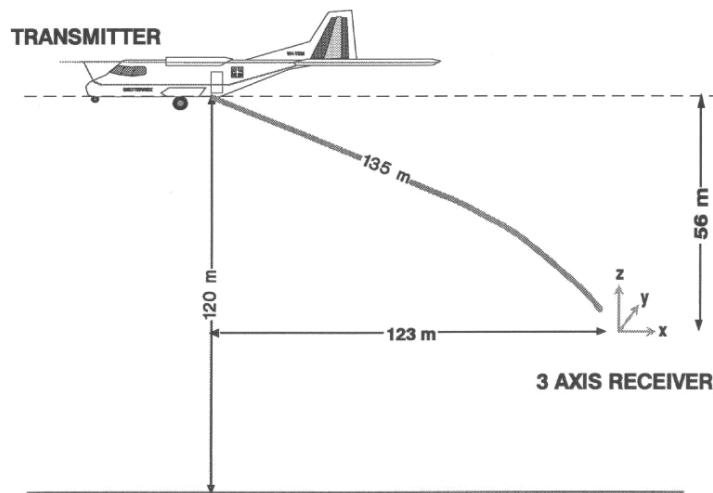


Fig. 1: The geometric configuration of the GEOTEM system. The system comprises a transmitter on the aircraft and a receiver sensor in a "bird" towed behind the aircraft. The z direction is positive up, x is positive behind the aircraft, and y is into the page (forming a right-hand coordinate system).

SOUNDING IN LAYERED ENVIRONMENTS

In a layered environment, the induced current flow is horizontal (Morrison et al., 1969) so the z component of the secondary response (V_z) is much larger than the x component (V_x), particularly in resistive ground and/or at late delay times. At the same time, the spheric noise in the z direction is 5 to 10 times less than in the horizontal directions (Macnae, 1984; McCracken et al., 1986), so V_z has a greater signal-to-noise ratio. Figure 2 shows theoretical curves over two different, but similar, layered earth models. One model is a half-space of $500 \Omega\cdot\text{m}$ and the other is a 350 m thick layer of $500 \Omega\cdot\text{m}$ overlying a highly resistive basement. In this plot the data have been normalized by the total primary field. The z component (V_z) is 6 to 10 times larger than V_x , and both curves are above the noise level, at least for part of the measured transient. On this plot, a noise level of 30 ppm has been assumed, which would be a typical noise level for both components when the spheric activity is low. To distinguish between the response of the half-space and thick layer, the difference between the response of one model and the response of the other model must be greater than the noise level. Figure 3 shows this difference for both components. Only the V_z difference is above the noise level. Hence for the case shown, V_z is more useful than V_x for determining whether there is a resistive layer at 350 m depth. Because V_z is generally larger in a layered environment, the vertical component will generally be better at resolving the conductivity at depth.

In the above discussion, we have assumed that corrections have been made for the coil rotation. An alternative approach is to calculate and model the magnitude of the total field, as this quantity is independent of the receiver orientation. Macnae et al. (1991) used this strategy when calculating the conductivity depth sections for SPECTREM data.

The symmetry of the secondary field of a layered environment is such that the y component response (V_y) will always be zero. In fact, the V_y component will be zero whenever the conductivity structure on both sides of the aircraft is the same. A non-zero V_y is therefore useful in identifying off-line lateral inhomogeneities in the ground.

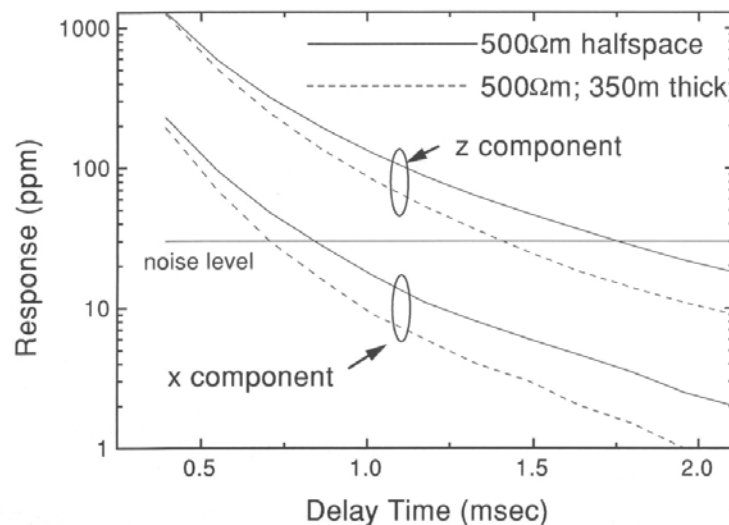


Fig. 2. The response for a $500 \Omega\cdot\text{m}$ half-space (solid line) and a $500 \Omega\cdot\text{m}$ layer of thickness 350 m overlying a resistive half-space (dashed line). The z -component responses are the two curves with the larger amplitudes and the two x -component response curves are 6 to 10 times smaller than the corresponding z component. A noise level of 30 ppm is considered to be typical of both components in the absence of strong spherics.

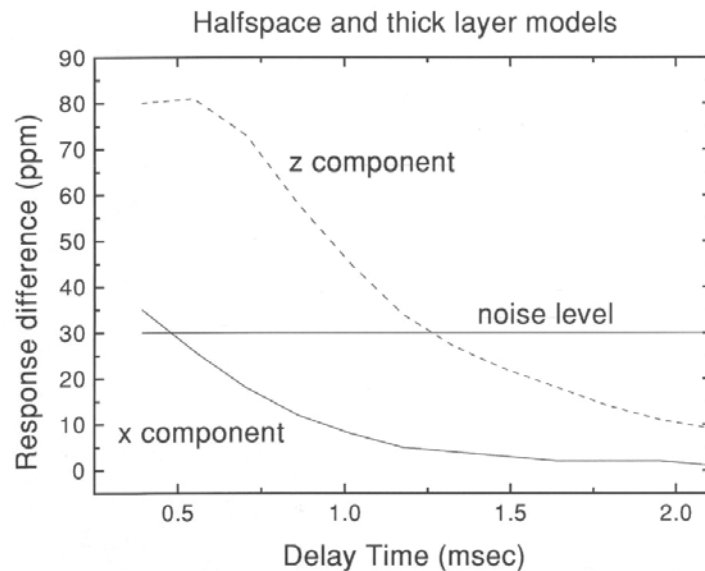


Fig. 3: The difference in the response of each component for the half-space and thick layer models of Figure 2. Only the z-component difference is above the noise level for a significant portion of the transient. Therefore, this is the only component capable of distinguishing between the responses of the two models.

DISCRETE CONDUCTORS

In our discrete conductor study, models have been calculated using a simple plate in free-space model (Dyck and West, 1984) to provide some insight into the geometry of the induced field. The extension to more complex models, such as those incorporating current gathering, will not be considered in this paper.

Historically, airborne transient electromagnetic (TEM) data have been used for conductor detection. The old INPUT system was designed to measure V_x because this component gave a large response when the receiver passed over the top of a vertical conductor. The bottom part of Figure 4 shows the response over a vertical conductor, which has been plotted at the receiver position. The V_x profile (smaller of the two solid lines) has a large peak corresponding with the conductor position. Note that there is also a peak at 200 m, just before the transmitter passes over the conductor, and a trailing edge negative to the left of the conductor. The z component (dashed line) has two peaks and a large negative trough just before the conductor. Because of the symmetry, the V_y response (dotted line) is zero.

All the peaks, troughs and negatives make the response of a single conductor complicated to display and hence interpret. The display can be simplified by plotting the "energy envelope" (EE) of the response. This quantity is defined as follows:

$$EE = \sqrt{V_x^2 + \bar{V}_x^2 + V_y^2 + \bar{V}_y^2 + V_z^2 + \bar{V}_z^2},$$

where $\bar{\quad}$ denotes the Hilbert transform of the quantity. The energy envelope plotted on Figure 4 (the larger of the two solid curves) is almost symmetric, and would be a good quantity to present in plan form (as contours or as an image). For flat-lying conductors, the energy envelope has a maximum at the leading edge (just after the aircraft flies onto the conductor).

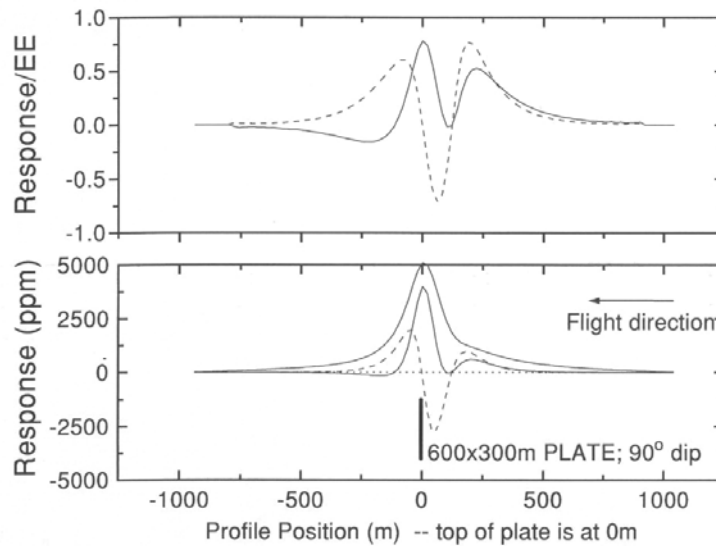


Fig. 4. (Bottom) the response of a 600 by 300 m plate 120 m below an aircraft flying from right to left. The plotting point for the response is below the receiver. The x-component response is the smaller amplitude solid line, the z-component is the dashed line, and the y-component response is the dotted line. The larger amplitude solid line is the “energy envelope” of all three components. (Top) the z- and x-components normalized by the energy envelope. These and all subsequent curves are for a delay time of 0.4 ms after the transmitter current is turned off.

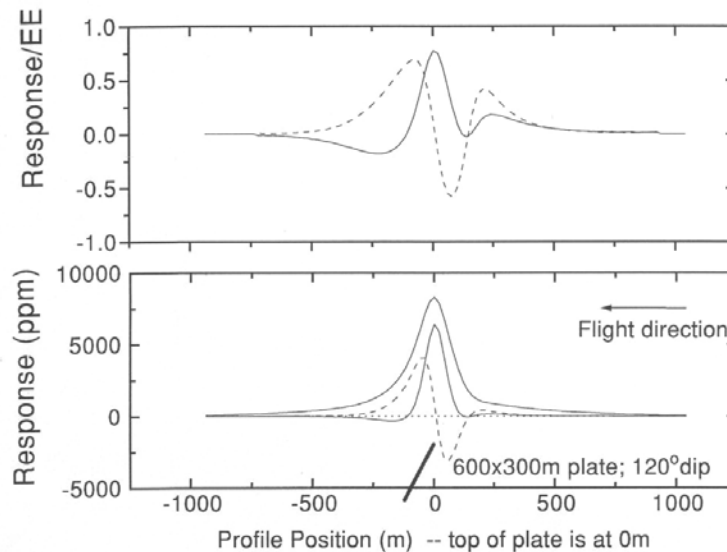


Fig. 5 (Bottom) same as Figure 4, except the plate is now dipping at 120°. On the top graph note the down-dip (left) peak on the normalized z-component response is larger than the right peak (c.f. Figure 4).

What little asymmetry remains in the energy envelope is a good indication of the coupling of the AEM system to the conductor. If the response profile for each component is normalized by the energy envelope, then the effect of system coupling will be removed (at least partially) and the profiles will appear more symmetric. For example, the top part of Figure 4 shows the V_x and V_z normalized by the energy envelope at each point. The size of the two x peaks and the two z peaks are now roughly comparable.

Dip determination

The response of a plate with a dip of 120° is shown on Figure 5. For the V_x/EE and V_z/EE profiles, the peak on the down dip side is larger. For shallow dips, it becomes difficult to identify both V_x/EE peaks, but the two positive V_z/EE peaks remain discernable. Plotting the ratio of the magnitudes of these two V_z/EE peaks, as has been done with solid squares on Figure 6, shows that the ratio is very close to the tangent of the dip divided by 2. Hence, calculating the ratio of the peak amplitudes (R) will yield the dip angle θ using

$$\theta = 2 \tan^{-1}(R).$$

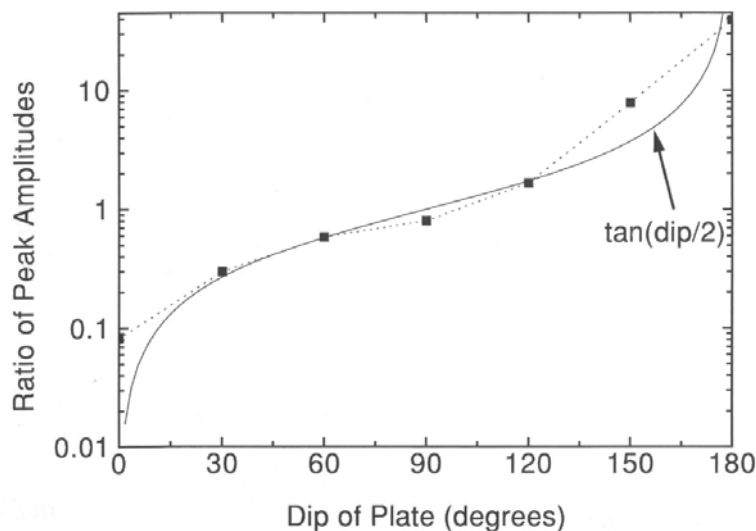


Fig. 6. The ratio of the peak amplitudes of the normalized z-component response (left/right) plotted with solid squares. The ratio plots very close to the tangent of half the dip angle θ of the plate.

Depth Determination

As the depth of the body increases, there is a corresponding increase in the distance between the two positive peaks in the V_z/EE profile. As an example of this, Figure 7 shows the case of a plate 150 m deeper than the plate of Figure 4. The peaks are now 450 m apart, as compared with 275 m on Figure 4. A plot of the peak-to-peak distances for a range of depths is shown on Figure 8 for plates with 60° , 90° and 120° dips. Because the points follow a straight line, it can be concluded that for near vertical bodies (60° to 120° dips), the depth to the top of the body d can be determined from the measured peak-to-peak distances using the linear relationship depicted in Figure 8. The expected error would be about 25 m. Such an error is tolerable in airborne EM interpretation. More traditional methods for determining d analyze the rate of decay of the measured response (Palacky and West, 1973). Our method requires only the V_z/EE response profile at a single delay time. Analyzing this response profile for each delay time allows d to be determined as a function of delay time, and hence any migration of the current system in the conductor could be tracked.

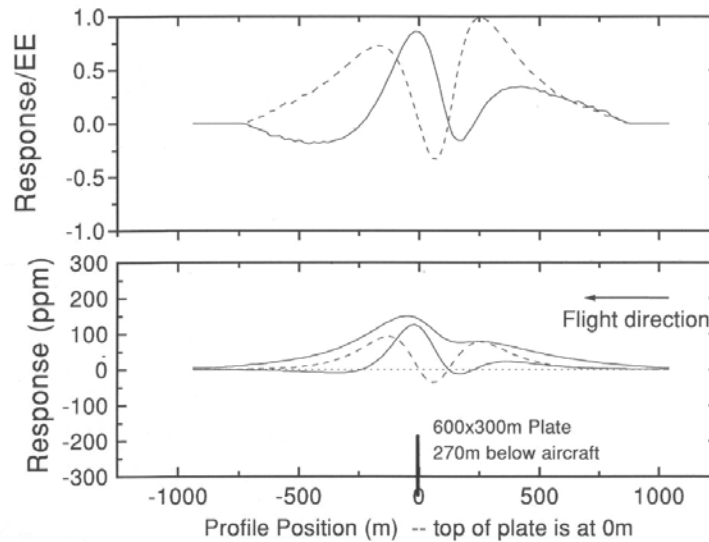


Fig. 7. The same as Figure 4, except the plate is now 270 m below the aircraft. Note that the distance between the z-component peaks is now much greater.

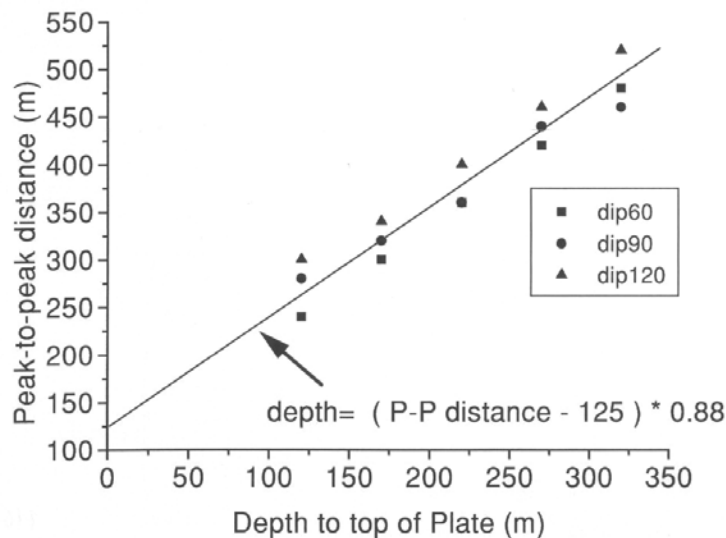


Fig. 8. The peak-to-peak distance as a function of plate depth for three different dip angles θ . A variation in dip of $\pm 30^\circ$ does not result in a large change in the peak to peak distance.

Strike and offset determination

The response shown in Figure 4 varies in cases when the plate has a strike different from 90° or the flight path is offset from the center of the plate.

Figure 9 shows the response for a plate with zero offset and Figure 10 shows the plate when it is offset by 150 m from the profile line. The calculated voltages V_z and V_x are little changed from the no offset case, but the V_y response, is no longer zero. In fact, the shape of the V_y curve appears to be the mirror image of the V_z curve.

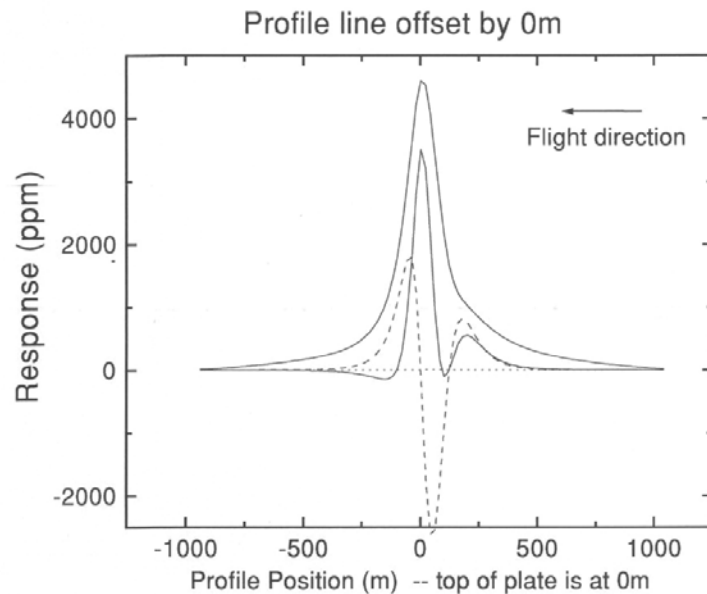


Fig. 9 The response of a 300 by 300 m plate traversed by a profile line crossing the center of the plate in a direction perpendicular to the strike of the plate (the strike angle ζ of the plate with respect to the profile line is 90°).

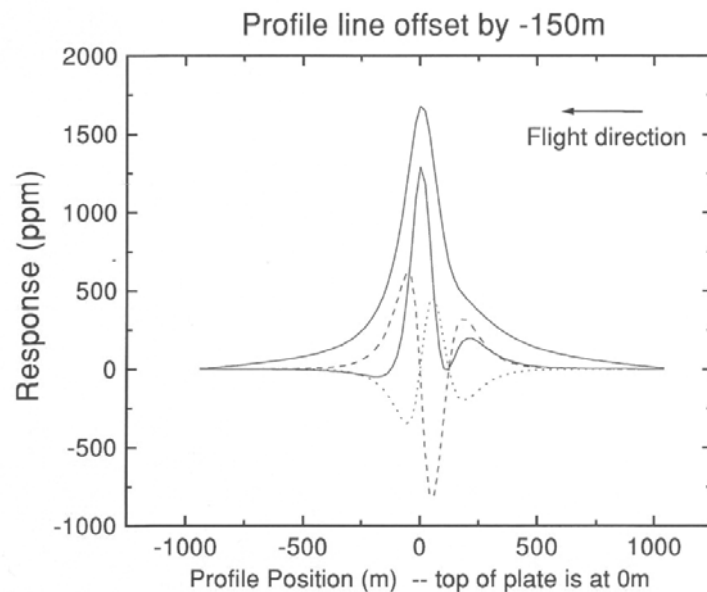


Fig. 10. Same as Figure 9, except the profile line has been offset from the center of the plate by -150 m in the y direction (equivalent to a $+150$ m displacement of the plate).

In the case when the plate strikes at 45° , the y component is similar in shape but opposite in sign to the x-component response (Figure 11).

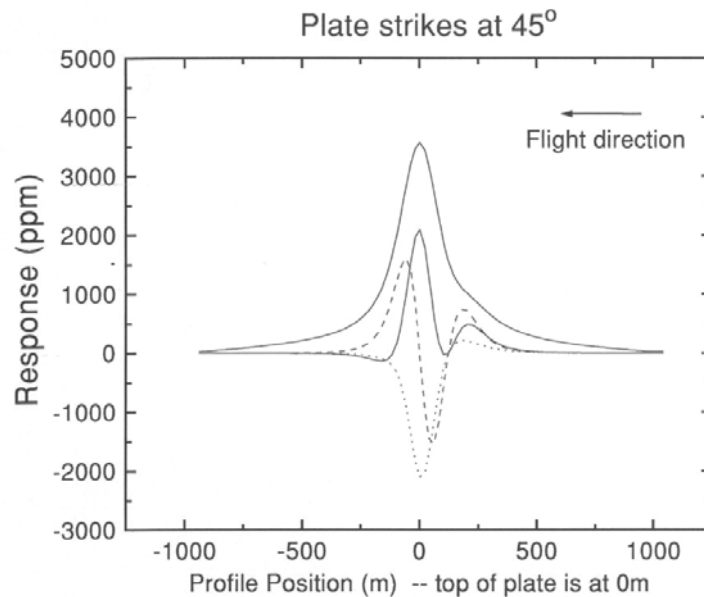


Fig. 11 Same as Figure 9, except the profile line traverses the plate such that the strike angle ζ of the plate with respect to the profile line is 45° .

These similarities can be better understood by looking at schematic diagrams of the secondary field from the plate. Figure 12 shows a plate and the field in section. For zero offset, the field is vertical (z only). As the offset increases, the aircraft and receiver moves to the right and the measured field rotates into the y-component.

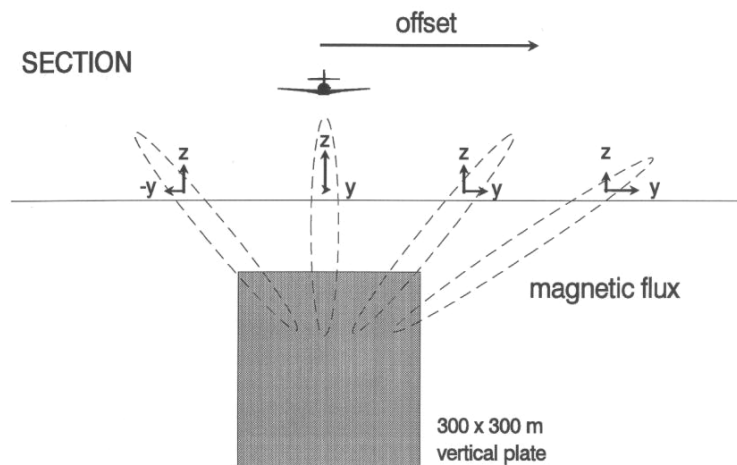


Fig. 12. A schematic diagram of the plate and the magnetic flux of the secondary field (section view). For increasing offset of the aircraft and receiver from the center of the plate, the magnetic field at the receiver rotates from the z to the y component.

The secondary field is depicted in plan view in Figure 13. Variable strike is simulated by leaving the plate stationary and changing the flight direction. When the strike of the plate is different from 90° , the effective rotation of the EM system means that the secondary field, which was previously measured purely in the x direction, is now also measured in the y direction.

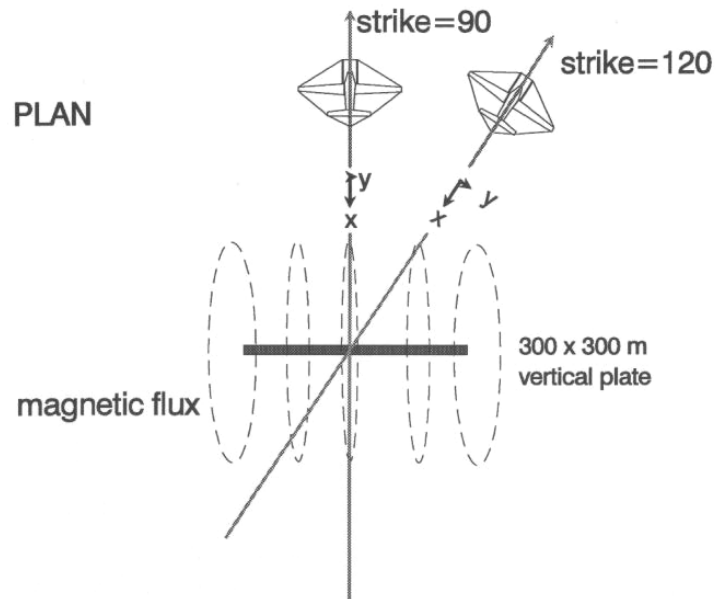


Fig. 13. A schematic diagram of the plate and the magnetic flux of the secondary field (plan view). Here varying strike is depicted by an equivalent variation of the flight direction. As the flight direction rotates from a strike angle of 90°, the receiver rotates so as to measure a greater response in the y direction.

The y component (V_y) can thus be considered to be a mixture of V_x and V_z components, viz

$$V_y = C_{stk} V_x + C_{off} V_z ,$$

an equation that is only approximate. The response for a variety of strike angles and offset distances has been calculated and in each case the y-component response has been decomposed into the x and z components by solving for the constants of proportionality C_{stk} and C_{off} .

A plot of C_{stk} for the case of zero offset and varying strike direction ξ is seen on Figure 14. The values of C_{stk} determined from the data are plotted with solid squares and compared with the $\tan(90^\circ - \xi)$. Because the agreement is so good, the formula

$$\xi = 90 - \tan^{-1} (C_{stk})$$

can be used to determine the strike. This relation was first obtained by Fraser (1972).

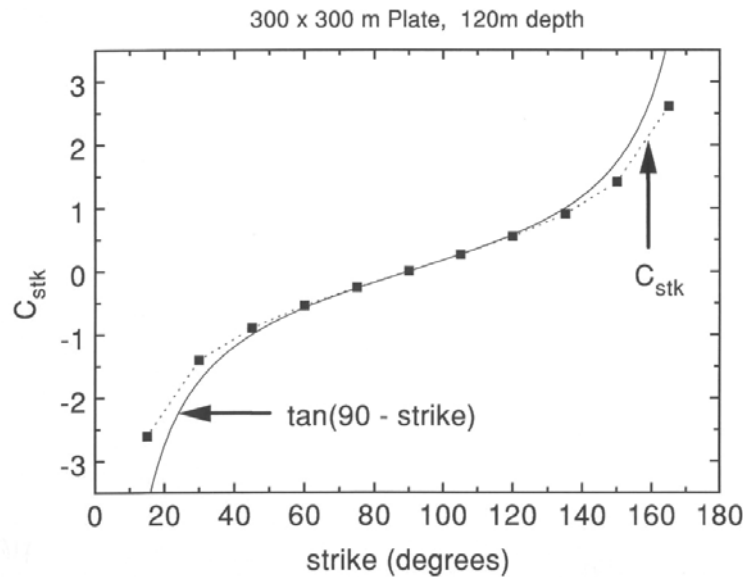


Fig. 14. The ratio $C_{stk} = V_y/V_x$ plotted as a function of varying strike angle (solid squares). The data agree very closely with the cotangent of the ζ .

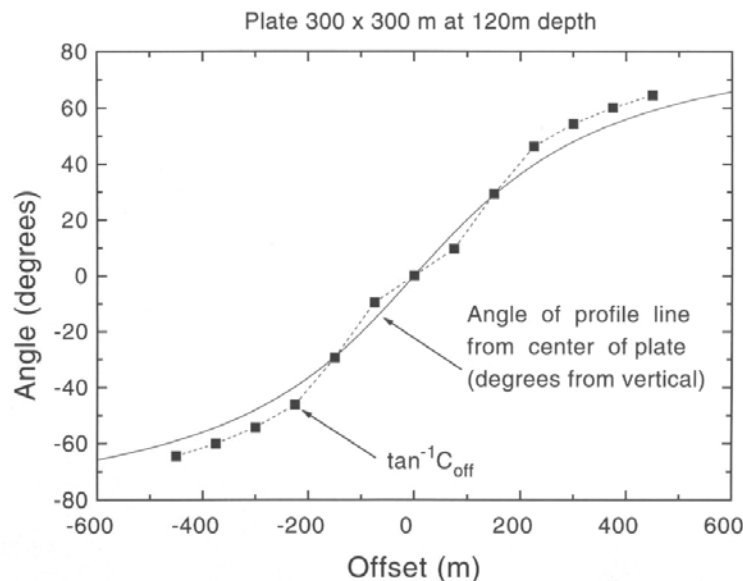


Fig. 15. The arctangent of $C_{off} = V_y/V_z$, plotted as a function of varying offset (solid squares). There is good agreement between this quantity and the angle ϕ between a vertical line and the line from the center of the top edge of the plate to the profile line.

When the strike is fixed at 90° , and the offset varies, the corresponding values obtained for C_{off} have been plotted with solid squares on Figure 15. Again, there is good agreement with the arctangent of C_{off} and the angle ϕ between a vertical line and the line that joins the center of the top edge of the plate with the position where the aircraft traverse crosses the plane containing the plate. If an estimate of the distance to the top of the conductor D is already obtained using the method described above, or by the method described in Palacky and West (1973), then

$$D = \sqrt{(O^2 + d^2)},$$

(where d is the depth below surface). Hence, the offset distance O can be written as follows

$$\begin{aligned} O &= d \tan(\phi) \\ &= d C_{\text{off}} \\ &= C_{\text{off}} \sqrt{D^2 - O^2} \end{aligned}$$

which can be rearranged to give

$$O = C_{\text{off}} D / \sqrt{1 + C_{\text{off}}^2}.$$

Lateral delectability

Figure 12 illustrates that V_y becomes relatively strong as the lateral displacement from the conductor is increased. Thus, if V_y is measured, then the total signal will remain above the noise level at larger lateral displacements of the traverse line from the conductor. This has been illustrated by assuming a flat-lying conductor, here approximated by a wire-loop circuit of radius 125 m (Figure 16). The x , y and z components of the response have been computed using the formula for the large-loop magnetic fields in Wait (1982). The results are plotted on Figure 17 as a function of increasing lateral displacement L of the transmitter/receiver from the center of the conductor. The transmitter and receiver are separated in a direction perpendicular L to simulate the case when the system is maximal coupled to the conductor, but the flight line misses the target by an increasing amount. The effect of varying the conductance or measurement time has been removed by normalizing the response to the total response measured when the system is at zero displacement. At displacements greater than 80 m, the y component is clearly larger than any other component. Assuming the same sensitivity and noise level for each component (which is a realistic assumption if the data are corrected for coil rotation and the spheric activity is low), it is clearly an advantage to measure V_y , as this will increase the chances of detecting the target when the flight line has not passed directly over the conductor.

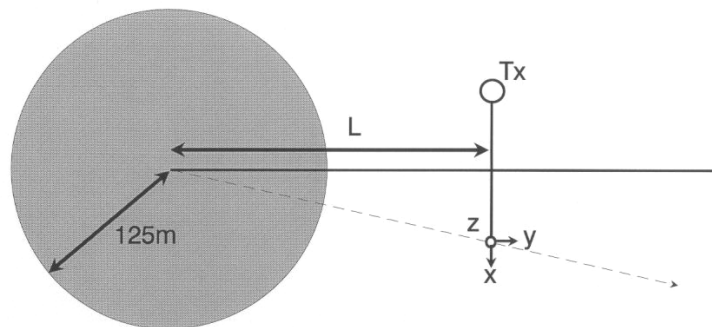


Fig. 16. Plan view of a flat-lying conductor (a circular loop with a radius of 125 m). The AEM system is offset a distance L from the center of the conductor in a direction perpendicular to the traverse direction. The traverse direction of the system is from the bottom to the top of the figure.

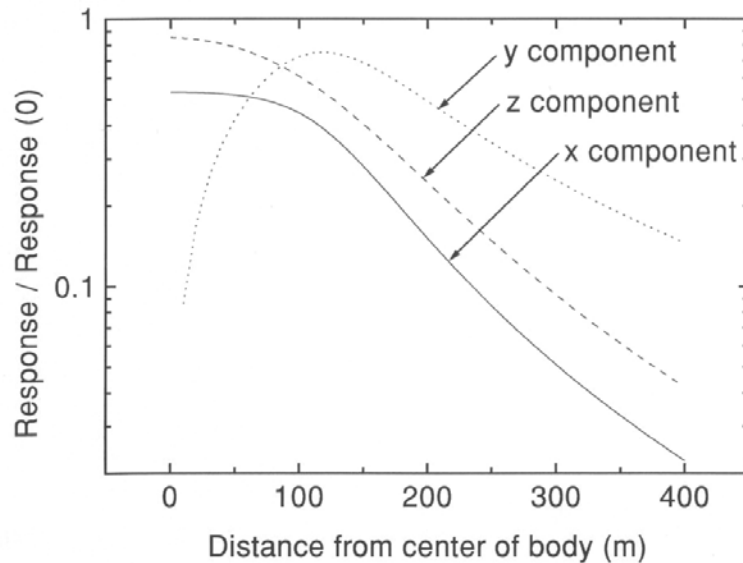


Fig. 17. The normalized response of the EM system plotted as a function of increasing offset distance L . The x component falls off most rapidly and the y component most slowly with increasing offset distance.

CONCLUSIONS

AEM systems measuring three components of the response can be used to infer more and/or better information than those systems that measure with only one component, i.e., V_x .

The z -component data enhances the ability of the AEM system to resolve layered structures as the z -component has a larger signal and a smaller proportion of spheric noise than any other component. If all the components are employed to correct for coil rotation, then the data quality and resolving power is increased further, as individual components are not contaminated by another component. Having better signal-to-noise and greater fidelity in the data will allow deeper layers to be interpreted with confidence.

A non-zero y component is helpful in identifying when the conductivity structure has a lateral inhomogeneity that is not symmetric about the flight line.

All components can be used to calculate the energy envelope, which is a valuable quantity to image. The energy envelope has a single peak over a vertical conductor and two peaks over a dipping conductor (one at either end). The asymmetry in the response profile of each individual component can be reduced by normalizing each profile by the energy envelope.

All three components are of great use in determining the characteristics of discrete conductors. For example, the distance between the two positive peaks in the V_z/EE profile can be employed to determine the depth. Also, the ratio of the magnitude of the two V_z/EE peaks helps to ascertain the dip of the conductor. The x component has been used in the past for these purposes, but is not as versatile, as it requires the data at all delay times, or an ability to identify a very small peak.

The y component can be utilized to extract information about the conductor that cannot be

obtained from single component AEM data. The degree of mixing between the y and z components can give the lateral offset of the conductor (provided the depth is known), while the mixing between the y and x component gives the strike of a vertical conductor.

Finally, because the y component decreases most slowly with increasing lateral offset, this component gives an enhanced ability to detect a conductor positioned at relatively large lateral distances from the profile line, either between lines or beyond the edge of a survey boundary.

ACKNOWLEDGMENTS

The authors wish to thank Geotrex for the permission to publish the results of this model study. This paper has been allocated Geological Survey of Canada Contribution No. 36894.

REFERENCES

- Annan, A. P., 1986, Development of the PROSPECT I airborne electromagnetic system, in Palacky, G. J., Ed., Airborne resistivity mapping : Geol. Surv. Can. Paper **86-22**, 63-70.
- Annan, A. P., and Lockwood, R., 1991, An application of airborne GEOTEM in Australian conditions: Expl., Geophys., **22**, 5-12.
- Barnett, C. T., 1984, Simple inversion of time-domain electromagnetic data: Geophysics, **49**, 925-933.
- Cull, J. P., 1993, Downhole three component TEM probes: Expl. Geophys., **24**, 437-442.
- Dyck, A. V., and West G. F., 1984, The role of simple computer models in interpretations of wide-band, drill-hole electromagnetic surveys in mineral exploration: Geophysics, **49**, 957-980.
- Fraser, D. C., 1972, A new multicoil aerial electromagnetic prospecting system: Geophysics, **37**, 518-537.
- Frischknecht, F. C., Labson, V. F., Spies, B. R., and Anderson, W. L., 1991, Profiling methods using small sources, in Nabighian M. N., Ed., Electromagnetic methods in applied geophysics, Vol. 2, Applications: Soc. Expl. Geophys. Investigations in geophysics, no. 3, 105-270.
- Hodges, D. G., Crone, J. D., and Pemberton, R., 1991, A new multiple component downhole pulse EM probe for directional interpretation: Proc. 4th Int. MGLS/KEGS Sym. on Borehole Geophys. For Min. Geotech. And Groundwater Appl.
- Hogg, R. L. S., 1986, The Aerodat multigeometry, broadband transient helicopter electromagnetic system, in Palacky, G. J., Ed., Airborne resistivity mapping: Geol. Surv. Can. Paper **86-22**, 79-89.
- Lee, J., 1986, A three component drill-hole EM receiver probe: M.Sc. thesis, Univ. of Toronto.
- Macnae, J. C., 1984, Survey design for multicomponent electromagnetic systems: Geophysics, **49**, 265-273.
- Macnae, J. C., Smith, R. S., Polzer, B. D., Lamontagne, Y., and Klinkert, P. S., 1991, Conductivity-depth imaging of airborne electromagnetic step-response data: Geophysics, **56**, 102-114.
- McCracken, K. G., Oristaglio, M. L., and Hohmann, G. W., 1986, Minimization of noise in electromagnetic exploration systems: Geophysics, **51**, 819-132.
- McNeill, J.D., and Labson, V., 1991, Geological mapping using VLF radio fields, in Nabighian M. N., Ed., Electromagnetic methods in applied geophysics, Vol. 2, Applications: Soc. Expl.

Geophys. Investigations in geophysics, no. 3, 521-640.

Morrison, H.F., Phillips, R.J., and O'Brien, D.P., 1969, Quantitative interpretation of transient electromagnetic fields over a layered earth: *Geophys. Prosp.* **17**, 82-101.

Palacky, G. J., and West, G. F., 1973, Quantitative measurements of Input AEM measurements: *Geophysics*, **38**, 1145-1158.

Palacky, G. J., and West, G. F., 1991, Airborne electromagnetic methods, in Nabighian M. N., Ed., *Electromagnetic methods in applied geophysics, Vol. 2, Applications: Soc. Expl. Geophys. Investigations in geophysics, no. 3*, 811-879.

Spies, B. R., and Frischknecht, F. C., 1991, Electromagnetic sounding, in Nabighian M. N., Ed., *Electromagnetic methods in applied geophysics, Vol. 2, Applications: Soc. Expl. Geophys. Investigations in geophysics, no. 3*, 285-425.

Vozoff, K., 1990, Magnetotellurics: Principles and practices: *Proc. Indian Acad. Sci.*, **99**, 441-471.

Vozoff, K., 1991, The magnetotelluric method, in Nabighian M. N., Ed., *Electromagnetic methods in applied geophysics, Vol. 2, Applications: Soc. Expl. Geophys. Investigations in geophysics, no. 3*, 641-711.

Wait, J. R., 1982, *Geo-electromagnetism*: Academic Press Inc.

Zonge K. L., and Hughes, L. J., 1991, Controlled-source audio-magnetotellurics, in Nabighian M. N., Ed., *Electromagnetic methods in applied geophysics, Vol. 2, Application: Soc. Expl. Geophys. Investigations in geophysics, no. 3*, 713-809.

Appendix E

Data Archive Description

Data Archive Description:

Survey Details

Survey Area Name: Edmonton - Red Deer Area
Job number: 07427 & 08401
Client: Alberta Energy Resources Conservation Board
Survey Company Name: Fugro Airborne Surveys
Flown Dates: November 21st - December 18th, 2007 and
February 6th - February 18th, 2008
Archive Creation Date: March, 2008

Survey Specifications

Northern Blocks (30Hz and 90Hz), 2007 Flying

Traverse Line Azimuth: 150° - 330°
Traverse Line Spacing: 800m
Tie Line Azimuth: 65° - 245°
Tie Line Spacing: 15000m

Southern Block (30Hz Extension), 2008 Flying

Traverse Line Azimuth: 65° - 245°
Traverse Line Spacing: 800m
Tie Line Azimuth: 150° - 330°
Tie Line Spacing: 15000m

Flying Elevation: 120 m Mean Terrain Clearance
Average Aircraft Speed: 65 m/s

Geodetic Information for map products

Projection: Alberta 10 TM Projection
Datum: NAD83
Central meridian: 115° West
False Easting: 500000 metres
False Northing: 0 metres
Scale factor: 0.9992
I.G.R.F. Model: 2007
I.G.R.F. Correction Date: 2007.9 & 2008.1

Equipment Specifications:

Navigation

GPS Receiver: NovAtel OEM4, 12 Channels
Aircraft: Casa (Twin Turbo Propeller)
Video Camera: Panasonic WV-CL302

Magnetics

Type: Scintrex CS-2 Cesium Vapour
 Installation: Towed bird
 Sensitivity: 0.01 nT
 Sampling: 0.1 s

Electromagnetics

Type: GEOTEM[®], 20 channel multicoil system
 Installation: Vertical axis loop (231m² area with 6 turns) mounted on the aircraft.
 Receiver coils in a towed bird.
 Coil Orientation: X, Y and Z
 Frequency: 30 Hz & 90 Hz
 Pulse width: 4045 μ s (30Hz) & 2110 μ s (90Hz)
 Off-time: 12589 μ s (30Hz) & 3346 μ s (90Hz)
 Geometry: Tx-Rx horizontal separation of ~130 m
 Tx-Rx vertical separation of ~45 m
 Sampling: 0.25 s

30 Hz Data Windows:

Channel	Start (p)	End (p)	Width (p)	Start (ms)	End (ms)	Width (ms)	Mid (ms)
1	6	21	16	0.041	0.171	0.130	0.106
2	22	179	158	0.171	1.457	1.286	0.814
3	180	337	158	1.457	2.743	1.286	2.100
4	338	495	158	2.743	4.028	1.286	3.385
5	496	510	15	4.028	4.150	0.122	4.089
6	511	522	12	4.150	4.248	0.098	4.199
7	523	537	15	4.248	4.370	0.122	4.309
8	538	557	20	4.370	4.533	0.163	4.451
9	558	582	25	4.533	4.736	0.203	4.635
10	583	617	35	4.736	5.021	0.285	4.879
11	618	662	45	5.021	5.387	0.366	5.204
12	663	717	55	5.387	5.835	0.448	5.611
13	718	787	70	5.835	6.405	0.570	6.120
14	788	872	85	6.405	7.096	0.692	6.750
15	873	972	100	7.096	7.910	0.814	7.503
16	973	1097	125	7.910	8.927	1.017	8.419
17	1098	1247	150	8.927	10.148	1.221	9.538
18	1248	1447	200	10.148	11.776	1.628	10.962
19	1448	1697	250	11.776	13.810	2.035	12.793
20	1698	2048	351	13.810	16.667	2.856	15.238

90 Hz Data Windows:

Channel	Start (p)	End (p)	Width (p)	Start (ms)	End (ms)	Width (ms)	Mid (ms)
1	6	26	21	0.027	0.141	0.114	0.084
2	27	146	120	0.141	0.792	0.651	0.467
3	147	264	118	0.792	1.432	0.640	1.112
4	265	384	120	1.432	2.083	0.651	1.758
5	385	406	22	2.083	2.203	0.119	2.143
6	407	426	20	2.203	2.311	0.109	2.257
7	427	446	20	2.311	2.420	0.109	2.365
8	447	466	20	2.420	2.528	0.109	2.474
9	467	486	20	2.528	2.637	0.109	2.582
10	487	511	25	2.637	2.772	0.136	2.705
11	512	536	25	2.772	2.908	0.136	2.840
12	537	566	30	2.908	3.071	0.163	2.989
13	567	596	30	3.071	3.234	0.163	3.152
14	597	636	40	3.234	3.451	0.217	3.342
15	637	676	40	3.451	3.668	0.217	3.559
16	677	721	45	3.668	3.912	0.244	3.790
17	722	771	50	3.912	4.183	0.271	4.047
18	772	831	60	4.183	4.508	0.326	4.346
19	832	906	75	4.508	4.915	0.407	4.712
20	907	1024	118	4.915	5.556	0.640	5.235

ASCII and Geosoft Line Archive File Layout (*_ascii.xyz & *.gdb):

Field	Variable	Description	Units
1	Line	Line Number	
2	Fiducial	Seconds after midnight	sec.
3	Flight	Flight number	-
4	Date	Date of the survey flight	ddmmyy
5	Lat_NAD83	Latitude in NAD83	degrees
6	Long_NAD83	Longitude in NAD83	degrees
7	X_NAD83	Easting (X) in NAD83 Alberta 10TM Projection	m
8	Y_NAD83	Northing (Y) in NAD83 Alberta 10TM Projection	m
9	GPS_Z	GPS elevation (above WGS84 datum)	m
10	Radar	Radar altimeter	m
11	DTM	Terrain (above WGS84 datum)	m
12	Diurnal	Ground Magnetic Intensity	nT
13	TMI_raw	Raw Airborne Total Magnetic Intensity	nT
14	IGRF	International Geomagnetic Reference Field	nT
15	RMI	Final Airborne Residual Magnetic Intensity	nT
16	Primary_field	Electromagnetic Primary Field	μ V
17	Hz_monitor	Powerline Monitor (60 Hz)	μ V
18-37	x01-x20	Final dB/dt X-Coil Channels 1-20	pT/s
38-57	y01-y20	Final dB/dt Y-Coil Channels 1-20	pT/s
58-77	z01-z20	Final dB/dt Z-Coil Channels 1-20	pT/s
78-97	Bx01-Bx20	Final B-Field X-Coil Channels 1-20	fT
98-117	By01-By20	Final B-Field Y-Coil Channels 1-20	fT
118-137	Bz01-Bz20	Final B-Field Z-Coil Channels 1-20	fT
138-157	Raw_x01-Raw_x20	Raw dB/dt X-Coil Channels 1-20	pT/s
158-177	Raw_y01-Raw_y20	Raw dB/dt Y-Coil Channels 1-20	pT/s
178-197	Raw_z01-Raw_z20	Raw dB/dt Z-Coil Channels 1-20	pT/s
198-217	Raw_Bx01-Raw_Bx20	Raw B-Field X-Coil Channels 1-20	fT
218-237	Raw_By01-Raw_By20	Raw B-Field Y-Coil Channels 1-20	fT
238-257	Raw_Bz01-Raw_Bz20	Raw B-Field Z-Coil Channels 1-20	fT
258	VD1	First Vertical Derivative of RMI	nT/m
259	Res_hs_z1	Apparent Resistivity (Half Space Model) from dB/dt Z Ch 01	ohm-m

ASCII and Geosoft CDT File Layout (*_RDI_array_ascii.xyz and *_RDI_array.gdb):

Field	Variable	Description	Units
1	Line	Line Number	
2	Fiducial	Seconds after midnight	sec.
3	X_NAD83	Easting (X) in NAD83 Alberta 10TM Projection	m
4	Y_NAD83	Northing (Y) in NAD83 Alberta 10TM Projection	m
5	GPS_Z	GPS elevation (above WGS84 datum)	m
6	Radar	Radar altimeter	m
7	DTM	Terrain (above WGS84 datum)	m
8	Hz_monitor	Powerline Monitor (60 Hz)	μV
9 – 159	Resistivity	Resistivity at Depth Below surface from 0 - 300m at 2 m intervals	ohm-m
	Depth*	Depth Below Surface (0 - 300m)	m

Note – The Depth field is in the Geosoft database only.

The null values in the ASCII archive are displayed as –9999999.000000

Grid Archive File Description:

The grids are in Geosoft and ArcInfo format. A grid cell size of 200 m was used for all area grids.

File	Description	Units
ERDA_RMI	Residual Magnetic Intensity	nT
ERDA_VD1	First Vertical Derivative	nT/m
(30Hz or 90Hz)_Res_z1(_deh)	Apparent Resistivity (Half Space Model) from dB/dt Z Ch 01	ohm-m
ERDA_RDI_Slice_10m(_deh)	Resistivity Depth Slice at 10m	ohm-m
ERDA_RDI_Slice_30m(_deh)	Resistivity Depth Slice at 30m	ohm-m
ERDA_RDI_Slice_60m(_deh)	Resistivity Depth Slice at 60m	ohm-m
ERDA_RDI_Slice_120m(_deh)	Resistivity Depth Slice at 120m	ohm-m

The *_deh files are the grid files corrected for asymmetry (“de-herringboned”).

Due to the nature of the Apparent Resistivity, it is not suitable to merge data from the two different base frequencies.

Resistivity Depth Section grid archive Description:

The surface referenced resistivity depth section grids are named according to the following convention:

*rdi***LINE***_trc*.grd

where **LINE** is the line number of the section grid and **trc** refers to sections that are terrain corrected. Grids are in Geosoft binary format with units in Ohm-metres.

SEG-Y Archive Description:

Two sets of the resistivity SEG-Y files were archived. One set relative to surface and one set shifted to be referenced to a datum of 1035 metres above the WGS84 spheroid. Both the shifted and non-shifted SEG-Y files have identical names and are differentiated by the directories in which they are contained (surface_referenced, datum_shifted). The SEG-Y files are named according to the following convention:

*sgy***LINE**.sgy

where **LINE** is the survey line number.

Appendix F

Map Product Grids

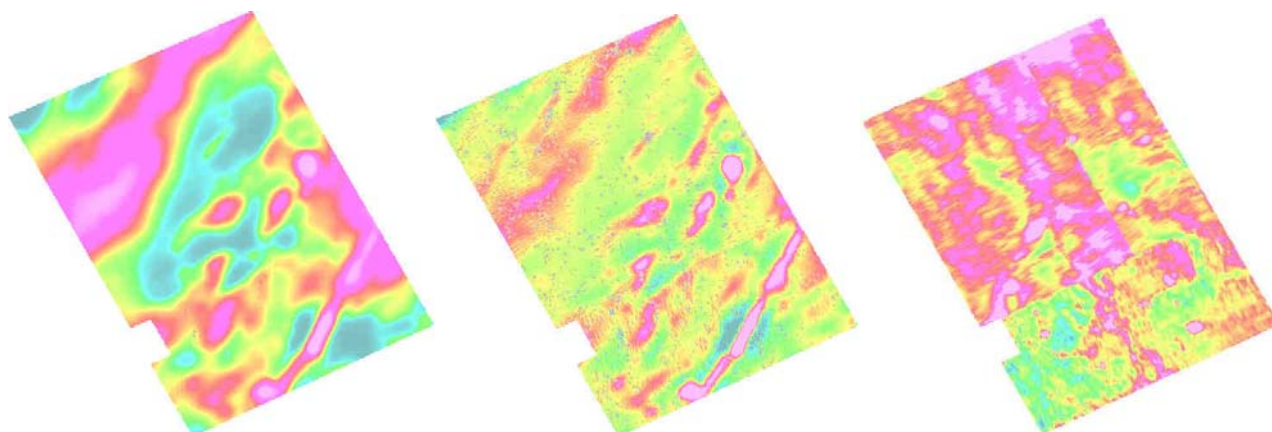


Figure 1. Residual Magnetic Intensity (left), First Vertical Derivative of RMI (middle), and Apparent Resistivity (right)

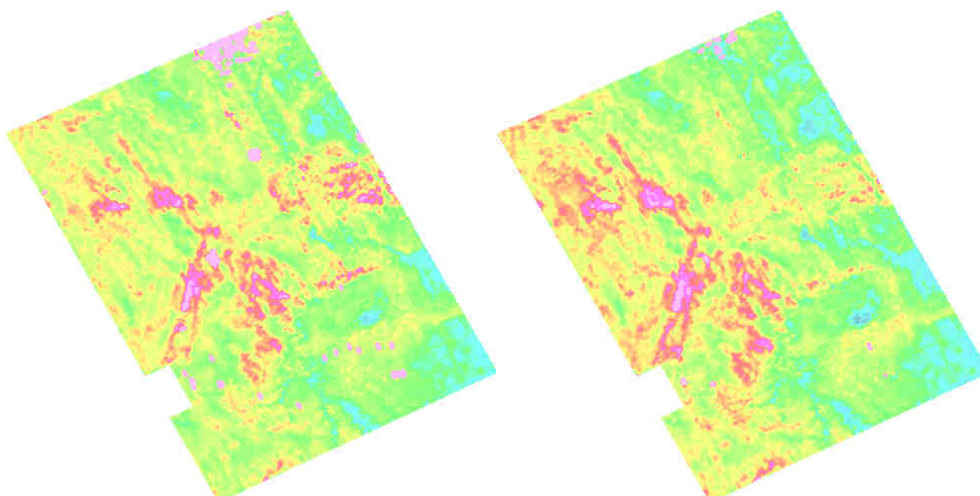


Figure 2. Resistivity Depth Section (RDS) at 10 metres (left), and RDS at 30 metres (right)

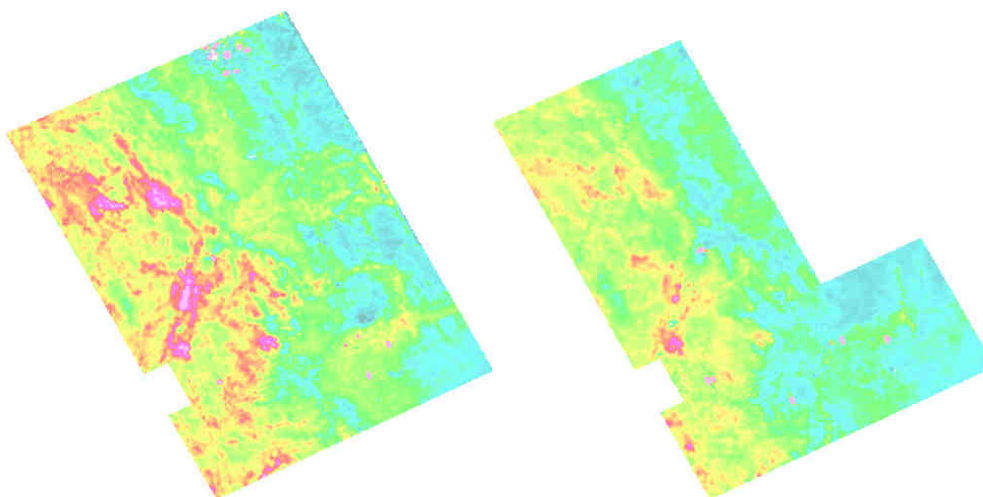


Figure 3. RDS at 60 metres (left), and RDS at 120 metres (right)

Appendix G

Reference Waveform

Reference Waveform Descriptor:

The information shown is only an example. The actual reference waveforms are provided on CD-ROM or DVD and will have been renamed to ptaFLTpre.out / ptaFLTpost.out, "FLT" represents the flight number.

The reference waveform can be divided into four main sections, which are described below.

Section 1

This section contains the name of the raw reference waveform file (i.e. **D0050704.002**). The approximate horizontal and vertical offsets (i.e. **125 m** and **50 m**) of the EM bird position in meters are listed. These are followed by the base frequency (i.e. **90Hz**) in Hertz and the sample interval (i.e. **43.4 μs**) in microseconds.

```

GEOTEM Calibration Data - Version 31 July 1998
'D0050704.002' = Name of original saved parameter table file
 125.000000000000000 = Horizontal TX-RX separation in meters
  50.000000000000000 = Vertical TX-RX separation in meters
  90.000000000000000 = Base Frequency in Hertz
 43.402777777777779 = Sample Interval in micro-seconds
  
```

Section 2

This section displays the gate configuration for channels 1 to 20.

20 Time Gates: First and Last Sample number, RMS chart position:

Start & end samples of each channel			
1	4	11	1
2	12	25	2
3	26	39	3
4	40	53	4
5	54	59	5
6	60	61	6
7	62	64	7
8	65	67	8
9	68	71	9
10	72	75	10
11	76	79	11
12	80	83	12
13	84	87	13
14	88	92	14
15	93	97	15
16	98	102	16
17	103	108	17
18	109	114	18
19	115	121	19
20	122	128	20

} Channels 1 to 20

Appendix 3 – Interpretation of the GEOTEM® Airborne EM Data from the Alberta Energy Resources Conservation Board Groundwater Mapping Project, Red Deer–Edmonton Corridor Survey

Interpretation of the GEOTEM™ Airborne EM Data
from the
Alberta Energy Resources Conservation Board
Groundwater Mapping Program
Red Deer – Edmonton Corridor Survey

November 15, 2008

Larch Consulting Ltd
and
Fugro Airborne Surveys
Project 08411

Table of Contents

Introduction.....	3
Data Preparation and Analysis.....	4
Data Inversion and Interpretation	8
Results	19
Integration of the March and November 2008 GEOTEM™ Results	44
Data Interpretation.....	52
Summary and Conclusions.....	77
References	78
APPENDIX I - Definitions	79



Introduction

On behalf of the Alberta Energy Resources Conservation Board (AGS) Fugro Airborne Surveys (hereafter FUGRO) has flown an adjoining area along the western boundary of the earlier airborne surveys that were part of the groundwater mapping program in the region referred to as the Edmonton-Calgary corridor. The objective is to map buried aquifers to a depth of 200 m in both bedrock and unconsolidated drift strata using electromagnetic (EM) and magnetic data. The scope of the work includes both the collection and the processing of airborne geophysical data. FUGRO Airborne Surveys acquired data for an area shown in Figure 1, the heavier outline, with an 800 m line spacing using the GEOTEM™ time-domain airborne EM system. The earlier GEOTEM™ surveys are shown in Figure 1 in lighter outline and the RESOLVE™ survey in pink. The latest survey was flown in June and July 2008 and the data processing was completed in early August 2008. Some additional processing was done prior to doing the inversion work reported here and was not completed until late September. The survey specifications, data products and data processing have been described in a separate FUGRO report. The processed data and the processing report were submitted to the AGS in August. The processed data interpretation is reported here.

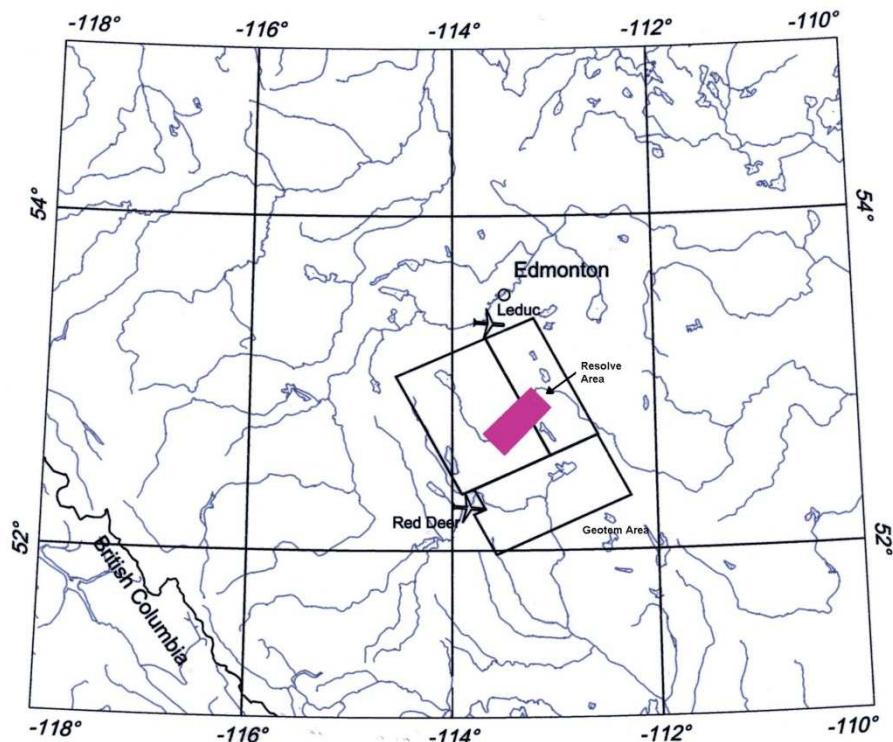


Figure 1: Airborne EM Survey Area Location Map

The first step in the data interpretation was to operate an inversion process on the data. The inversion process is described in a following section. The inversion results were imported to GEOSOFT OASIS™ (hereafter GEOSOFT™) where they were gridded.



Images and maps were generated from the grids. These products were used to conduct a simple geological analysis of the data. Additionally, comments are made about data quality and earth model resolution. Magnetic data are measured with the EM data and are briefly interpreted here and integrated with the EM data.

A brief discussion and comparison of the interpretation reported here and the one done earlier in 2008 is presented.

Data Preparation and Analysis

The fixed wing, time domain system (GEOTEM™) was flown using a base frequency of 30 Hertz along 800m (approximate) spaced flight lines in a north 30 degrees west direction. Tie lines were nominally 1500 m apart in a north 60 east direction. The GEOTEM™ data were recorded approximately at 8m intervals along the flight lines. The area flown was about *102X136km*.

The processing report explains in some detail the steps taken to prepare the raw, observed data for further interpretation and analysis. The processed data were loaded into GEOTEM™ data base. A process was used for the GEOTEM™ data that created apparent resistivity depth sections, called RDIs™. The process was also described in the respective processing report.

The data were processed for interpretation using a layered inversion method described in the next section. It is likely that additional insight will be gained upon a study of these results and from future water well studies and new drilling by the client. A revisit of the inversions results is commonly done after such studies and the acquisition of new information to extract additional information from the electromagnetic survey data.

The data base prepared in the post flight processing step was used as input for the inversion process and the inversion results were placed back into the same data base. The data base and any maps or grids made from the data base can be viewed using a GEOSOFT OASIS Viewer™ that can be downloaded free from GEOSOFT™. Several grids were made from the inversion results and are included in this report as shaded relief images (figures) and as maps (pocket).

Four inversion models were done on the GEOTEM™ data following the results obtained in the earlier study concluded in May 2008, Models n, nn, m and mm, Table 1. As before, the Model nn results were deemed the best and have been provided to the client in the requested grid formats and are discussed in this report. The four models were done to better assess any changes that might have arisen due to the current survey area lying west of the previous surveys areas and possible containing a somewhat different resistivity profile with depth. However, the models remain consistent with the ones used for the earlier surveys.



Model	R ₁	R ₂	R ₃	R ₄	R ₅	t ₁	t ₂	t ₃	t ₄
m	20	80	15	8		30	15	25	
mm	100	50	20	10	5	10	20	30	50
n	75	45	25	10		15	15	15	
nn	75	45	30	15	8	15	20	20	20

Table 1: List of four inversion models run on the 30hz GEOTEM™ data. R is layer resistivity and t is the layer thickness, with the subscript identifying the layer.

Data from the current GEOTEM™ survey is reported here but were merged with the previous survey data to make a complete data set for the current status of the Edmonton Red Deer airborne EM survey data. Some comment is made on the consistency of the results across the four separate surveys that have been completed to date.

In this report, some discussion accompanies each figure that includes both an interpretation of the data and of the method used to create the image shown in the Figure under discussion. The final results have been provided to the client in the special Alberta projection. The image scales are quite small. In fact, the area covered by the GEOTEM™ survey is quite large and various map parameters are too small to see at the image scale in the figures. However, they can be seen on maps and any computer viewed images.

A feature of the inversion process for the time domain system is to use only the off time of the measured response. A second, common analysis technique is not to invert every measurement point along the line. Again to save some time, and not losing significant detail, one might invert every 10th point and interpolate the intervening points. This represents about an 80 meter averaging along the line for the GEOTEM system. It is viewed acceptable, since the geometry of the system tends to average over a 300 m “foot print”.

The township and range grids, major drainage and the US government 90m elevation data were imported into the project and are shown overlain on many of the data images. These overlays provide a frame of reference, and in the case of the drainage and elevation data provide a basis for evaluation whether any topographic influences may be present in the data and the inversion results.

Figure 2a shows the flight line pattern for the survey interpreted here. The line directions are designed to maximize coverage of the anticipated geological strike directions of the features of interest. The tie lines provide of means to level data across the flight lines, particularly the magnetic data. It is important to know that the spatial sampling of the features of interest is best in the flight line direction. The data have been gridded at 200m so it decreases the recorded resolution along the flight line direction and it “creates” data



between the 800m spaced tie lines. There is the possibility of some spatial aliasing to occur in the tie line direction.

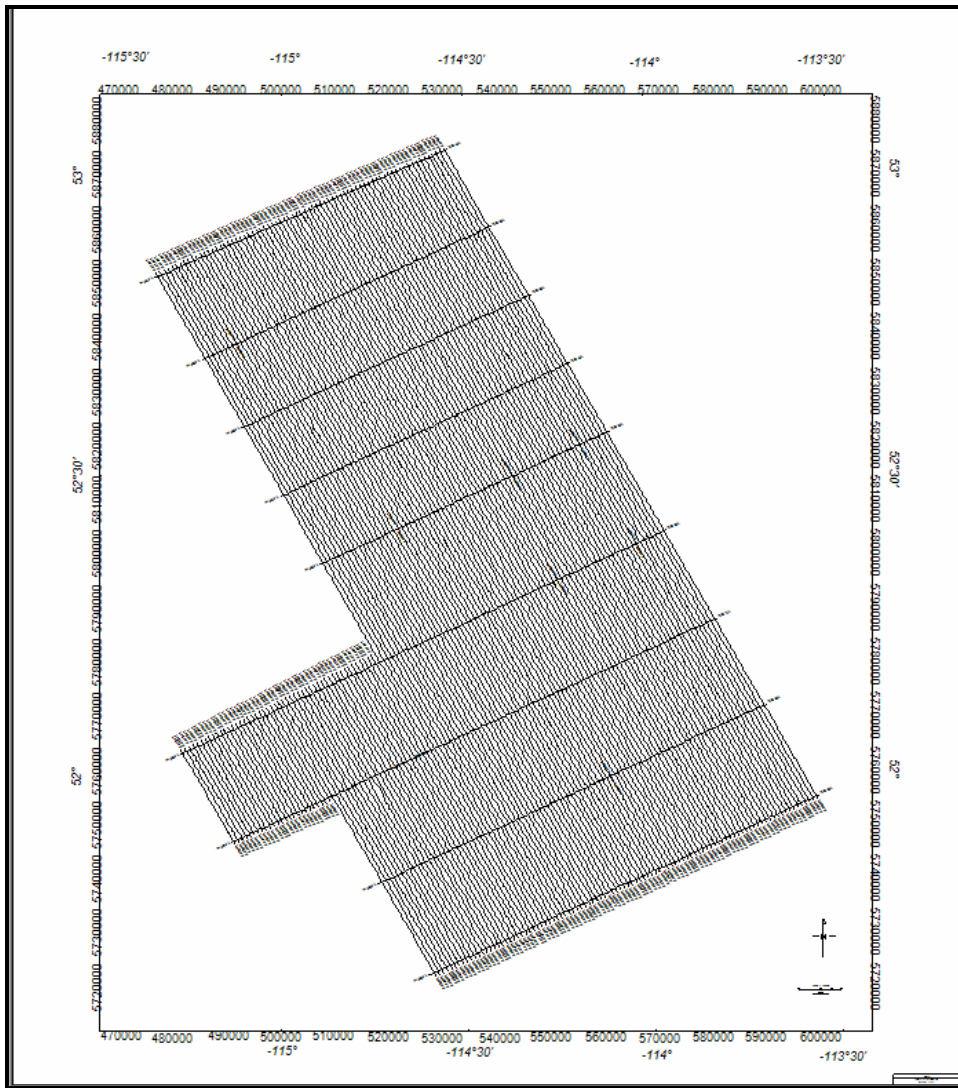


Figure 2a: An image of the flight line pattern for the survey. The township and range grid and major drainage is overlain. The image co-ordinates are in the Alberta TM10 projection.

Figure 2b shows the US government 90m elevation data. It is relevant because the EM system may investigate up to some depth, depending on the subsurface resistivity, which most likely will be a different formation across the survey area. The elevation data are important for several reasons: 1) the problem posed later in Figures 4 and 5, 2) the possibility that surficial deposits or bedrock geology follow terrain and the EM results



follow these trends, 3) drape flying the terrain is an objective but in areas of rugged terrain and large relief it may not be possible. Drainage is part of this evaluation since surface and near surface features will influence the EM results. Water saturation and lithology are important influences on resistivity

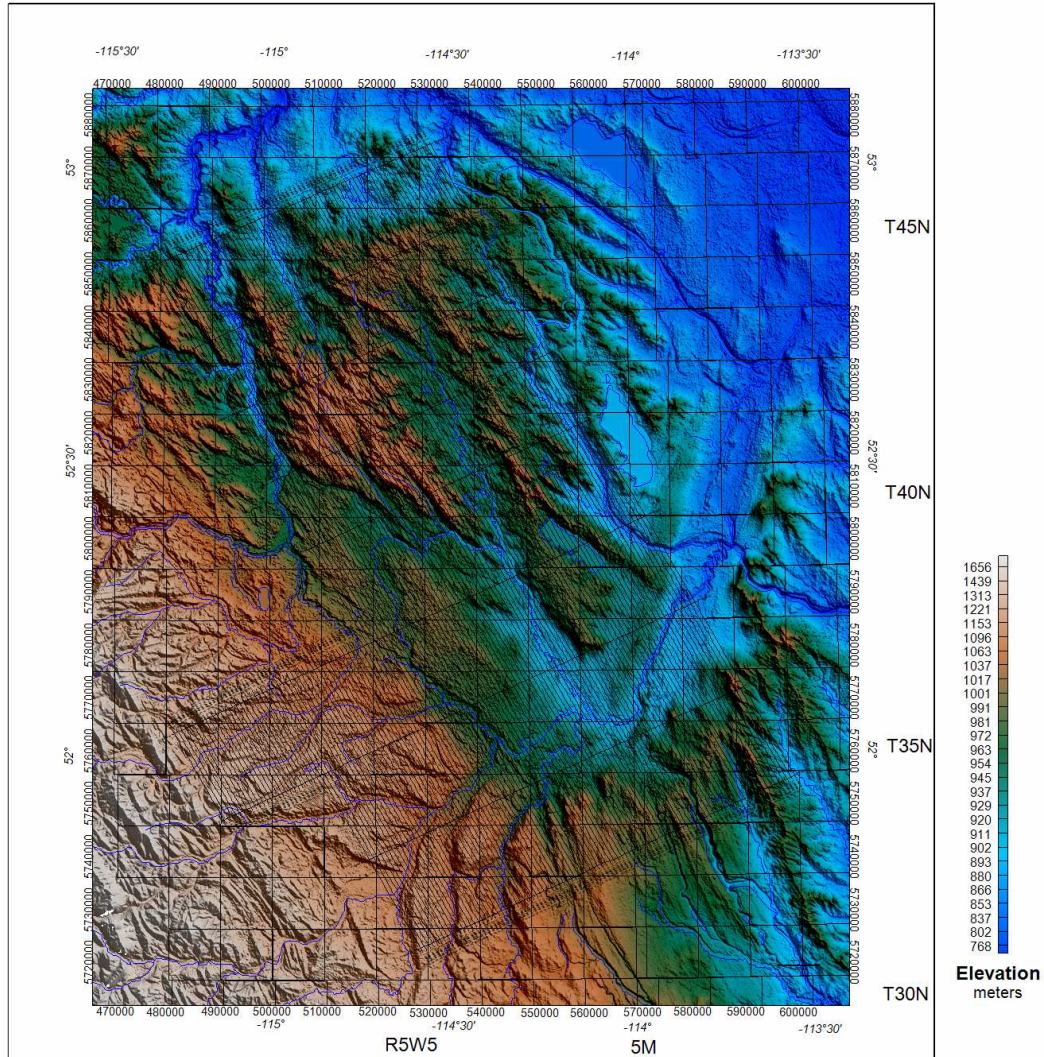


Figure 2b: Image of the flight line pattern for the GEOTEM survey on the US Government 90m elevation data, downloaded from their website and shown as a color shaded relief image Principal drainage and the township and range grid are also shown on the image. Note, that, in the some parts of the survey area, the NW-SE flight lines are somewhat parallel to the relief. The drainage and elevation data do not exactly overlay due to inaccuracies in their respective compilations.



Data Inversion and Interpretation

The data inversion for the GEOTEMTM data was done using software developed in Australia for a consortium of companies that included FUGRO. The program is called AIRBEOTM (Raiche, 1998) and operates on single measurement points along the flight line and assumes a simple layered earth resistivity structure, Figure 3. The model may be any number of layers but is commonly six or less. Three layers are shown in Figure 3, with the third layer basically an infinite half space. Basic inversion principles can be found described in Glenn et al., 1973, Tripp et al. 1984; Hohmann and Raiche, 1988; Chin and Raiche, 1998. The AIRBEOTM algorithm uses a 1D singular value decomposition inversion.

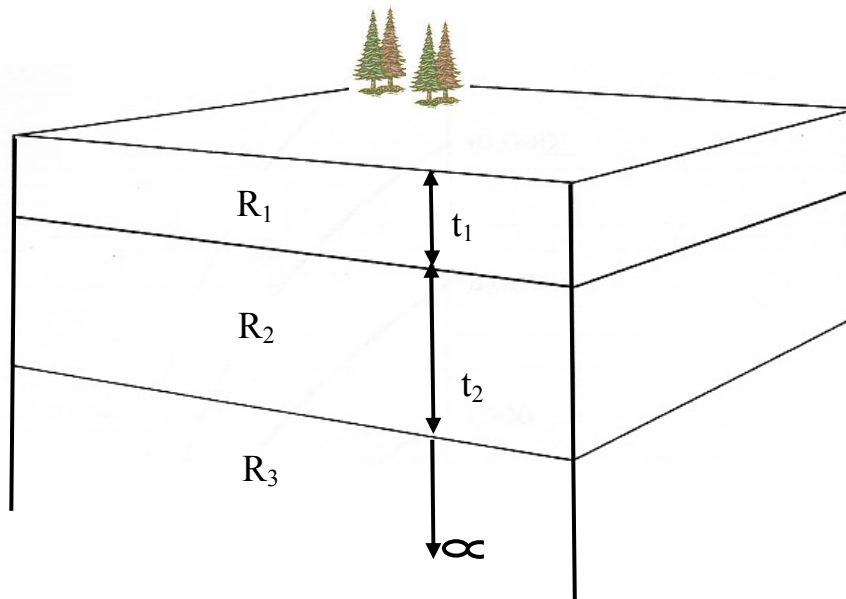


Figure 3: Layered earth model used in the inversion process. The earth may be any number of layers, but typically is six or less. The layer parameters found by inversion are each of the layer resistivities, R , and thicknesses, t . The lowermost layer is “infinite”.

The inversion process, simply described, compares the theoretical electromagnetic fields from the layered earth model to the observed data. The process continues until a “goodness of fit” is reached, commonly measured by the least square error of fit between the measured and calculated data. AIRBEOTM permits some flexibility to control the inversion process in an attempt to find a good fit between the observed data and the calculated data from the layered model. However, the process is non-linear and can reach a number of reasonable data fits. The result is sensitive to the starting layer model used. Experience, a priori information, and well data can be used to establish starting models. The RDITM results for the GEOTEMTM system can also be a guide to the starting model



for this system. Although these data sets provide a guide for resistivities, they are less able to provide more than a general indication of depth associated with the resistivities.

The individual layered inversion results are then plotted along the survey lines to create a “2D” map view representation of the subsurface resistivity and layer thickness variation over the survey area. One can view the individual lines in a stacked form to create a “3D” image of the subsurface. Alternatively the data can be imported to a 3D volume software system to create a “3D” image of the inversion results. The results are plotted referenced to topography so an actual depth model is presented. However, the depth is variable and is dependent on the resistivity of the subsurface. The results, then, are 2D and 3D constructs and not actual 2D and 3D results. Any real 2D and 3D variations in the subsurface could make the 1D approximation inaccurate. Since airborne systems average both horizontally and vertically due to their geometries and physical size, many of these effects are smoothed to some extent. The significant exceptions are relatively narrow, good conductors, such as metallic mineralization which is a major objective of these survey systems in mineral exploration and sharp lateral boundaries, such as channels, important in many applications, including oil and gas exploration and water resource investigations.

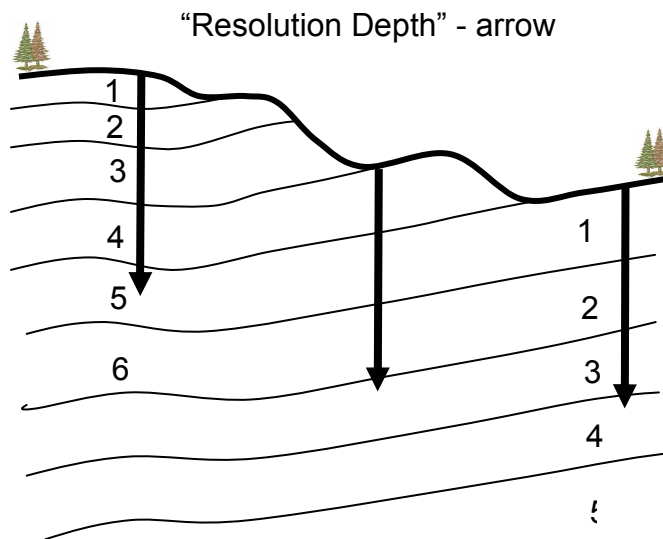
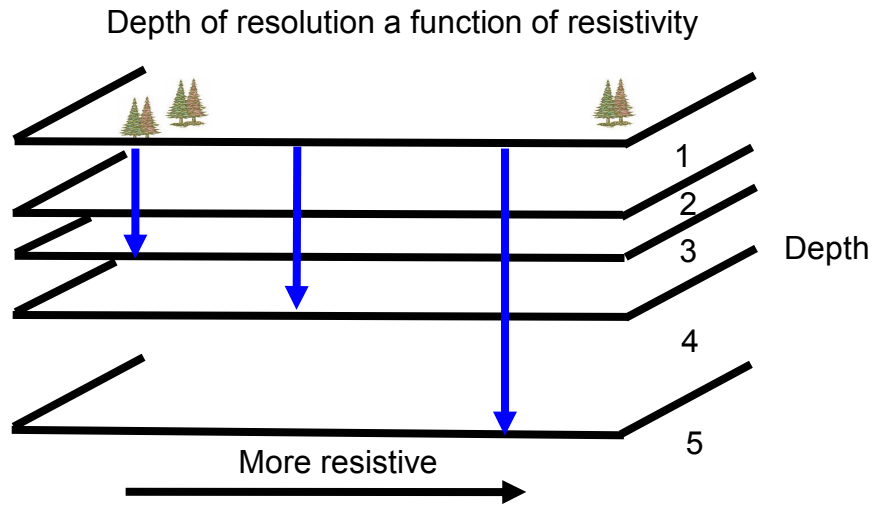
The more resistive the subsurface, the greater the depth the electromagnetic energy transmitted from the airborne system will penetrate the earth with amplitude sufficient to create a secondary field in the subsurface that can be detected in the receiver system on the aircraft. The nominal depth that this occurs with the GEOTEM™ system is typically quoted to be between 250m and 300m. However, in areas of low resistivities, values around 5 – 10 ohm for example, this depth may be much less. A second feature of this limited depth of investigation is depicted in Figure 4. If the geology is near horizontal layers, and there is some topographic variability, then the formation probed by the system at the maximum depth of investigation will vary over the survey area. This variability is depicted in Figure 4.

The vertical arrows in the top cartoon in Figure 4 show how the depth of exploration increases with higher resistivity. In the lower cartoon in Figure 4 the arrows indicate how the depth of exploration, if constant, will probe to different formation levels due to changes in topography. If the formations change in resistivity across this type of model, not only are the formations changing, but so is the depth of exploration. For example, layer 3 in the inversion results will be a different layer 3 in the subsurface over the area covered by the survey. See Figure 5 or an illustration of this result. These two variations can lead to results that take some consideration to interpret.

The inversion process, as noted above, predicts a layered earth beneath each survey point that is inverted. This layer geometry would be imposed on the models shown in Figure 4. Hence, the layers from the inversion process are not the geological layers as depicted in Figure 4 since they would follow some depth below the surface across the model (see Figure 5). However, one can interpret the geological layer from the results since the resistivity and the thickness of the layer varies along the profile. This problem is particularly true where the layered inversion results are presented in map views. It is not



as easy to recognize that lateral changes that may be due to a depth of investigation change.



Layer number and resolution of formation changes across a region with constant depth of investigation

Figure 4: Illustration of changing depth of exploration (top) and formation examined over an area with variable resistivity and topography.



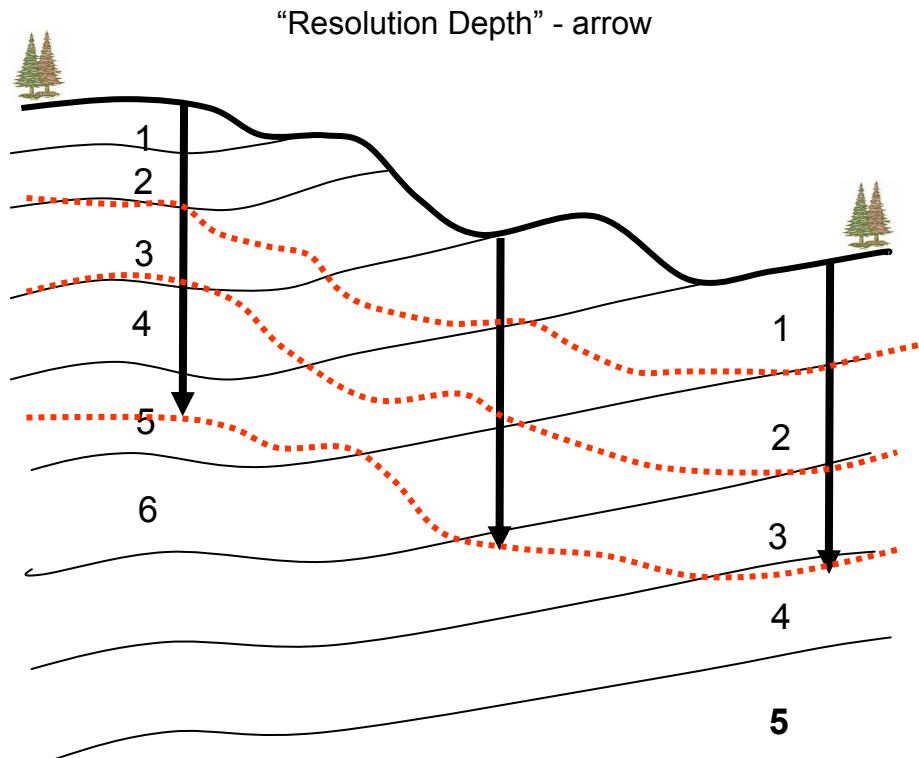


Figure 5: The cartoon of Figure 4 repeated here to show how the inversion layers (dotted red lines) might cross the model. However, one would expect the distinct resistivities of the actual layers to be mapped in each of the inversion layers where they cross the actual layers.

One of the main issues doing an inversion analysis is choosing the starting model. This model may be known a priori, from some well data, and mapping. Some indication may be available in the apparent resistivities calculated from the decay curves in the time domain GEOTEMTM data. It is customary and done here, to invert the data using several starting models and examine the changes the program attempts from each start (see Figure 6). The changes and final results are examined and a final starting model is selected and the inversion done one more time. These results are then accepted as the most likely representation of the subsurface. The other models may be included in the interpretation discussions to illustrate some aspects of the model and to provide some support for choosing the final model. Note, in the example shown here, the behavior of the parameter changes, and particular, the changes of the least square error indicate that the first starting model was the better of the two. The iterative process becomes more complex with a greater number of layers (i. e., model parameters). In this study, the results from the previous survey were used for the inversion models.



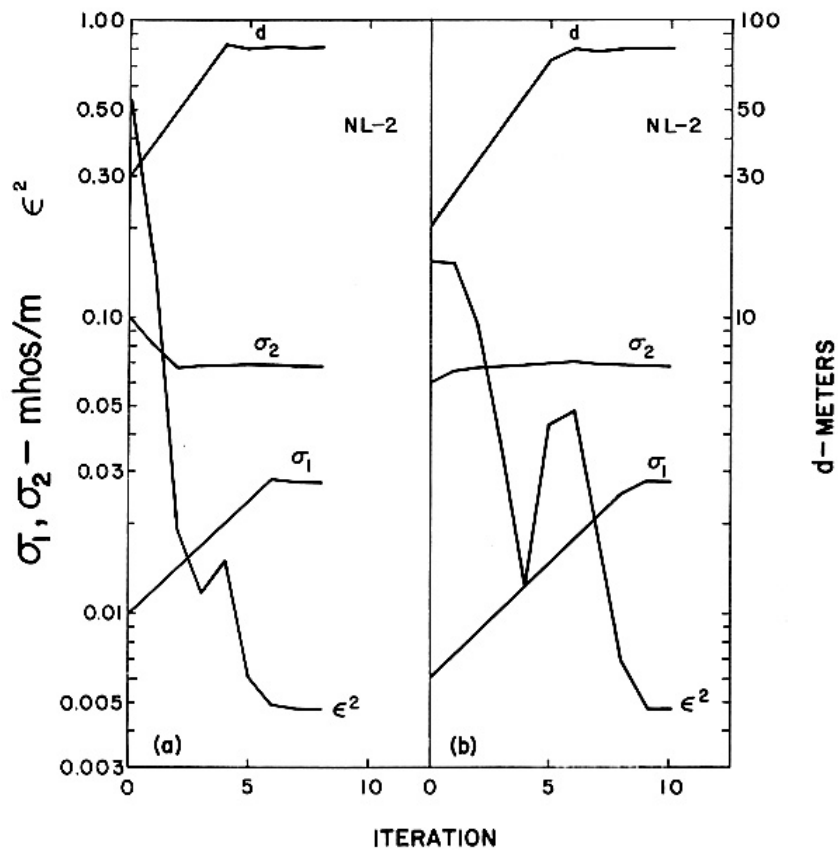


Figure 6: Figure shows the changing conductivity, σ , (inverse of resistivity) and first layer thickness, d , with iteration for a two layer model. The least square error, ϵ , is also shown. The left and right views show the iterative process converge to nearly identical models starting with different starting values for the two layer conductivities and the first layer thickness (After Glenn et al., 1973).

Figure 7 shows the inversion fit a two layer model to a set of frequency domain, loop-loop electromagnetic survey data. Note that there are fifteen measured data points that define the response curve. The position of the curve with respect to the square root of frequency is also dependent on the resistivity. The time domain inversion converts a number of frequency domain calculations to the time domain for the least square determinations.



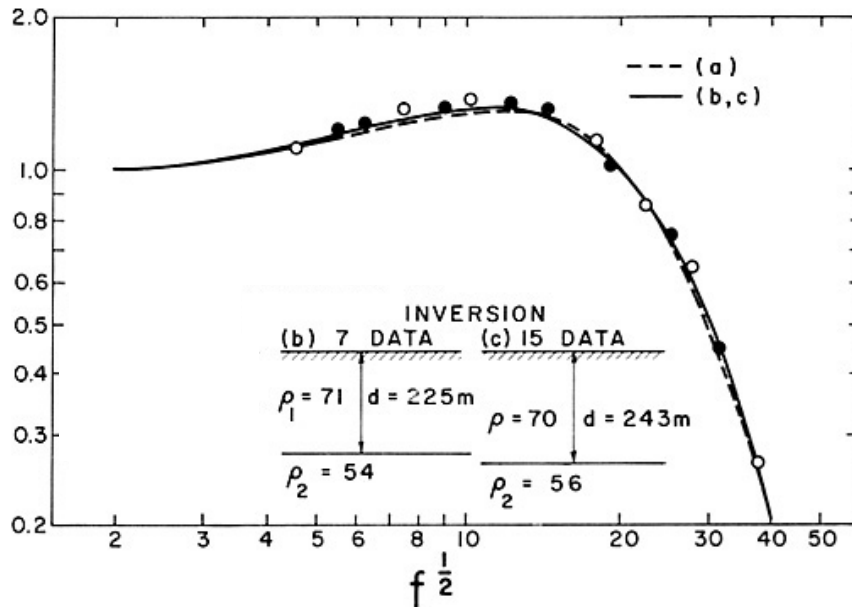


Figure 7: The fit between the observed data, dots, and the calculated response for a two layer model for an inversion process. The data were collected from a ground frequency domain loop – loop system. The vertical axis is the normalized magnetic field strength and the horizontal axis is square root of frequency, (after Glenn et al., 1973).

One objective of this survey was to map any shallow channels that may be located in the survey area. In this case, the channels would be recognized from their expected cross-sectional shape and from their “stream-like” pattern in map view. However, the constraints noted in a previous paragraph apply. A simple sketch in Figure 8 is drawn to show that channels may be found at any depth. In fact, not shown is an incised channel system which is also quite likely to occur in an area. One can imagine how the simple view seen in Figure 5 could be made more complex if the surface has some topography. Channels could “disappear” beneath topography due to the channel moving to a depth deeper than the depth of investigation. Channels could truncate against a topographic edge. The data would also map any other resistive or conductive feature such as sand rich tills, clay rich lake bottoms, eskers and other glacial features.

The preceding examples were for a frequency domain analysis but the process is the same of the time domain data measured by the GEOTEMTM system. In this case the match is made to the time domain decay curve, Figure 9.



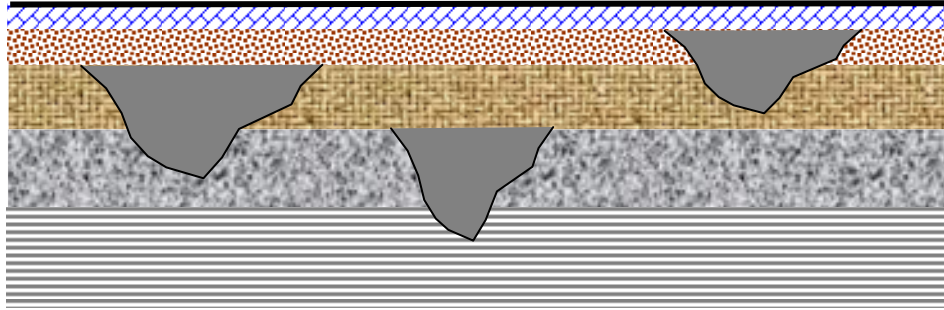


Figure 8: Cartoon of a layered earth with three buried channels.

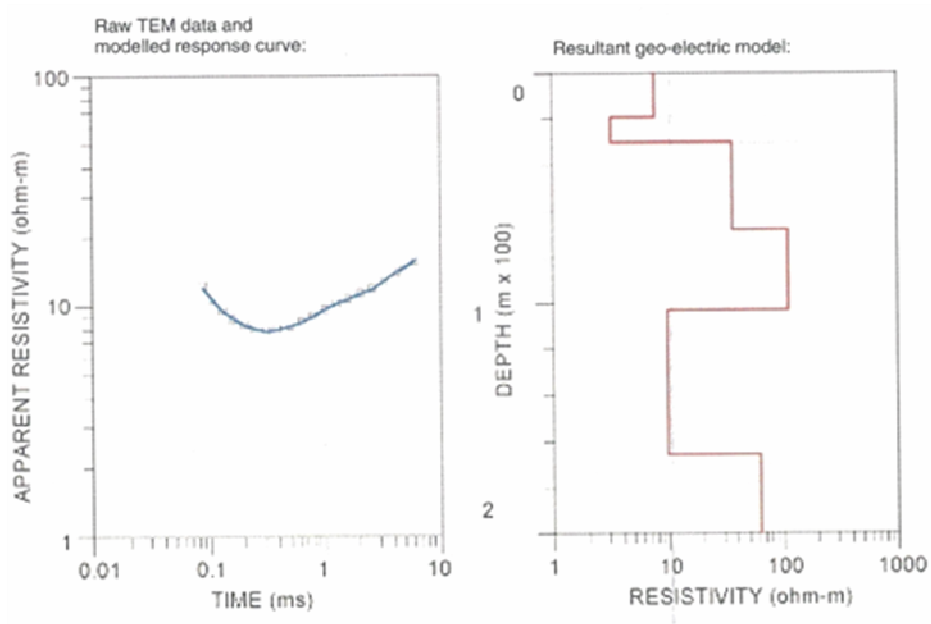


Figure 9: Layered earth inversion of a time domain decay curve, left, using a 6 layered model, right (from Associated Geosciences). The measured points are small boxes in the left figure and the model result is the smooth curve through these points. These data are from a ground survey.

Magnetic data are collected with the electromagnetic data. These data may indicate channels if certain conditions are met. Two common conditions found in Alberta are depicted in Figure 10. Either the channel is magnetic or a non-magnetic channel cuts through a magnetic horizon. The anomaly characteristics of the two cases are different and can, in most instances, be differentiated on magnetic maps. The anomaly amplitudes



due to channels are typically weak and need to be accentuated by filtering the measured total magnetic field.

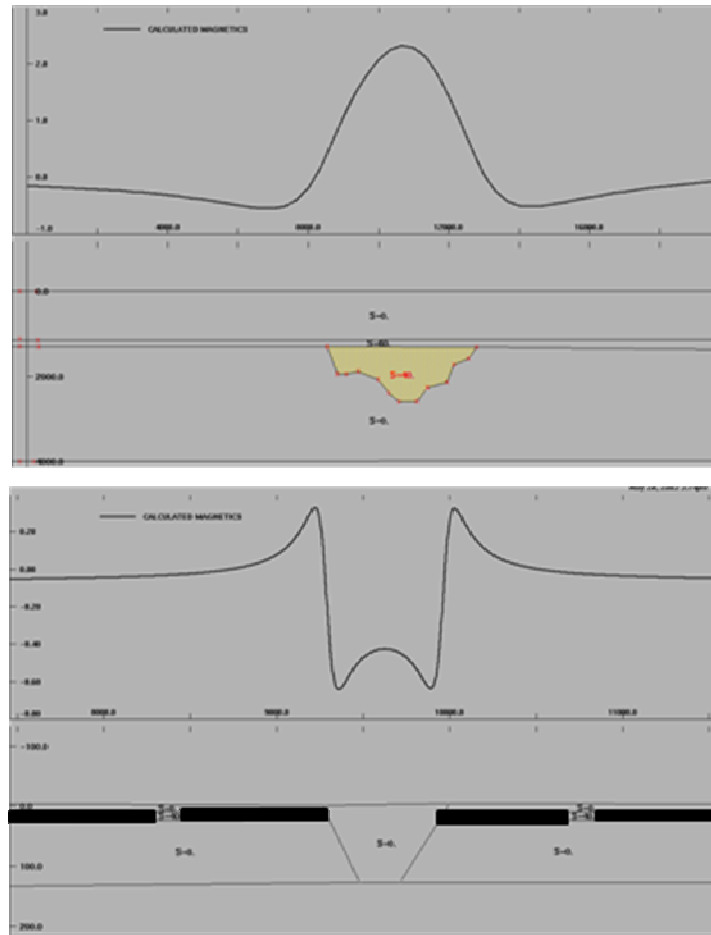


Figure 10: Bottom diagram illustrates the magnetic anomaly characteristics over an outcropping or buried channel cutting a magnetic horizon. The upper diagram is a model result showing the magnetic response of a channel that is magnetic. Note the very different anomaly shape for the two types of magnetic sources.

Channels are commonly mapped with ‘high resolution’ aeromagnetic (HRAM) data (Peirce et al, 1998). The line spacing of HRAM data is considered to be 800m or less. The GEOTEMTM survey has 800m line spacing. For good channel mapping a line spacing of 400m or less is preferred. The magnetic data are examined, briefly, in this study.

One complication of data interpretation, whether it is magnetic or electromagnetic data, is the spatial aliasing that arises because the surveys do not completely sample the total geological variation in the subsurface, Figure 11. The simple geometric forms in Figure 11 indicate that the chosen line spacing and direction do not completely sample the strike length, direction and size of all the geological targets (the geometric shapes). There will



be a natural width, sinuosity, and distribution of channels that would not be resolved by any survey and that is true for the survey studied here.

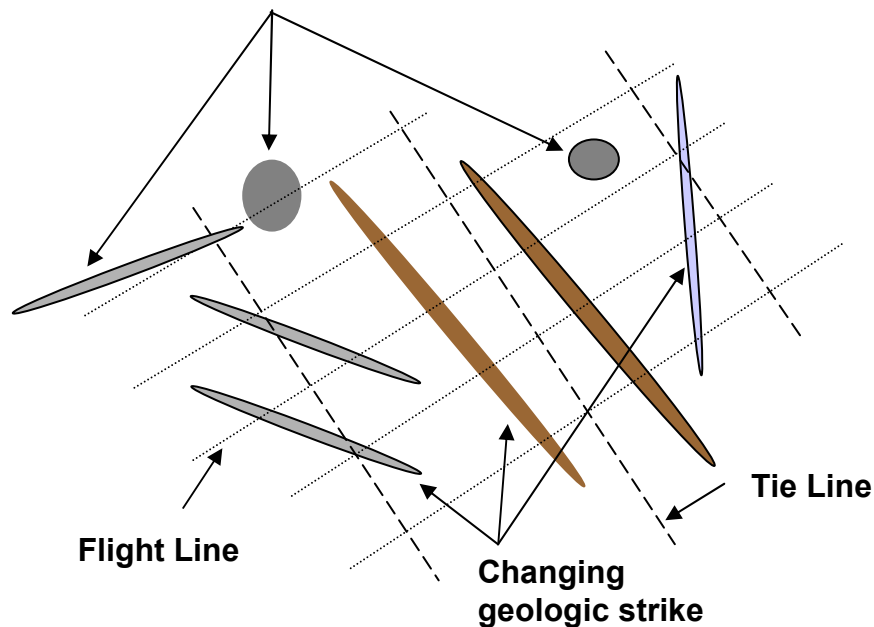


Figure 11: Illustration of aliasing due to flight line spacing

It is not practical to do the highest spatial resolution survey and the geological strike of objectives may vary considerably within the survey area. The flight line spacing and direction are chosen with these limitations in mind and an attempt is made to optimize both within the financial and logistical limitations placed on the survey design.

The resolution of layers is also an issue. The deeper and thinner a layer, the more difficult it becomes, if not impossible, to resolve. The more resistive the layer becomes, the more difficult it becomes to define the absolute resistivity of the layer. This model problem is depicted in Figure 12a.

The resolution of layers is also an issue. The deeper and thinner a layer, the more difficult it becomes, if not impossible, to resolve. The more resistive the layer becomes, the more difficult it becomes to define the absolute resistivity of the layer. Thin layers may be modeled as one thick layer close to the accumulative thickness of the several thin layers. A thin layer may not be detected at all. It may simply average up or down the resistivity of the surrounding, thicker layers. This model problem is depicted in Figure 12a.

Despite the number of limitations and interpretation cautions raised in the preceding discussion, an electromagnetic survey can provide a wealth of information to map subsurface geological features. Airborne EM surveys have been a successful tool for mapping the first few tens of meters to the first 200 meters of the subsurface and have



been widely applied in Alberta for the mapping of buried channels. The channel targets may be important to finding coarse aggregate, water, and gas. The gas may be resource target or it may be a drilling hazard. Overpressure water may also pose a drilling hazard. The interpretation used is to attribute the higher resistivity channels to porous zones containing either fresh water or gas. The magnetic data may simply outline the channels and will not provide information on the material in the channel, Figure 4. However, the magnetic data may define aspects of the channel geometry that does not have a resistivity contrast. Therefore, magnetic data may complement the electromagnetic data.

As with any resource exploration and geophysical methods, drilling of interpreted targets is necessary to calibrate and to verify the interpretations.

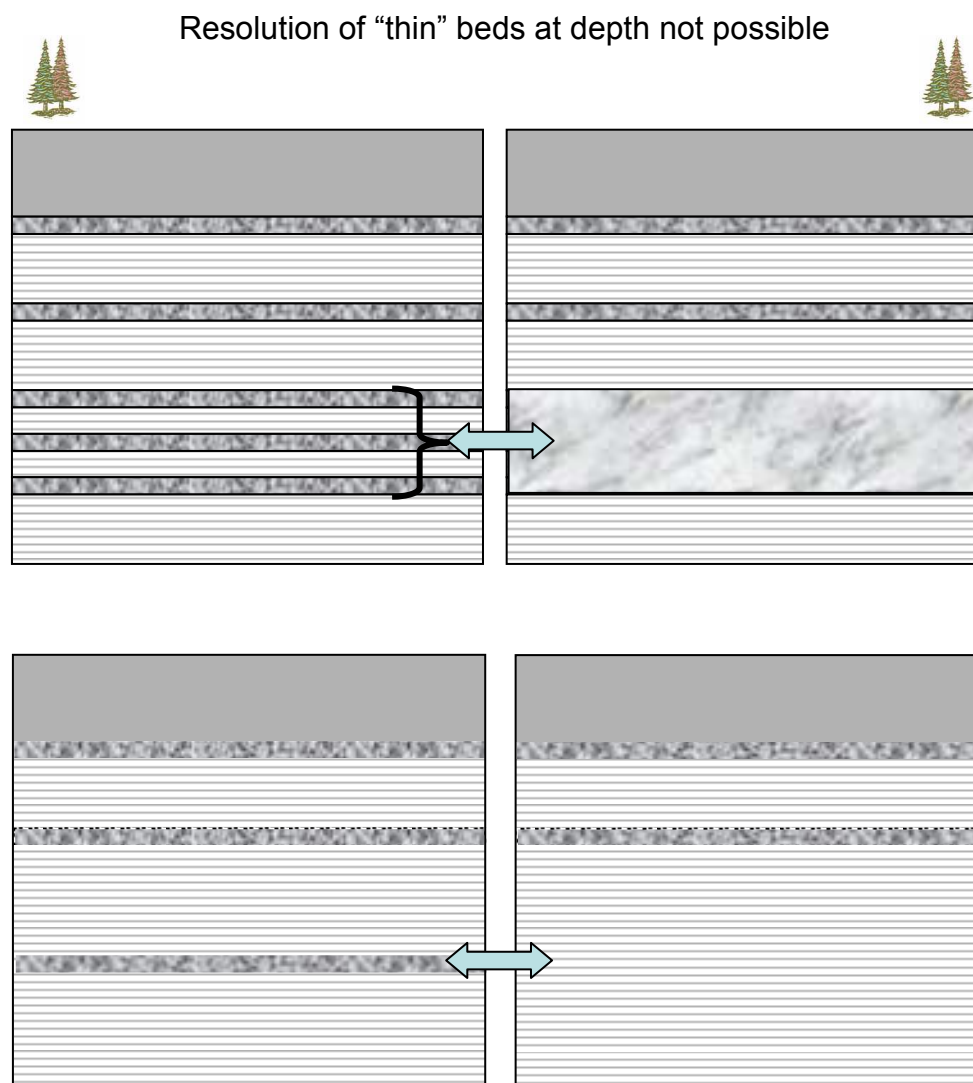


Figure 12a: A cartoon layered earth model showing on the left layering that may give inversion results such as shown on the right. Thin layers may appear as one layer, single thin layers may not be seen in the results.



To summarize, a model that may be similar to the current survey area, without the topography indicated, is shown in Figure 12b. The till may be very complex, somewhat layered in part, variably thick and contain quite different materials, and have an irregular unconformity at its base. The various till components may have quite different resistivities. The interpretation will assume that the more coarse aggregate portions of the till will be more resistive and that these zones may be the best aquifers. The Cretaceous rocks beneath the till are expected to be low resistivity shale. However, there could be incised, more resistive channels in these rocks. Also, there may be relatively more resistive facies within the shale that may be mapped by the airborne EM systems. In some cases, as suggested in Figure 12b, faults may be present and could be mapped, in some cases, by either the magnetic or the electromagnetic data.

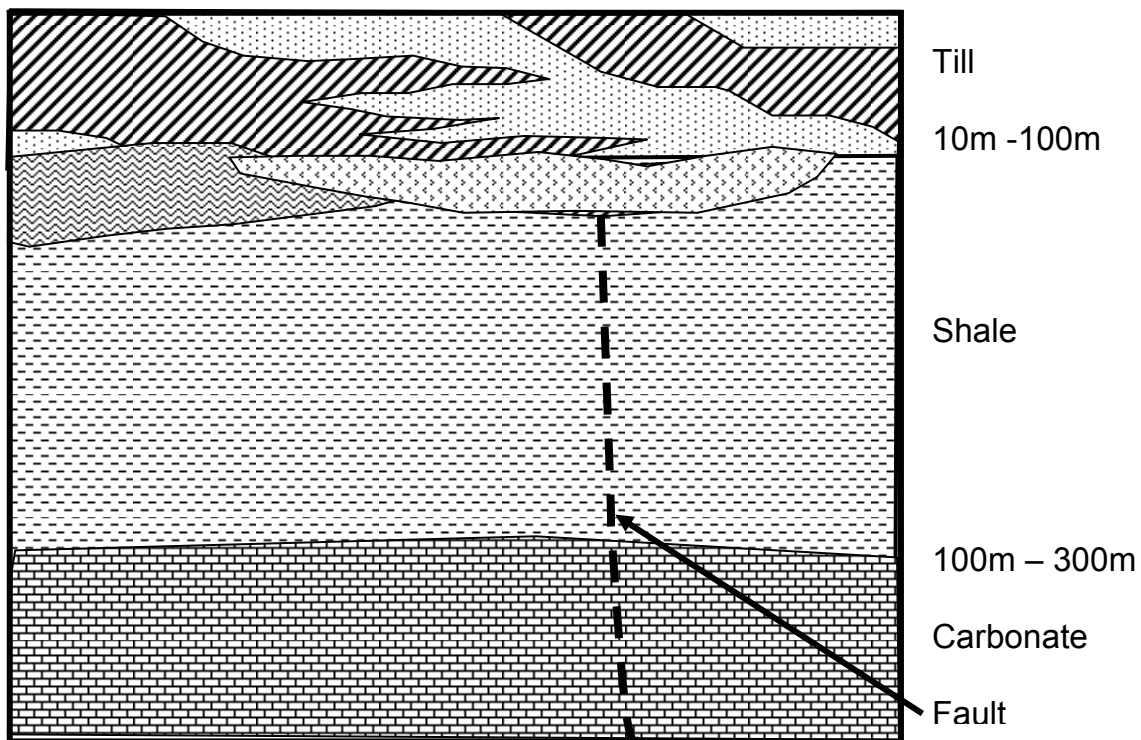


Figure 12b: A cartoon of the possible subsurface geology of the survey area. The model shows till over Cretaceous bedrock shale.

The cartoon in Figure 12b indicates that several features would not be resolved by the GEOTEM™ system in the till section. The cross-hatched lithology, for example, would be difficult to resolve where it tapers and thins. The small wedge of the stipple lithology on the left end of the line would not likely be detected.



Results – GEOTEM™ System

Four multilayered models were run on the 30hz GEOTEM™ survey data, Table 1. The four models n, nn, m, and mm were selected based on the results of the work done on the previous surveys and reported to the AGS in May 2008. The model name, e. g. “n”, and the layer resistivities, R, and thickness, t, up to 5 layers are listed across the table. The model has only the number of layers that a parameter is given a value. Note that the models are 4 and 5 layers. The starting models use a set of constant input values for the starting model resistivities and thicknesses for each layer. As stated earlier only the on-time data and every tenth sample along the survey line were used in the inversion. Model nn was selected as the “best” result and is discussed here. The other model results are available to the AGS.

The shaded relief images of each of the model nn layer resistivity, thickness, and the model error of fit are shown in the following figures. Some discussion is associated with the presentation of the data images but more complete discussion and interpretation follows in a later section. Not all results are shown in the text but are included in the data base.

The Alberta TM10 projection is used for all plots. The latitude – longitude lines and Township and Range grid are also shown for reference. The major drainage (approximate) is overlain on many of the images. The final data products and maps are also in the Alberta TM10 projection.

The shaded relief image of the 90 m US government elevation data that is available free on the internet is shown in Figure 2b. It is clear from the data that the topographic relief in the survey area is close to or exceeds the nominal 250 to 300 m exploration depth of the GEOTEM™ system. The elevation varies approximately between 720 and 1500 metres within the survey area. This issue was discussed earlier and it means that the layers beneath the highest topography are not the same as those beneath the lowest topography in the inversion layer results. Also, the system most likely does not reach any formation under the highest topography that it “sees” under the lowest topography. See Figure 4. The inversion results suggest the GEOTEM™ system may have sensed some variations to its nominal exploration depth. However, if no significant resistivity boundary occurs in this depth interval then it does not appear in the inversion results and the depth of investigation is unknown. Without any mapable changes, it is not possible to assess the exploration depth. Later drill tests may determine what depth of exploration was achieved.

One feature of the images shown here in the “a” part of the figure is that the same color palette is used for all resistivities, another one for all thickness or depths and another one for the error data. The common palette for each type of layer parameter, called a zonal palette, means one is always comparing the same color ranges in all images. Another set of plots can be made where a simple rainbow, histogram equalization palette is used for each image. In these plots a particular color, such as red, would represent different parameter values in the various images. Therefore, one cannot make a direct comparison



of relative values very easily among the various images. One could always look back and forth at all the individual color bars but this becomes a tedious and commonly confusing process. However, one benefit of the rainbow palette is that commonly emphasizes the subtle features in the data to greater extent than the zonal palette.

To illustrate this effect, the first layer resistivity, *rnn1*, image is shown in Figure 13a using the common zonal palette, and is repeated in Figure 13b using a simple histogram color palette. One can see all the same features in both Figures 13a and 13b; however, the eye can more easily see the subtle trends in the data in the color histogram image. Note the limited dynamic range is captured in the histogram plot and the color bar increment is only 2-3 ohm-m over most of the color bar range. The higher values (red end) have a larger increment. However, as one finds in many geophysical data, variations can be mapped while the absolute “true” value of a parameter may not be known. Any histogram palette of the data will be consistently shown in the “b” part of the figure just as was done for the first layer resistivity in Figure 13.

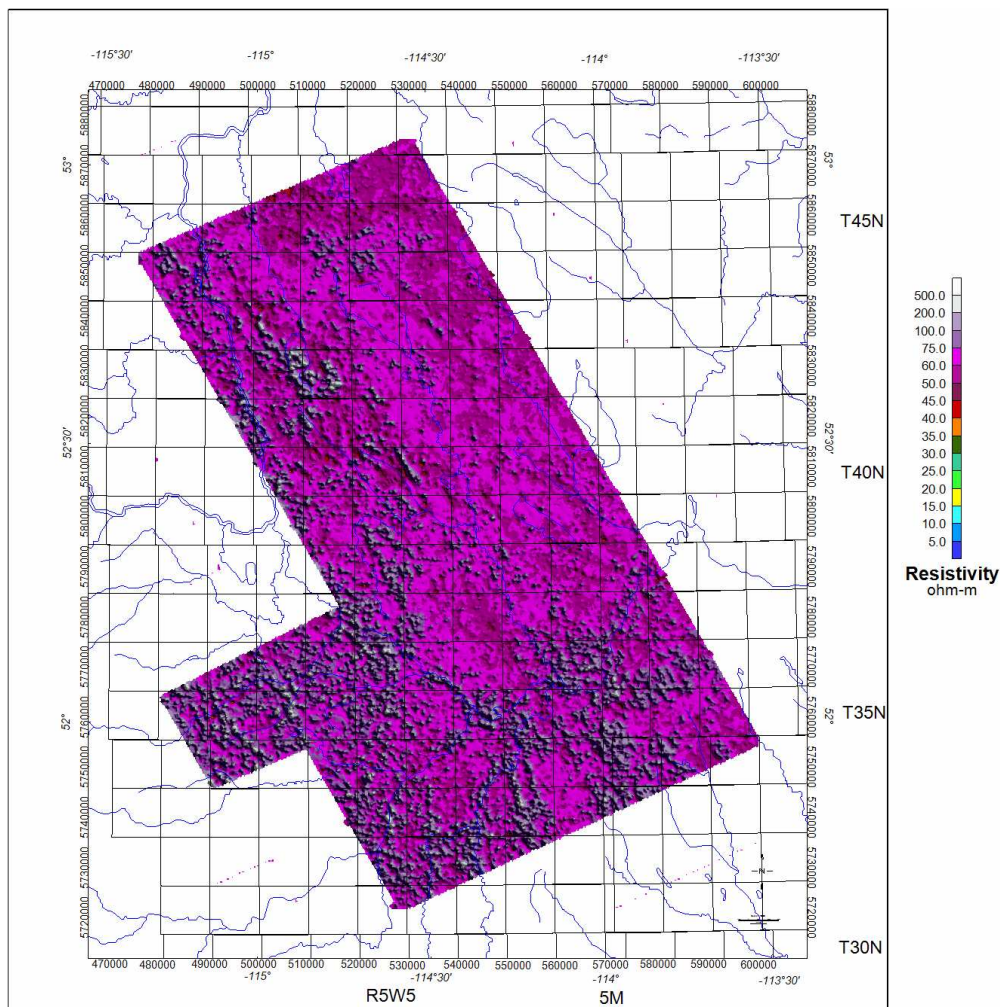


Figure 13a: The first layer resistivity shaded relief image, *rnn1*



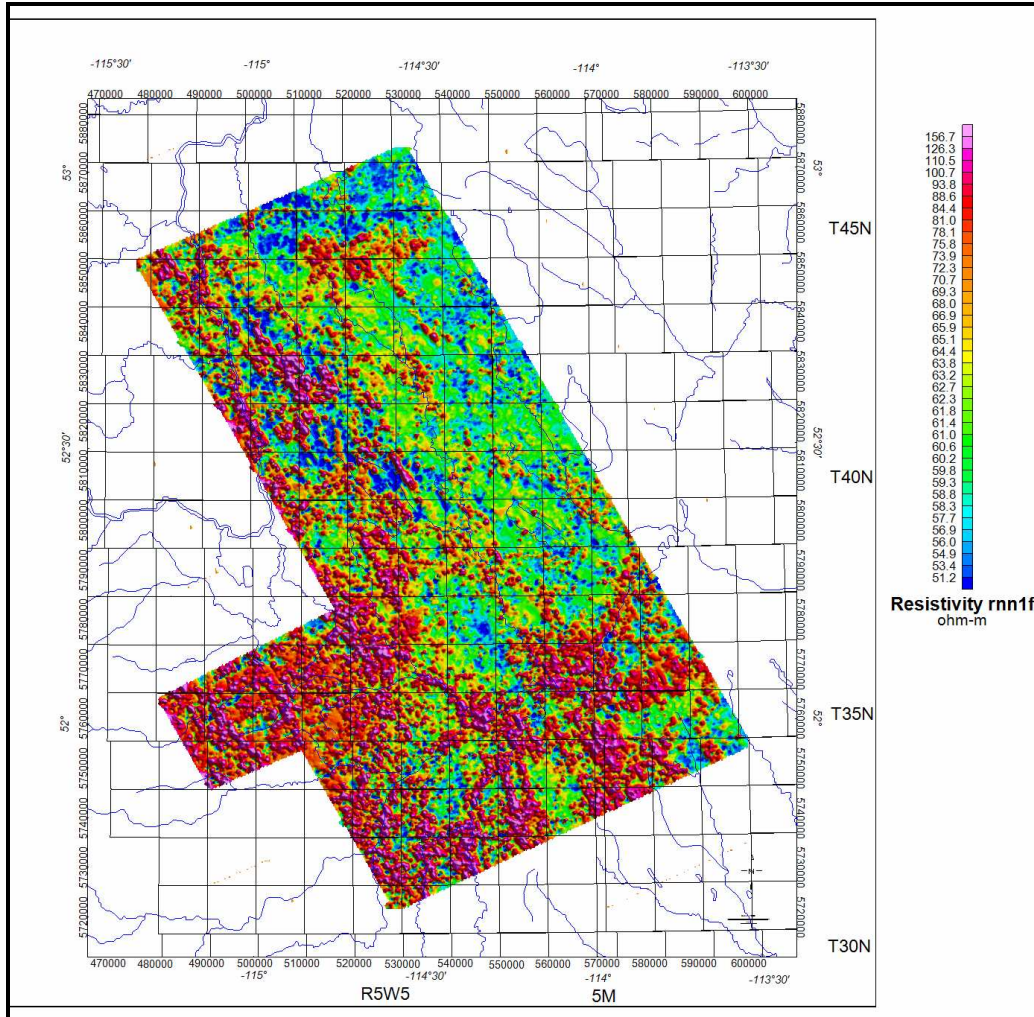


Figure 13b: The first layer resistivity shaded relief image, rnn1 using a rainbow, histogram equalization palette.

Figures 14a, 14b, and 15a, 15b and 16a, 16b and 17a, 17b show the shaded relief images of the rnn2, rnn3, rnn4 and rnn5 data, the second through fifth layer resistivities for the nn model. One can see that the resistivity decreases with depth through the fourth layer and then becomes somewhat more resistive at depth to the west in the fifth layer. Also, there are clear patterns in the data having patterns that could be mapping buried drainage systems. These features, relative to the surrounding resistivity in each layer, have some common characteristics, shape and location between layers but there are changes within the layers as well. Most, if not all these features, are more resistive than the surrounding areas. More will be noted about these features in the interpretation section.



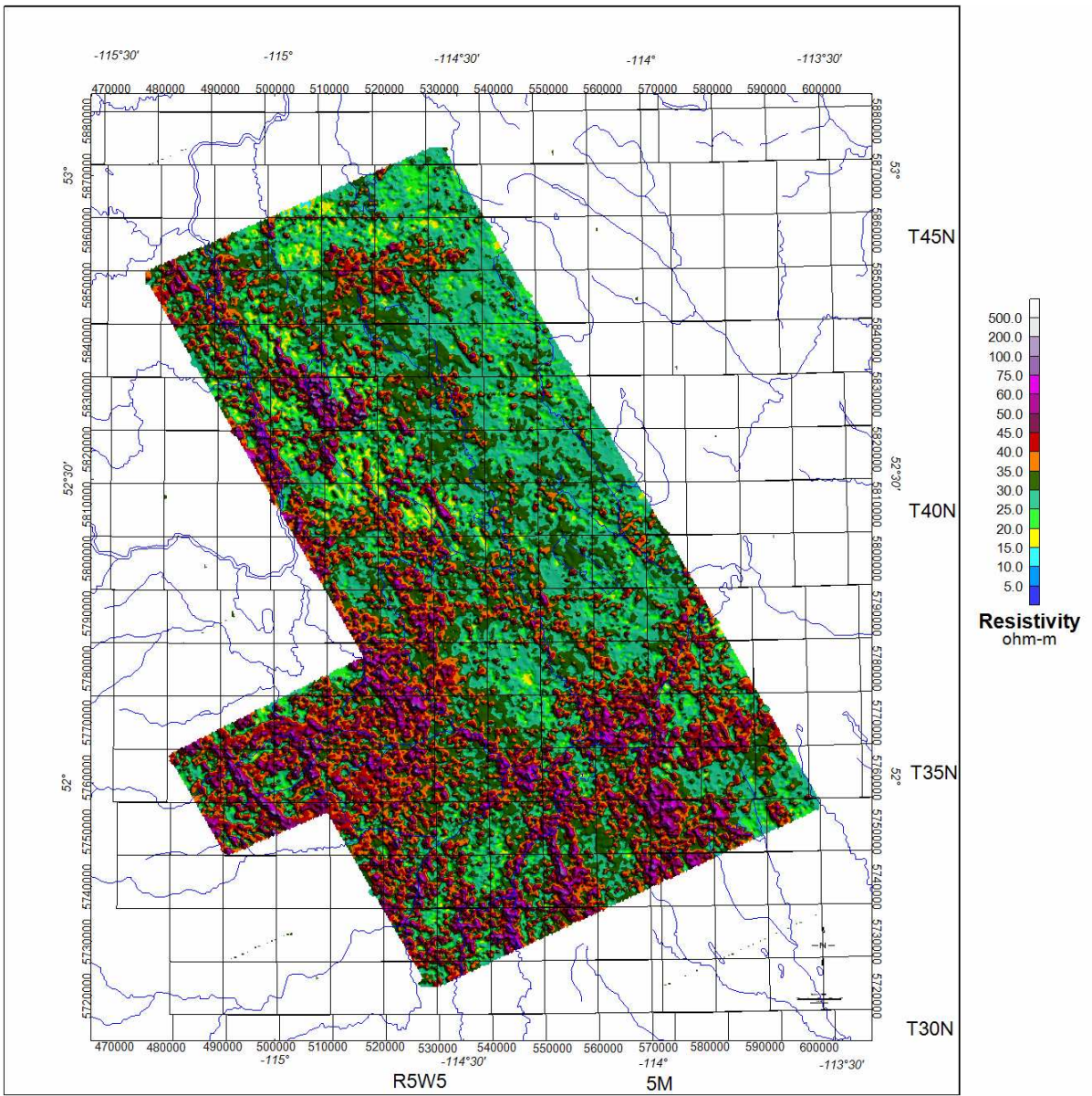


Figure 14a: Shaded relief image of the second layer resistivity, Rnn2.



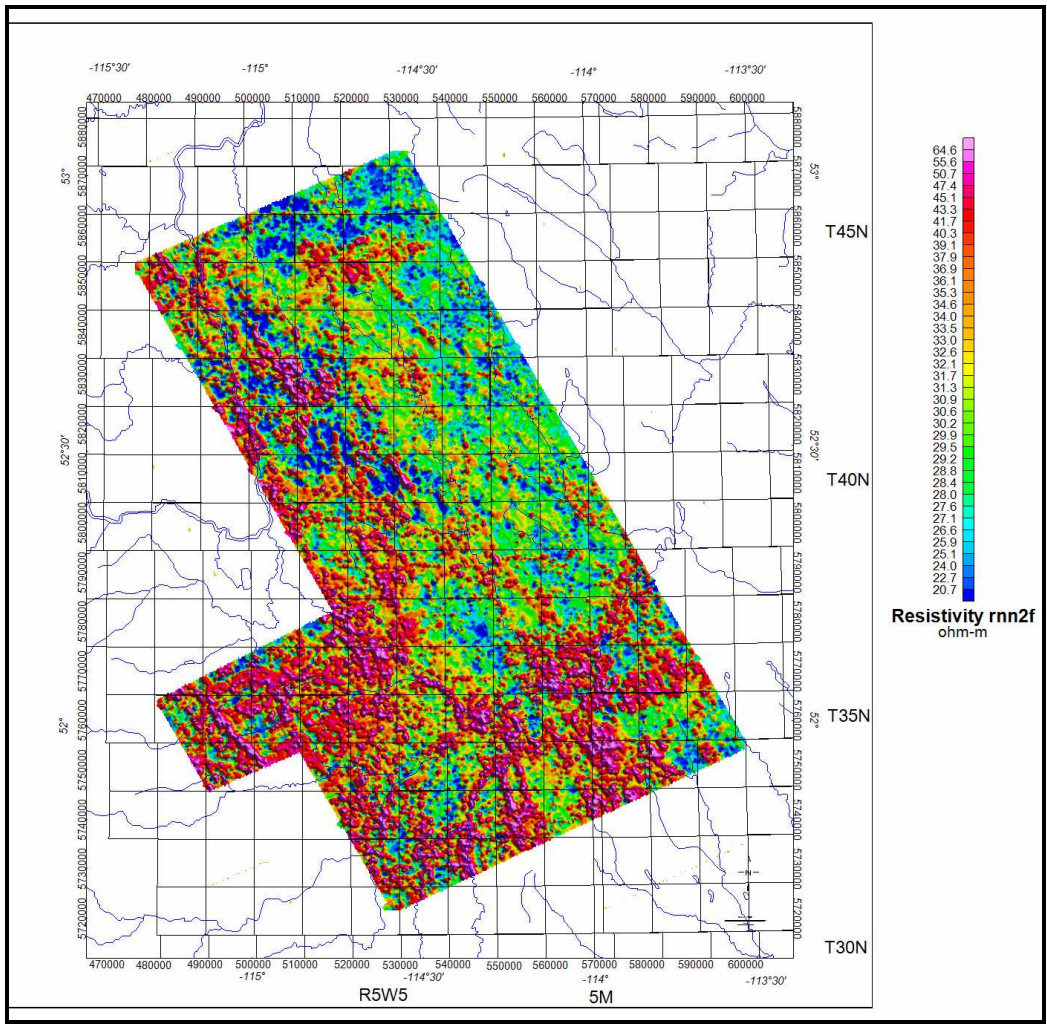


Figure 14b: Shaded relief image of the second layer resistivity, Rnn2, with a rainbow palette.



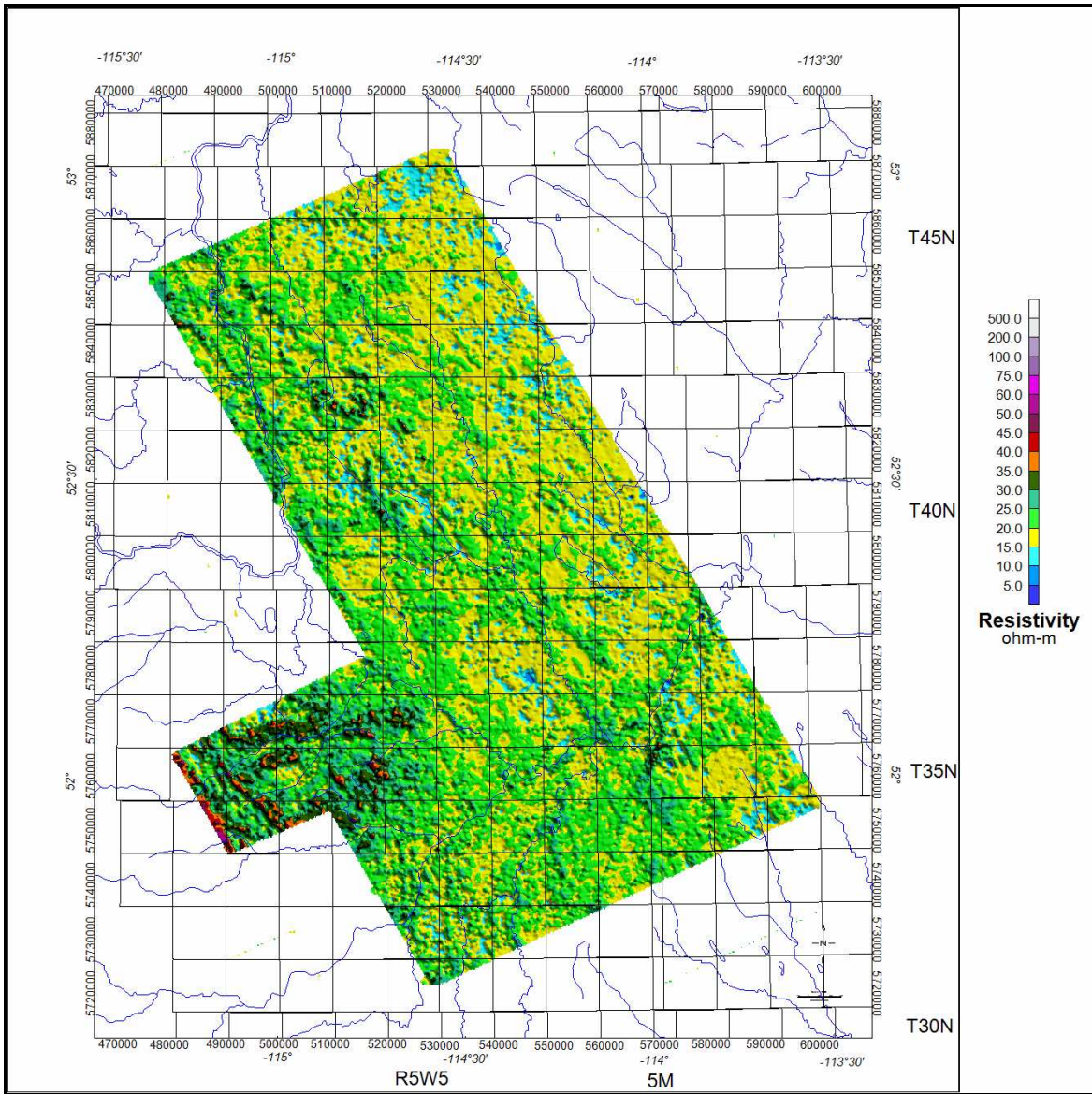


Figure 15a: Shaded relief image of the third layer resistivity, Rnn3



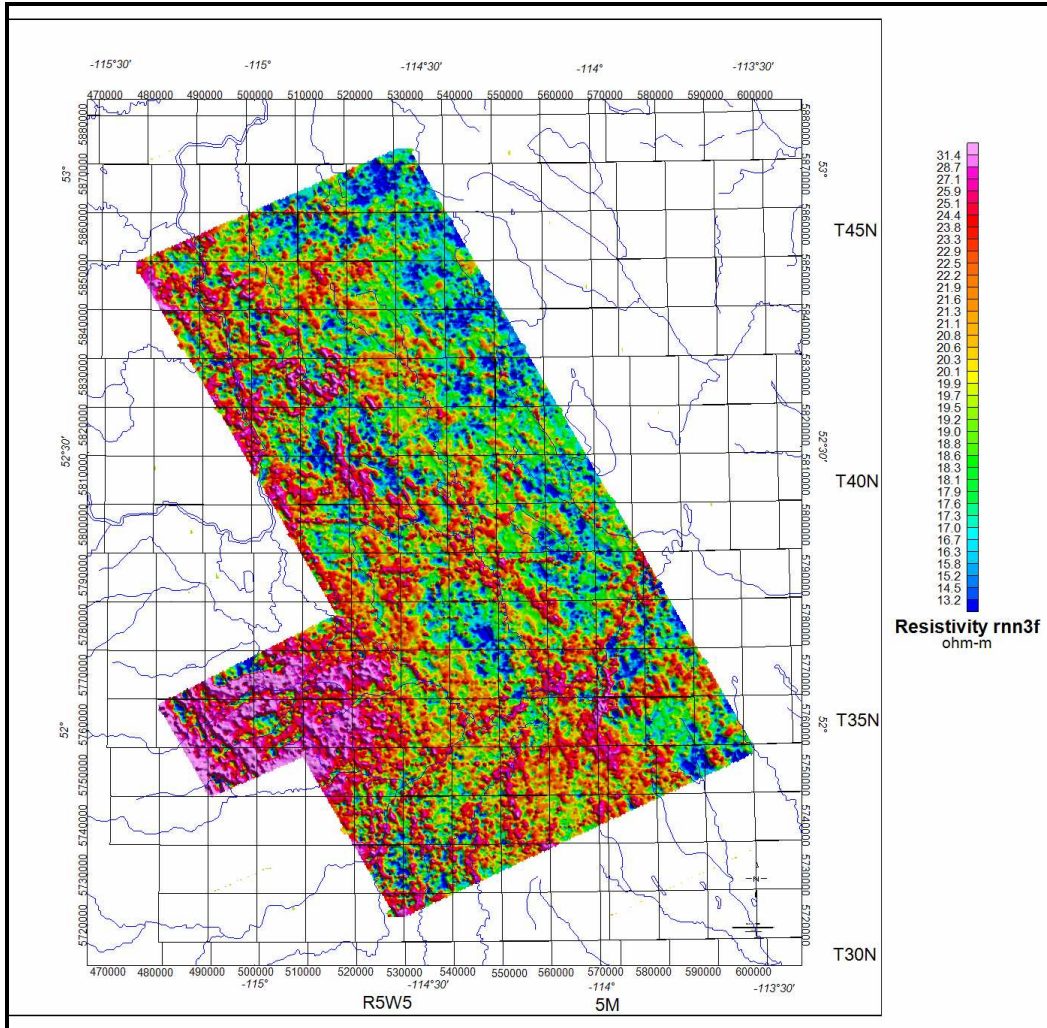


Figure 15b: Shaded relief image of the third layer resistivity, Rnn3, rainbow palette



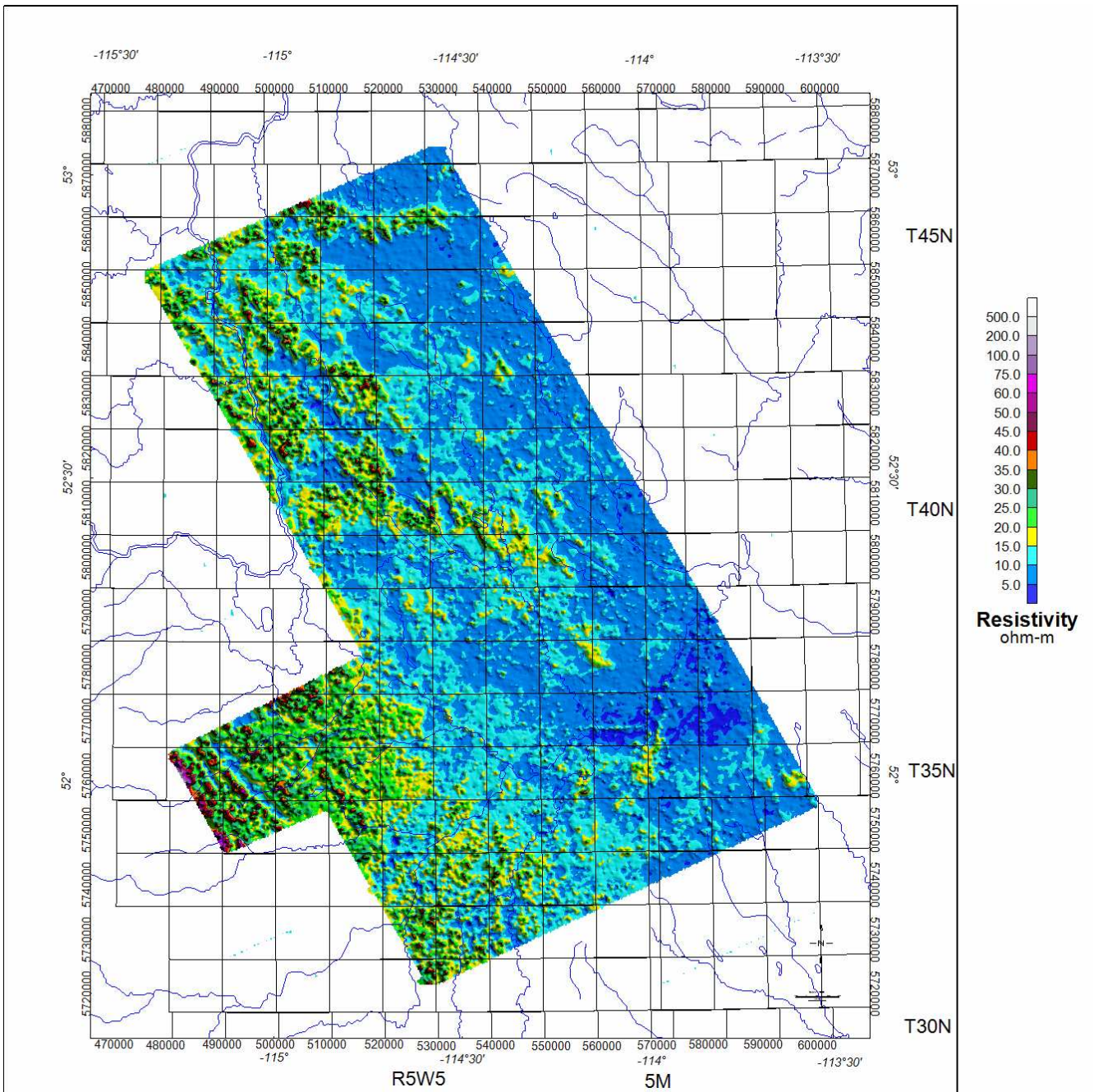


Figure 16a: Shaded relief image of the fourth layer resistivity, Rnn4



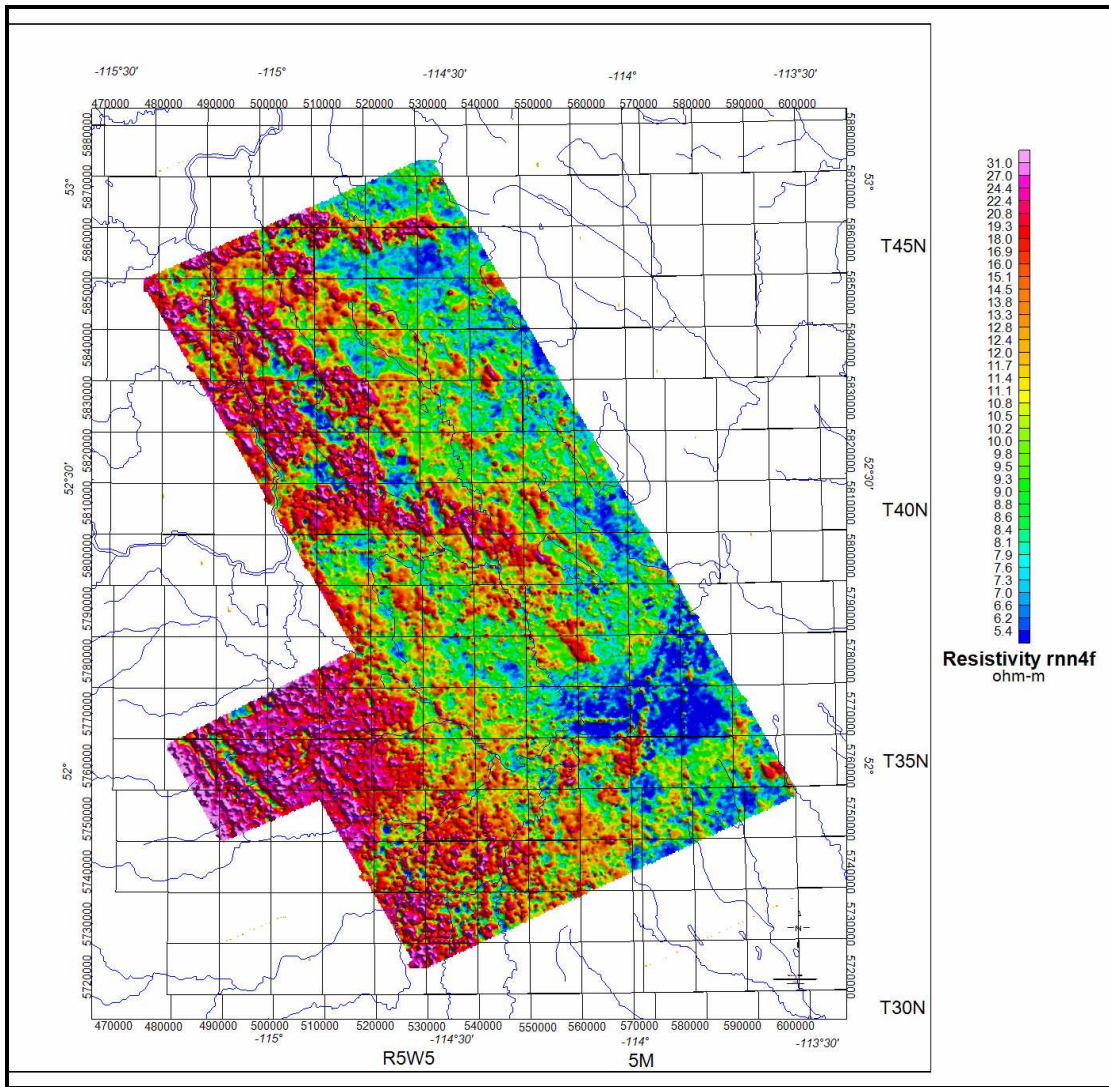


Figure 16b: Shaded relief image of the fourth layer resistivity, Rnn4, with a rainbow palette



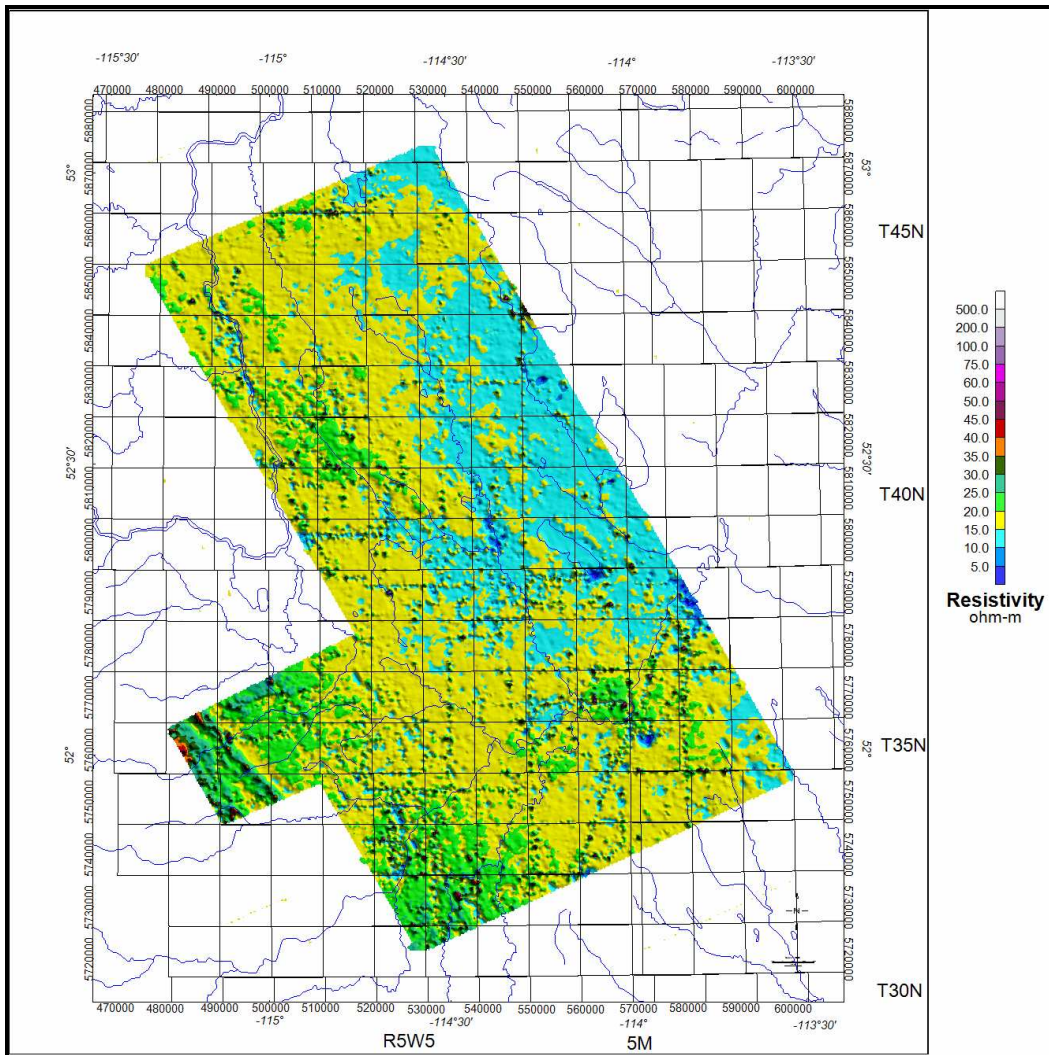


Figure 17a: Shaded relief image of the fifth layer resistivity, Rnn5



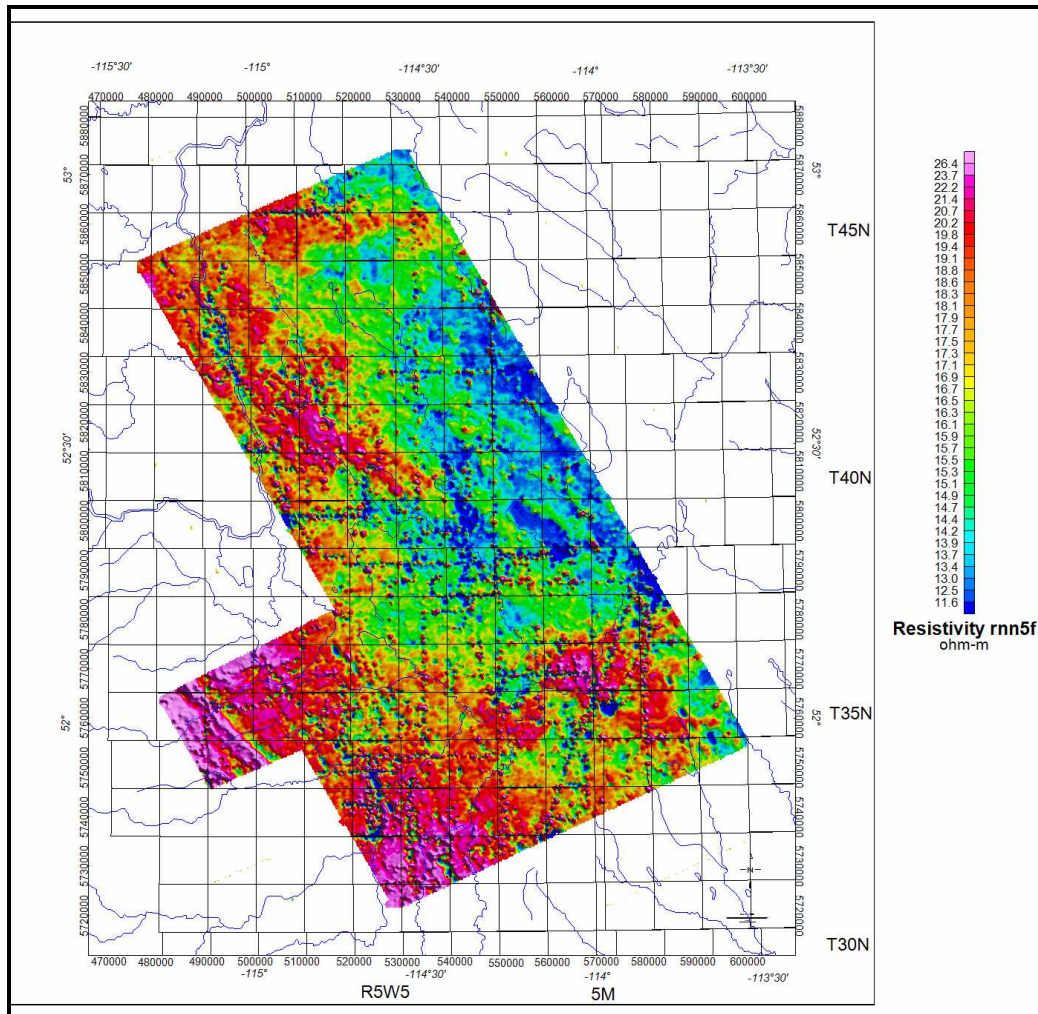


Figure 17b: Shaded relief image of the fifth layer resistivity, Rnn5, with a rainbow palette

Figures 18a, 18b, and 19a, 19b and 20a, 20b and 21a, 21b, show the shaded relief images of the Thnn1, Thnn2, Thnn3 and Thnn4, the thickness images (the four layer thicknesses respectively of the nn model, again with a zonal and a histogram palette. The thickness patterns are similar but not identical to the resistivity ones. Both the thickness and resistivity can be used together to map out possible channels and other features that may have hydrological interest. The differences between the features' resistivity characteristics may be attributed to the data resolution of a channel or lithological differences among the sources.

One can see that the first layer is relatively thin, Figure 18, except in the higher elevation western part of the survey. The area is also relatively more resistive, Figure 13.



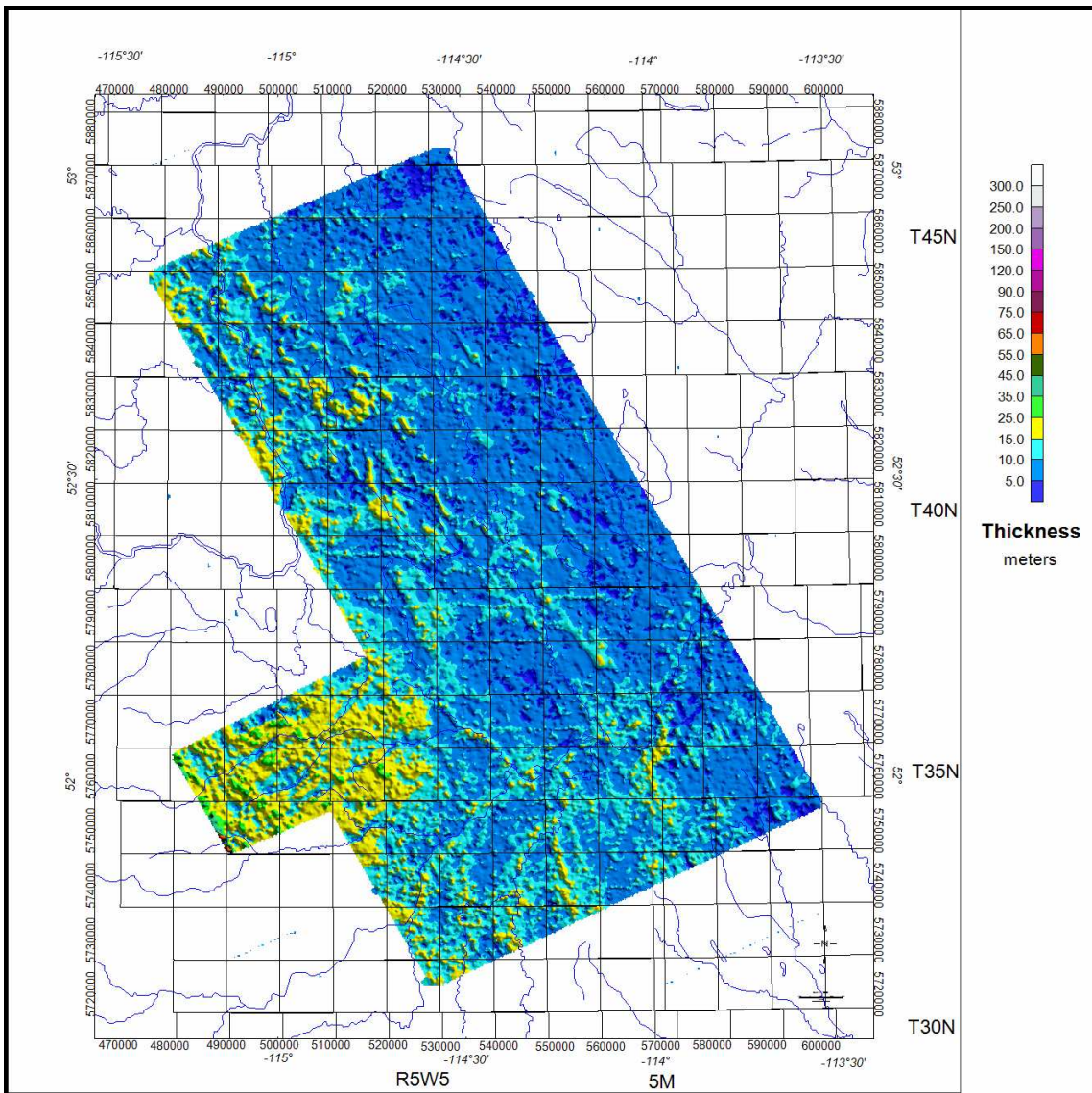


Figure 18a: Shaded relief image of the first layer thickness, Thnn1

The second layer thickness is similar to the first layer, both in thickness and resistivity patterns, Figures 14 and 19. However, the second layer is uniformly less resistive than the first layer. The third layer thickness is somewhat greater in the west and remains relatively thin in the east which is the lowest resistivity area of the survey. The fourth layer thickness also is greater and is more uniform over the entire survey area, Figure 21.

Most of the patterns in both resistivity and thickness data for both the first and second layers lie in the western half of the survey area. The rainbow palettes show the dynamic range in each of the data sets best and can be viewed to identify some of the more resistive features in the data. Some of these features may be older, buried channel features which will be noted later.



These features can be seen in the third layer data and fourth layer data as well, Figures 20 and Figure 21.

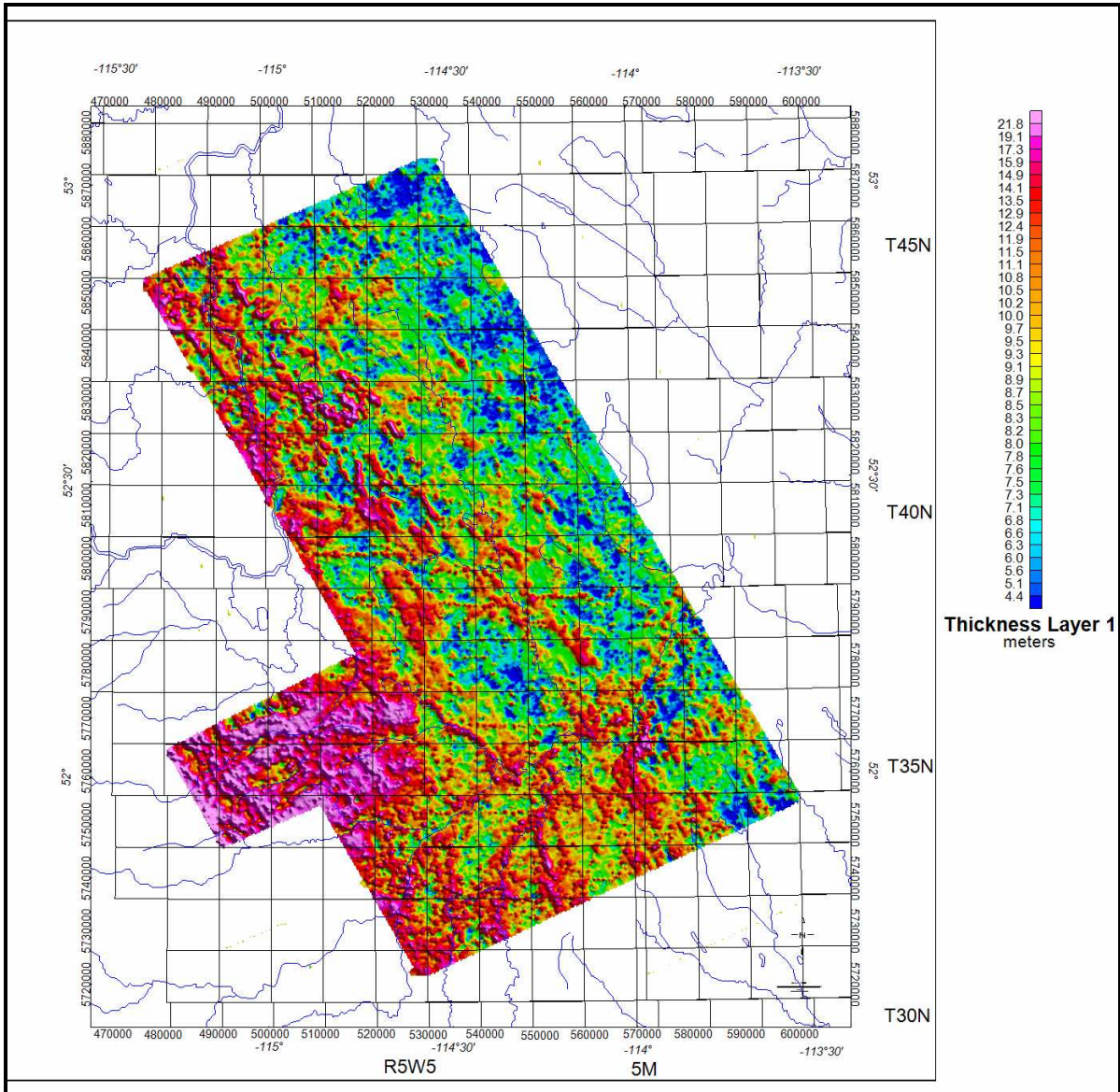


Figure 18b: Shaded relief image of the first layer thickness, Thnn1, with a rainbow palette.



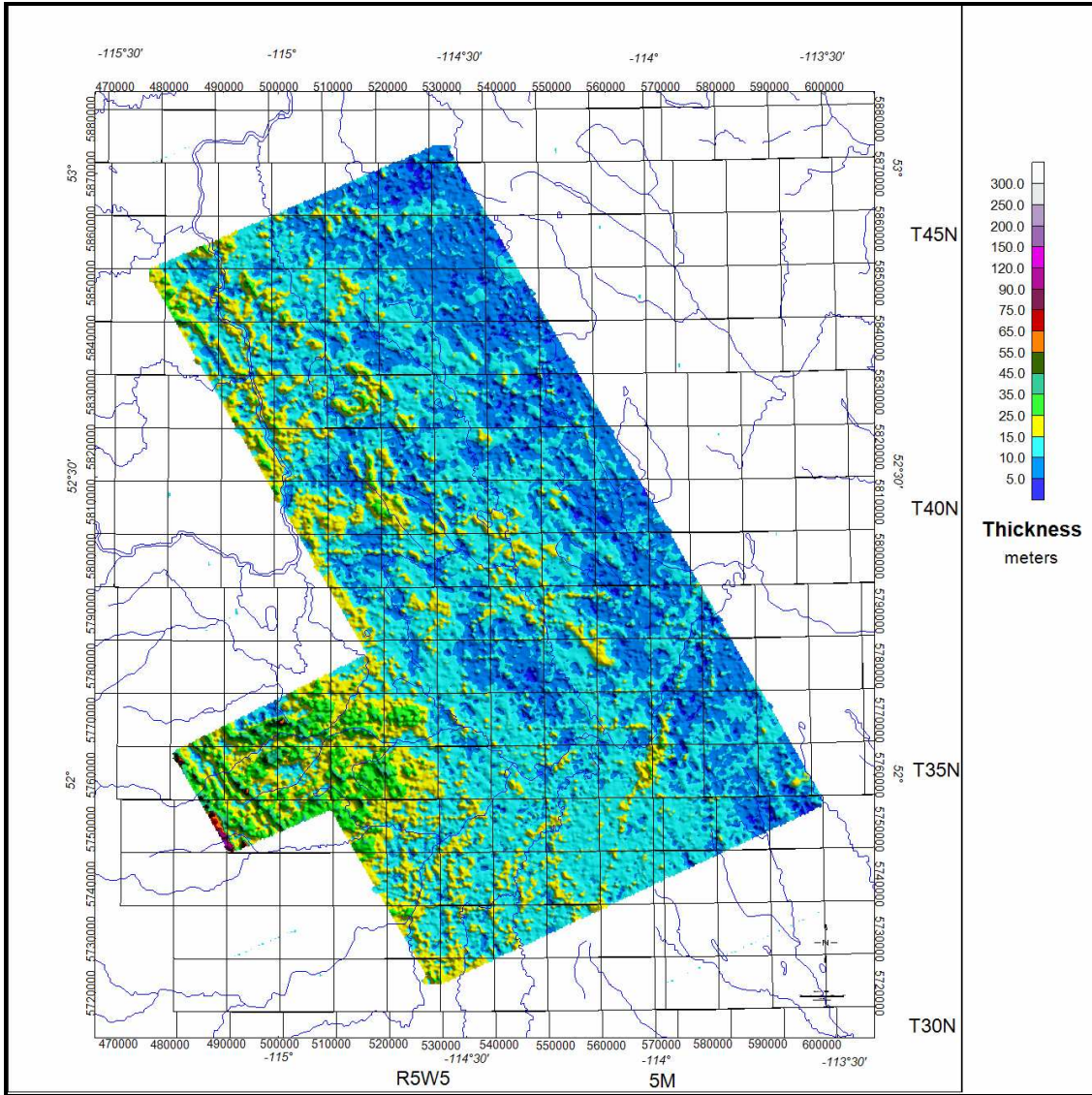


Figure 19a: Shaded relief image of the second layer thickness Thnn2



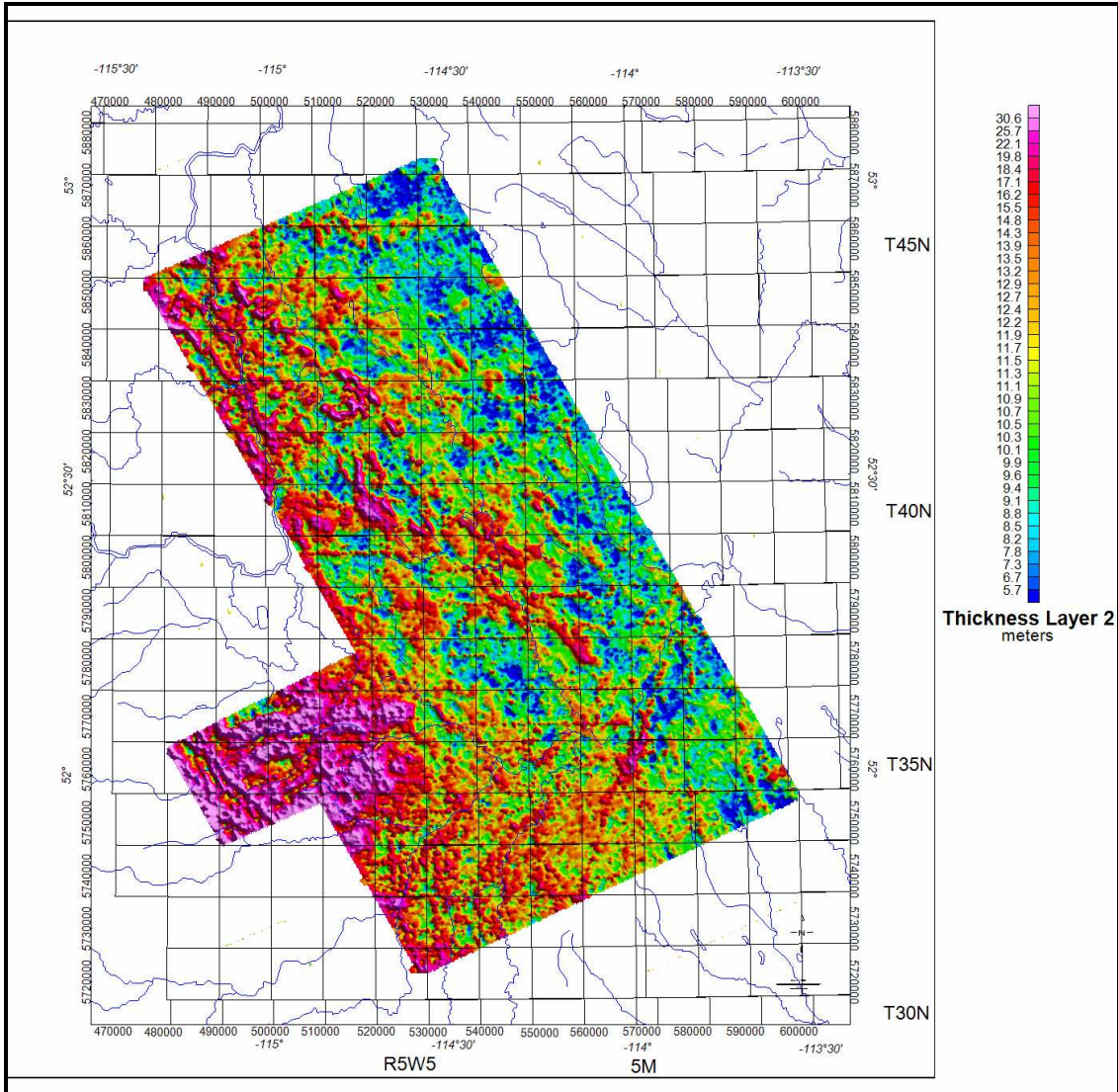


Figure 19b: Shaded relief image of the second layer thickness Thnn2, with a rainbow palette



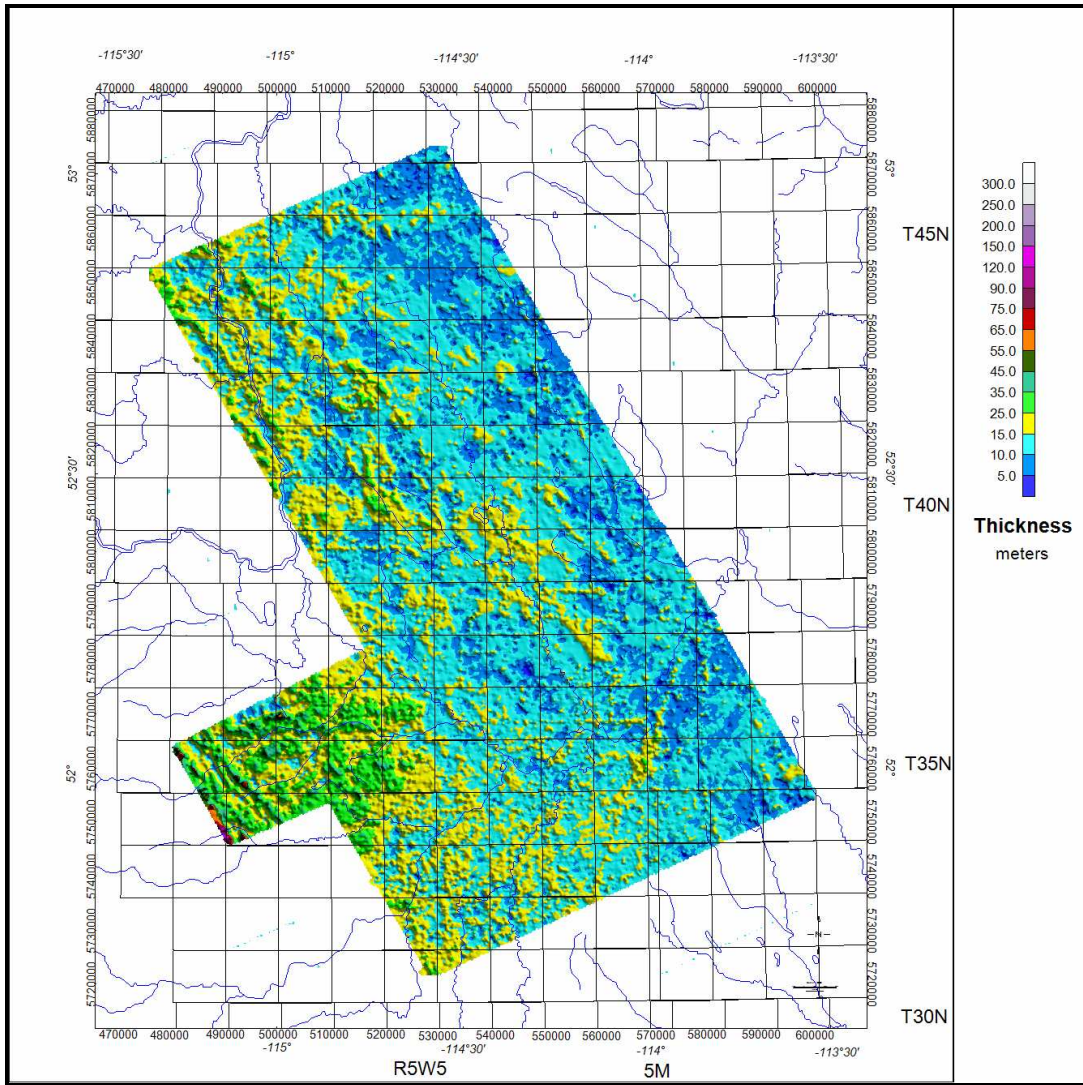


Figure 20a: Shaded relief image of the third layer thickness Thnn3



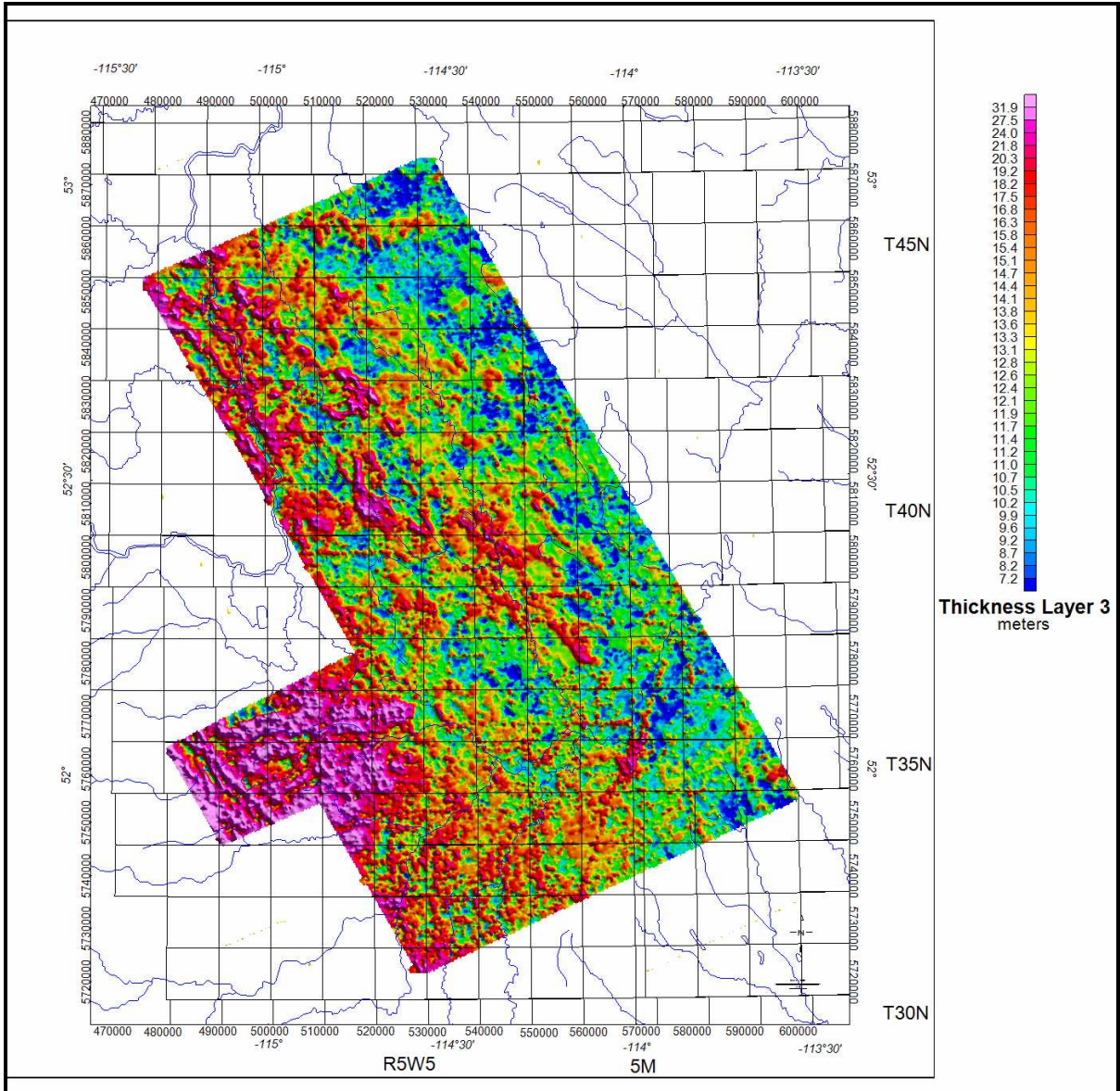


Figure 20b: Shaded relief image of the third layer thickness Thnn3, with a rainbow palette



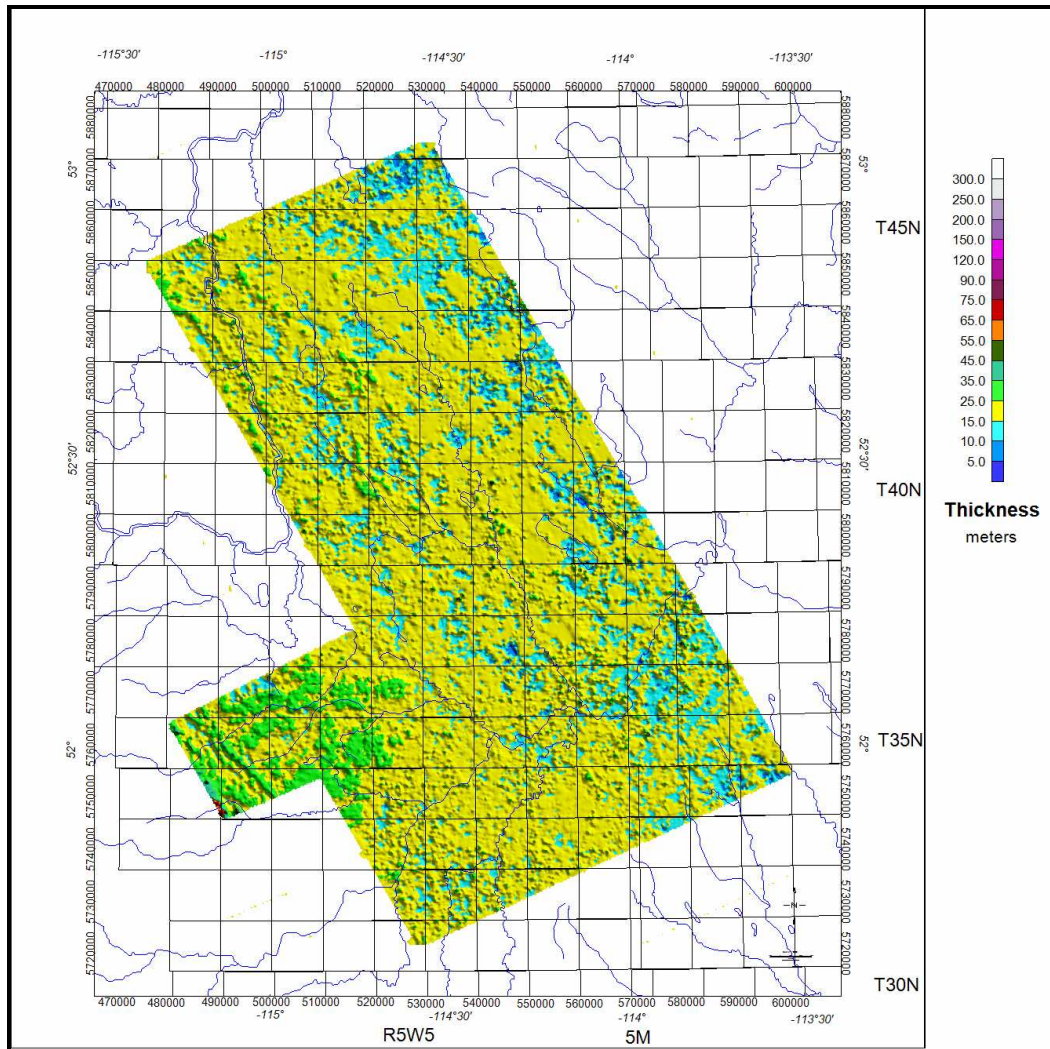


Figure 21a: Shaded relief image of the fourth layer thickness, Thnn4



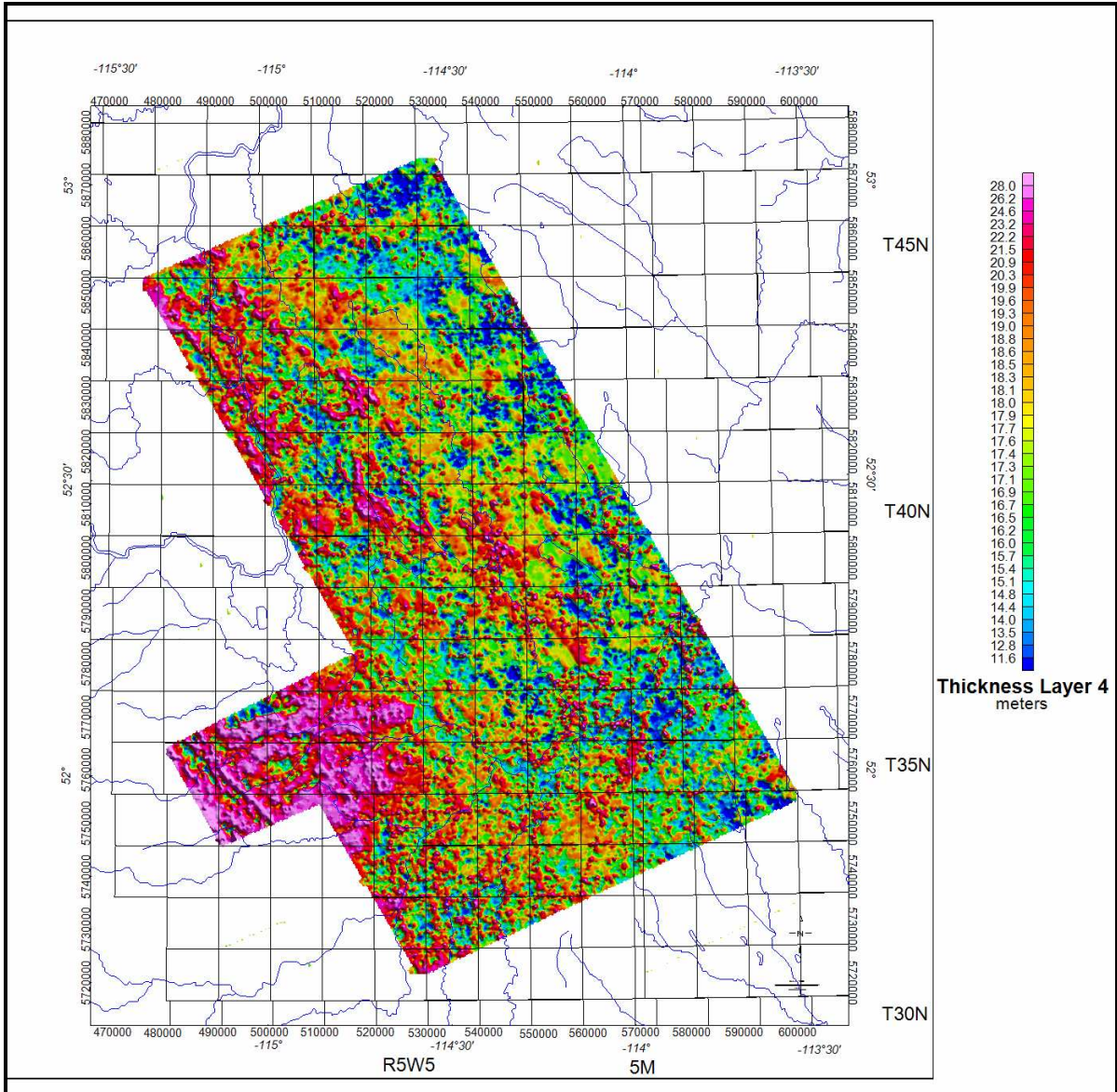


Figure 21b: Shaded relief image of the fourth layer thickness, Thnn4, with a rainbow palette



Figure 22 shows the shaded relief image of the total thickness of the four layers, or the depth to the fifth layer, the deepest layer or half space resolved in the inversion process, Figure 4.

Note how variable the depth to the fifth layer is over the survey area. It varies from about 20 meters to over 100 meters. However, since the thickness of the fifth layer, or half-space, is not known, then the total depth of investigation is not known. If a resistivity change at depth is known and not seen in these data, it would provide some depth limit for the GEOTEMTM survey. Most of the thinner depths are in the eastern part of the survey area. It is also the area with lower elevation. The higher resistivities to the west indicate this area is underlain by quite different geological section in the near surface.

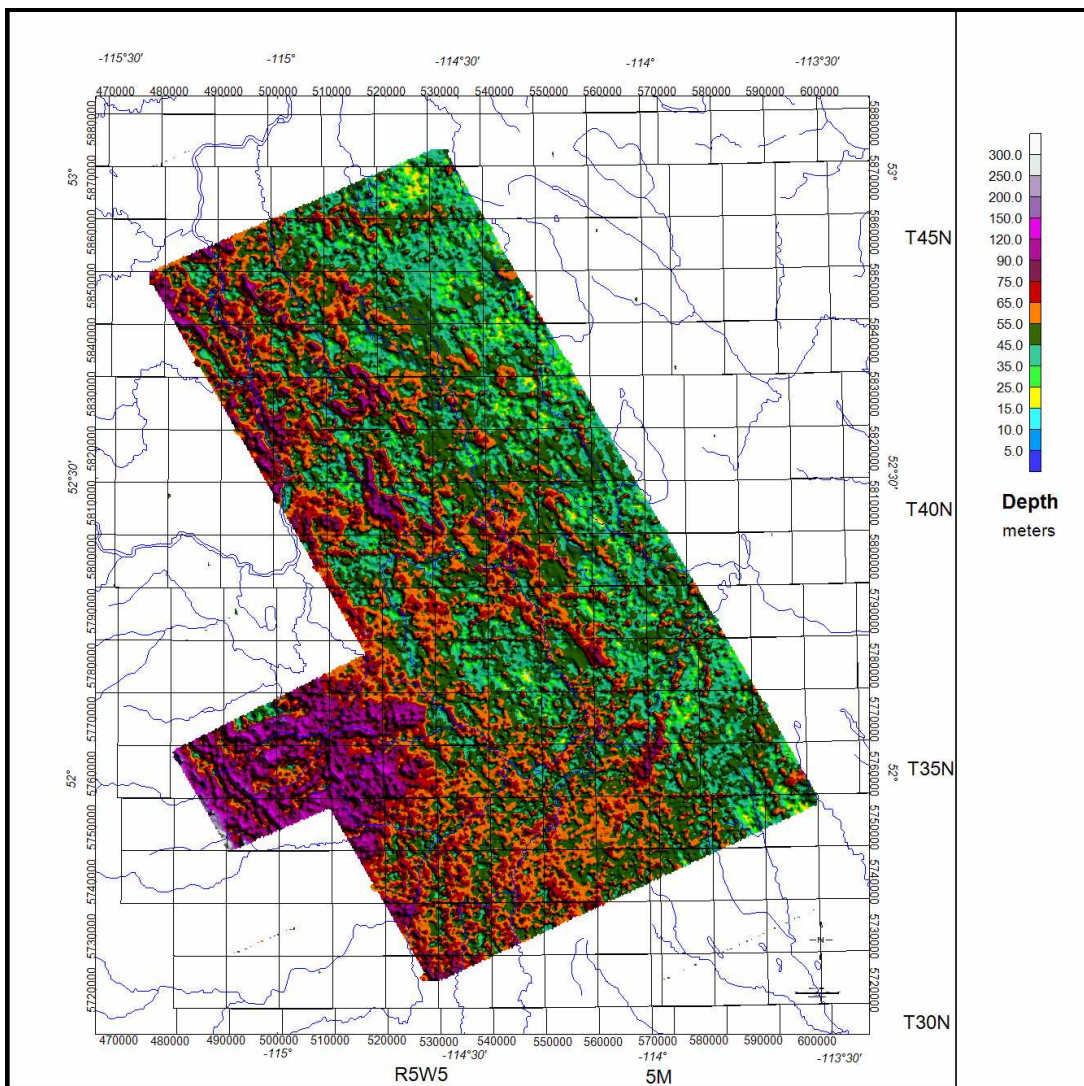


Figure 22: Sum of the four layer thicknesses or depth to fifth layer



Figure 23 shows the shaded relief image of the least square error of fit for the nn model. The error of fit is quite good. Most of the area is less than 2.5% and much of the remaining area error of fit is less than 5%. The main exceptions are over what appears to be pipelines and oil fields with many wells. Despite these cultural affects, the regional inversion data gives quite good continuity results. If you examine the many data images seen in the previous figures, you do not see much correlation of either the resistivity or thickness with the cultural features seen in the least square image. Some culture noise appears in the fifth layer data but is not significant and does not detract from interpretation of the data. The noise levels are best seen in the rainbow palette images.

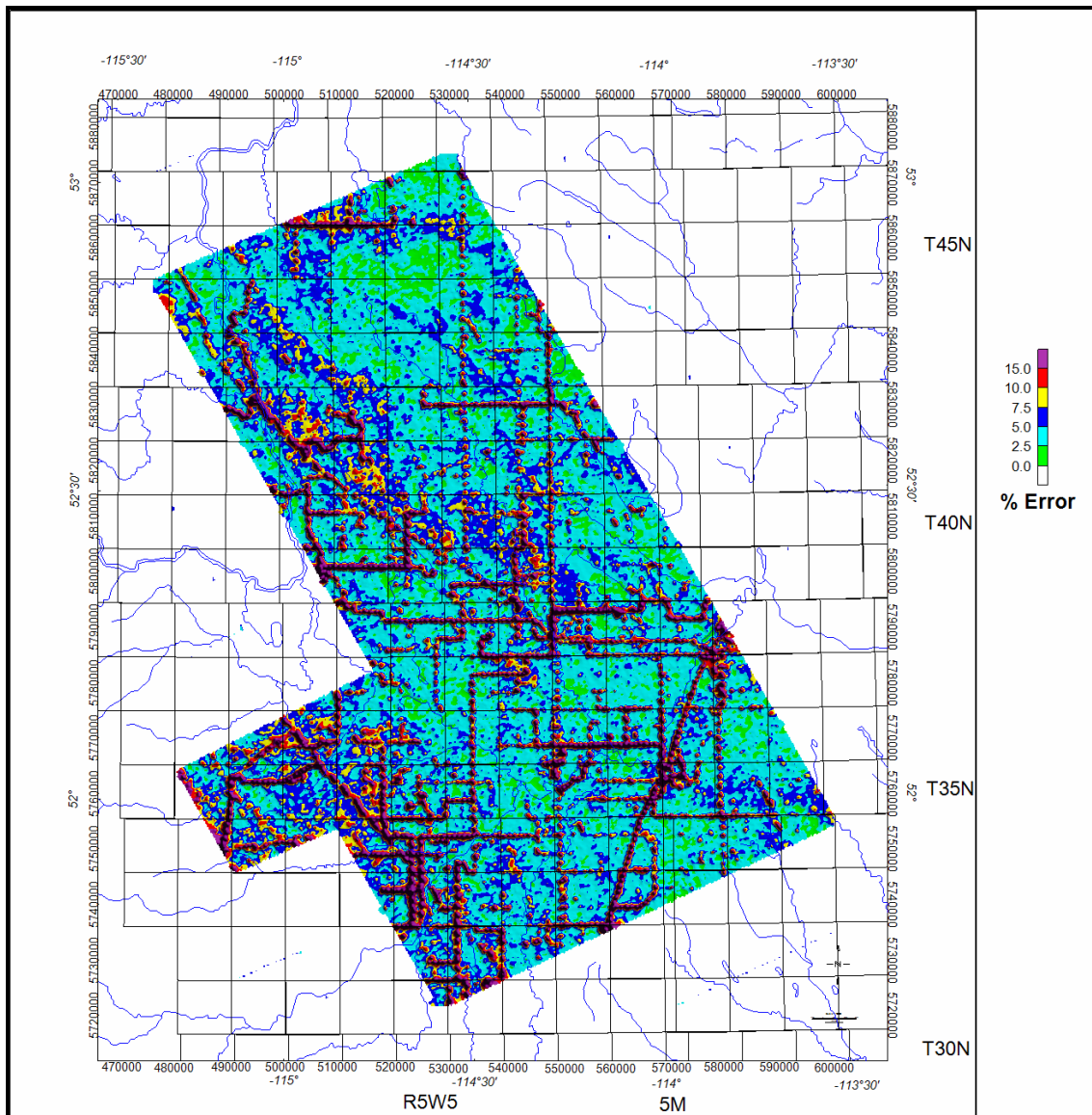


Figure 23: Shade relief image of the error of fit from the inversion process



Four RDI depth slices for the GEOTEM™ data prepared by FUGRO are shown in Figure 24, for depths of 10, 30, 60 and 120 meters. The images are overlain on the topographic image and have the township and range grids and major drainage overlain. The histogram color palette is used for all four images. Two things to note are: 1) the resistivity patterns change very little through the depth slices, 2) the small changes show some decrease in resistivity with depth in the eastern part of the survey area. One can compare these images with the layered inversion results shown in Figures 13-17.

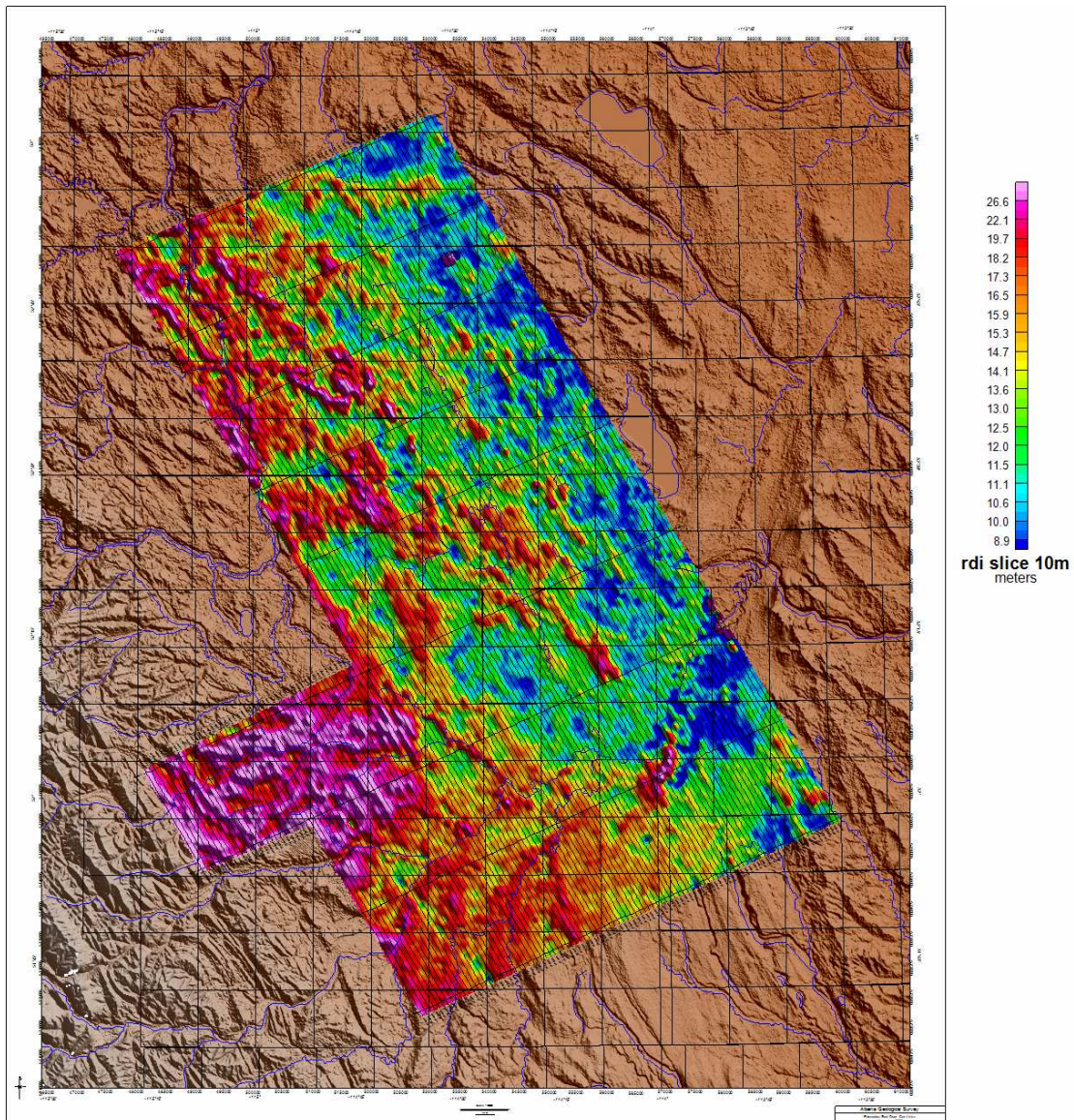


Figure 24a: The shaded color image of the RDI depth slice from 10 m depth.

It is clear from that comparison that patterns are very similar but the layer changes from the inversion show a greater change than one sees in the RDI slices. Also, no claim is made that the depth slice depth is accurate. The inversion results indicate a very different



layer depth profile. Inversions are not unique; however, the depths appear reasonable and can be checked with drill hole and other data.

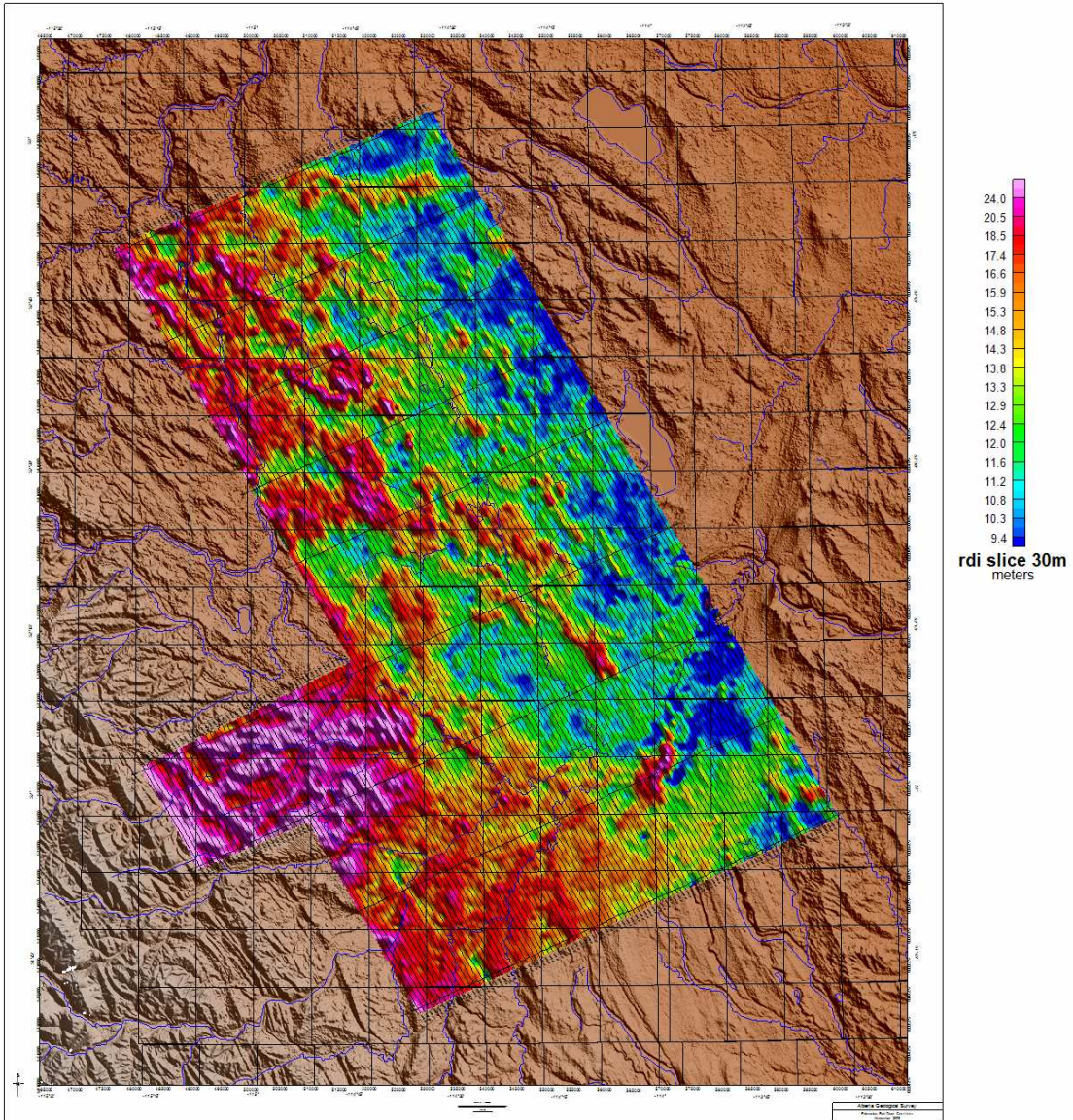


Figure 24b: The shaded color image of the RDI depth slice from 30 m depth.



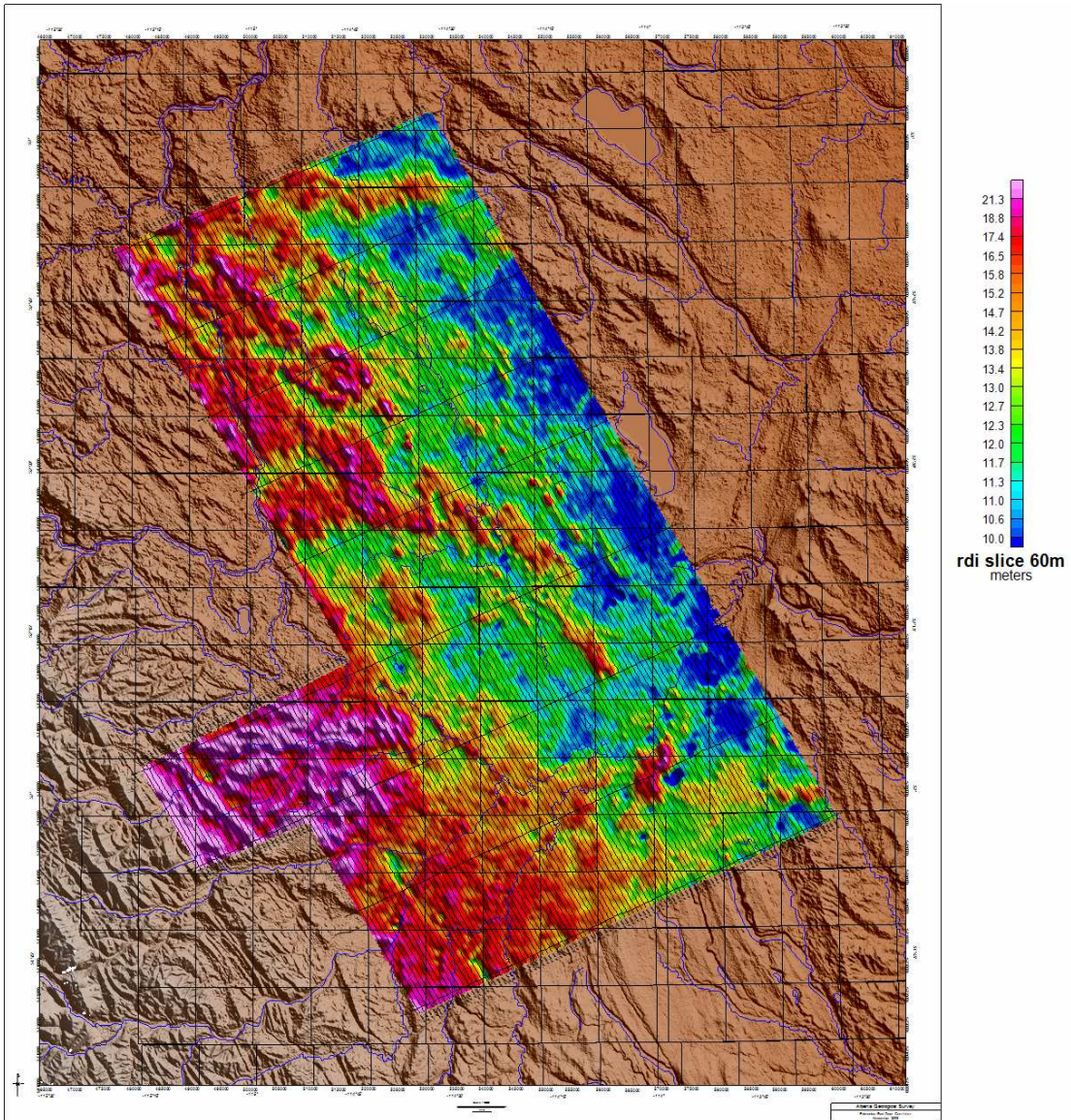


Figure 24c: The shaded color image of the RDI depth slice from 60 m depth.



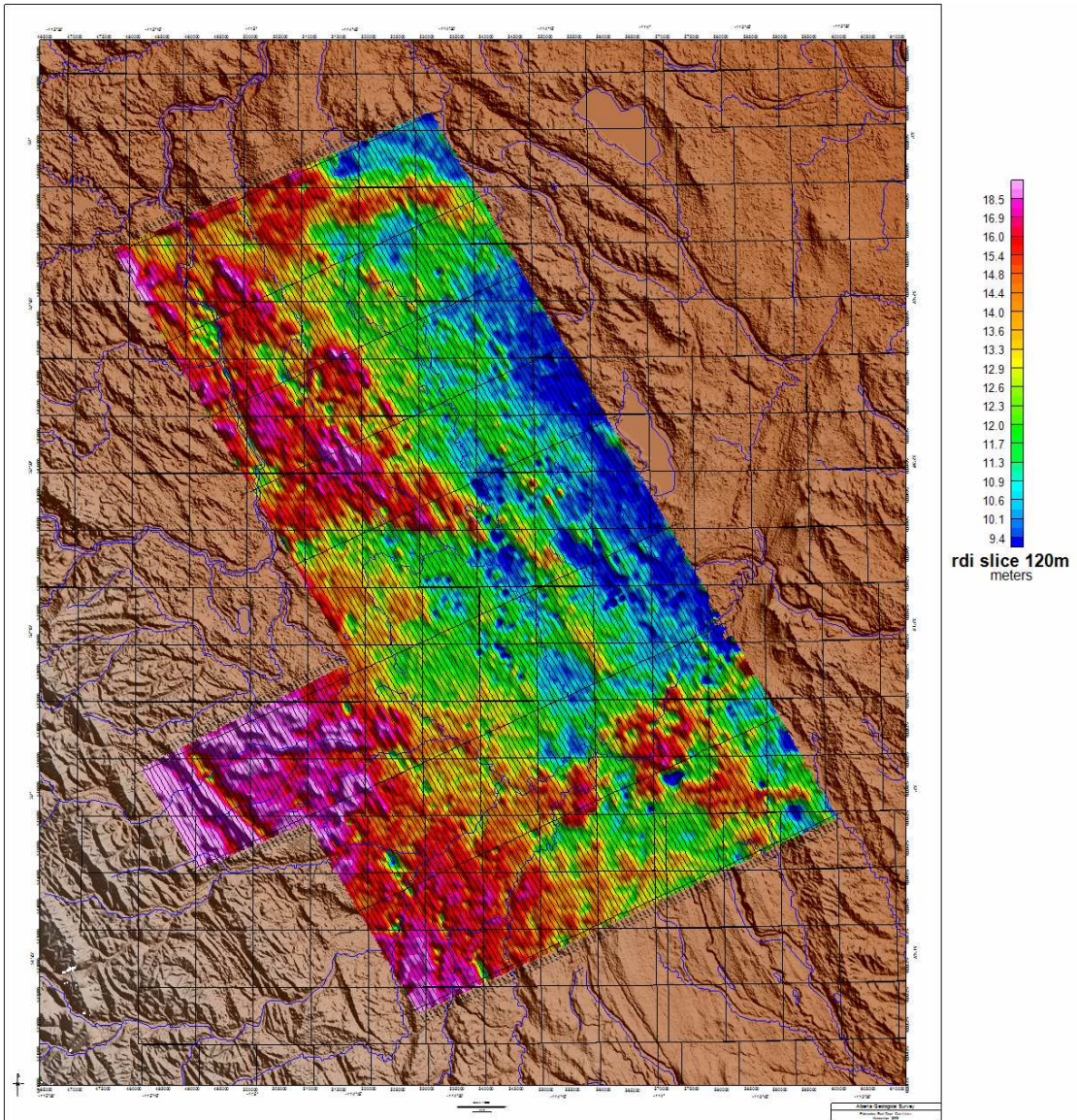


Figure 24d: The shaded color image of the RDI depth slice from 120 m depth.



Integration of the March and November 2008 GEOTEM™ Results

A short discussion is presented to examine the integration of the most recent GEOTEM™ results with the ones reported earlier in 2008. Figure 25 shows the shaded relief image of the first layer resistivities from both inversion results using the zonal palette. The results look quite good. There is only a modest difference along the eastern boundary of the recent survey with the western boundary of the very first 30 Hertz GEOTEM™ survey. One might expect some differences in the near surface layer since the surveys were flown at different times of the year and the near surface could have very different water saturation.

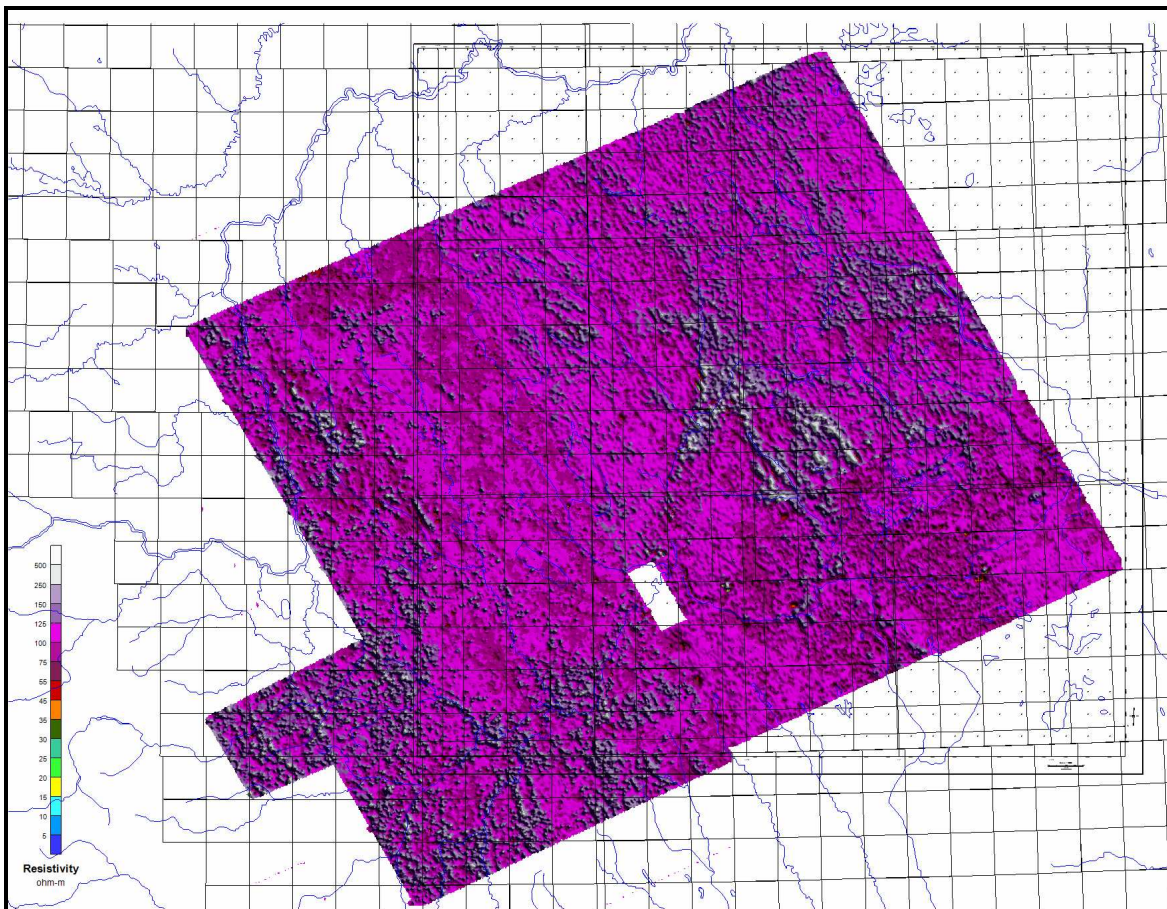


Figure 25: The rnn1, first layer resistivity, merged for the current and previous GEOTEM™ surveys.

The second layer resistivity match, Figure 26, is not as good as seen in the first layer in the northwest part of the survey. It is quite good in the south east. It is not known why



this difference has occurred. Attempts were made by FUGRO to find an explanation in the data processing. A statistical process was used to adjust the db/dt amplitudes for all areas subsequent to the original 07427 areas which subsequently improved the fit. A more detailed description is included in the 08411 Fugro Report.

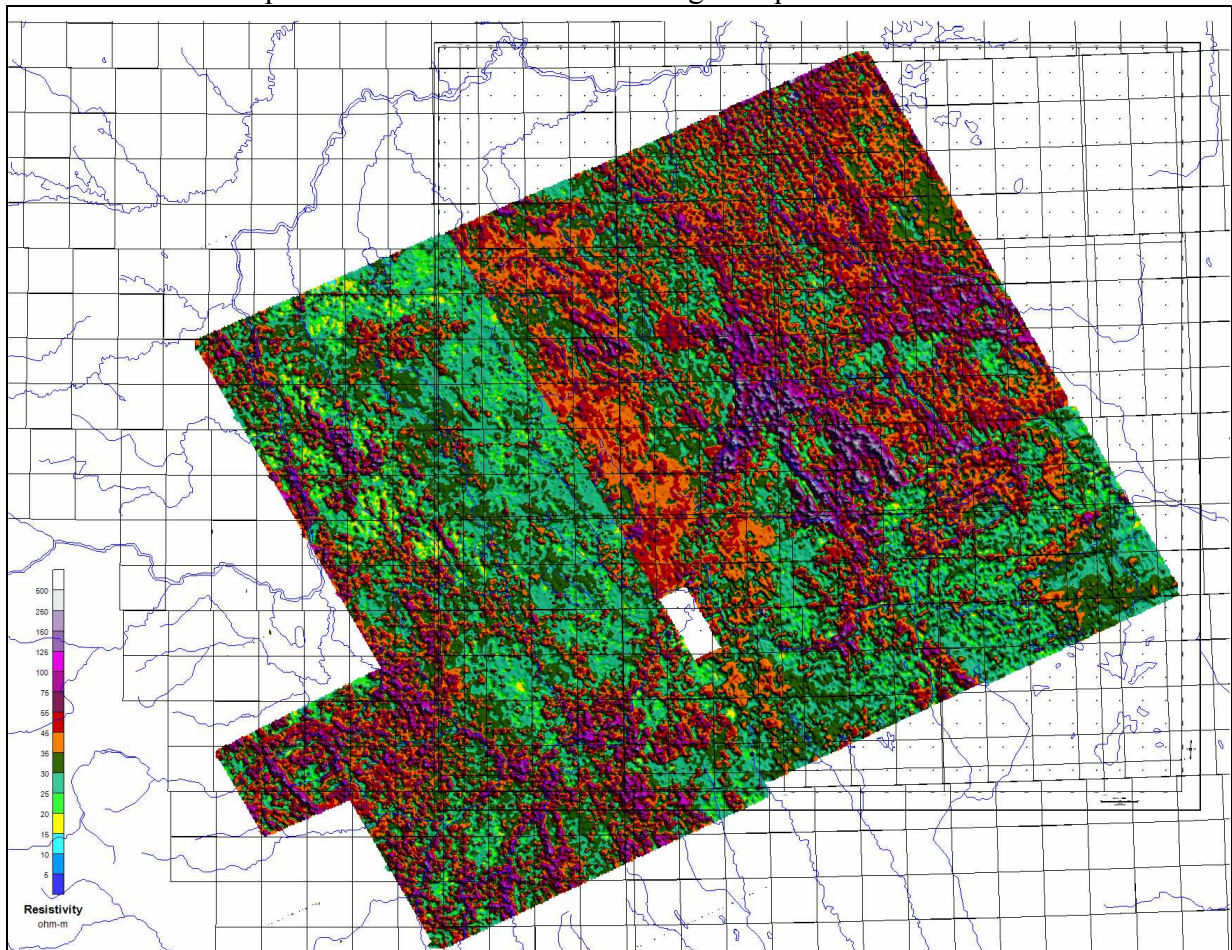


Figure 26: The rnn2, second layer resistivity, merged for the current and previous GEOTEMTM surveys.

The third layer data resistivity data are shown in Figure 27. Here the match is not bad. The colors across the eastern boundary of the current survey and the earlier survey are adjacent colors in the color bar and would suggest the match is within a few ohm-m, well within the accuracy one might expect from an airborne survey. Again, it is the southeast part of the boundary that is the best fit. One can see some continuity of features across the survey boundary.



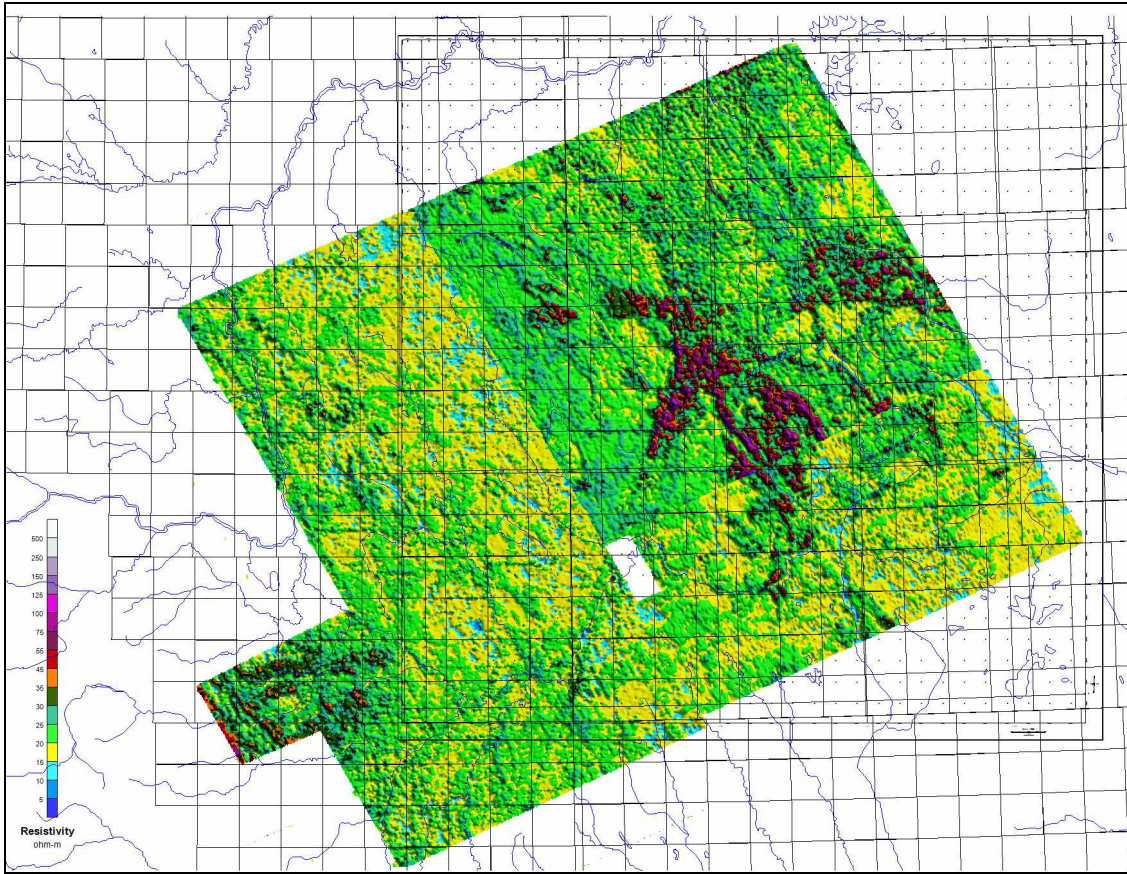


Figure 27: The rnn3, third layer resistivity, merged for the current and previous GEOTEM™ surveys

The merged fourth layer resistivity data are shown in Figure 28. The match is not perfect but is quite good. One can see continuity of some features across the boundary.

The merged first through fourth layer thicknesses are shown in Figures 29 through 32. It is the fourth layer that shows the best fit across the boundary. The other three layers are not perfect but are close. One can see the data patterns, where they occur, continue across the boundaries in most cases. Again it is the second layer that shows the poorest fit.



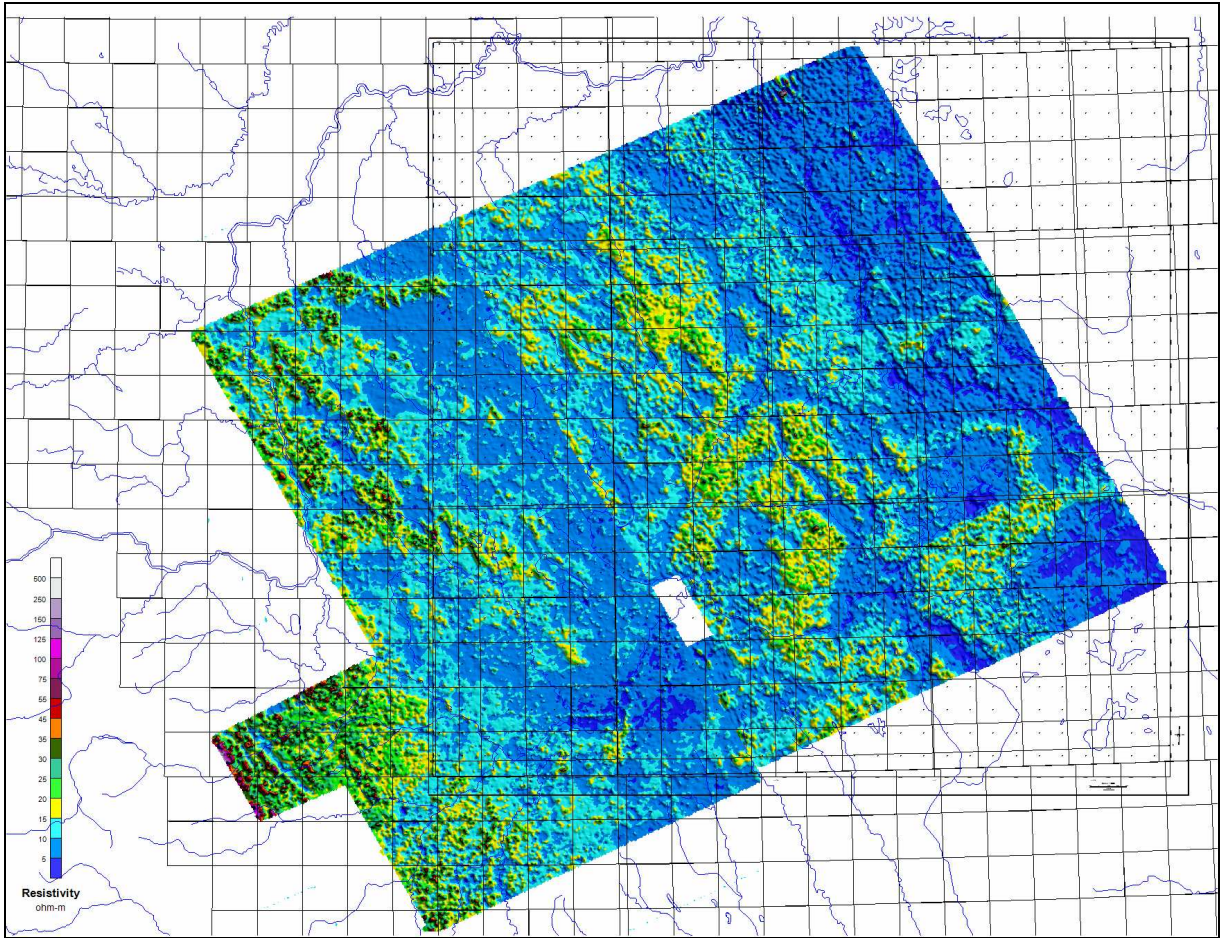


Figure 28: The rnn4, fourth layer resistivity, merged for the current and previous GEOTEM™ surveys



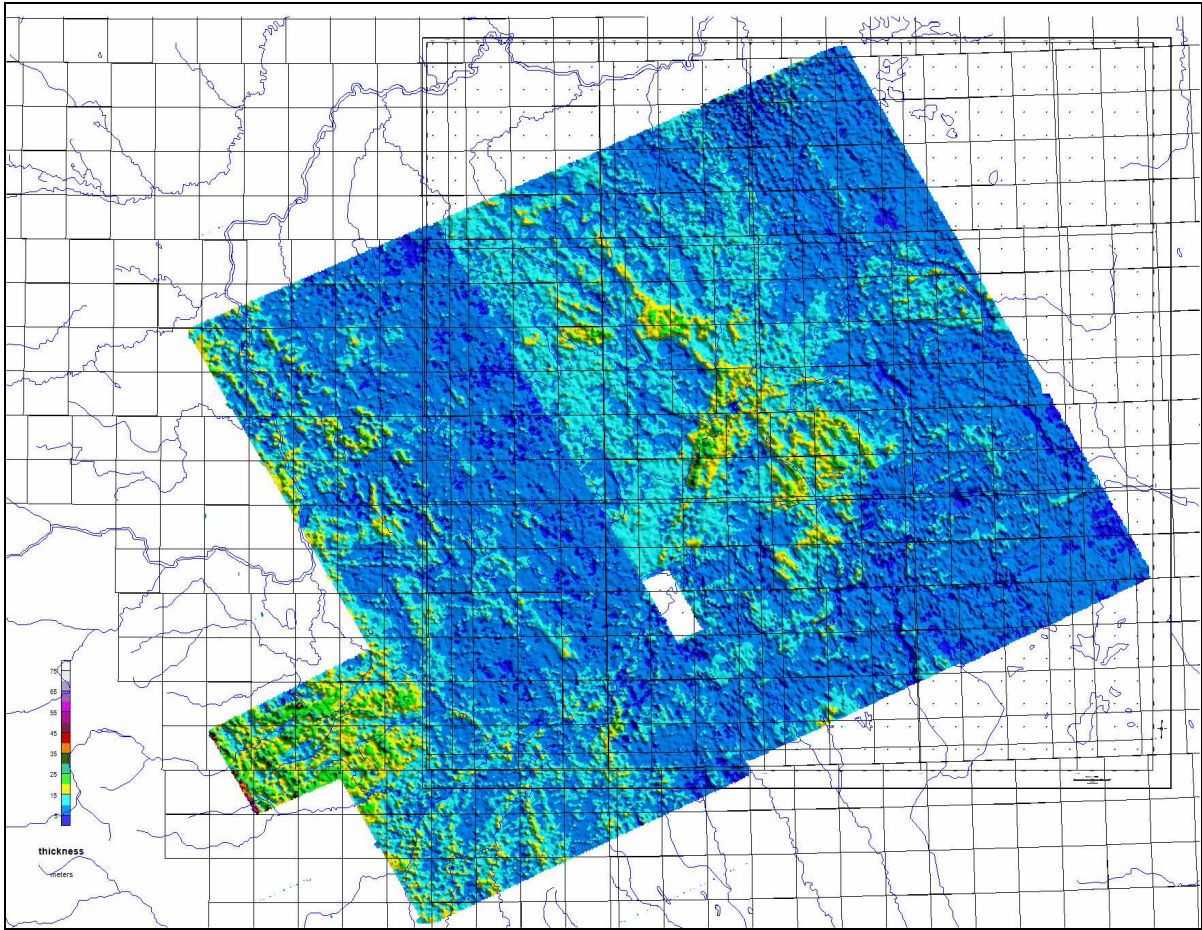


Figure 29: The T_{hnn1} , thickness for first layer, merged for the current and previous GEOTEMTM surveys



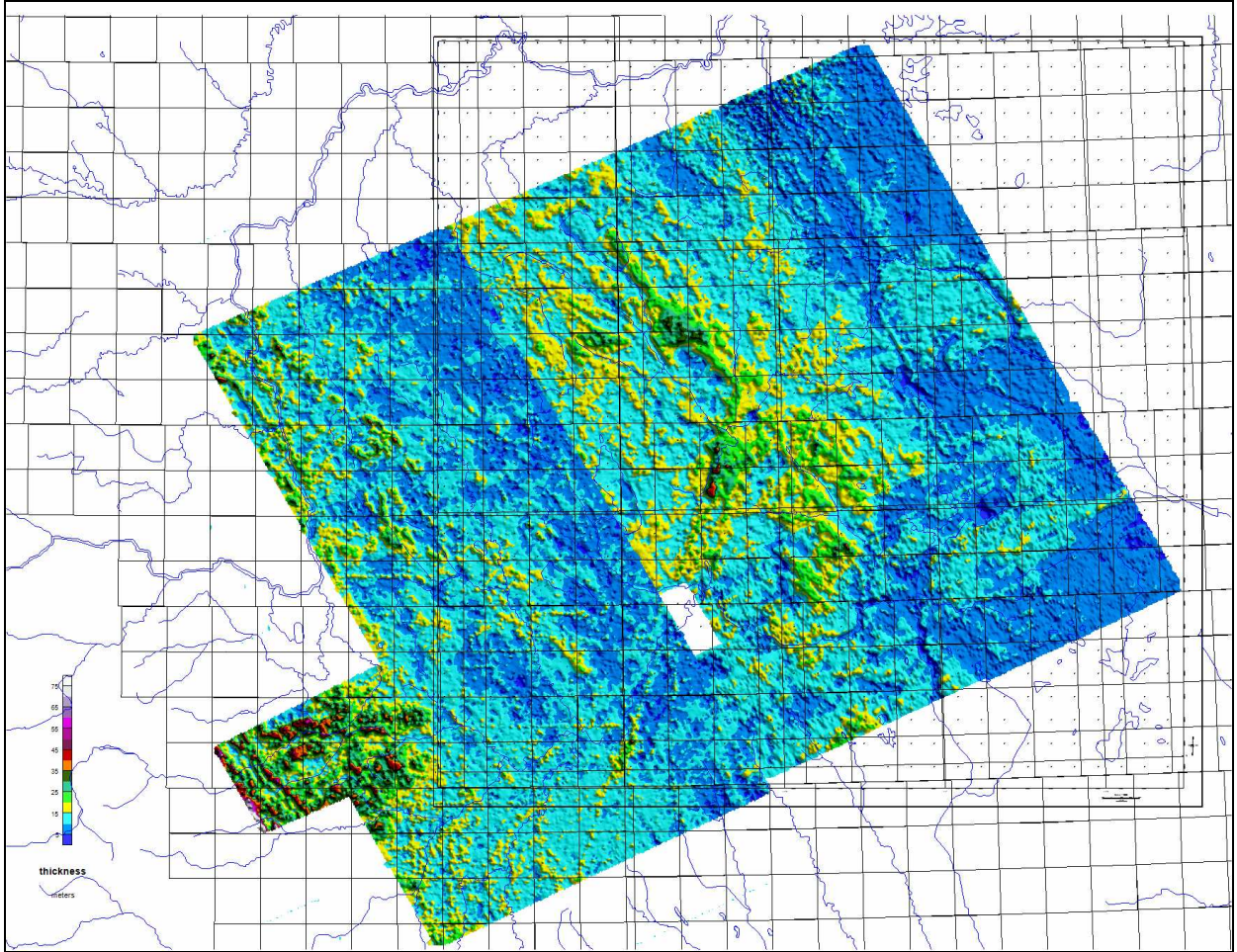


Figure 30: The Thnn2, thickness for second layer, merged for the current and previous GEOTEM™ surveys



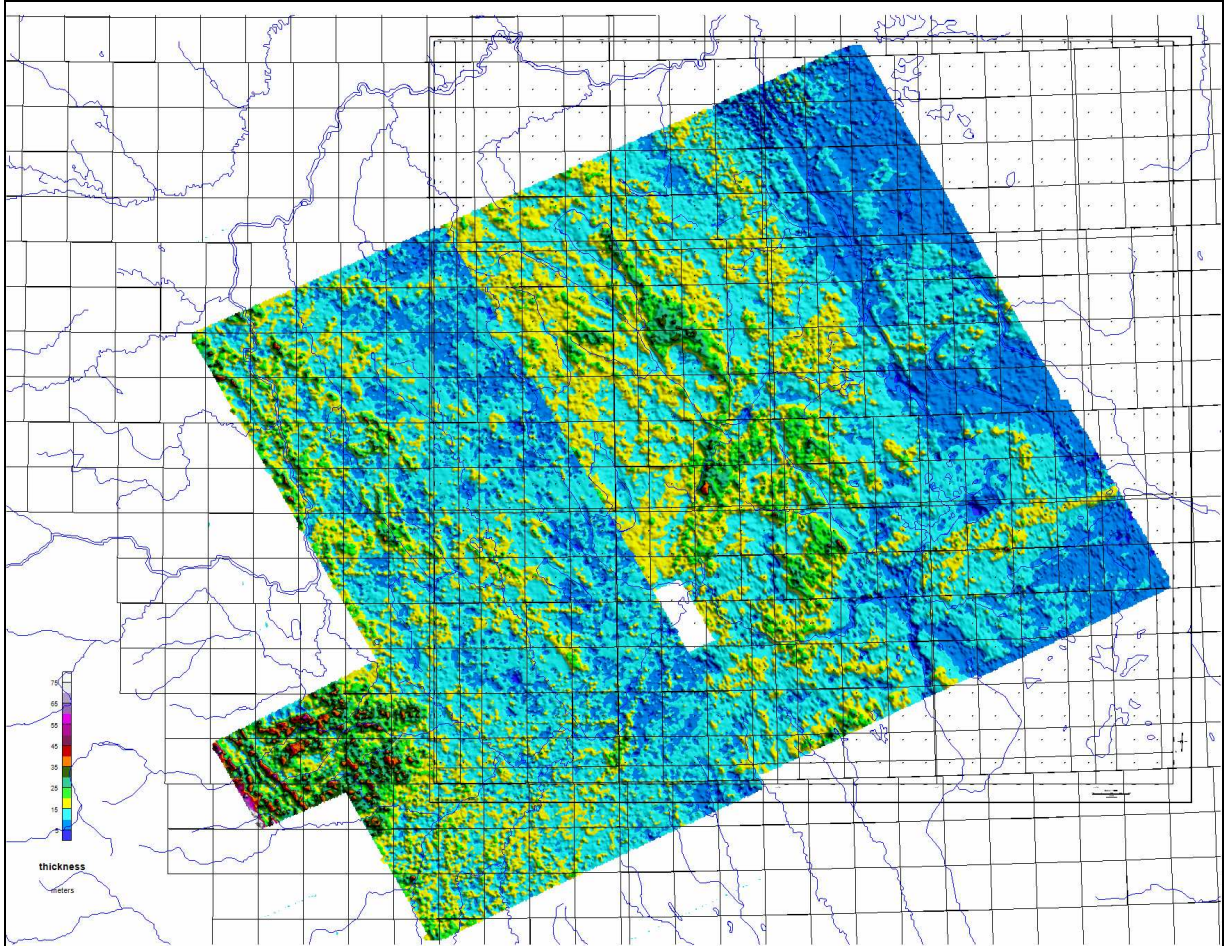


Figure 31: The Thnn3, thickness for third layer, merged for the current and previous GEOTEM™ surveys



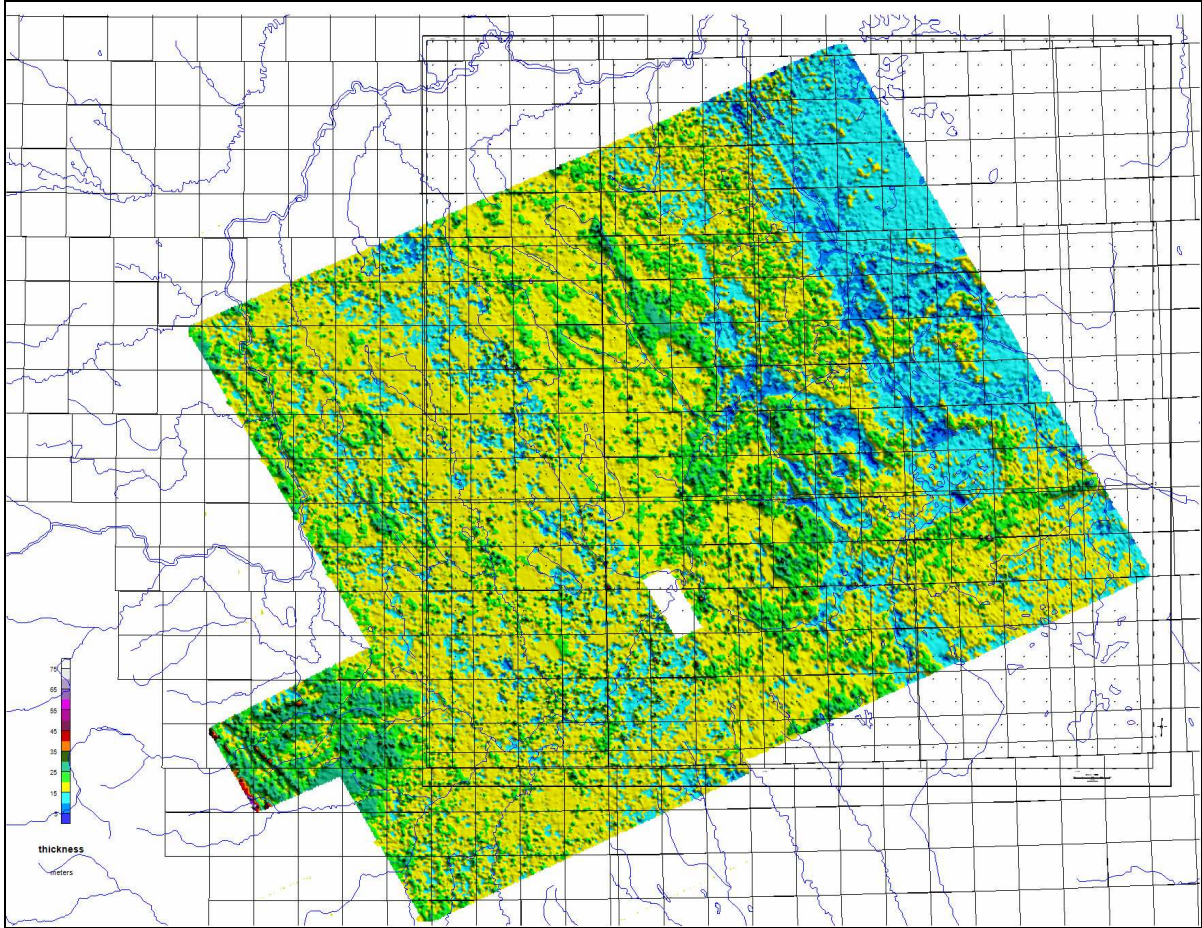


Figure 32: The Thnn4, thickness for fourth layer, merged for the current and previous GEOTEM™ surveys



Data Interpretation

The compilation of regional, shallow data from water wells, oil wells and other sources is under way at the Alberta Geological Survey (AGS). The lithologies in the wells are from the drillers and may vary with the driller on the rig. The drillers do not have formal geological training and the drilling process does not keep the integrity of the chip samples. However, it is useful information and can be a guide to the likely lithological profile of the subsurface. Also, there is the deliverability of the wells that can contribute to an understanding of the characteristics of the aquifers. Additional drilling may be done directly by the AGS which would provide a good subsurface data set to help understand the resistivity distributions seen in the airborne data. An integration of all these compiled data should help refine the airborne data interpretation. The details of this kind of interpretation will be left to the client. Only a general interpretation of the inversion data will be presented here.

Several airborne surveys were flown in late 2007 and provided to the AGS in early 2008. An interpretation report on these surveys was provided in March 2008. The survey discussed in this report lies along the western boundary of the previous surveys. The current survey results were merged with the previous results and were shown in the previous section.

Some discussion of the current survey data will note any similarities or apparent correlation of features seen the previous survey data. Some data were provided by the AGS for the previous study and these data extended to varying amounts westward over the current survey area, Figure 33. Overlays of some of these data are discussed in a limited way. Note how many of the mapped features follow current drainage.

Portions of the first, second and third layer resistivity shaded relief images from the inversion results with the AGS overlays on them are shown in Figures 34 through 36. Selected, highest resistivity levels in each of the layer data sets have been contoured. The contoured areas can be directly compared to the outlined AGS aggregate and coarse sediment areas. One can see that there is only a partial correlation. It is possible that the resistivity may be mapping the thickest, most saturated and coarsest material areas. There is nothing in the results to determine if this conclusion has merit. However, it is one reasonable explanation. Most interesting is that there are a number of these resistive areas that do not correlate in any way with the mapped features. It is possible that these resistive areas represent unmapped coarse sediment or aggregate areas.

Note that the resistivity of the layers and the relative higher resistivity areas within each area decreases with depth. This decrease may be a property of the sediment facies, its water salinity or both.

Figure 34a shows a zoomed portion of the first layer resistivity around T36N, R1W5. The AGS overlays from Figure 33 are included in the images. The first layer resistivity is quite high everywhere. However, the highest values are dark colors.



Resistivity contours at 70, 90 and 120 ohm-m are also in the image. The objective was to see if any of the most resistive areas were coincidental with the mapped AGS features. The result shows only a partial coincidence.

Figure 34b shows a similar zoomed image of an area around T42N, R6-7W5. Again, there is only a partial correlation between highest resistivities and the mapped AGS features. There are several reasons for the lack of correlation, assuming the AGS map is correct. The mapped features do not have a significant resistivity contrast with material around these deposits. The mapped features are relatively thin and do not create a measureable EM response.

Figure 34c shows a zoomed area in the NW part of the survey area around T44N, R8-9W5. Here there are few mapped AGS features and those few areas present show no correlation to the highest resistivity.

Figure 35 show the same series of images for the second layer resistivity. There appears to be a bit more correlation between the mapped AGS features and the second layer resistivities. Resistivity contours at 40, 60 and 70 ohm-m are included in the images to highlight again the highest resistivity values in the data.

Figure 36 shows similar zoomed areas for layer three. Note the resistivities continue to become lower in each deeper layer. One of the best correlations between the resistivity patterns and the AGS contours occurs in the south central part of figure 36a, along the east side of the river. The curvilinear aspect of the data pattern suggests it may be an older, buried channel.

Figure 37a shows the hatched filled patterns interpreted, approximately, as the area highest resistivity in layer 1. The areas are interpreted, in part, using a resistivity-thickness product data set, Figure 38. It is possible that a more resistive, thicker layer could be the best hydrologic targets. It would need to be verified by well data. The same data are shown in Figure 37b with the AGS overlays on the image.

Similar resistivity-thickness products are shown for layers 2 and 3 in Figures 39 and 40. All the resistivity-thickness product data have been divided by 100 to simply place their data range within the range of the color palettes used for other data.

Figure 41 shows the resistivity thickness product for the first three layers, zoomed for the extreme western part of the survey area. The patterns in the data along the western block suggest that the resistivity is mapping possible Cretaceous bedrock sub crop edges. These edges might be expected to follow this NW-SE trend seen in the data. The patterns to east also resistive areas but trend more ENE-WSW. It may be that drainage systems have incised the Cretaceous sub crop to form this resistivity pattern. Note that most the drainage, approximate, follows the lower resistivity areas. Perhaps the resistive Cretaceous rocks have been removed. Note the good correlation between topography and the third layer resistivity thickness product. This correlation would support the interpretation that there is a relationship between the sub crop and resistivity



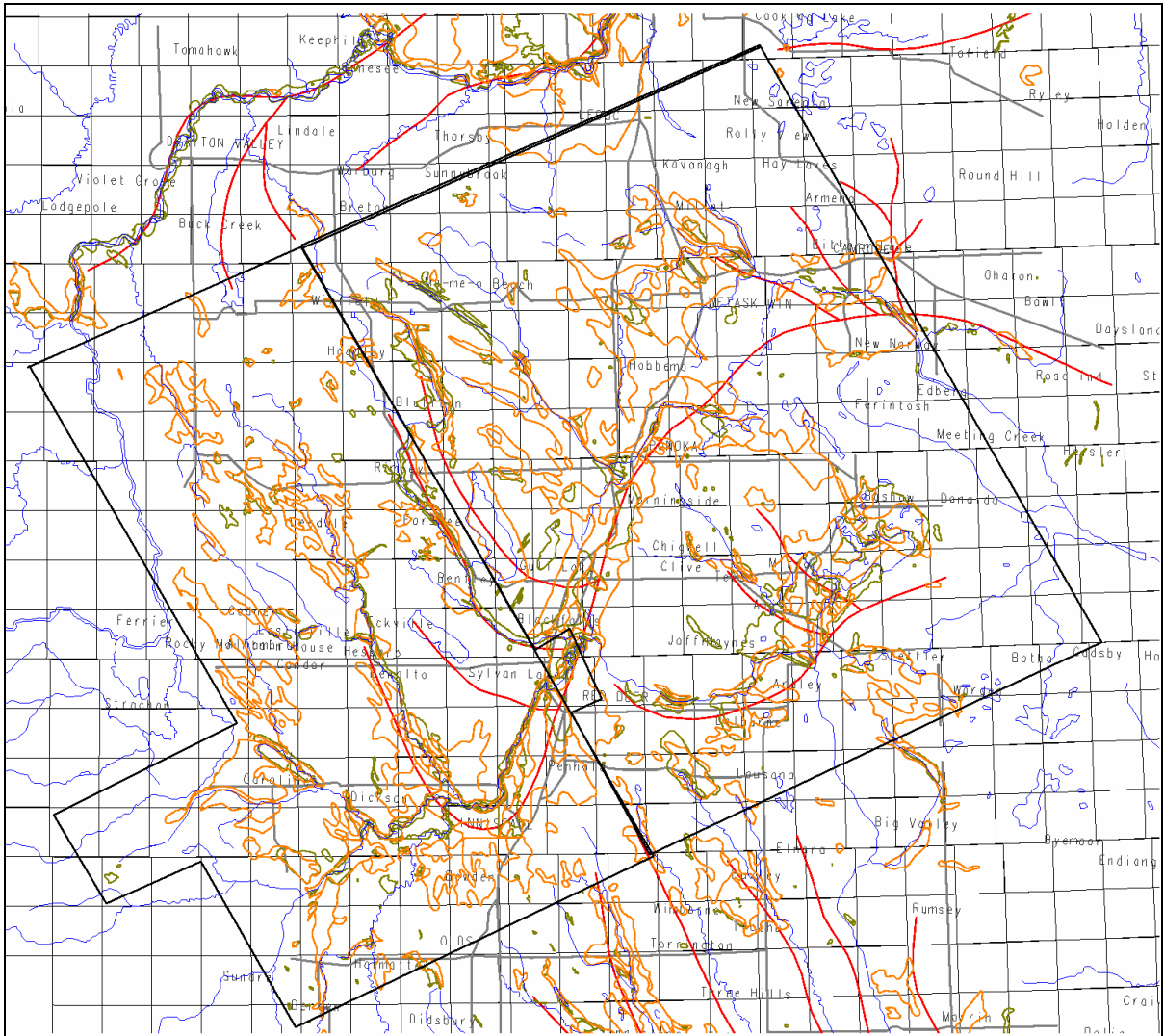


Figure 33a: Map of AGS data: Red color is buried channels, Green color is aggregate, Orange color is coarse sediments. Black lines outline the current survey area on the west and the several earlier surveys on the east. The small rectangle in along the south west border of the older survey is a data gap over the city of Red Deer. The survey outlines are approximate. Township and range grid is shown on the figure, as well as the major drainage (approximate).



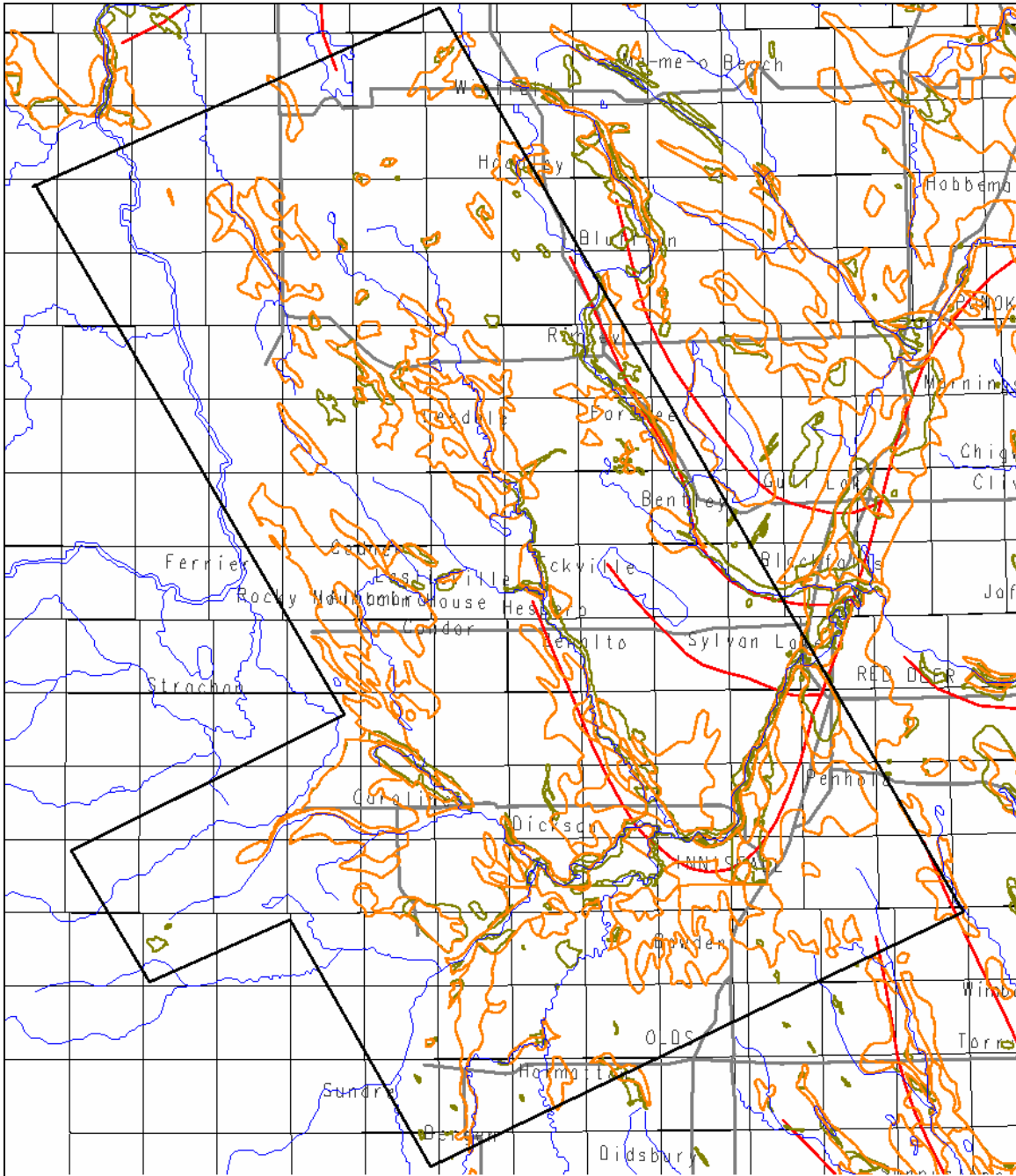


Figure 33b: Zoomed western portion of Figure 33a over the newer survey area. All overlays are the same as described in the caption to Figure 33a.



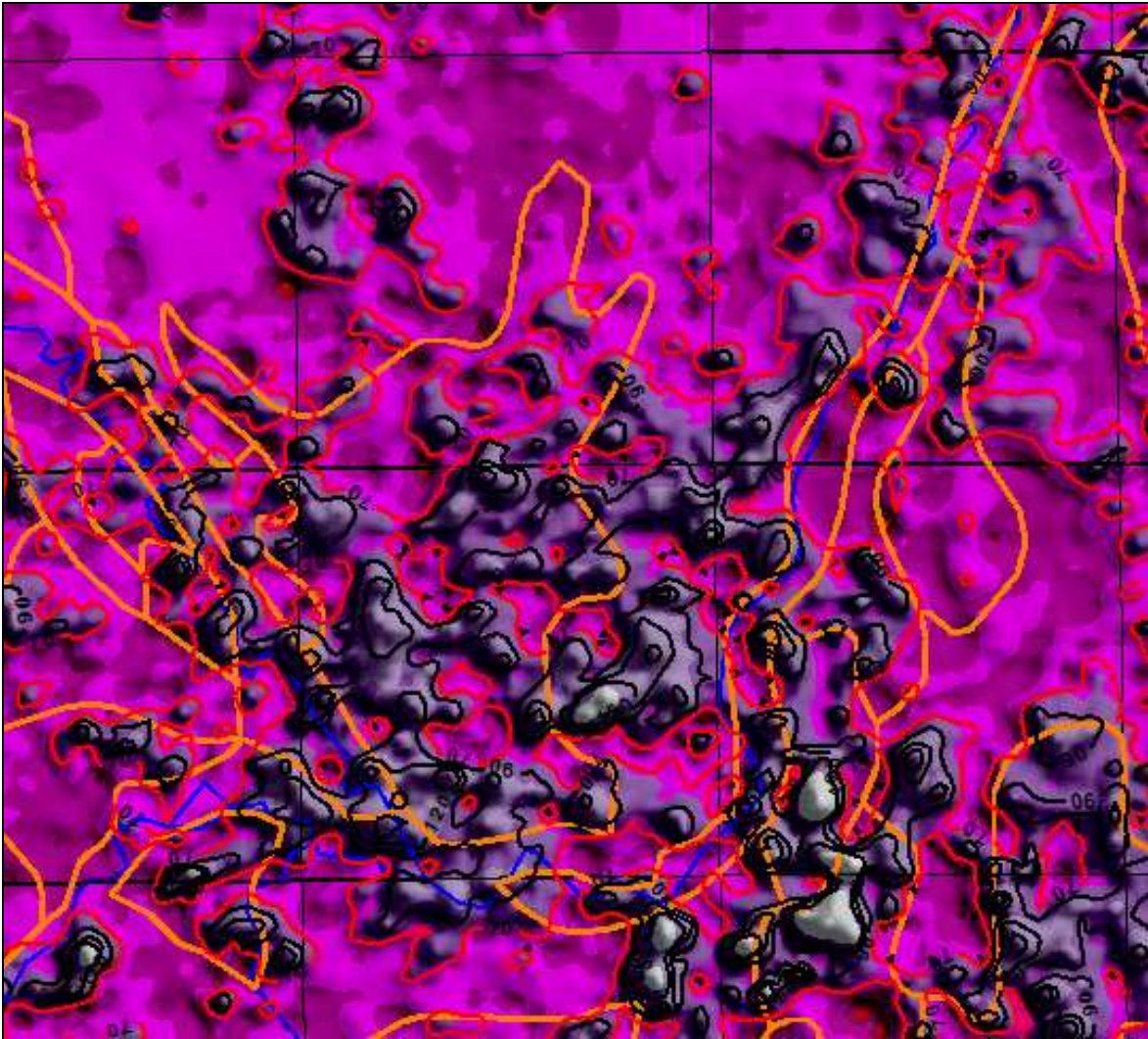


Figure 34a: Shaded relief image of the first layer resistivity with the coarse sediment contours in orange overlain for an area Township36 and Range 1W5. Black contours are overlain at 70, 90 and 120 ohm-m levels.



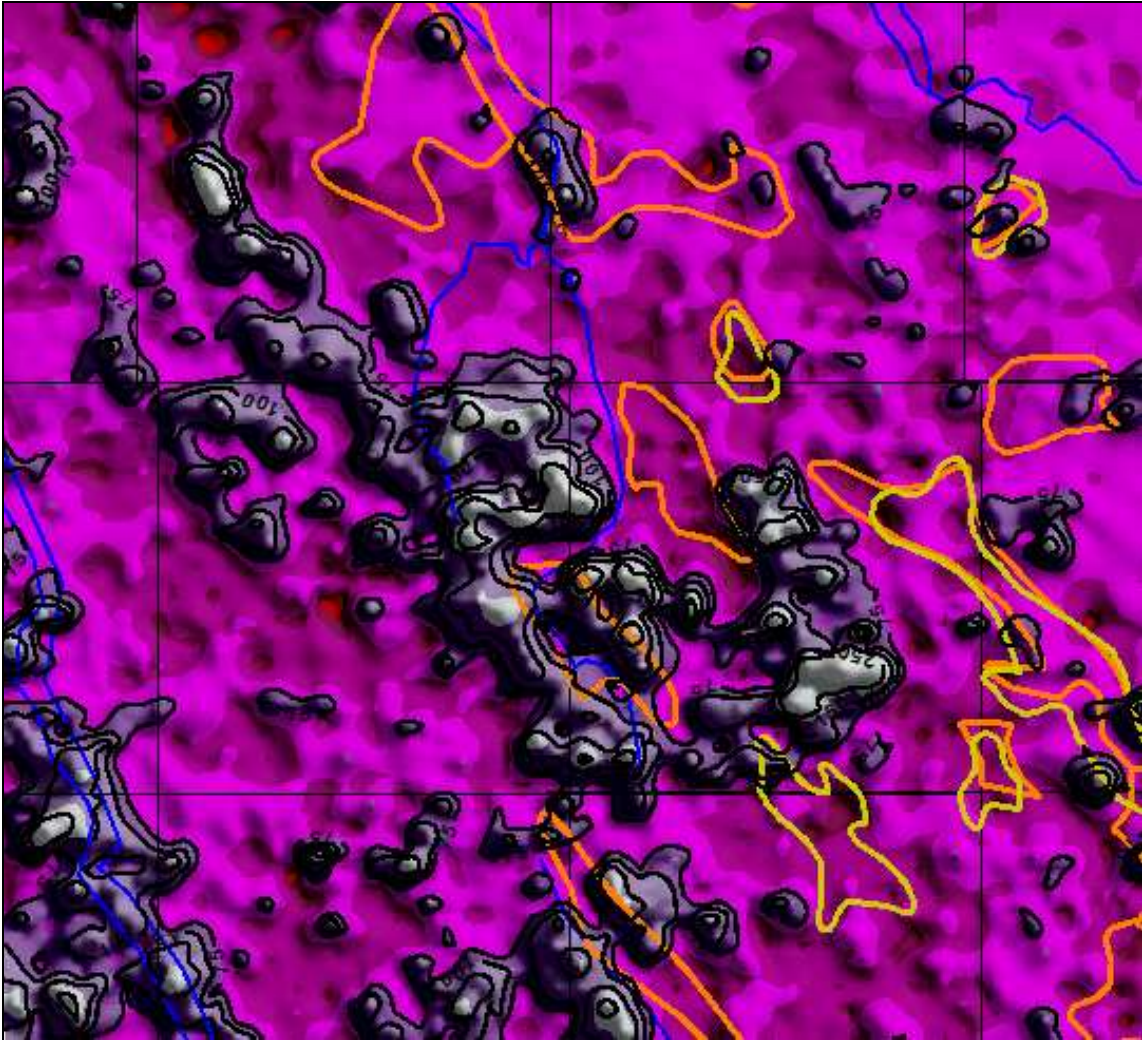


Figure 34b: Shaded relief image of the first layer resistivity with the coarse sediment contours in orange overlain in an area around Township 42, Ranges 6 and 7W5. Black contours are overlain at 70, 90 and 120 ohm-m levels.



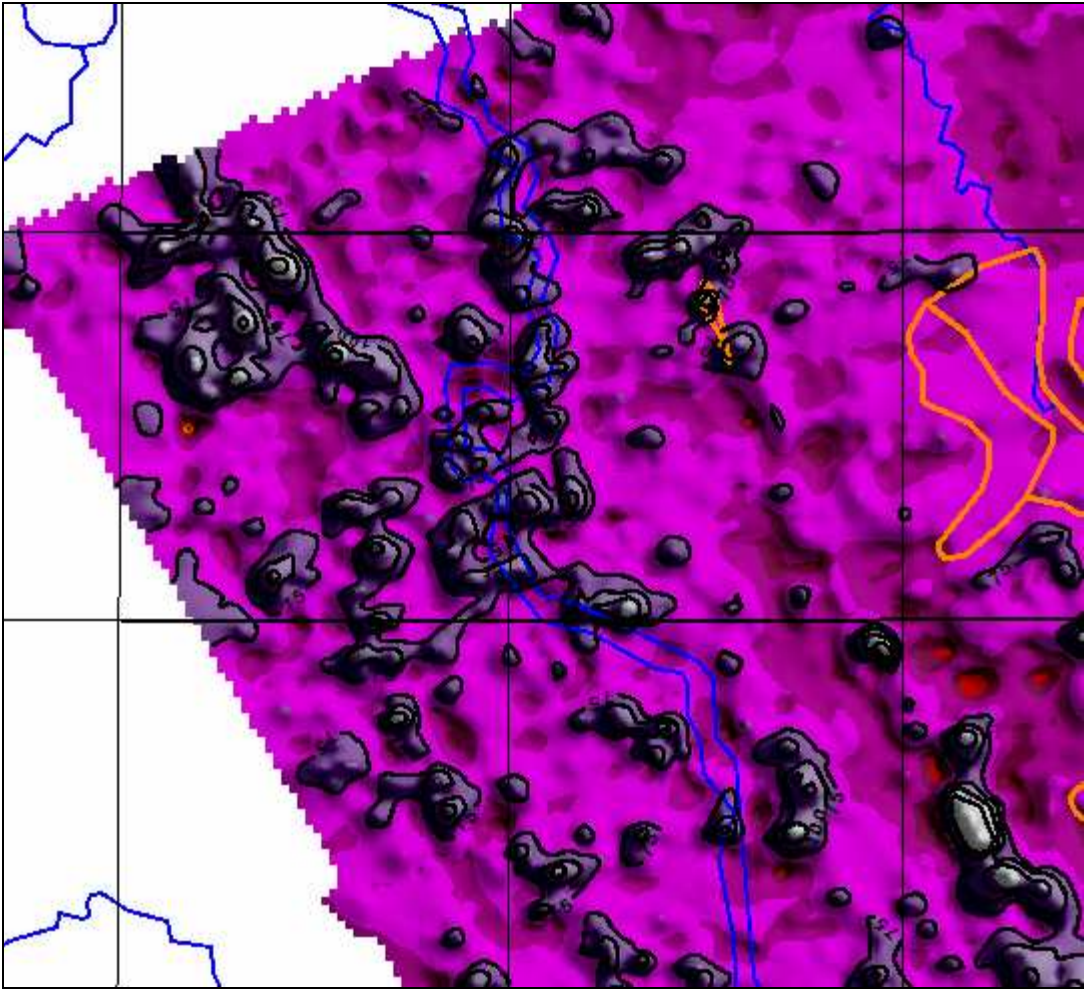


Figure 34c: Shaded relief image of the first layer resistivity with the coarse sediment contours in orange overlain in an area around Township 44, Ranges 8 and 9W5. Black contours are overlain at 70, 90 and 120 ohm-m levels.



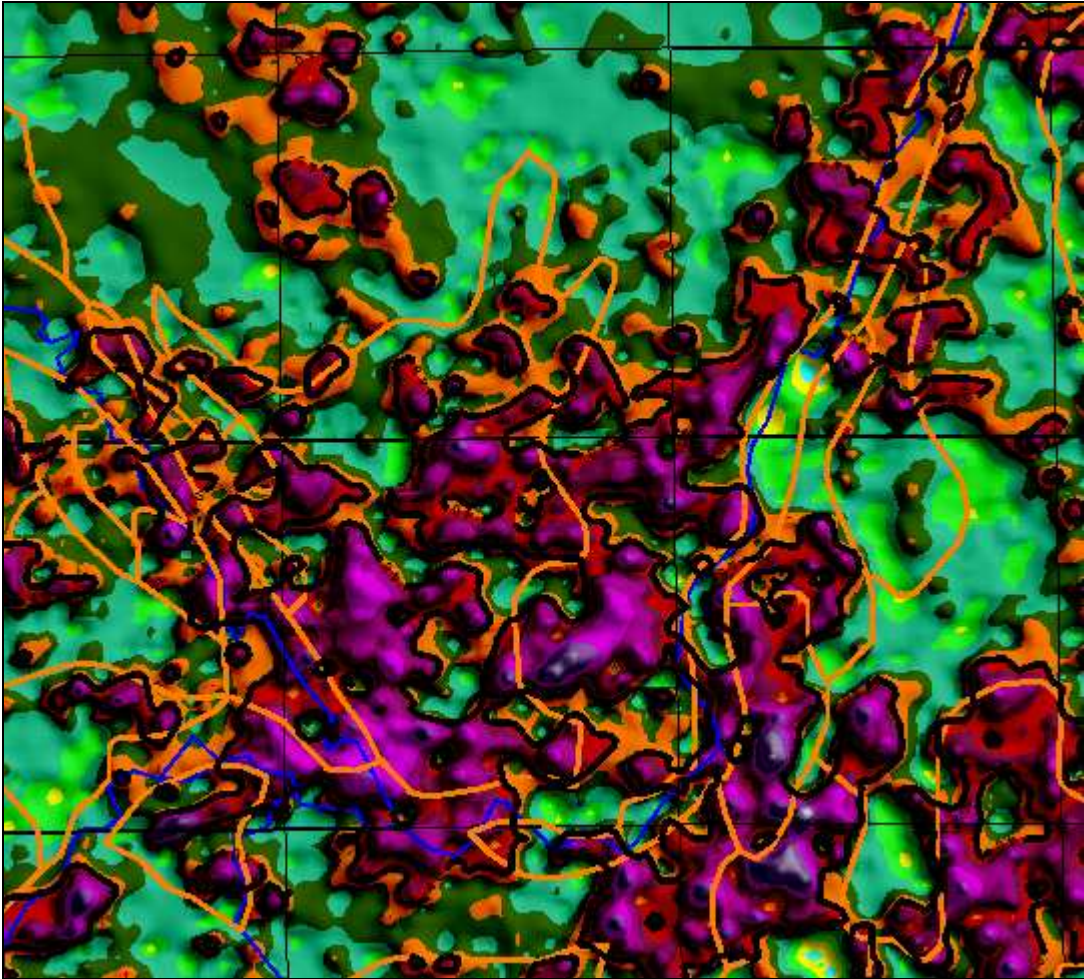


Figure 35a: Shaded relief image of the second layer resistivity with the coarse sediment contours in orange overlain in an area around Township 36 and 37, Range 1W5. Black contours are overlain at 40, 60 and 70 ohm-m levels.



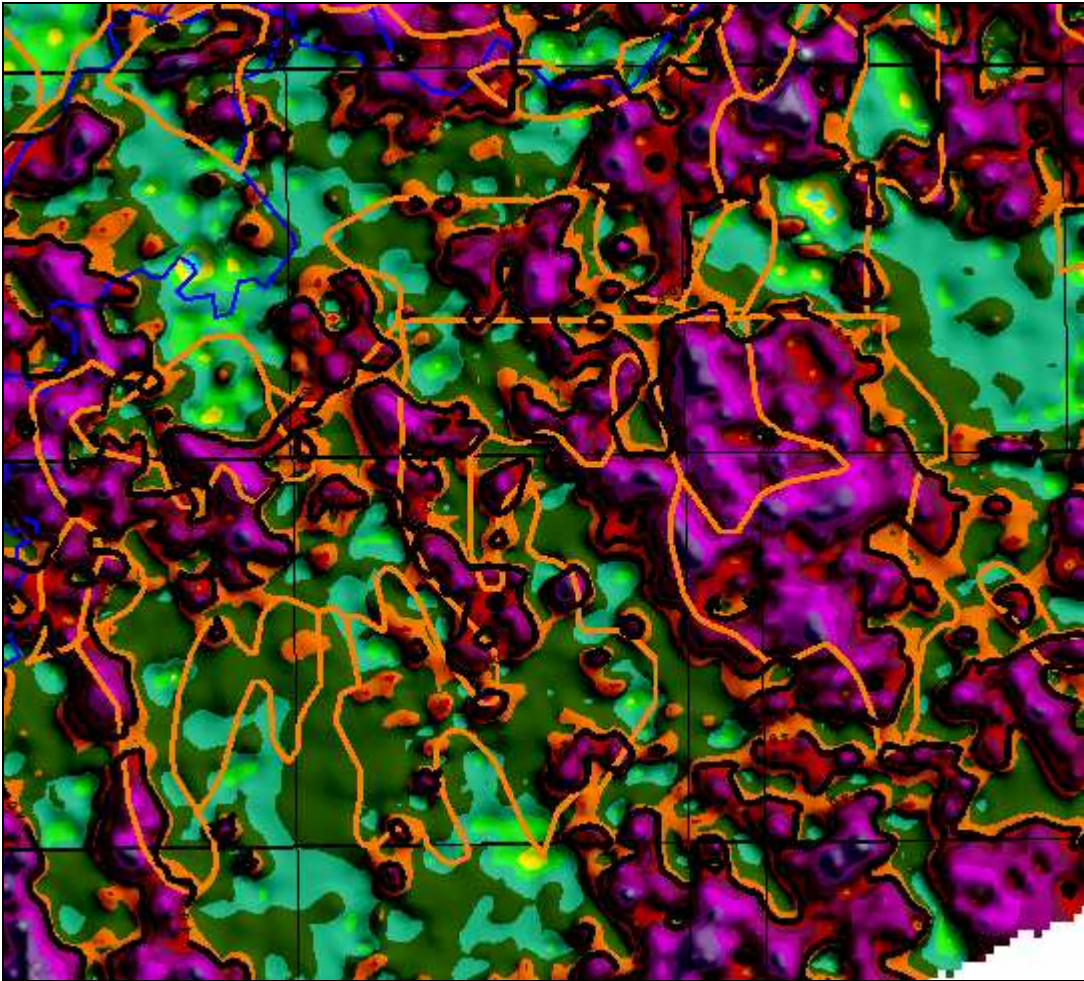


Figure 35b: Shaded relief image of the second layer resistivity with the coarse sediment contours in orange overlain in an area around Townships 34 and 35, and the fifth meridian. Black contours are overlain at 40, 60 and 70 ohm-m levels.



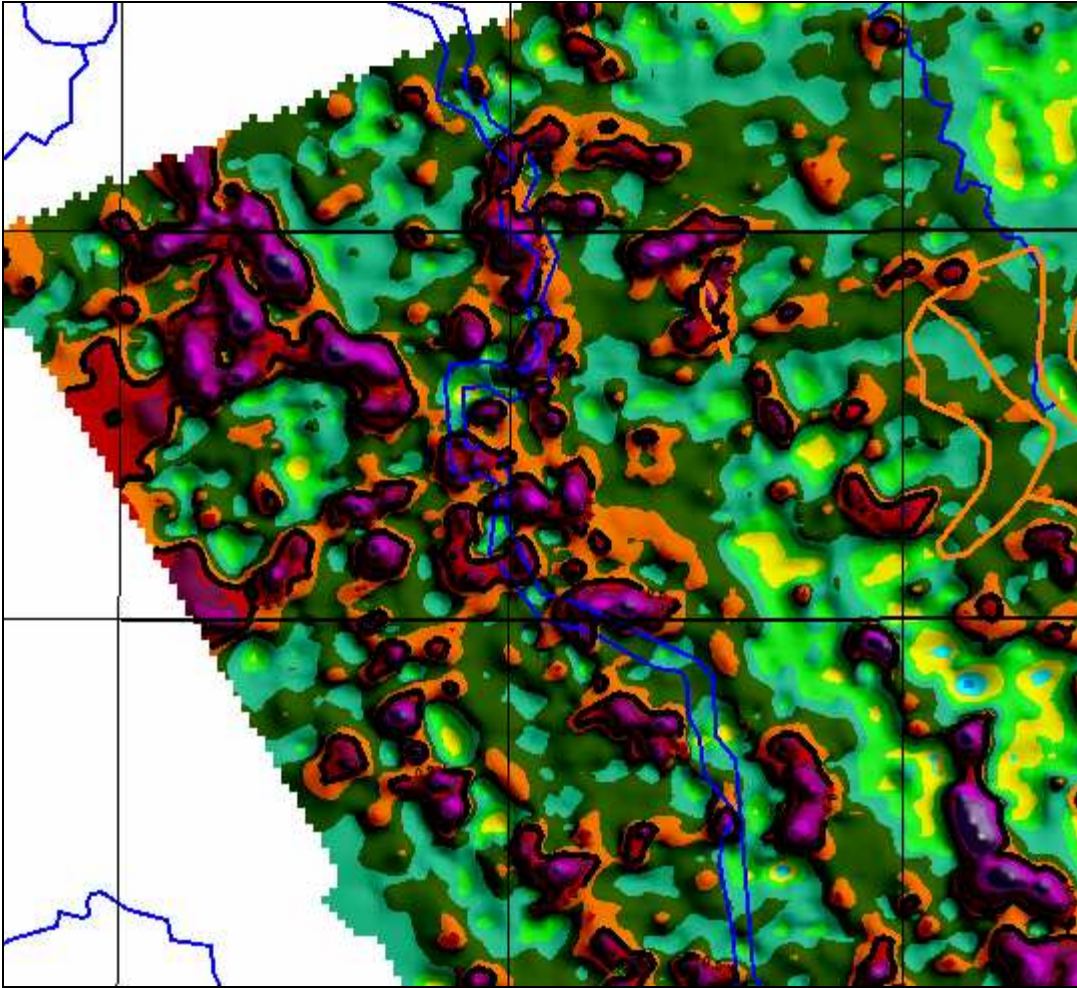


Figure 35c: Shaded relief image of the second layer resistivity with the coarse sediment contours in orange overlain in an area around Township 44, and Ranges 8 and 9W5. Black contours are overlain at 40, 60 and 70 ohm-m levels.



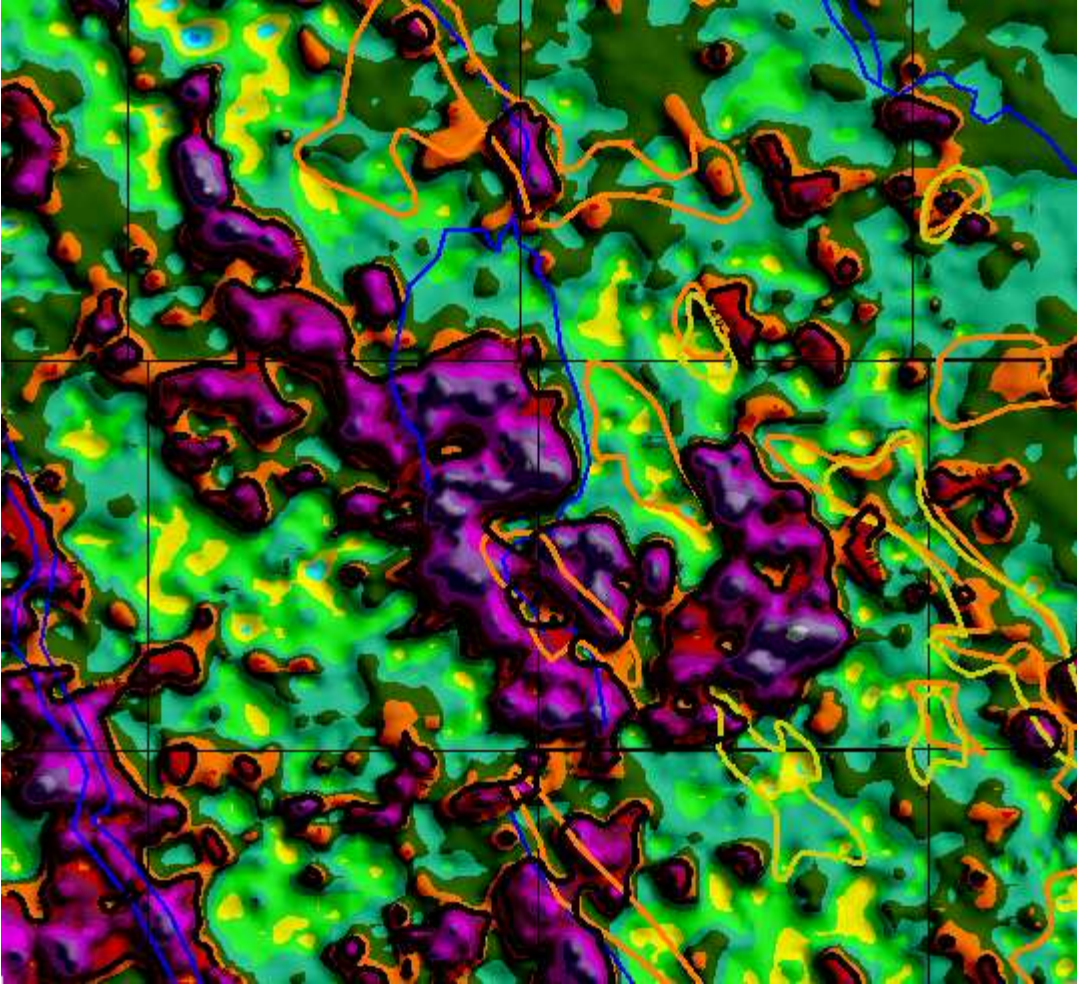


Figure 35d: Shaded relief image of the second layer resistivity with the coarse sediment contours in orange overlain in an area around Township 42, and Ranges 6 and 7W5. Black contours are overlain at 40, 60 and 70 ohm-m levels.



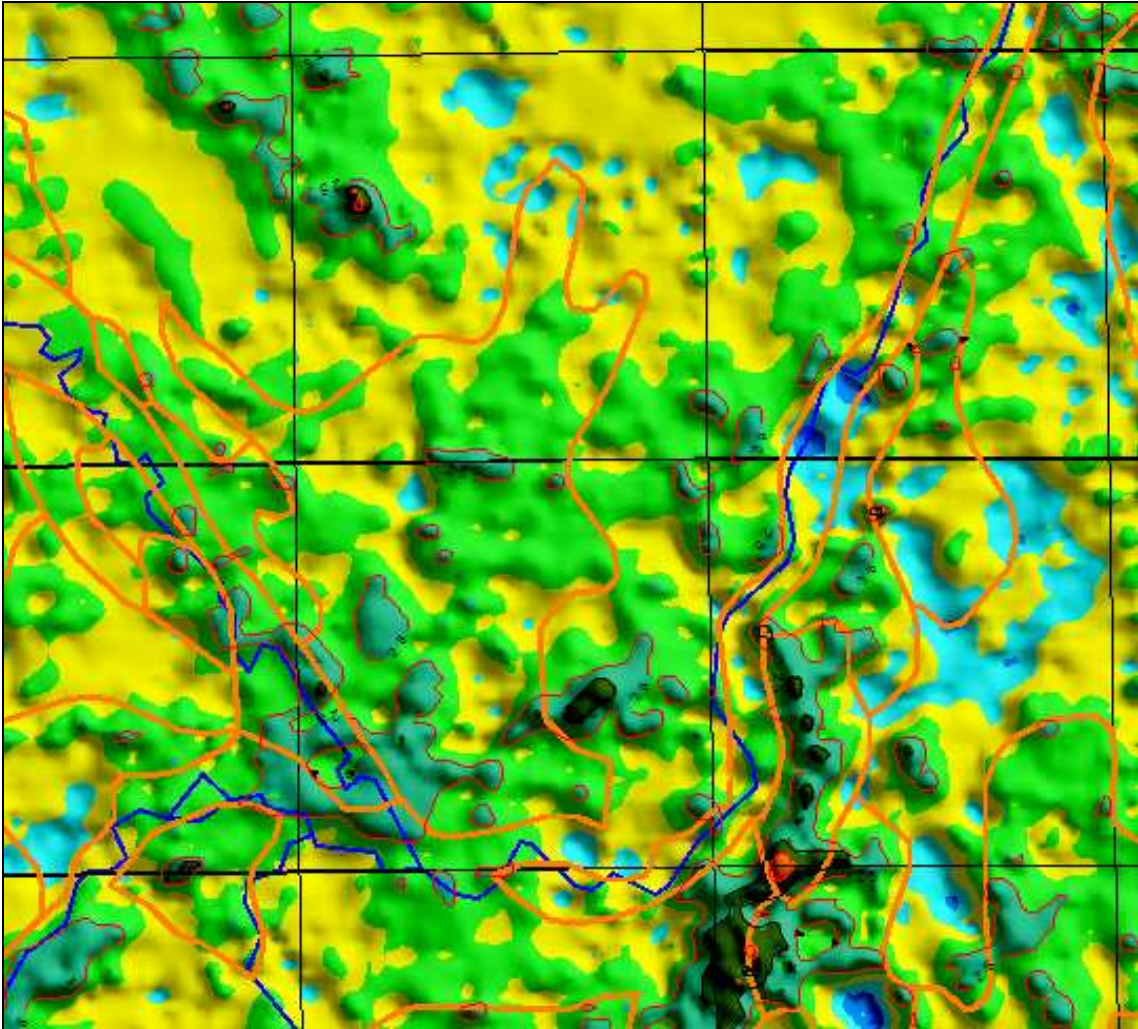


Figure 36a: Shaded relief image of the third layer resistivity with the coarse sediment contours in orange overlain in an area around Townships 36 and 37, and Range 1W5. Black contours are overlain at 25, 30, 35 and 40 ohm-m levels.



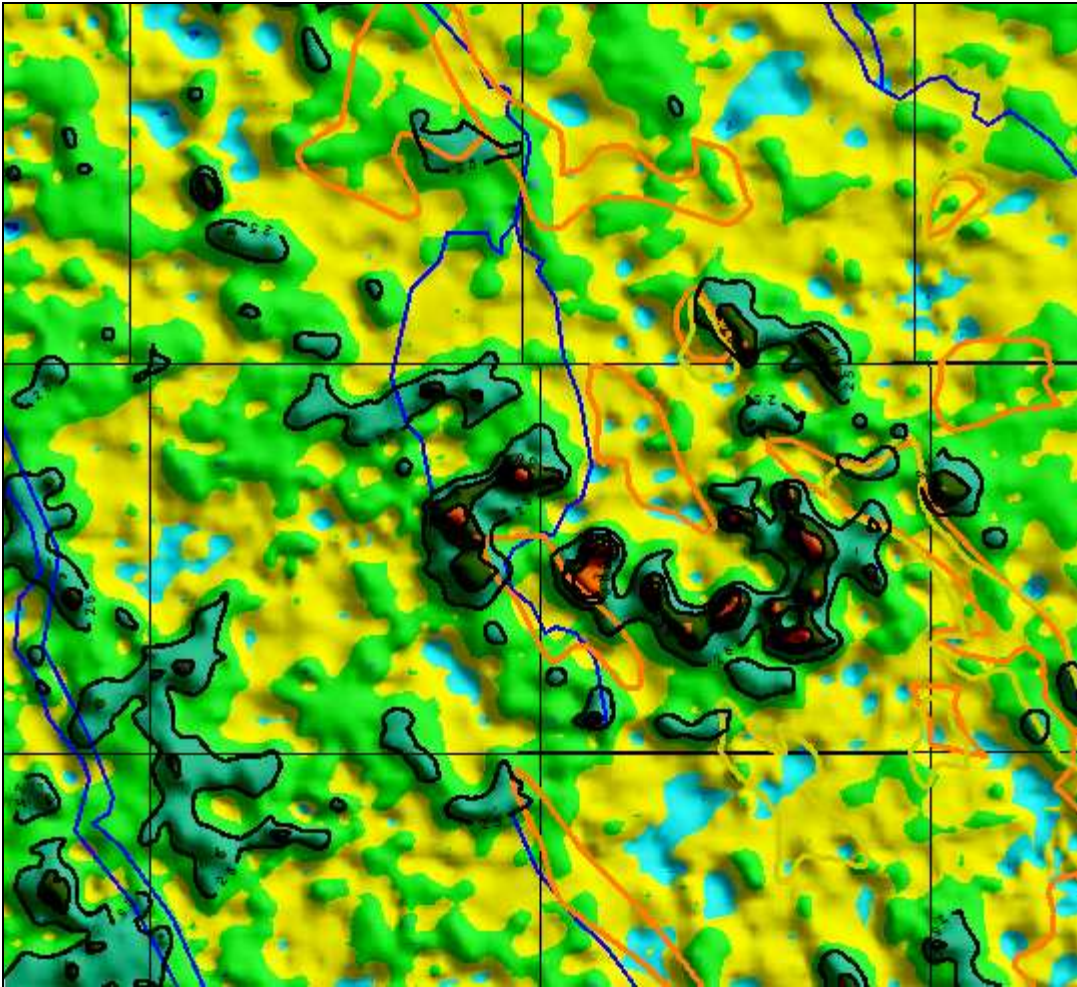


Figure 36b: Shaded relief image of the third layer resistivity with the coarse sediment contours in orange overlain in an area around Townships 36 and 37, and Ranges 1W5. Black contours are overlain at 25, 30, 35 and 40 ohm-m levels.



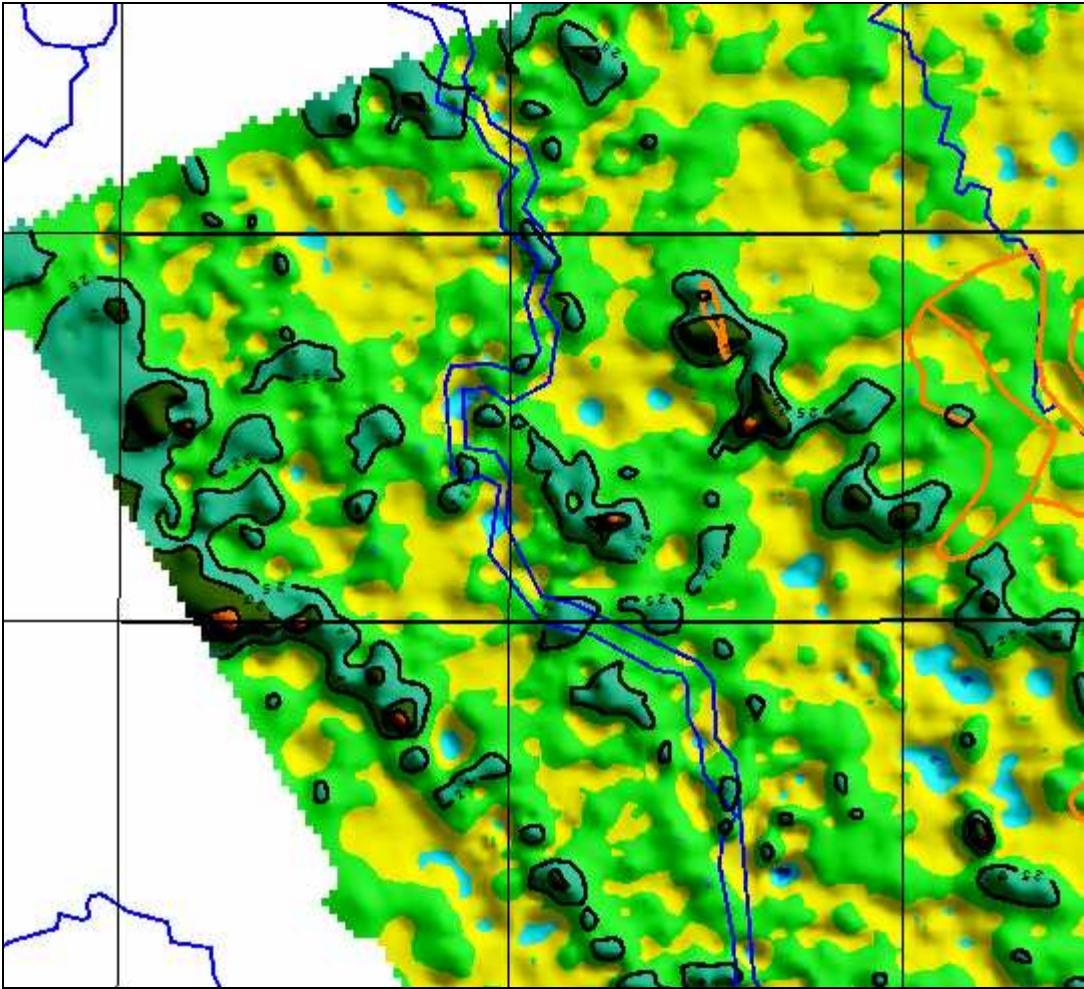


Figure 36c: Shaded relief image of the third layer resistivity with the coarse sediment contours in orange overlain in an area around Township 44, and Ranges 8 and 9W5. Black contours are overlain at 25, 30, 35 and 40 ohm-m levels





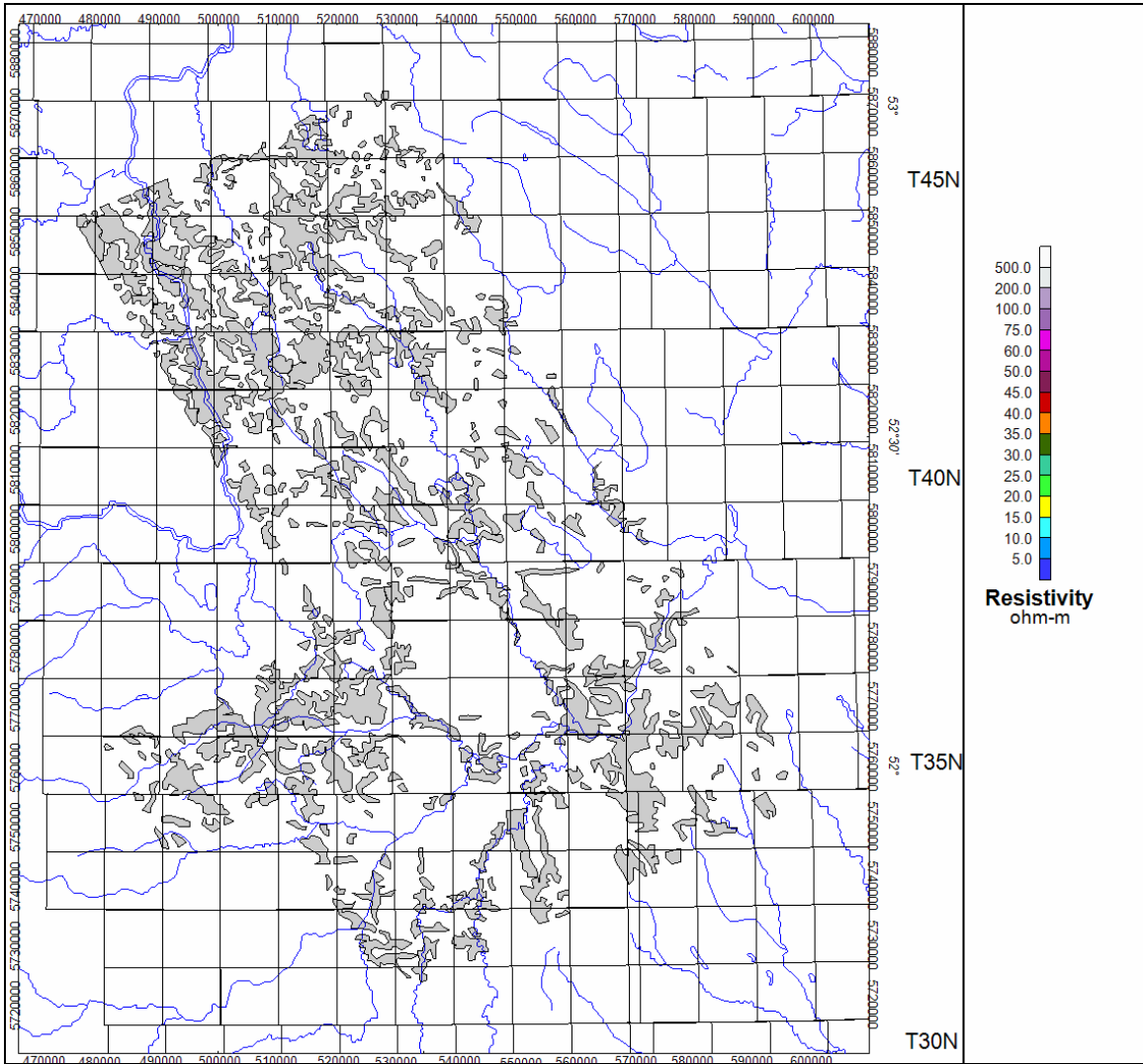


Figure 37a Areas of highest resistivities from the first layer resistivity.



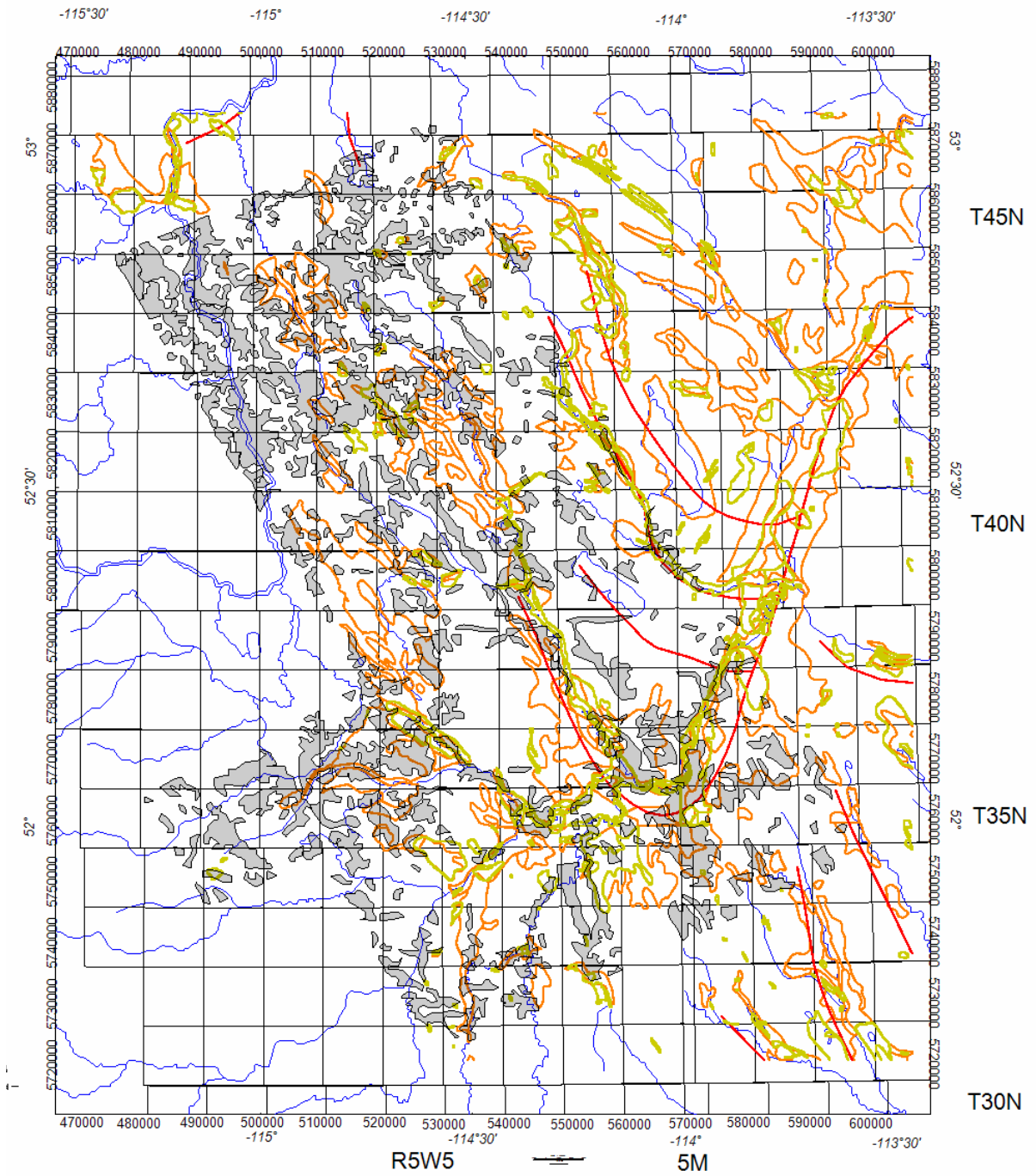


Figure 37b Areas of highest resistivities from the first layer resistivity with the AGS overlays.



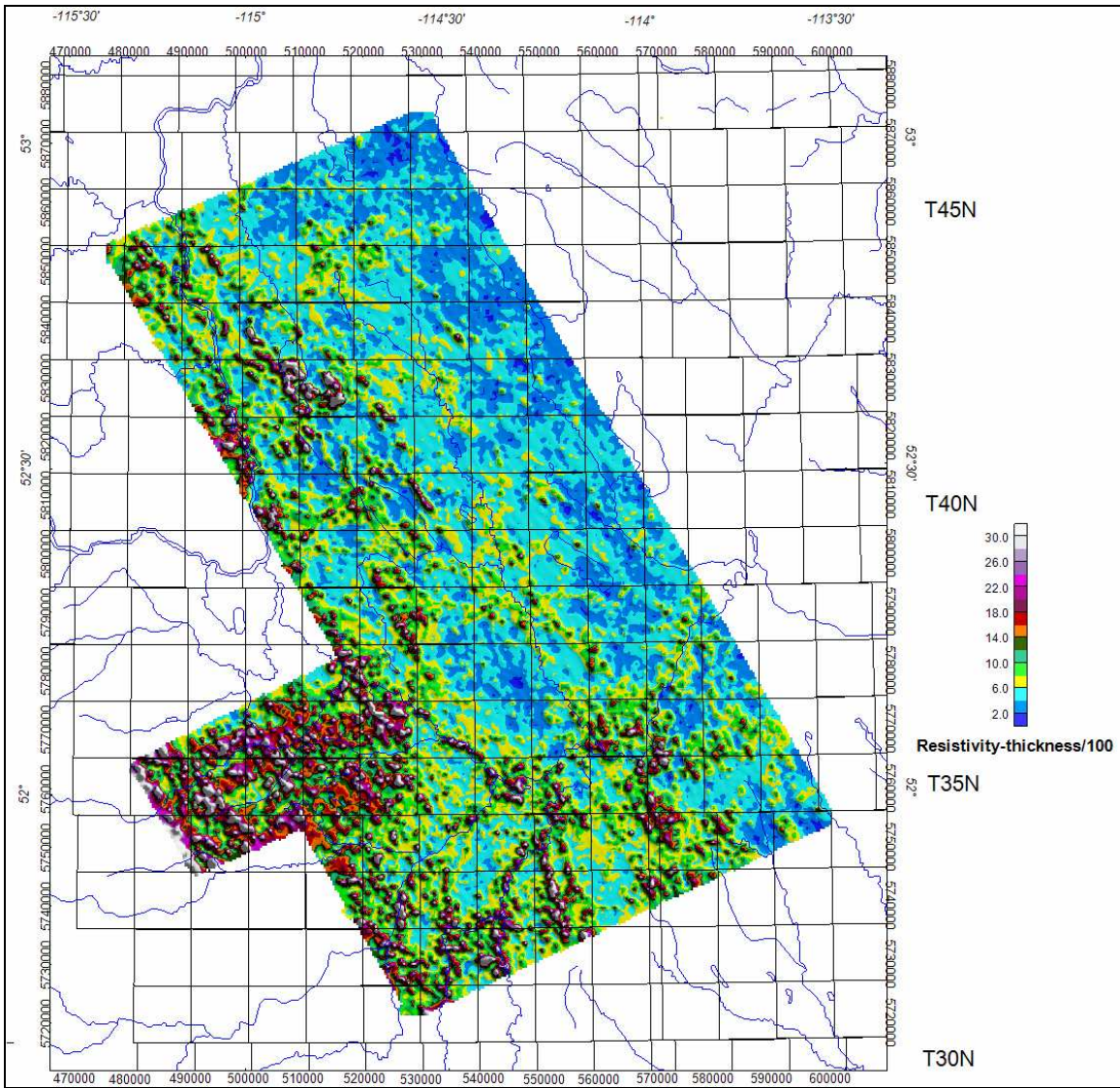


Figure 38: Resistivity-thickness for layer 1 (divided by 100), zone palette



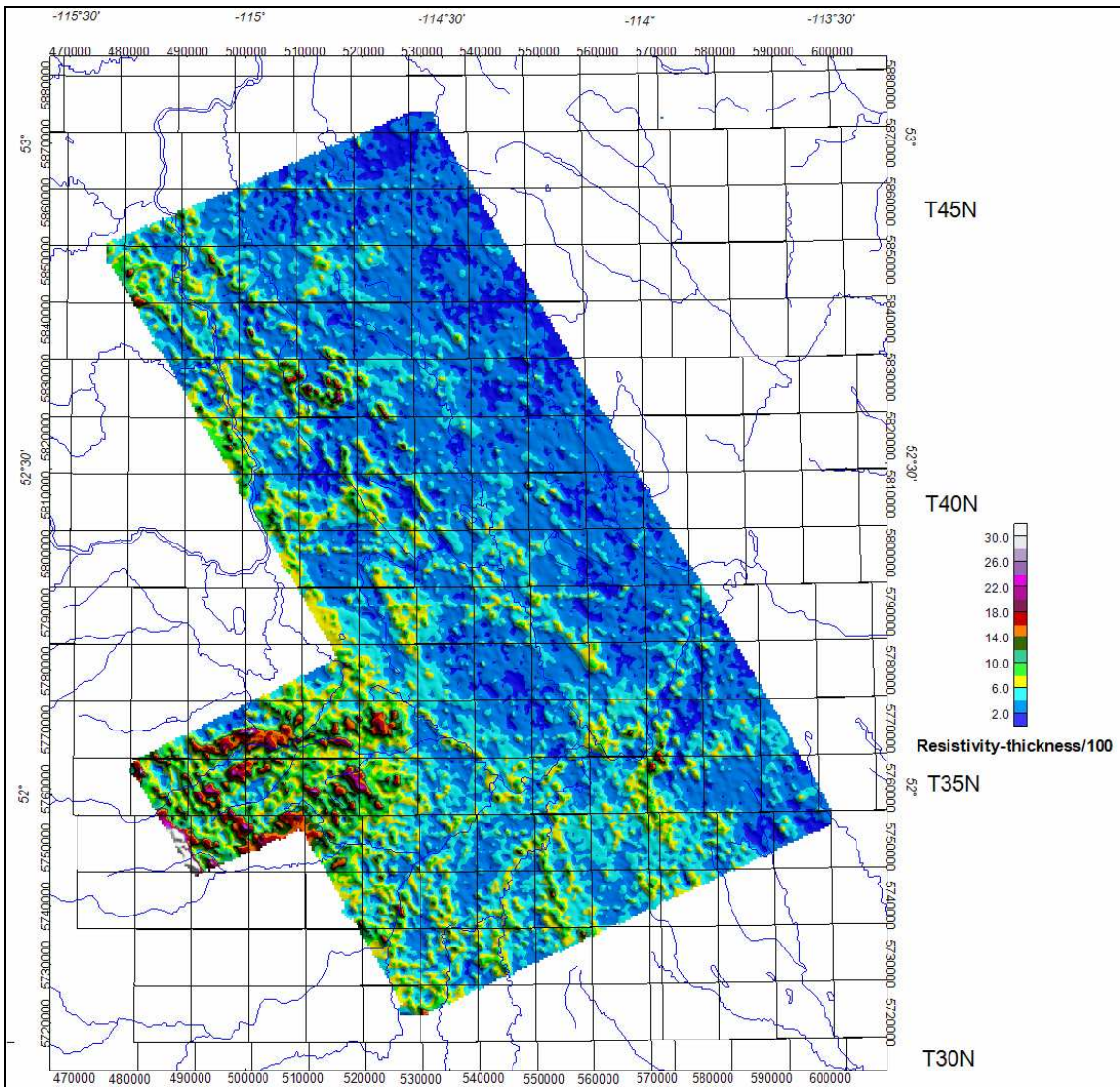


Figure 39: Resistivity-thickness product layer 2 (divided by 100), zone palette



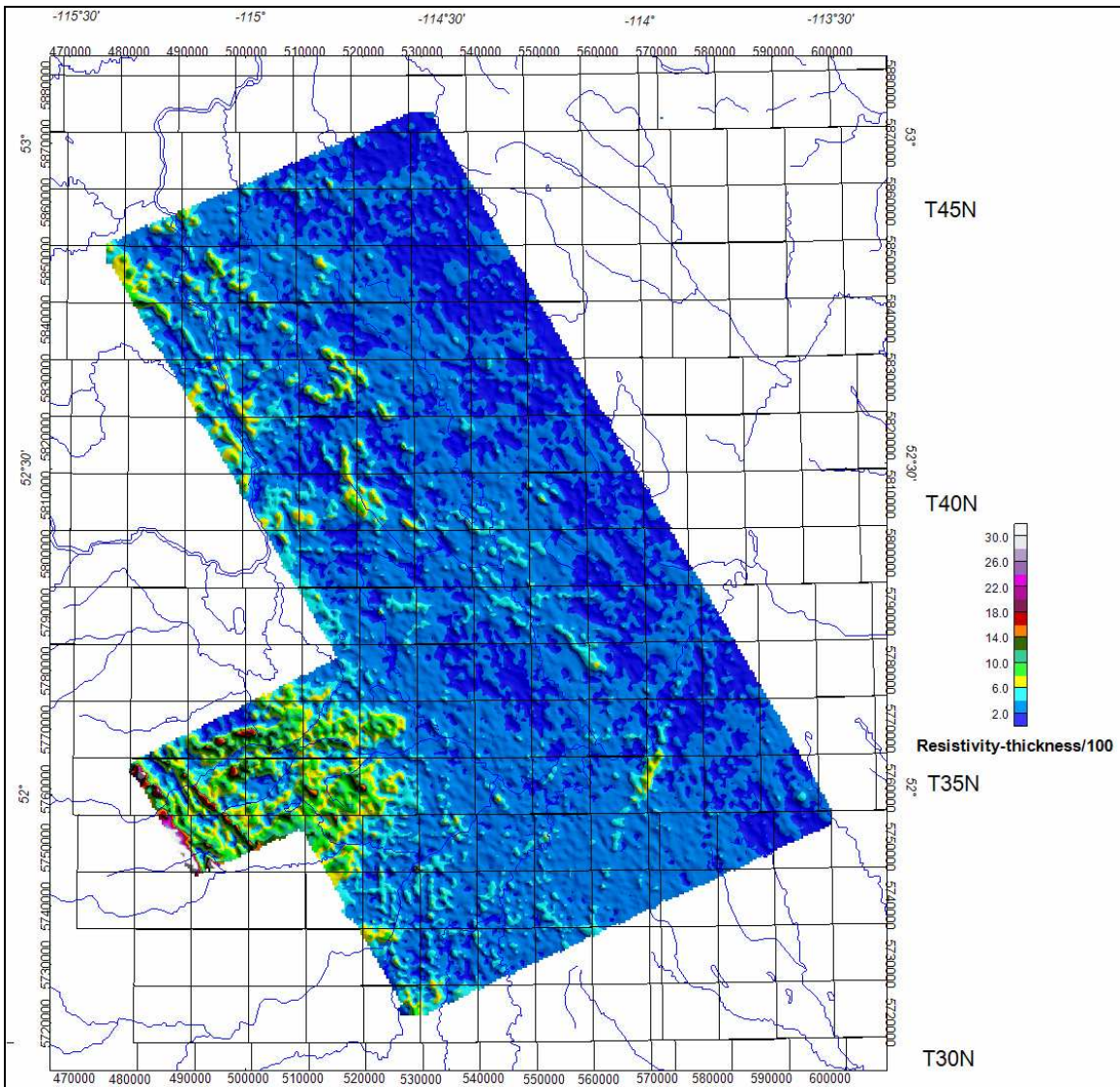


Figure 40: Resistivity-thickness product for layer 3 (divided by 100), zone palette



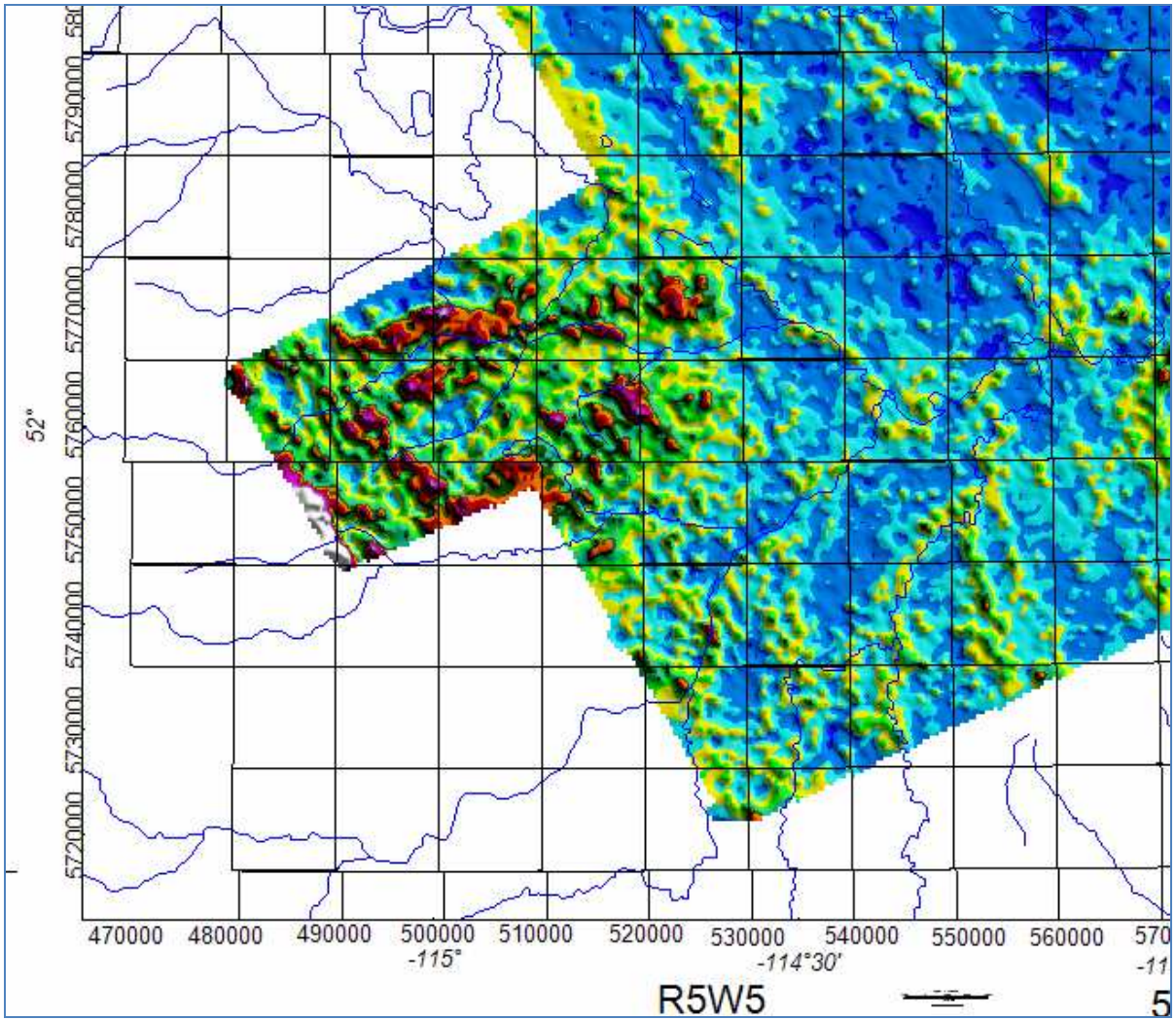


Figure 41a Zoomed western area of Rnn2Thnn2 product, zone palette



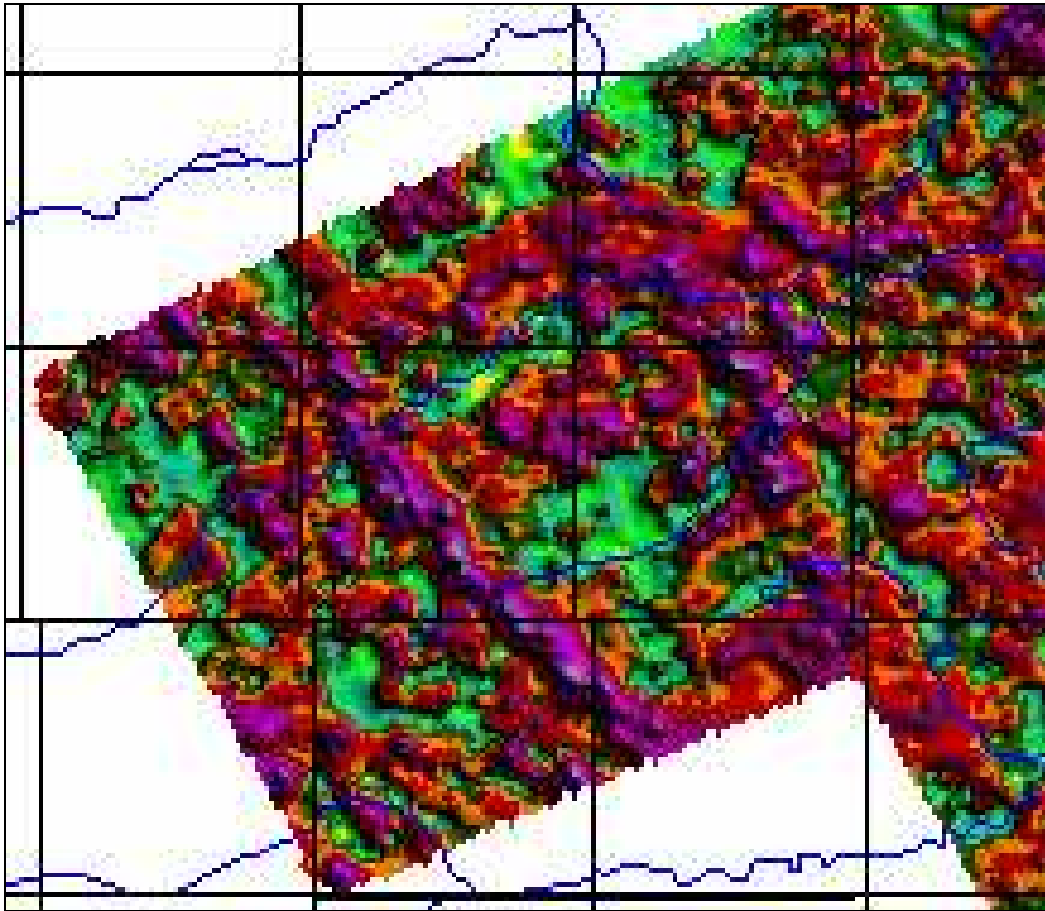


Figure 41b Zoomed western area of Rnn2Thnn2 product, color histogram palette



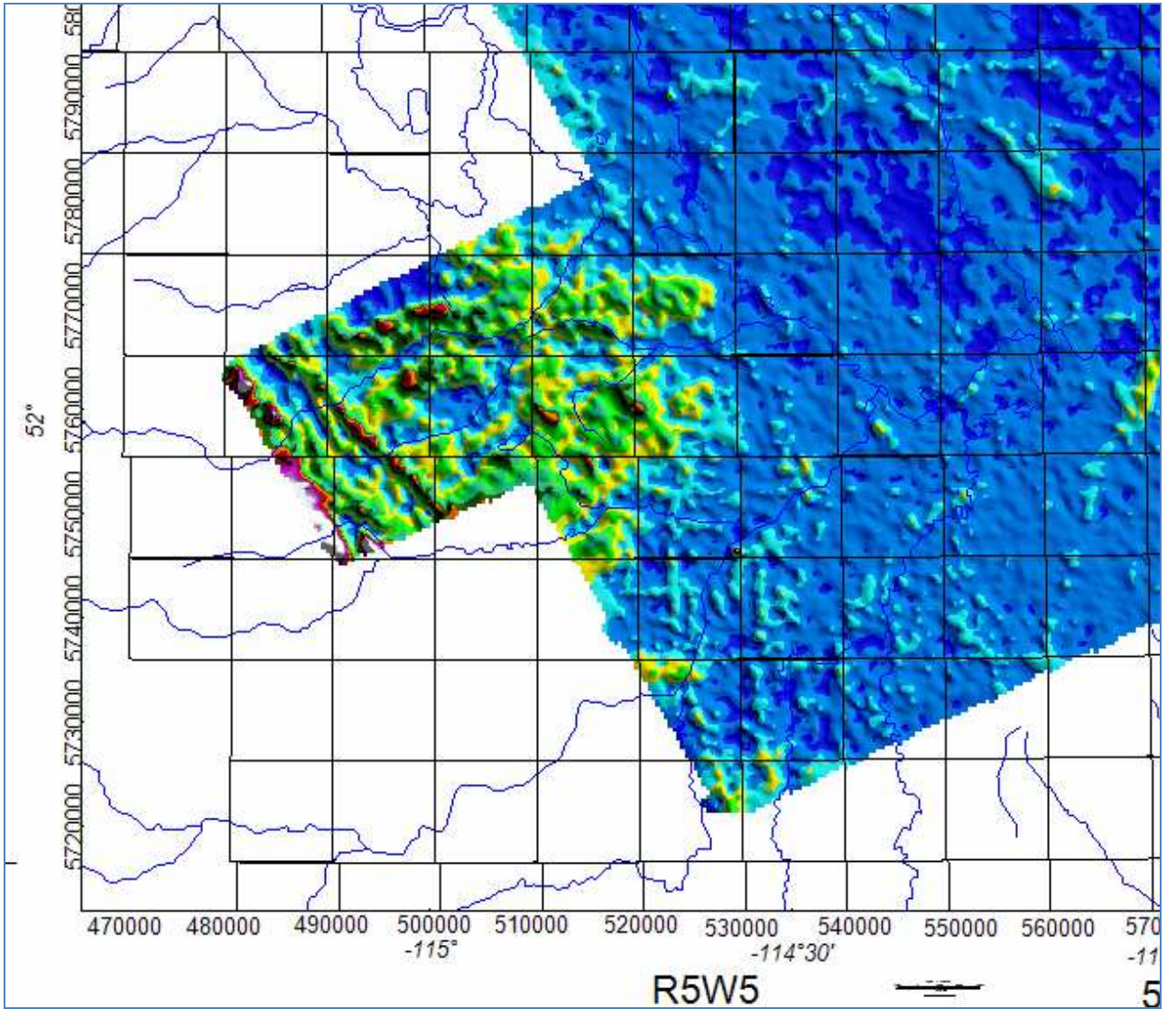


Figure 41c Zoomed western area of Rnn3Thnn3 product, zone palette



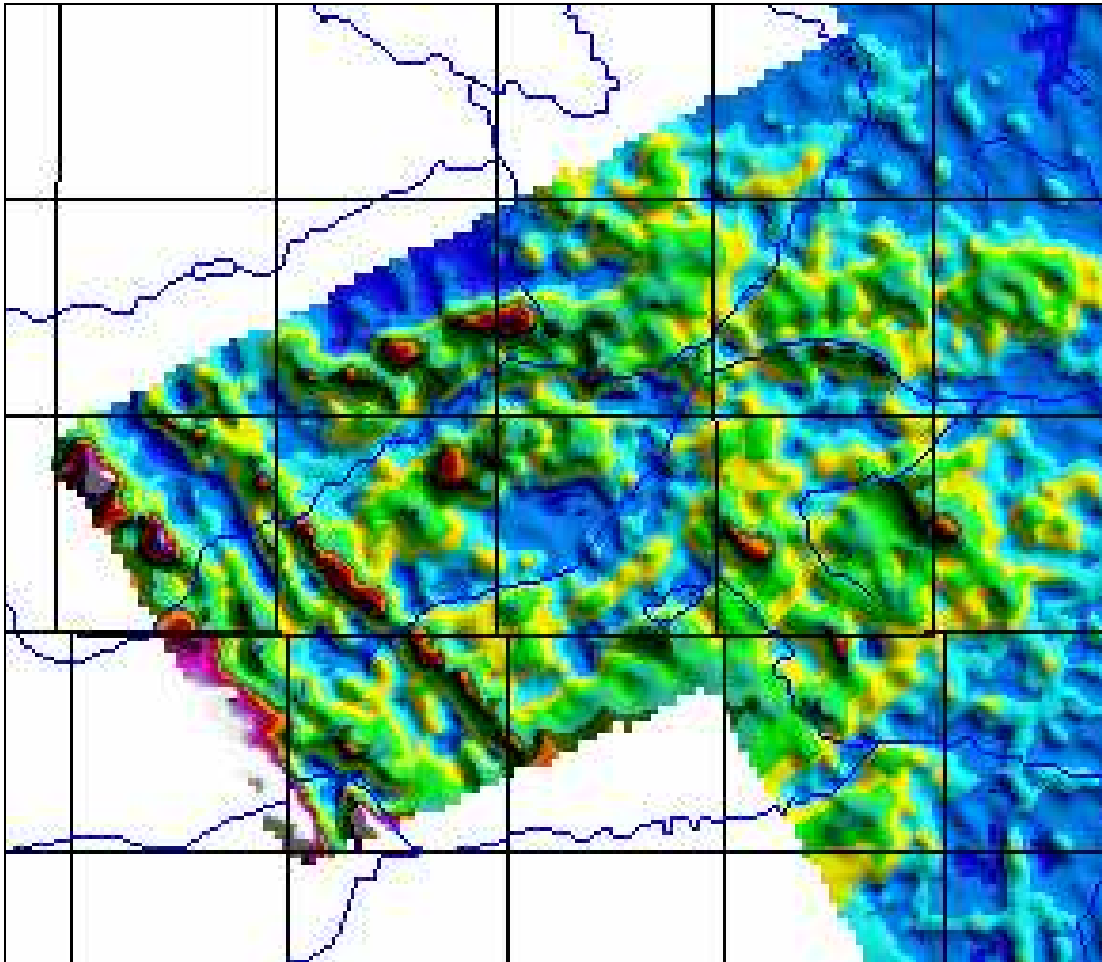


Figure 41d Additional Zoomed western area of Rnn3Thnn3 product, zone palette, shown in Figure 41c



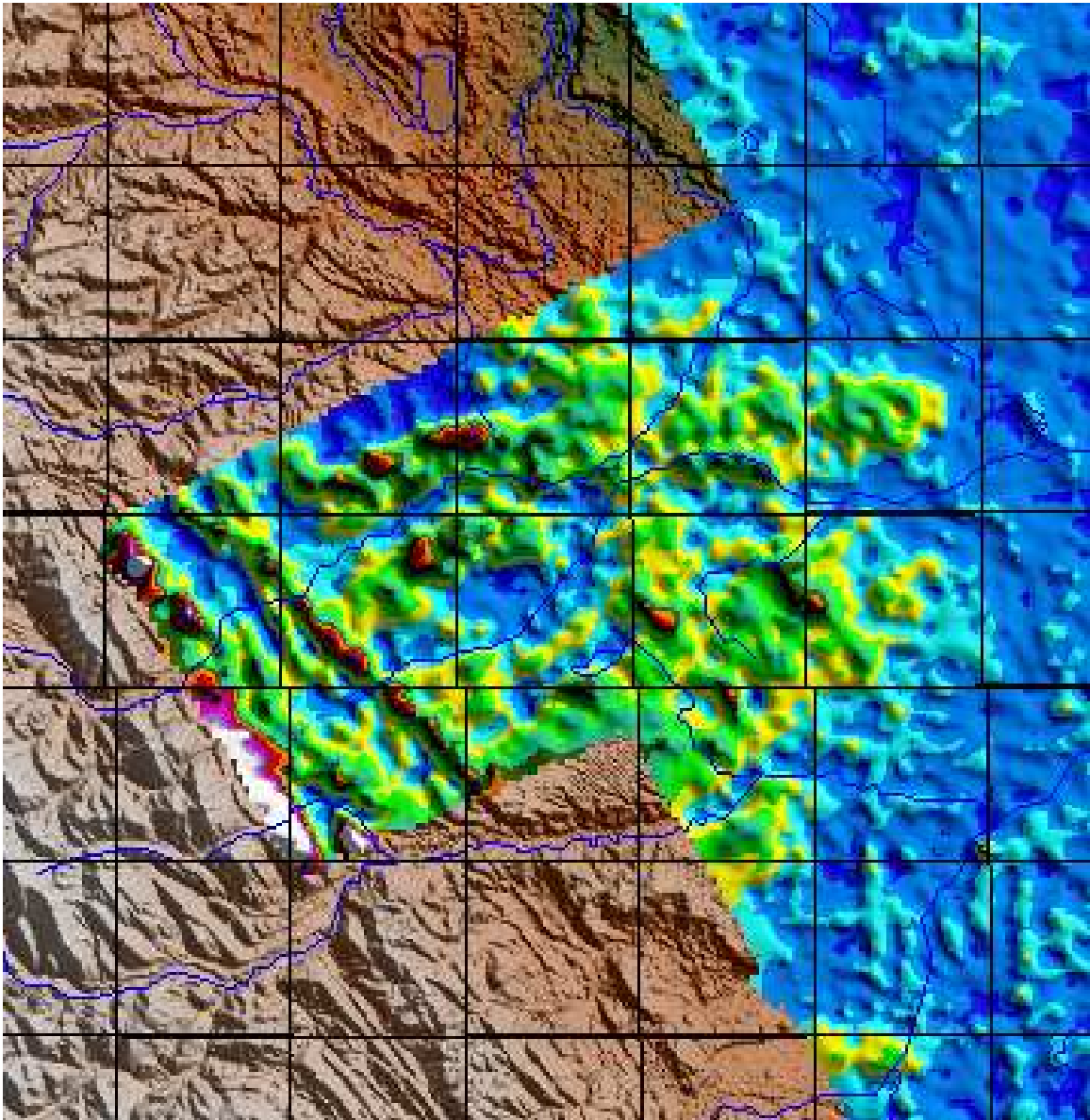


Figure 41e The resistivity-thickness product for layer 3 is overlain on the SRTM topography data. One can readily see the good correlation between the topography and the resistivity.



The following figure shows the Rnn2 data with the color histogram palette. Some dendritic features have been highlighted in the data pattern. It is possible that these patterns map buried channels. Some of the channels follow current drainage.

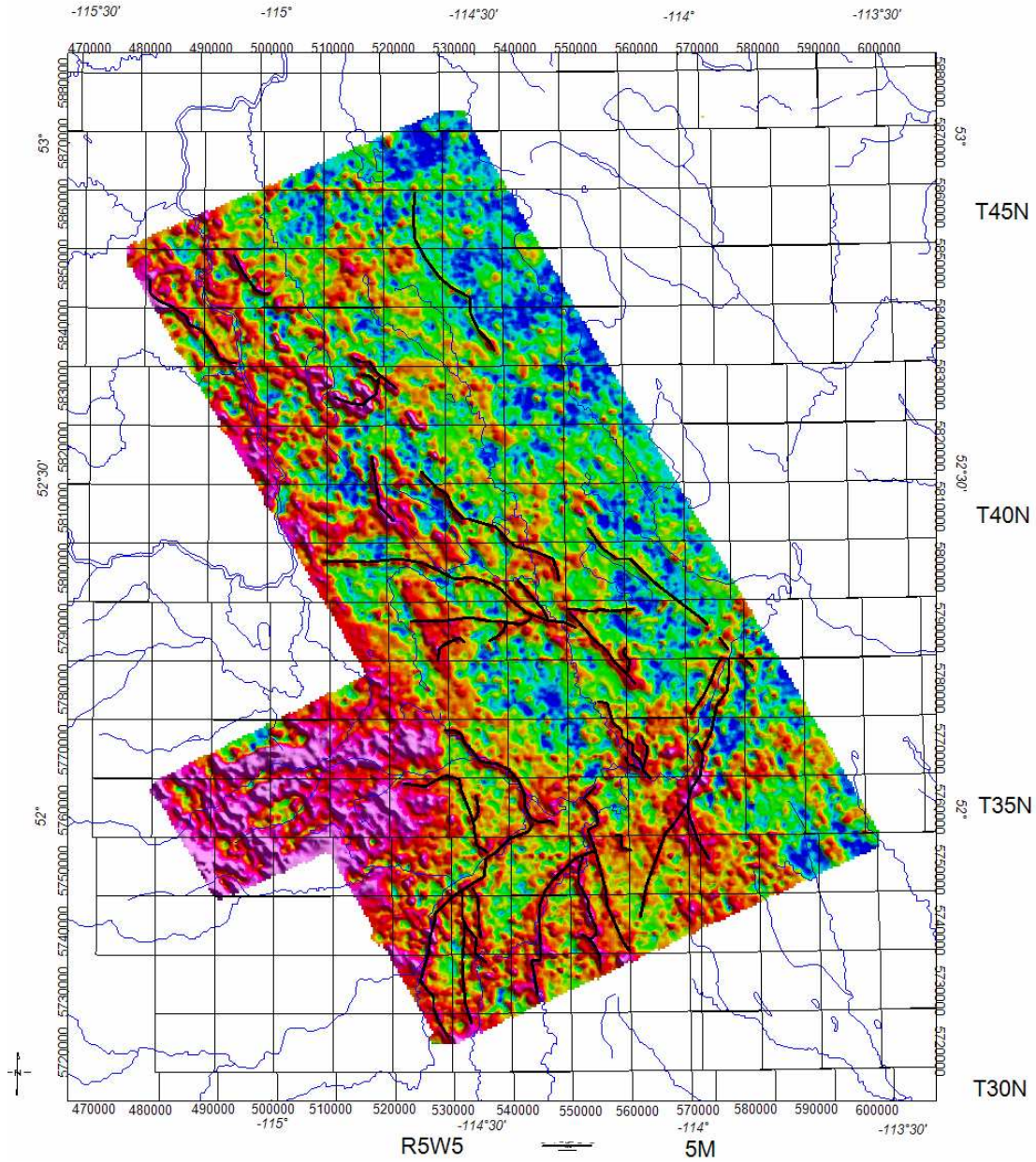


Figure 42 Second layer resistivity, Rnn2, with possible drainage features sketched on the image.



Lineaments were interpreted from the magnetic data. The lineaments could follow deeper faults. The interpreted lineaments are overlain on the Rnn1 high resistivity area map to see if any correlation might exist between any lineaments and the resistivity trends. There does seem to be a general strike correlation between several lineaments and resistive trends, particularly in the northern part of the survey area.

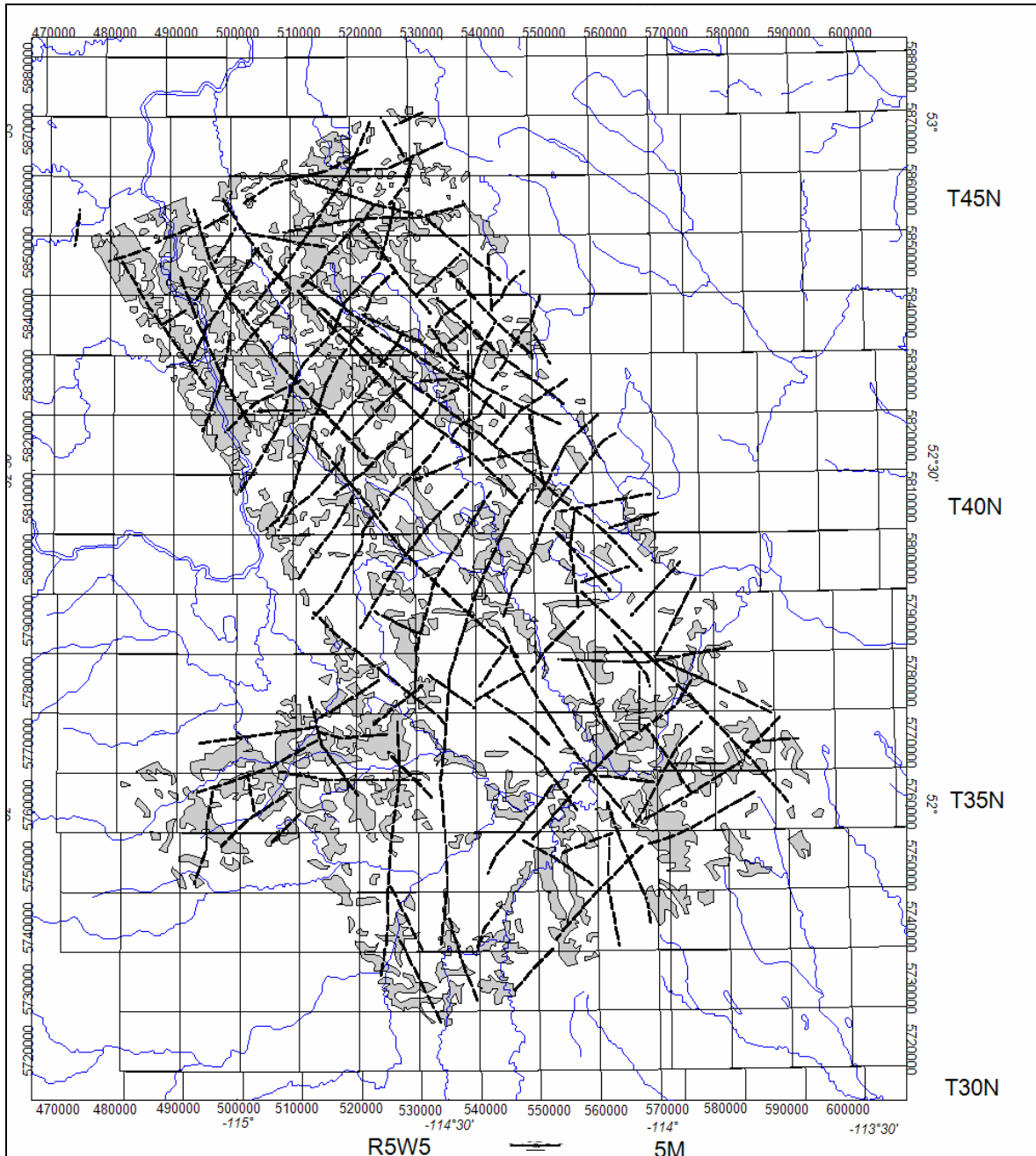


Figure 41 Rnn1 highest resistivity outlines and magnetic lineaments



Summary and Conclusions

A number of conclusions can be made from the results obtained here.

1. The GEOTEMTM data appears to have mapped a number of interesting features that could describe distribution of higher resistivity areas in the subsurface. These areas may have some hydrologic interest.
2. Inversion models included four models used in the March 2008 study with the same model, nn, chosen as the best result.
3. In some areas the resistivity patterns have the appearance of a channel-like character and they have been interpreted in that fashion.
4. The magnetic data did not show any significant correlation with the resistivity. In particular, no channel-like features were seen in the magnetic data.

In general it the airborne surveys met the objectives set out for the program.



References

Chin J., and Raiche A. 1998 Inverting AEM data using a damped eigen-parameter method *Exploration Geophysics* Vol. 29, pp. 128-132

Glenn, W. E., Ryu, J., Ward, S. H., Peeples, W. J., and Phillips, R. J., 1973, The inversion of vertical magnetic dipole sounding data: *Geophysics*, Vol. 38, p. 1109-1129.

Hohmann, G. W. and Raiche, A. P., 1988, Inversion of Controlled-Source Electromagnetic Data, in *Electromagnetic Methods in Applied Geophysics*, Vol. 1, Theory, Ed. M. N. Nabighian, p. 469-503.

Peirce, J. W., Glenn, W. E., and Brown, K. C., 1998, Ed. Special Issue on High Resolution Aeromagnetism for Hydrocarbon Exploration, *Can. Jour. Expl. Geophys.*, Vol. 34.

Raiche A. 1998 Modelling the time-domain response of AEM systems. *Exploration Geophysics* Vol. 29, pp. 103-106.

Tripp, A. C., Hohmann, G. W., and Swift, C. M. Jr., 1984, Two-dimensional resistivity inversion: *Geophysics*, Vol 8, p. 1708-1717.



APPENDIX I

Some EM terms defined

R is electrical resistance (sometimes used for resistivity)

ρ is electrical resistivity

σ is electrical conductivity

μ is magnetic permeability

ϵ is dielectric permittivity

t is time in seconds

T is period in seconds

f is frequency in Hertz, cycles/second

ω is angular frequency radians/second

E or e is electric field intensity, volts/m

H or h is magnetic field intensity, A/m

B or b is magnetic induction, Wb/m², Tesla

D is dielectric displacement

J is electrical current density, A/m²

I is electrical current, coulombs/ second

q is electrical charge, coulombs

